



---

Universidad de Valladolid



PROGRAMA DE DOCTORADO EN INGENIERÍA QUÍMICA Y  
AMBIENTAL

TESIS DOCTORAL:

**Encapsulation of hydrophobic drugs with  
elastin-like recombinamers by supercritical  
antisolvent process for advanced biomedical  
applications**

Presentada por Reinaldo Vallejo Vicente para optar al  
grado de  
Doctor por la Universidad de Valladolid

Dirigida por:  
Francisco Javier Arias Vallejo  
Soraya Rodríguez Rojo  
Mercedes Santos García



# INDEX



---

|  |    |
|--|----|
| 1. ABSTRACT.....   | 1  |
| 2. INTRODUCTION.....   | 11 |
| 2.1 Active pharmaceutical ingredient .....                                   | 16 |
| 2.1.1 Pharmacodynamics.....  | 17 |
| 2.1.2 Pharmacokinetics.....  | 18 |
| 2.1.3 Hydrophobic APIs.....  | 24 |
| 2.2 Elastin like recombinamers (ELRs) .....                                  | 32 |
| 2.2.1 ELR biosynthesis.....  | 36 |
| 2.2.2 ELRs as controlled drug delivery carriers .....                        | 38 |
| 2.2.3 Hydrogels as macroscopic devices for controlled release.....           | 39 |
| 2.2.4 ELR nanoparticles as devices for controlled drug release .....         | 41 |
| 2.3 Encapsulation of active agents into biomaterials.....                    | 43 |
| 2.4 Processes with supercritical CO <sub>2</sub> .....                       | 45 |
| 2.4.1 Rapid expansion of supercritical solution (RESS) .....                 | 45 |
| 2.4.2 Supercritical solvent impregnation (SSI) .....                         | 46 |
| 2.4.3 Particles from gas saturated solutions (PGSS) and PGSS-<br>drying..... | 47 |
| 2.4.4 Supercritical fluid extraction of emulsion (SFEE) .....                | 48 |
| 2.4.5 Supercritical anti-solvent (SAS) precipitation.....                    | 49 |
| 2.5 REFERENCES.....  | 50 |
| 3. HYPOTHESIS .....  | 63 |
| 4. OBJECTIVES .....  | 63 |
| 4. MATERIALS.....  | 67 |
| 4.1.Reagents.....  | 67 |
| 4.2.Elastin-like Recombinamers (ELRs).....                                   | 68 |
| 5. METHODS .....   | 69 |
| 5.1.ELRs synthesis .....   | 69 |
| 5.2.Supercritical Antisolvent (SAS) pilot plan description. ....             | 70 |
| 5.3.Particle characterization .....  | 72 |
| 5.3.1. Proton Nuclear Magnetic Resonance <sup>1</sup> H-NMR.....             | 72 |

|  |     |
|--|-----|
| 5.3.2. Mass spectrometry (MALDI-TOF).....  | 73  |
| 5.3.3. Fourier transform infrared spectroscopy (FTIR) .....  | 73  |
| 5.3.4. Differential scanning calorimetry (DSC) .....   | 74  |
| 5.3.5. Dynamic light scattering and zeta potential .....   | 75  |
| 5.3.6. Scanning electron microscopy (SEM).....   | 76  |
| 5.3.7. Transmission Electron microscopy (TEM) .....  | 76  |
| 5.3.8. Atomic force microscopy (AFM).....  | 77  |
| 5.3.9. Confocal microscopy .....   | 78  |
| 5.3.10. Fluorescence microscopy.....   | 79  |
| 5.4. <i>In vitro</i> release studies .....   | 79  |
| 5.6. <i>Ex vivo</i> assays.....  | 83  |
| 5.7. <i>In-vivo</i> assays.....  | 84  |
| 5.8. REFERENCES.....   | 88  |
| CHAPTER 1: ACETAZOLAMIDE ENCAPSULATION WITH<br>ELASTIN LIKE RECOMBINAMERS BY SUPERCRITICAL<br>ANTISOLVENT (SAS) PROCESS FOR GLAUCOMA<br>TREATMENT..... | 95  |
| 6. RESULTS & DISCUSSION .....  | 96  |
| 6.1. Microencapsulation of ELR with acetazolamide.....   | 96  |
| 6.2. <sup>1</sup> H-NMR study for acetazolamide and ELR-Acetazolamide<br>mixture .....   | 98  |
| 6.3. Macroscopic characterization .....  | 102 |
| 6.4. Behaviour in aqueous solution.....  | 104 |
| 6.5. Characterization of the formulations by Atomic Force Microscopy<br>.....  | 107 |
| 6.6. Drug delivery studies.....  | 112 |
| 6.7. <i>Ex vivo</i> studies of the acetazolamide formulations.....   | 114 |
| 6.7.1. Transcorneal permeation study .....   | 115 |
| 6.8. <i>In vivo</i> studies of the acetazolamide formulations.....   | 116 |
| 6.8.1. Intraocular pressure <i>in vivo</i> assay .....   | 116 |
| 6.8.2. Ocular irritation tests .....   | 118 |
| 6.9. Final remarks.....  | 121 |

---

|  |     |
|--|-----|
| 6.10. REFERENCES.....  | 122 |
| CHAPTER 2: PRODUCTION OF ELASTIN-LIKE RECOMBINAMERS-BASED NANOPARTICLES FOR DOCETAXEL ENCAPSULATION AND USE AS SMART DRUG-DELIVERY SYSTEMS USING A SUPERCRITICAL ANTI-SOLVENT PROCESS..... | 125 |
| 7. RESULTS & DISCUSSION .....  | 126 |
| 7.1.Optimization of the supercritical antisolvent process (SAS) .....  | 126 |
| 7.2.Characterization of the particles obtained after SAS process ....  | 131 |
| 7.2.1. Characterization of the particles by SEM.....   | 131 |
| 7.2.2. Behaviour in aqueous solution.....  | 134 |
| 7.2.3. <sup>1</sup> HNMR study for Docetaxel and ELR-Docetaxel mixture..   | 140 |
| 7.3.Encapsulation of DTX by ELRs .....   | 142 |
| 7.3.1. Behaviour in an aqueous solution of the encapsulated DTX in ELRs .....  | 145 |
| 7.3.2. Drug-release study.....   | 153 |
| 7.4. <i>In vitro</i> cell assays .....   | 155 |
| 7.5.Final remarks.....   | 160 |
| 7.6.REFERENCES.....  | 161 |
| CHAPTER 3: QUERCETIN AND RESVERATROL ENCAPSULATION IN A SINGLE DRUG DELIVERY SYSTEM WITH ELASTIN-LIKE RECOMBINAMERS BY SUPERCRITICAL ANTISOLVENT PROCESS (SAS).....                        | 165 |
| 8. RESULTS & DISCUSSION .....  | 166 |
| 8.1.Optimization of the operational conditions for ethanol-water-scco <sub>2</sub> encapsulation with ELRs. ....   | 166 |
| 8.2.Particle characterization .....  | 171 |
| 8.2.1. NMR study for quercetin, resveratrol and their mixture with ELRs. ....  | 171 |
| 8.2.2. Particle analysis by SEM.....   | 176 |
| 8.2.3. Behaviour in aqueous solution.....  | 178 |
| 8.3.Drug delivery study .....  | 179 |
| 8.4.Final remarks.....   | 185 |

|                        |     |
|------------------------|-----|
| 8.5.REFERENCES.....    | 186 |
| 9. CONCLUSIONS.....    | 189 |
| 10. ABBREVIATIONS..... | 193 |
| ANNEX I.....           | 195 |
| ANNEX II.....          | 201 |



**RESUMEN /  
ABSTRACT**



## 1. ABSTRACT

Nowadays science tends to form multidisciplinary teams, where experts in different areas converge to achieve the same objective. This thesis is one of those examples where knowledge from areas such as genetic engineering, molecular biology, biotechnology, chemistry and chemical engineering is gathered together to achieve a small step forward in the world of science.

The development of advanced materials that improve the features of devices already on the market is a general challenge in all technological areas. The emergence of new therapeutic molecules and their validation stimulates the progress of new biomaterials, either as excipients or by exerting an active effect on the dosage and efficacy of the drug. Among the most frequently promoted are those of natural origin: polysaccharides and proteins. The first ones have excellent biocompatibility and capacity to protect the active ingredients but lack the flexibility and multifunctionality of proteins. Proteins perform numerous functions in living organisms and viruses, with great efficiency and selectivity, interacting specifically with other biomolecules and adapting to different physiological environments.

Currently, Elastin Like Recombinamers (ELRs) are biopolymers that form unique molecules of completely defined structure with the strength, self-assembly capacity and natural mechanical properties of human elastin. But also with the unparalleled versatility of proteins, where all 20 amino acids can be used in infinite combinations to complement the functionalities not present in elastin. ELR polymers are polypeptides whose sequence consists of repeats of the (VPGXG)<sub>n</sub> sequence, or permutations thereof, conferring unique mechanical properties similar to natural elastin. They are currently produced by recombinant DNA technology using *Escherichia coli* bacteria and their properties include

some of the most remarkable features of elastin: extraordinary elasticity, self-assembly capacity, and excellent resistance to stress.

Controlled drug delivery systems from biodegradable polymer nanoparticles are having a major medical impact in a wide range of therapeutic areas. However, difficulties remain in formulating protein-based nanoparticle systems. For example, there are difficulties in the encapsulation in water-based hydrogels, resulting in very low loadings of this type of drugs, in the exposure of protein polymers to high temperatures, leading to their denaturation, or in the use of organic solvents, in some cases toxic, which implies the design of a subsequent process for their elimination. For these reasons, new production processes have been developed to protect the functionality of these polymers. The use of supercritical fluids (SCFs) is a viable option to consider when producing nanoparticulate systems for controlled drug release.

High-pressure technologies, especially those involving supercritical carbon dioxide (scCO<sub>2</sub>), were studied as sustainable alternatives for polymer processing because of the moderate pressure and temperature at which the supercritical state is reached (73.8 bar and 304.1K) allow the processing of polymers at lower temperatures.

The first chapter is focused on acetazolamide, an active compound used in the treatment of glaucoma that is considered the second most common cause of blindness in the world after cataracts and one of the main causes of permanent blindness. In this case, an ELR has been used, which consists of a tetrablock design involving two hydrophilic blocks containing glutamic acid (E) and two hydrophobic blocks containing isoleucine (I) as guest residues. Acetazolamide (AZM) is encapsulated by SAS using DMSO as a solvent in three different ELR:AZM ratios achieving high a process yield, up to 62%. The powder obtained after SAS technique was characterized by SEM and chemically characterized by NMR H<sup>+</sup> obtaining a residual amount of DMSO between 6.6 and 12.3%. After dispersion

under physiological conditions, the microparticles disintegrate into stable monodisperse nanoparticles due to low PDI (between 0.132 to 0.155) and high Z-potential (between -33 to -34mV). Topographies were confirmed by TEM and by a novel AFM characterization. The in vitro release profiles show a Fick diffusion-governed release with a more sustained release of the drug over time. Transcorneal permeation results show a higher permeation level than the control solution, reaching significant differences of more than 30% after 2h. In vivo intraocular pressure (IOP) tests performed on hypertensive rabbits show higher effectiveness for the three formulations analyzed, suggesting a higher bioavailability of the drug in the treatment. Finally, ocular irritation tests did not reveal any ocular alteration or damage.

In the second chapter of this work, a coaxial nozzle was designed, which, combined with the implementation of a bypass line in the installation, allowed us to reduce the residual amount of solvent in the final product. The chemotherapeutic agent Docetaxel (DTX) is encapsulated with a block copolymer ELR containing the RGD peptide, a specific target sequence for cancer cells. The amount of residual DMSO found in the final product after implementing the process improvements was found to be between 3.5 and 3.7%. Physical characterization of the powder obtained after SAS process shows spherical microparticles by SEM and after dispersion under physiological conditions, microparticles disaggregate into stable monodisperse nanoparticles. This protects the drug, as confirmed by NMR analysis, thereby increasing the water solubility of DTX up to fifty orders of magnitude. The delivery process is governed by the Fick diffusion mechanism and indicates that the presence of DTX on the surface of the particles is practically negligible. Cellular assays showed that, due to the presence of the cancer target sequence RGD, breast cancer cells were more affected than human endothelial cells, thus meaning that the strategy

developed in this work opens the way to new controlled release systems more precise than non-selective chemotherapeutic drugs.

The last chapter covers the treatment of dry eye disease using a combination of two active compounds, resveratrol and quercetin. In this part of the work, the use of DMSO for encapsulation with ELRs was avoided and an ethanol/water mixture was used, for which new operating conditions had to be investigated, based on the CO<sub>2</sub>-Ethanol-Water ternary diagram. A final product was obtained with different ratios that were physically and chemically characterised. In addition, stability tests showed that the encapsulated active principles display a prolonged degradation over time.

**RESUMEN**

Hoy en día la ciencia tiende a formar equipos multidisciplinares, en los que convergen expertos de diferentes áreas para conseguir un mismo objetivo. Esta tesis es uno de esos ejemplos donde se reúnen conocimientos de áreas como la ingeniería genética, la biología molecular, la biotecnología, la química y la ingeniería química para conseguir un pequeño avance en el mundo de la ciencia.

El desarrollo de materiales avanzados que mejoren las prestaciones de los dispositivos ya comercializados es un reto generalizado en todas las áreas tecnológicas. La aparición de nuevas moléculas terapéuticas y su validación estimula el progreso de nuevos biomateriales, ya sea como excipientes o ejerciendo un efecto activo en la dosificación y eficacia del fármaco. Entre los más promocionados están los de origen natural: polisacáridos y proteínas. Los primeros tienen una excelente biocompatibilidad y capacidad para proteger los principios activos, pero carecen de la flexibilidad y multifuncionalidad de las proteínas. Las proteínas desempeñan numerosas funciones en los organismos vivos y en los virus, con gran eficacia y selectividad, interactuando específicamente con otras biomoléculas y adaptándose a diferentes entornos fisiológicos. En la actualidad, los recombinantes similares a la elastina (ELR) son biopolímeros que forman moléculas únicas de estructura completamente definida con la fuerza, la capacidad de autoensamblaje y las propiedades mecánicas naturales de la elastina humana. Pero también con la inigualable versatilidad de las proteínas, donde los 20 aminoácidos pueden utilizarse en infinitas combinaciones para complementar las funcionalidades no presentes en la elastina. Los polímeros ELR son polipéptidos cuya secuencia consiste en repeticiones de la secuencia (VPGXG)<sub>n</sub>, o permutaciones de la misma, que confieren propiedades mecánicas únicas similares a la elastina natural. Actualmente se producen mediante tecnología de ADN recombinante utilizando bacterias

*Escherichia coli* y sus propiedades incluyen algunas de las características más notables de la elastina: extraordinaria elasticidad, capacidad de autoensamblaje y excelente resistencia a la tensión.

Los sistemas de administración controlada de fármacos a partir de nanopartículas poliméricas biodegradables están teniendo un gran impacto médico en una amplia gama de áreas terapéuticas. Sin embargo, siguen existiendo dificultades en la formulación de sistemas de nanopartículas basados en proteínas. Por ejemplo, existen dificultades en la encapsulación en hidrogeles de base acuosa, lo que da lugar a cargas muy bajas de este tipo de fármacos, en la exposición de los polímeros proteicos a altas temperaturas, lo que provoca su desnaturalización, o en el uso de disolventes orgánicos, en algunos casos tóxicos, lo que implica el diseño de un proceso posterior para su eliminación. Por estas razones, se han desarrollado nuevos procesos de producción para proteger la funcionalidad de estos polímeros. El uso de fluidos supercríticos (SCF) es una opción viable a tener en cuenta en la producción de sistemas nanoparticulados para la liberación controlada de fármacos.

Las tecnologías de alta presión, especialmente las de dióxido de carbono supercrítico (scCO<sub>2</sub>), se estudiaron como alternativas sostenibles para el procesamiento de polímeros, ya que la presión y la temperatura moderadas a las que se alcanza el estado supercrítico (73,8 bar y 304,1K) permiten el procesamiento de polímeros a temperaturas más bajas.

El primer capítulo se centra en la acetazolamida, un compuesto activo utilizado en el tratamiento del glaucoma que se considera la segunda causa de ceguera en el mundo, después de las cataratas, y una de las principales causas de ceguera permanente. En este caso, se ha utilizado un ELR, que consiste en un diseño de tetrabloque que incluye dos bloques hidrofílicos que contienen ácido glutámico (E) y dos bloques hidrofóbicos que contienen isoleucina (I) como residuos invitados. La acetazolamida (AZM) se encapsuló



mediante SAS utilizando DMSO como disolvente en tres proporciones diferentes de ELR:AZM logrando un alto rendimiento del proceso, hasta el 62%. El polvo obtenido tras la técnica SAS fue caracterizado por SEB y químicamente por  $^1\text{H-NMR}$  obteniendo una cantidad residual de DMSO entre el 6,6 y el 12,3%. Tras la dispersión en condiciones fisiológicas, las micropartículas se desintegran en nanopartículas monodispersas estables debido a su baja PDI (entre 0,132 y 0,155) y su alto potencial Z (entre -33 y -34mV). Las topografías fueron confirmadas por TEM y por una novedosa caracterización por AFM. Los perfiles de liberación in vitro muestran una liberación gobernada por difusión de Fick con una liberación más sostenida del fármaco en el tiempo. Los resultados de permeación transcorneal muestran un nivel de permeación superior al de la solución de control, alcanzando diferencias significativas de más del 30% después de 2h. Las pruebas de presión intraocular (PIO) in vivo realizadas en conejos hipertensos muestran una mayor eficacia para las tres formulaciones analizadas, lo que sugiere una mayor biodisponibilidad del fármaco en el tratamiento. Finalmente, las pruebas de irritación ocular no revelaron ninguna alteración o daño ocular.

En el segundo capítulo de este trabajo se diseñó una boquilla coaxial que, combinada con la implementación de una línea de bypass en la instalación, permitió reducir la cantidad residual de disolvente en el producto final. El agente quimioterapéutico Docetaxel (DTX) se encapsula con un copolímero en bloque ELR que contiene el péptido RGD, una secuencia diana específica para las células cancerosas. La cantidad de DMSO residual encontrada en el producto final tras la implementación de las mejoras en el proceso resultó estar entre el 3,5 y el 3,7%. La caracterización física del polvo obtenido tras el proceso SAS muestra micropartículas esféricas por SEM y, tras la dispersión en condiciones fisiológicas, las micropartículas se disgregan en nanopartículas monodispersas estables. Esto protege al fármaco, tal y como confirma el análisis de RMN, aumentando así la

solubilidad en agua del DTX hasta cincuenta órdenes de magnitud. El proceso de suministro se rige por el mecanismo de difusión de Fick e indica que la presencia de DTX en la superficie de las partículas es prácticamente insignificante. Los ensayos celulares mostraron que, debido a la presencia de la secuencia diana del cáncer RGD, las células de cáncer de mama se vieron más afectadas que las células endoteliales humanas, lo que significa que la estrategia desarrollada en este trabajo abre el camino a nuevos sistemas de liberación controlada más precisos que los fármacos quimioterapéuticos no selectivos. El último capítulo aborda el tratamiento de la enfermedad del ojo seco mediante una combinación de dos compuestos activos, el resveratrol y la quercetina. En esta parte del trabajo se evitó el uso de DMSO para la encapsulación con ELRs y se utilizó una mezcla de etanol/agua, para la que hubo que investigar nuevas condiciones de operación, basadas en el diagrama ternario CO<sub>2</sub>-Etanol-Agua. Se obtuvo un producto final con diferentes proporciones que se caracterizó física y químicamente. Además, las pruebas de estabilidad mostraron que los principios activos encapsulados presentan una degradación prolongada en el tiempo.

# INTRODUCTION



## 2. INTRODUCTION

The use of nanotechnology in the development of new medicines is a reality in every sense [1,2] and has been recognised in the European Union as one of the key strategies [3] capable of providing new innovative solutions to address unmet medical needs. The application of nanotechnology for medical purposes has been termed nanomedicine and the European Science Foundation defines it as “the science and technology of diagnosing, treating, and preventing disease and traumatic injury, of relieving pain, and of preserving and improving human health, using molecular tools and molecular knowledge of the human body” [4]

Over the past 50 years, advances in nanomedicine have gone almost hand in hand with technology. A liposomal formulation of doxorubicin (Doxil®) was approved by the US Food and Drug Administration (FDA) in 1995 [5] to treat AIDS-related Kaposi's sarcoma. In 2005, the FDA approved an albumin-based nanoparticle, protein-bound paclitaxel (Abraxane®) [6], for clinical use in the treatment of breast cancer, non-small cell lung cancer and pancreatic cancer. More recently, in 2019, ado-trastuzumab emtansine (DM1) (Kadcyla®) was approved by FDA [7] for targeted use in patients with HER2-positive breast cancer.

Hence, currently, numerous examples of dosages forms of drugs have appeared either as macromolecular substances [8] or incorporated into a support, nanocapsules as well as reservoir systems [9][10]. In this context, the controlled release of drugs has been the subject of research in recent decades. The interest of researchers in being able to administer a specific dose in a specific target has provided numerous contributions to the literature, achieving better and more effective systems [11].

Controlled drug delivery systems consist of technologies whose purpose is to release therapeutic agents in a specific target as needed to achieve the desired therapeutic dose

and maintain adequate drug levels for sufficiently prolonged periods of time. Therefore, in some cases, solubility is increased or the pharmacokinetics of the drug are modified, in order to reach its sustained and continuous presence. Thus, in recent years, different materials or formulations have been employed to achieve this goal which has been reported in the literature [12] for the treatment of different pathologies, such as cancer diseases. In this sense, drug delivery systems could be more ambitious, by designing carriers that could find specific sites to release the drug, thereby avoiding exposure to healthy tissues.

Nanomedicines have different *in vivo* characteristics depending on their formulation. In this context, Controlled drug delivery systems are classified according to their pharmacokinetic properties: dendrimers, engineered nanoparticles, lipid nanosystems, micelles and polymeric nanoparticles [13]. Figure 1 shows the nanomedicines approved by the Food and Drug Administration (FDA) until 2019 [14,15], where liposomes represent 44.8% of the approved products (13 products) and inorganic nanoparticles are in second place, representing 41.4% (12 products) [16]. It is worth noting that nanomedicines used in cancer therapies are in the first place, with 10 products on the market, followed by iron-replacement therapies (8 products) and imaging agents (6 products) [16]. In addition, the number of clinical trials of this category of nanomedicines has increased in recent decades (Figure 2), which reinforces the interest of the competent administrations in undertaking more and more efforts to approve new nanomedicines. Therefore, it is not surprising that in the forthcoming year's new products for different applications, especially for cancer therapies, will reach the market.

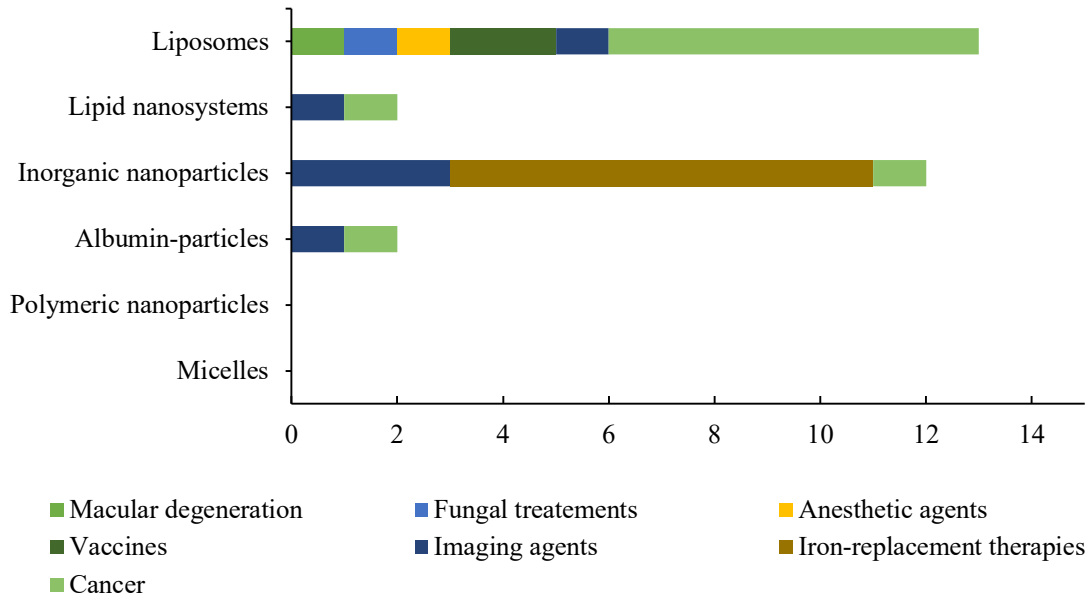


**Figure 1.** Clinically approved nanomedicines by FDA until 2019 for therapy and diagnostic. Figure adapted from ([16])

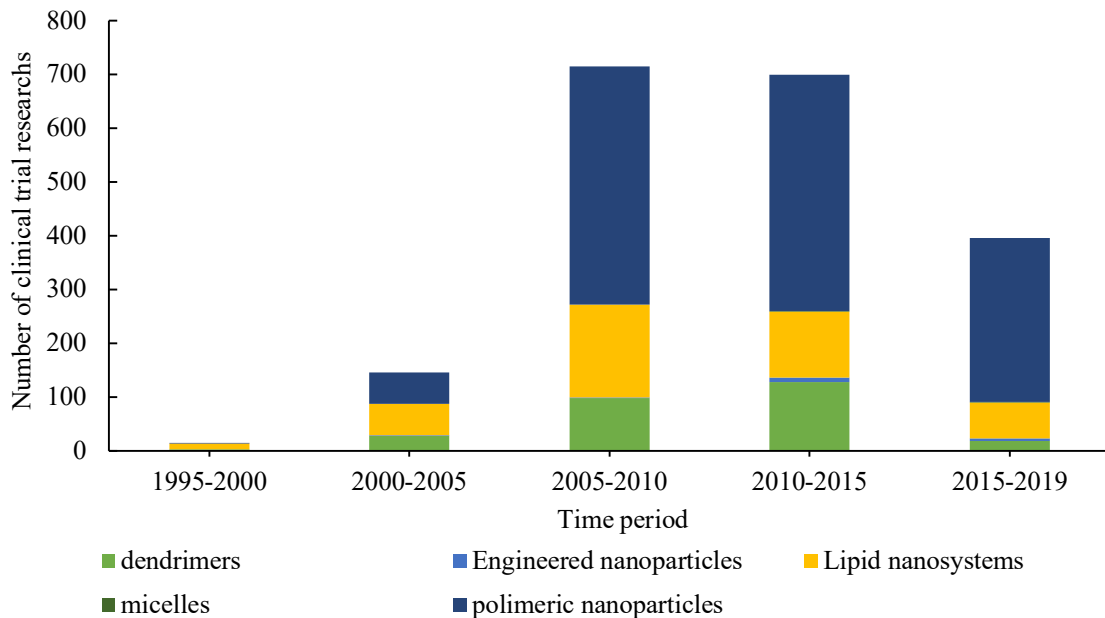


**Figure 2.** Number of clinical trials in the United States of America (USA) in which participants are assigned to groups that receive one or more intervention/treatment (or no intervention). Participants may receive diagnostic, therapeutic, or other types of interventions. The search was conducted on ClinicalTrials.gov [17] filtering studies with results.

European Medicine Agency (EMA) in 2009 established the European Nanomedicines Expert Group [18] composed of high profile academics and regulatory science specialists, which since its inception interact with regulatory scientists from the US Food and Drug Administration (FDA) and the Japan Pharmaceuticals and Medical Devices Agency (PMDA) and advances in this field have accomplished objectives such as more specific drug targeting, reducing toxicity without interfering with efficacy, achieving biocompatibility and developing new administration ways safer formulations [19] [20]. As a result, today the development of new supports based on biomaterials such as proteins, polymers, dendrimers, micelles/polymeric nanoparticles, liposomes, emulsions or nanoparticles (Figure 3) is having a great impact on nanomedicine [21].

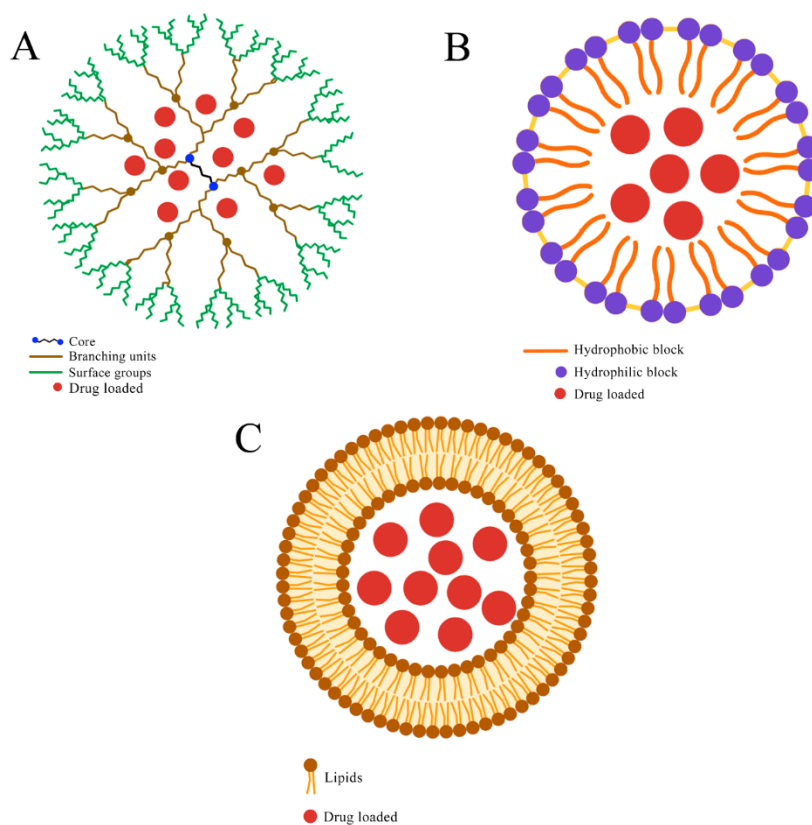


**Figure 3.** Different supports for drug delivery based on biomaterials. A, dendrimers; B, micelles/polymeric nanoparticles; C, liposomes.



Dendrimers are a type of three-dimensional macromolecule of arborescent construction that is part of polymers, but their difference lies in the fact that the distribution of the molecules that make up linear polymers is probabilistic, whereas, in the case of dendrimers, they are composed of a precise chemical structure, where the chemical bonds between atoms can be accurately described. In recent years, they have aroused interest in nanotechnology applied to medicine, as they are characterised by a very well-defined structure, with low polydispersity and a multivalent exterior with the possibility of functionalisation for interaction with a multitude of chemical species. Thus, in the field of medicine, they are promising agents for transporting drugs and genetic material to constitute new therapeutic formulations aimed at improving the efficacy and safety of active molecules[22].

Micelles/polymeric nanoparticles are structures that form spontaneously by self-assembly of amphiphilic polymeric molecules (usually block copolymers) once the critical micellar concentration (CMC) is exceeded. The hydrophobic blocks associate to form an internal domain called the micellar core, which is capable of solubilising and hosting lipid-soluble drugs, while the hydrophilic blocks form a corona that is in direct contact with the external, usually aqueous, environment, physically stabilising the micelle. In addition, the encapsulation of the drug within the micelle prevents its interaction with the external environment, increasing its physicochemical stability. The corona also constitutes the interface between the drug reservoir and the medium. Therefore, depending on properties such as micro-viscosity, thickness and porosity and the drug/core interaction, the release of the encapsulated drug will be more or less rapid. CMC, aggregation number (number of polymer molecules per micelle), micellar size, core size and micelle morphology depend on block length and hydrophilicity-lipophilicity balance (HLB). The amphiphilic polymer molecule can be designed to tailor these properties to specific requirements [23].

A liposome is a spherical vesicle with a membrane composed of a phospholipid bilayer, consisting of water-soluble and fat-soluble parts. Liposomes are characterised by advanced technology for delivering active molecules to the site of action, and several formulations are currently in clinical use. Research on liposome technology has progressed from conventional vesicles to "second generation liposomes" [24], where long-lasting liposomes are obtained by modulating the lipid composition, size and charge of the vesicle. Surface-modified liposomes have also been developed using various molecules, such as glycolipids. Medical research has supported the use of liposomes for the delivery of some drugs or even in novel applications such as imaging diagnosis disease [25].

### **2.1 Active pharmaceutical ingredient**

An Active Pharmaceutical Ingredient (API) is the chemical substance contained in a pharmaceutical, which is responsible for its therapeutic effect. Some pharmaceuticals contain more than one active ingredient (combination product). The terms drug, medicine and pharmaceutical product are commonly used interchangeably.

Drugs commonly interact with proteins in the body to affect physiological function [26]. This is the general idea behind all medicine. Once these chemicals are absorbed into the systemic circulation they bind with certain proteins and this changes the functioning of the cell slightly. For example, anticancer drugs bind to proteins on the surface of cancer cells and this stimulates the cells to die. In this case cell death is the physiological action of the drug. No drugs are specific to interacting with just one type of cell or one type of protein and this is what causes side effects. Again, using an anticancer drug as an example, the medication works by binding to very rapidly dividing cells, such as cancer cells, however, hair cells are also rapidly dividing and that is why one of the side effects

of anticancer drugs is hair loss. For most drugs, the amount of chemical needed to cause an effect is very small, often as small as 5 mg/L in blood [27] and this is a too low amount to package and handle, these ingredients are very expensive and give out little amounts like that will cause most of the drug to be lost and wasted. Therefore, most of the drugs that we take are also comprised of inactive ingredients that work to fill out the drug.

### **2.1.1 Pharmacodynamics**

Pharmacodynamics is responsible for studying how the body interacts with administered substances for the entire duration of exposure and it involves receptor binding, post-receptor effects, and chemical interactions. Our bodies are largely controlled by proteins that exist in many different forms in the body and have many different functions. Each protein has a specific function and is quite specific to the cell type that it acts on. For example, there are specific types of proteins called receptors that are embedded on the cell surfaces and there are different receptors for different types of cells, for example, a liver cell will have different receptors than a cardiac cell. The receptor binds to other proteins and chemicals on the outside of the cell and this, in turn, creates a change in the functioning of the cell. Proteins also act as drug targets. In order for a drug to exert an effect it needs to be bound to a protein then, it can have one of two main influences on the cell. It can produce a change in response or it can stop a normal response of the cell. Once the drug is bound to a protein it exerts a therapeutic effect on the body, this is the pharmacodynamics of a drug, being more accurate, it could be defined as, the study of what pharmaceutical products do to body systems once they are administered. The pharmacodynamics of a product will explain what effect they have on the body and accordingly how they work to achieve the desired therapeutic response. There is an

enormous list of different drugs and their actions in the body, some of the major treatment areas are, cancer, contraception, pain, respiratory, obesity and infection [26].

### **2.1.2 Pharmacokinetics**

Pharmacokinetics is closely related to, but distinctly different from pharmacodynamics, as, in this case, determines the onset, duration, and intensity of a drug's effect. The main stages include the absorption of the drug into the blood and across cell membranes to enter the cells; the distribution of the drug throughout the body; the metabolism or breakdown of the drug; and the excretion of the drug from the body.

Each drug will have a unique bioavailability, in other words, the amount of drug available to have an effect on the biological system. A drug's bioavailability is determined by its pharmacokinetics, for example, some drugs are poorly absorbed as they do not cross cell membranes as quickly or as effectively as others and so less of the drug will pass into the systemic circulation where it needs to be in order to have an effect. The proportion of the drug that does pass into the circulation is called the drug-plasma concentration. When a drug is absorbed into the circulation, the plasma concentration will increase until it reaches a peak and then as the drug is metabolised this plasma concentration will decline until the entire drug has been metabolised and then excreted from the body. Depending on the characteristics of the drug some will reach the peak plasma concentration quicker than others or be metabolised faster and so on.

Each drug has a range of dosages that can effectively treat a condition while still remaining safe. That is, the range between the lowest dose that has a positive effect, and the highest dose before the negative effects outweigh the positive effects. This is known as the therapeutic window. This can vary substantially between different types of drugs. For example, one drug could be safe and efficacious anywhere between 5mg to 20mg of

whereas another could have a therapeutic window between 15mg and 20mg. Hence, it is necessary to provide alternative delivery strategies for certain drugs that (i) have a broad therapeutic window, (ii) require low daily dose or (iii) are going to be used for long-term treatment of disease (Figure 4).

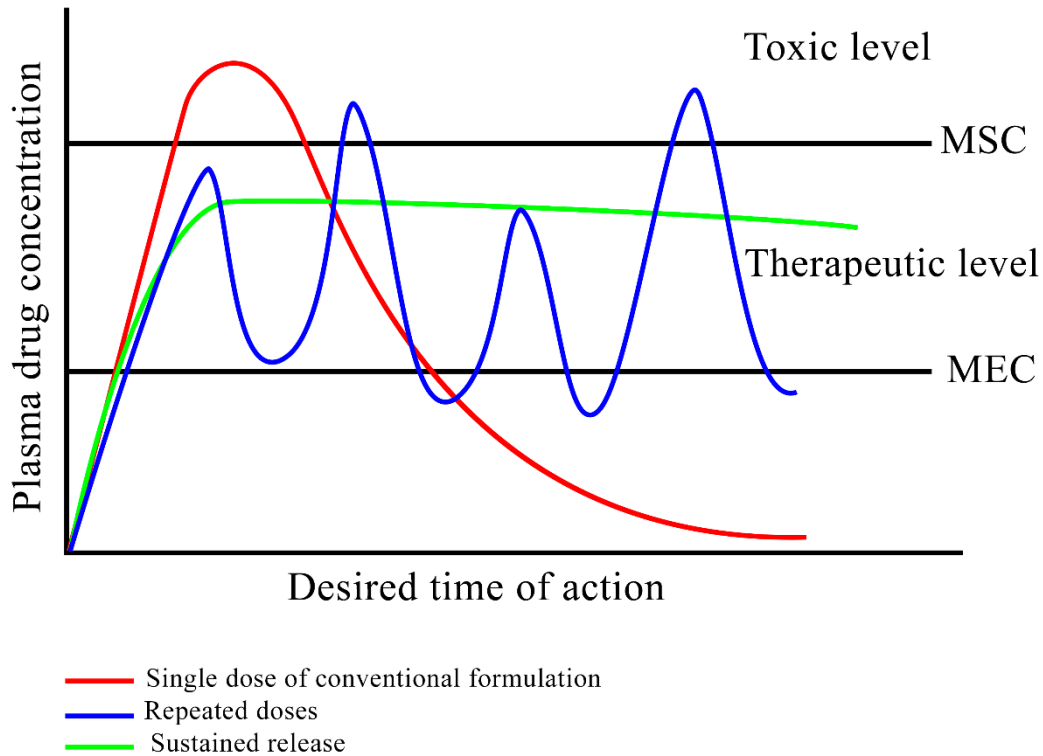


**Figure 4.** A hypothetical plasma concentration-time profile from conventional multiple dosing and single doses of sustained and controlled delivery formulations. Red, single dose of conventional formulation. Blue, repeated doses. Green, sustained release. MSC, maximum safe concentration. MEC, minimum effective concentration.

### 2.1.2.1 Mathematical models to describe drug release.

Drug release is an important property of a therapeutic system, which is a prerequisite for the absorption of the therapeutic agent and contributes to the rate and degree of active availability to the body. Therefore, controlled release dosage forms allow pharmacists and engineers to work together to design controlled release drug delivery systems in order to provide release profiles to understand the exact mass transport mechanisms involved in drug release and to quantitatively predict the resulting drug release kinetics.

Mathematical models are an important tool for the design of pharmaceutical formulations, the evaluation of in vitro and in vivo drug release processes and, in general, the optimal design of new systems. Thus, mathematical models should be able to transform the release curve as a function of some other parameter related to the dosage form and therefore predict the release of the encapsulated molecules as a function of time.

### **2.1.2.1.1 Zero-order kinetics.**

This mathematical model is used for drug releases where the active agent is rapidly absorbed and eliminated and can lead to periods of under-or over-exposure. When an active agent is administered from rapid release dosage forms, and the drug remains within the so-called therapeutic range for a short time and therefore frequent repetitive dosing is necessary in order to maintain the effective drug concentration. Zero-order models can be found in systems where the release of an active agent is only a function of time and the process takes place at a constant rate independent of the concentration of the active agent (e.g., transdermal slow-release matrix, coated, and osmotic systems) [28].

$$W_0 - W_i = k_0 \cdot t \text{ (Eq. 1)}$$

Where  $W_0$  is the initial mass of the active agent;  $W_i$  is the remaining mass in the dosage form, on-time  $t$  and  $K$  is a constant of the apparent velocity of dissolution.

### **2.1.2.1.2 First-order kinetics.**

This model has been used to describe the absorption and/or elimination of therapeutic agents. However, it is difficult to define first-order kinetics using a basic theory. In this sense, first-order release kinetics states that the change in concentration with respect to the change in time depends only on the concentration. There are a variety of therapeutic

systems that exhibit this type of first-order release. For soluble active agents incorporated in a porous matrix, the amount of drug released is proportional to the amount of drug remaining in the matrix. Therefore, the amount of active agents released tends to decrease as a function of time [29].

$$\log Q_1 = \log Q_0 + \frac{k_1 t}{2.303} \quad (\text{Eq. 2})$$

the equation corresponds to a linear function, and the graph of the nepierian or decimal logarithm of the mass release of the drug will result in a straight line, with a coefficient  $\alpha = K_1/2.303$  and a linear coefficient equal to  $\log Q_0$ . where  $Q_1$  is the amount of active agent released on time  $t$ ,  $Q_0$  is the initial amount of drug dissolved, and  $K_1$  is the first-order constant.

#### **2.1.2.1.3 Higuchi model.**

A mathematical model to describe the drug dissolution from matrix systems was not developed until the 1960s. In 1961, Higuchi published probably the most famous and widely used mathematical equation to describe the rate of drug release from matrix systems. The release of drugs from flat systems (creams) containing drugs in suspension was the subject of research [30–32].

$$f_i = Q = K_H \sqrt{t} \quad (\text{Eq. 3})$$

where  $K_H$  is the release constant of Higuchi.

There are assumptions that need to be followed with the use of the Higuchi model:

- The matrix contains an initial drug concentration much higher than the solubility of the drug.
- The diffusion is unidirectional because the edge effects are negligible.
- The thickness of the dosage form is much larger than the size of the drug molecules.
- The swelling or dissolution of the matrix is negligible.
- The diffusivity of the drug is constant.
- The perfect sink conditions are attained in the release environment.

### 2.1.2.1.4 Korsmeyer-Peppas model.

An approach that is also frequently used for drug release analysis is the equation proposed by Korsmeyer in 1983 and Peppas in 1985. This equation arises from the attempt to explain drug release mechanisms where erosion or dissolution of the matrix is present and is no further than a generalised version of the Higuchi equation [33].

$$\frac{M_t}{M_\infty} = kt^n \text{ (Eq. 4)}$$

$M_\infty$  is the amount of drug at the equilibrium state (sometimes very close to the amount of drug contained in the dosage form at the beginning of the release process),  $M_t$  is the amount of drug released over time  $t$ ,  $k$  is the constant of incorporation of structural modifications and geometrical characteristics of the system (also considered the release velocity constant), and  $n$  is the exponent of release (related to the drug release mechanism) in the function of time  $t$ .



**2.1.2.1.5 Lindner-Lippold model.**

To describe the drug release process, Lindner and Lippold in 1995 modified the Higuchi model equation by adding a term ( $b$ ) to describe the burst effect, in other words, the release of the drug on the surface of the release system, which is released into the medium immediately after contact with it [34].

$$\frac{M_t}{M_\infty} = kt^n + b \quad (\text{Eq. 5})$$

where  $b$  is the burst effect.

Depending on the value of  $n$  that better adjusts to the release profile of an active agent in a matrix system, it is possible to establish a classification, according to the type of observed behaviour:

- Fickian model (Case I)
- Non-Fickian models (Case II, Anomalous Case and Super Case II)

**2.1.2.1.6 Ritger-Peppas model.**

Ritger and Peppas proposed a semi-empirical expression to study the release kinetics of active ingredients from planar systems in which coupling of the Fickian and Case II mechanisms takes place [35].

$$\frac{M_t}{M_\infty} = k_1t^{1/2} + k_2t \quad (\text{Eq. 6})$$

Where  $k_1$  is the constant related to the contribution of the Fick-type mechanism and  $k_2$  is the constant of the contribution of the relaxation mechanism of the polymer chains.

### 2.1.2.1.7 Peppas-Sahlin model.

Peppas and Sahlin modified the equation proposed by Ritger and Peppas in order to generalise it and determine the contribution of the Fickian diffusion process as well as the contribution of the relaxation process of the polymer chains. As a result, they proposed a biexponential equation, which is independent of the geometry of the release system [36].

$$\frac{M_t}{M_\infty} = k_1 t^m + k_2 t^{2m} \quad (\text{Eq. 7})$$

Where  $k_1$  is the constant related to the contribution of the Fick-type mechanism and  $k_2$  is the constant of the contribution of the relaxation mechanism of the polymer chains. The coefficient  $m$  is the purely Fickian diffusion exponent for a system of any geometrical shape that exhibits controlled release. The coefficient  $m$  is related to the coefficient  $n$  of the power law, which was given for any shape, including films, cylinders and spheres.

### 2.1.3 Hydrophobic APIs

The interest in developing new substances without compromising safety and efficacy is a real challenge in biomedicine. However, despite the effort that the industry has made to develop new molecules and processes, it is estimated that about 40% of approved drugs and 90% of those under development are low water-soluble molecules [37]. In this sense, numerous drugs can be found on the marketplace, with low solubility, low permeability, rapid metabolism and elimination from the body and, in some cases, not very safe and tolerable [38].

The definition of "hydrophobic drugs" describes, in a very fleeting way, a heterogeneous group of substances that are soluble, although not in a categorical way, in organic solvents and present a very poor solubility in water, based on the terms defined as slightly soluble

(1-10 mg/mL) very slightly soluble (0.1-1 mg/mL) and practically insoluble (<0.1 mg/mL).

The Biopharmaceutics Classification System (BCS) is the most promising scientific framework for classifying drug agents as it has been endorsed by regulatory organizations and agencies [39]. According to BCS, active pharmaceutical ingredients (APIs) can be classified as follows (Figure 5):

**Class I:** High solubility and high permeability

**Class II:** Low solubility and high permeability

**Class III:** High solubility and low permeability

**Class IV:** Low solubility and low permeability.

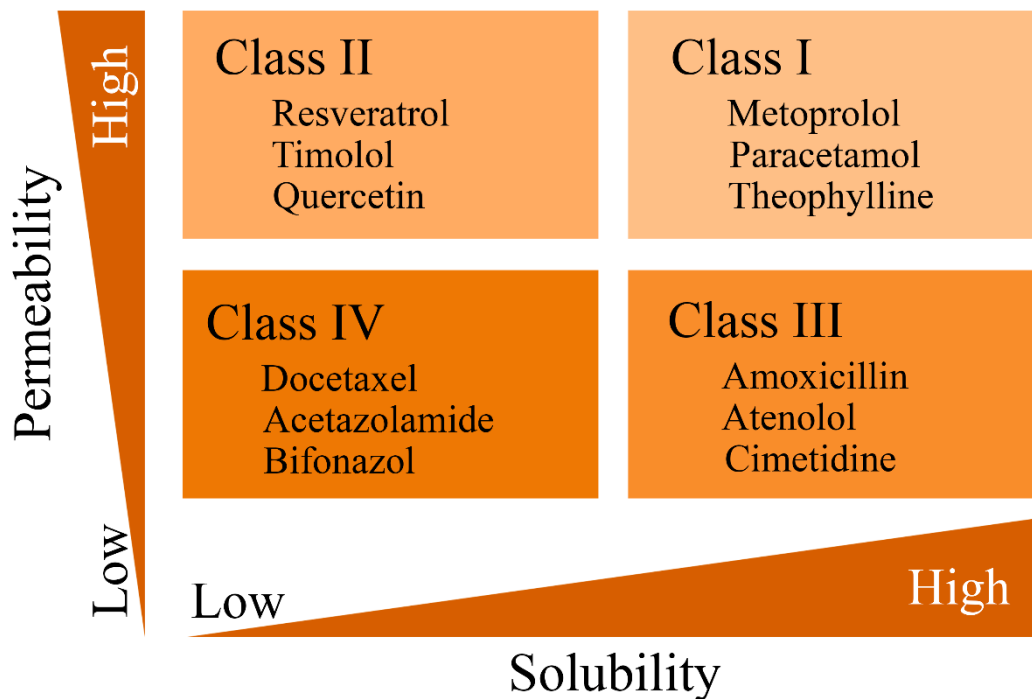


**Figure 5.** Illustration of how the Biopharmaceutics Classification System (BCS) may be used to distinguish different compounds with respect to permeability and solubility and examples of a few drugs in each class.

In recent years, the pharmaceutical industry has been working on the development of new formulations to improve the release of class II drugs by complexing, micronizing or modifying crystals. These techniques are focused on increasing the solubility of the drugs, but these strategies are not valid for class IV drugs due to their low permeability. Therefore, the best solution to improve the bioavailability of class IV drugs would be to return to the optimization phase of the drug to achieve the physical-chemical balance needed. However, returning to the optimization phase is not a viable option, as it is a long and very costly process [40] (Figure 6). Therefore, the formulation of drugs from their initial phase is a key factor for their subsequent commercialisation. However, what should be done with those class IV drugs that are already on the market? A large number of alternative approaches have been developed over the last few decades to overcome this issue [41] that involves, pH modification and salt form, co-solvency and surfactant solubilization, amorphous forms, solid dispersions and cocrystals, polymeric micelles or size reduction of the solid drug (micronization).

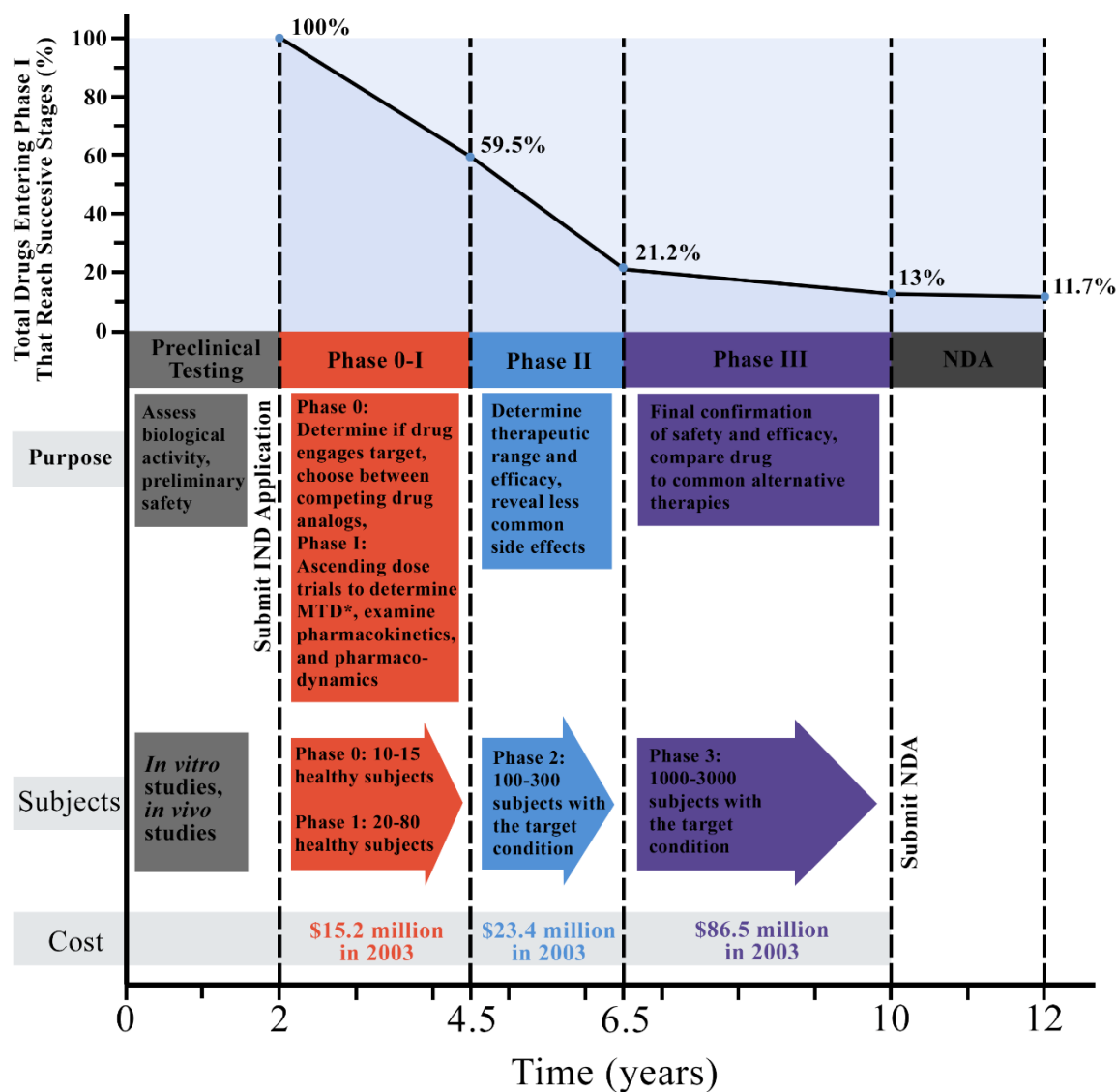
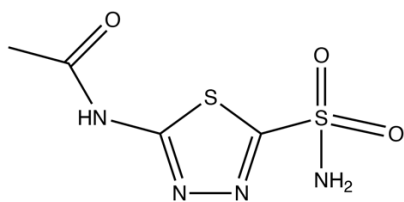
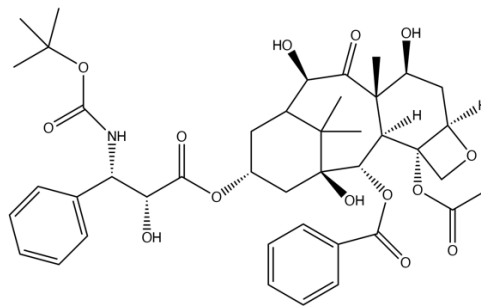


**Figure 6.** Time, cost and success stages in drug development. Maximum Tolerated Dose (MTD), New Drug Application (NDA). Figure reproduced from [40].

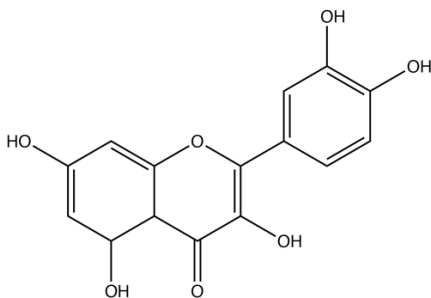
Figure 7 shows the drugs used in this thesis, all of them with low solubility in aqueous media. Docetaxel and acetazolamide are already used in cancer and glaucoma treatments, respectively, and two new proposals such as quercetin and resveratrol for the treatment of dry eye disease.



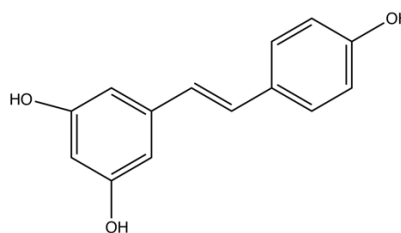
Acetazolamide



Docetaxel



Quercetin



Resveratrol

**Figure 7.** Chemical structure of the drugs employed in this Thesis.

### 2.1.3.1 Acetazolamide

In the last 40 years, acetazolamide has been used for the treatment of glaucoma. This disease is considered the second leading cause of blindness in the world after cataracts, one of the main causes of irreversible blindness, and is expected to affect 111.8 million patients in 2040 [42]. Glaucoma generally appears when fluid accumulates in the front of the eye causing increased intraocular pressure (IOP) through an imbalance between the production and drainage of aqueous humour which results in optic nerve damage. The main strategy to treat glaucoma is the administration of drugs aiming to decrease IOP. These drugs limit aqueous humour production in the ciliary body and/or enhance aqueous outflow through the trabecular meshwork or the uveoscleral pathway.

The drugs used in the long-term management of glaucoma include  $\beta$ -adrenergic blockers, miotics,  $\beta$ -adrenergic agonists, carbonic anhydrase inhibitors (CAIs), prostaglandin analogues and hyperosmotic. Among them, acetazolamide (Figure 7) has been used in the management of glaucoma for more than 40 years [43]. This sulfonamide derivative CAI is capable of acting as a powerful enzymatic inhibitor of the carbonic anhydrase, whose task is to catalyse the reversible reaction of hydration into carbonic acid, therefore, inhibiting the production of aqueous humour and thereby reducing the IOP. According to BCS, acetazolamide is a class IV drug with low solubility (0.7 mg/mL) and low permeability [44] ( $4.11 \cdot 10^{-6}$  cm/s) so, unfortunately, its topical administration in a simple solution is not effective.

Oral acetazolamide lowers IOP by about 30% depending on the administered dose [43]. In the treatment of open-angle glaucoma, one to four daily doses of 250 mg should be administered, depending on the symptoms and IOP. Secondary glaucoma and preoperative treatment of acute closed-angle glaucoma, between 250 to 1000 mg/day divided into several doses (250 mg every four hours) should be administered. Hence, acetazolamide is a drug which, in order to achieve the desired effect, requires the administration of high quantities of the active agent to the patient, which causes undesired side effects, as for example, lack of appetite and weight loss, diarrhoea, nausea, vomiting, allergic skin reactions, kidney damage and drowsiness among others [45].

### 2.1.3.2 Docetaxel

Currently, cancer represents the second most important cause of mortality in Europe with more than 3.7 million new cases and 1.9 million deaths each year [46] where breast and prostate cancer represents the major causes of death [47][48]. Docetaxel (DTX) (Figure 7) is the first-line drug for cancer treatment and is considered one of the most potent anticancer drugs in the clinical setting [49]. It is a well-established anti-mitotic chemotherapeutic active agent, member of the taxane group, that promotes tubulin assembly, stabilizes microtubules and inhibits their depolymerisation, thereby inducing cell apoptosis [50]. However, BCS classifies DTX as a class IV drug as the clinical application of docetaxel is limited by the poor aqueous solubility [51] (0.013 mg/mL), high toxicity and low bioavailability. The currently approved formulation contains 40 mg/mL of docetaxel and 26 mg of polysorbate 80 per mg of DTX and requires further dilution with 13% ethanol before addition to the intravenous infusion solution [52]. Serious dose-limiting toxicities and unpredictable adverse reactions due to either the drug itself or the solvent system have been reported in patients, such as hypersensitivity reactions [53] or neurotoxicity [54], requiring the oral administration of corticosteroids and antihistamines before infusion [55]. The occurrence of hypersensitivity reactions has, in part, been attributed to intrinsic toxic effects of polysorbate 80, more specifically to the oxidation products and oleic acid present in polysorbate 80, which are known to cause histamine release [56][57]. Furthermore, polysorbate 80 has been shown to increase plasma viscosity and produce changes in erythrocyte morphology, effects which have been suggested to contribute to mechanisms related to docetaxel-mediated cardiovascular side effects [58]. Hence, in this sense, considering the side effects associated with the current formulation of DTX, research has focused on avoiding the use of polysorbate 80, thus resulting in less toxic and better-tolerated polysorbate 80 free formulations, or



reducing the use of solvents, or developing advanced formulations which provide selective tumour delivery, thereby, increasing efficacy and selectivity while decreasing side effects related to nonspecific body distribution.

### **2.1.3.3 Resveratrol and Quercetin**

Dry eye is a chronic disease that affects the surface of the eye and causes annoyance, visual problems and, in some cases, damage to the cornea and conjunctiva affecting between 8-14% of the population worldwide [59]. However, the entire mechanism, both cellular and molecular, that causes dry eye disease (DED) is not completely defined [60]. Although recent research has been able to relate cellular apoptosis [61] in the conjunctiva and decreased tear production in the eye to increased levels of cytokines/chemokines [62] that are pro-inflammatory in the eye.

Anti-inflammatory drugs are commonly used in the treatment of DED and topical corticosteroids have been found to improve symptoms of DED, but their use is restricted because of the long-term side effects [63]. Therefore, the use of natural phytochemicals such as polyphenols [64] (flavonoids or stilbenes) with antioxidant and anti-inflammatory properties is an interesting alternative in the prevention and/or treatment of this type of eye disorder [65]

Quercetin (Figure 7) is a phenolic compound of the flavonoid family found in a variety of foods that has several biological properties, such as anticancer and neuroprotective effects [66]. Quercetin has also been reported as a strong anti-inflammatory, inhibiting many kinases [67], as well as interfering with cytokine/chemokine production [68] and as an antioxidant substance [69] since it has the ability to diminish the formation of reactive oxygen species (ROS) through different mechanisms [70].

Resveratrol (Figure 7) is a stilbene belonging to the phenolic compounds produced naturally by several plants whose antioxidant and anti-inflammatory properties have been widely demonstrated [71], as well as, chemotherapeutic [72] and anti-ageing activity [73]. However, both substances show poor water solubility, 0.003 mg/mL in the case of quercetin [74] and 0.03 mg/mL for resveratrol [75]; although they are considered class II compounds [75][76] by BCS since they have high permeability [77][78]. Despite the solubility limitations of both compounds, their potential as antioxidants or anti-inflammatory agents has already been successfully *in vitro* testing, decreasing the inflammatory response of ocular surface in epithelial cells [65], which was corroborated *in vivo* using a well-characterized murine model of DED followed by an adoptive transfer model [79].

Nevertheless, despite the numerous examples that have already appeared in the literature a large number of design possibilities for the controlled administration of drugs are still to be explored. The ultimate goal should be the formation of a vehicle capable of detecting a chemical abnormality and releasing the drug in response to it, in order to correct the imbalance, thereby acting in a similar manner to the human body, which closely controls the release and distribution of its own endogenous biological agents.

## **2.2 Elastin like recombinamers (ELRs)**

Elastin has properties that make it unique in the framework of biomedicine, and in recent years various studies have focused on the development of the so-called elastin-like recombinamers (ELRs) [80][81], where the term "recombinant" was introduced to define both tailor-made oligomeric composition and the method for producing these materials using recombinant DNA technologies [82]. These recombinant biopolymers, the sequence of which is inspired by natural elastin and comprises repeats of the sequence

(VPGXG)<sub>n</sub> where X can be any amino acid except proline due to steric hindrance when the transition occurs, preserve the unique mechanical properties found in elastin, i.e. extraordinary elasticity, ability to self-assembly, and excellent resistance to stress [83]. Moreover, ELRs are a new class of biomaterials with extraordinary biocompatibility [84]. The application of ELRs in the field of biomedicine is increasing [83][85] due to the significant advantages that they present, especially as genetic engineering allows total control of their architecture and design, as well as the ability to create monodisperse polymers with a complexity that is greater than in those synthesized chemically. Furthermore, their manufacture is easily scalable [86] and the natural ability of these polymers to self-assemble, and their stimuli responsiveness, allows the production of intelligent systems [87]. The smart nature of ELRs resides in their characteristic inverse temperature transition (ITT) [88] in which the folded and associated state is maintained by loss of the ordered water structures of hydrophobic hydration. Thus, below a temperature known as the transition temperature (T<sub>t</sub>) [89] (Figure 8) the polymer chains remain relatively extended and hydrated mainly by hydrophobic hydration and thus are soluble in cold aqueous solution. This hydration around its hydrophobic moiety is characterized by the existence of ordered, caged-like, clathrate water structures surrounding the moieties of the polymer and stabilized by hydrogen bonding among them. When the temperature increases, the polymer chain hydrophobically folds and aggregates to other polymer chains formation of intra- and inter-chain hydrophobic contacts. In this state, the polymer adopts a dynamic, regular, non-random structure, called β-spiral, formed by the concatenation of adjacent type II β-turns and stabilized by intra-spiral, inter-turn and inter-spiral hydrophobic contacts [90].

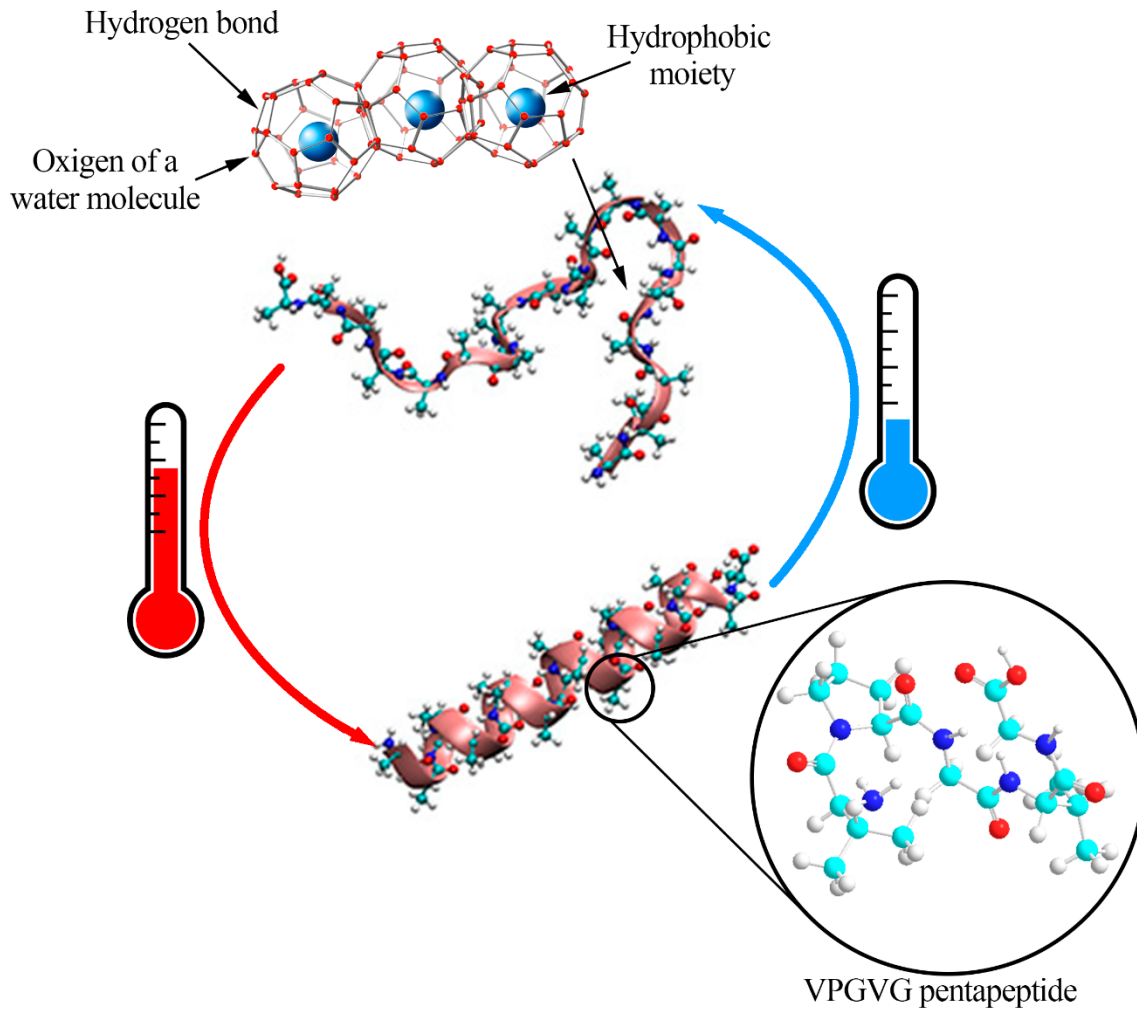


**Figure 8.** The thermal transition of Elastin-like Recombinamers from the extended state at low temperature to the folded state at high temperature. Clathrate structures surrounding the ELR chains and type II  $\beta$  turn in VPGVG pentapeptides are highlighted.

One of the most interesting features of ELRs is their capacity to show different properties depending on the guest amino acid they contain in the pentapeptides of the polymer chain. Thanks to genetic engineering techniques, it is possible to link different DNA sequences that encode the different pentapeptides that comprise the ELR structure obtaining, as a result, a biomaterial with advanced properties and functionalities in a simple way. Therefore, we can talk about ELRs designed for each specific application.

The physicochemical properties of the ELRs can be modulated by choosing the amino acid in the X position as guest residue in the pentapeptide (VPGXG)<sub>n</sub>, for example, the Tt is highly conditioned by the choice of guest amino acids (Figure 9), as well as, by the length of the polymer chain [91]; so that, when the polymer contains hydrophobic guest amino acids, such as phenylalanine (F), tyrosine (Y) or isoleucine (I), hydrophobicity and apolarity increase, resulting in a decrease [92] in Tt. As hydrophobicity decreases with the inclusion of aliphatic guest amino acids containing non-polar atoms such as Alanine (A), Valine (V) or Leucine (L), the transition temperature increases. However, when the guest amino acid is polar or has a charge, either positive or negative, such as Lysine (K) or Glutamic acid (E), the transition temperature increases considerably, most likely due to charge repulsion.

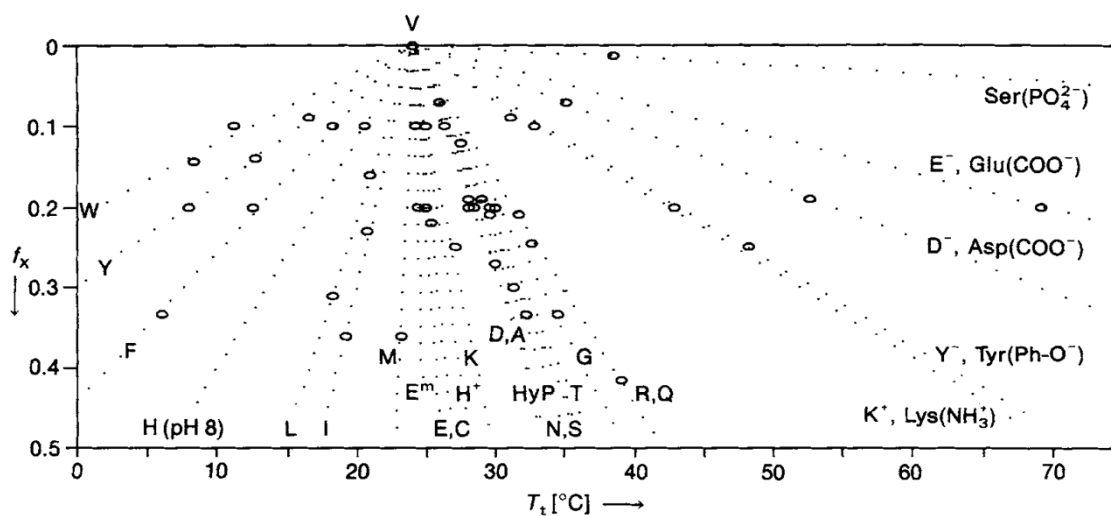


**Figure 9.** The effect of the amino acid composition at guest residue position on the Tt.  $f_x$  represents the mole fraction of pentamers containing the residue X. Reproduced from [88]

However, ELRs can show response to other stimuli, as has already been shown in the literature, such as pH [91], light [93], ELR concentration [94] or presence of other cosolutes [95] or cosolvents [96].

Within the multiple options that provide us with the inclusion of peptide sequences derived from other proteins, it is noteworthy those that have an interaction with the cells where the ELR has to be targeted. In this case, the sequence formed by the tripeptide, Arginine - Glycine - Aspartic (RGD) present in the human fibronectin protein, facilitates the cellular adhesion of ELRs in multiple types of cells, preferably in those that present an over-expression of integrin's type  $\alpha_5\beta_1$  y  $\alpha_v\beta_3$  [97]. Thus, the interaction between ELR-cells is enhanced, promoting their proliferation.

### 2.2.1 ELR biosynthesis

Thanks to the progress made in recent years in the field of biotechnology and genetic engineering, it has been possible to produce stable synthetic genes designed to express proteins of interest in heterogeneous systems, such as *Escherichia coli*. In addition to the biocompatibility [84] and non-immunogenicity of ELRs, the biosynthesis procedure ensures precise control of their amino acid sequence and molecular weight [98].

The iterative recursive directional ligation is an alternative method in which DNA segments with two different restriction sites flanking the insert are joined in sequential steps, with the length of the ligated segments growing geometrically in each step. This approach is suitable for the synthesis of repetitive polypeptides with a specific and predetermined chain length, as it seamlessly joins two monomeric inserts and, also, eliminates the restriction sites placed at either ends of the dimerized gene. However, the inclusion of new terminals in the restriction sites at the sequence of the gene itself can result in the formation of unwanted nucleotides that will be present at the final sequence. Therefore, when employing this method, type-IIS restriction endonucleases are used (Figure 10), as they are able to recognise specific base sequences in the DNA and then cut each strand at a specific location outside its recognition sequences, resulting in

seamless cloning of the genes and therefore avoiding the introduction of non-desired nucleotides [99]. After integration of the final expression vector, it is inserted into a host such as *Escherichia coli* that is capable of bioproducing the desired recombinant polymer.

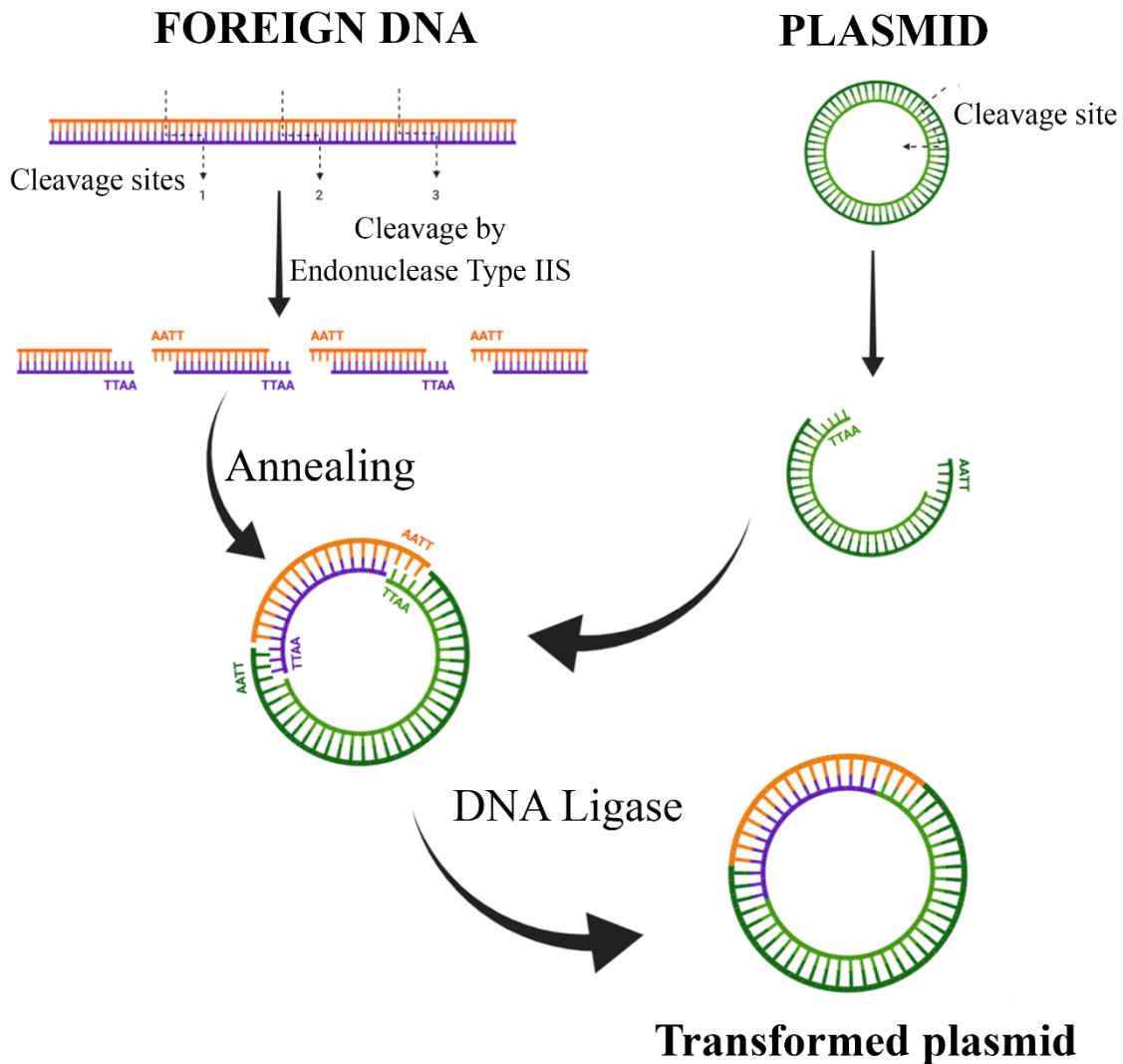


**Figure 10.** Schematic representation of DNA assembly using type IIS endonucleases. When a restriction enzyme cleaves a restriction site, the reaction creates highly reactive "sticky ends" on the broken DNA. By cutting open vector DNA itself with restriction enzymes used to cleave the target DNA, complementary "sticky ends" are created. This fosters the insertion of the target DNA into the vector. The fragment is "glued in" with DNA ligase, which creates the phosphodiester bonds necessary to complete the sugar-phosphate backbone of the new foreign DNA.

Once bioproduction is complete, a purification process is needed to isolate the ELR. The most straightforward process is to exploit the above-described ITT. For this purpose, different heating-cooling cycles (Inverse Transition Cycling) are implemented, followed by centrifugation and solubilisation, taking advantage of the ability of ELRs to aggregate reversibly above their transition temperature and allowing us to remove bacterial debris and endogenous material derived from the bioproduction [100]. After purification, endotoxins are removed by specific treatment to obtain a high purity final product suitable for *in vitro* and *in vivo* assays [101].

### **2.2.2 ELRs as controlled drug delivery carriers**

ELRs have become excellent candidates as they have been shown to allow controlled release of highly hydrophobic drugs that are difficult to dispense [102,103] by other routes, such as topical or intravenous ones [104–107]. Of the many different advanced ELR-based drug-delivery devices available, nanoparticulate delivery systems present great advantages since they provide a wide range of administration routes (oral, parenteral, transdermal, nasal, ocular, etc.) (Figure 11).



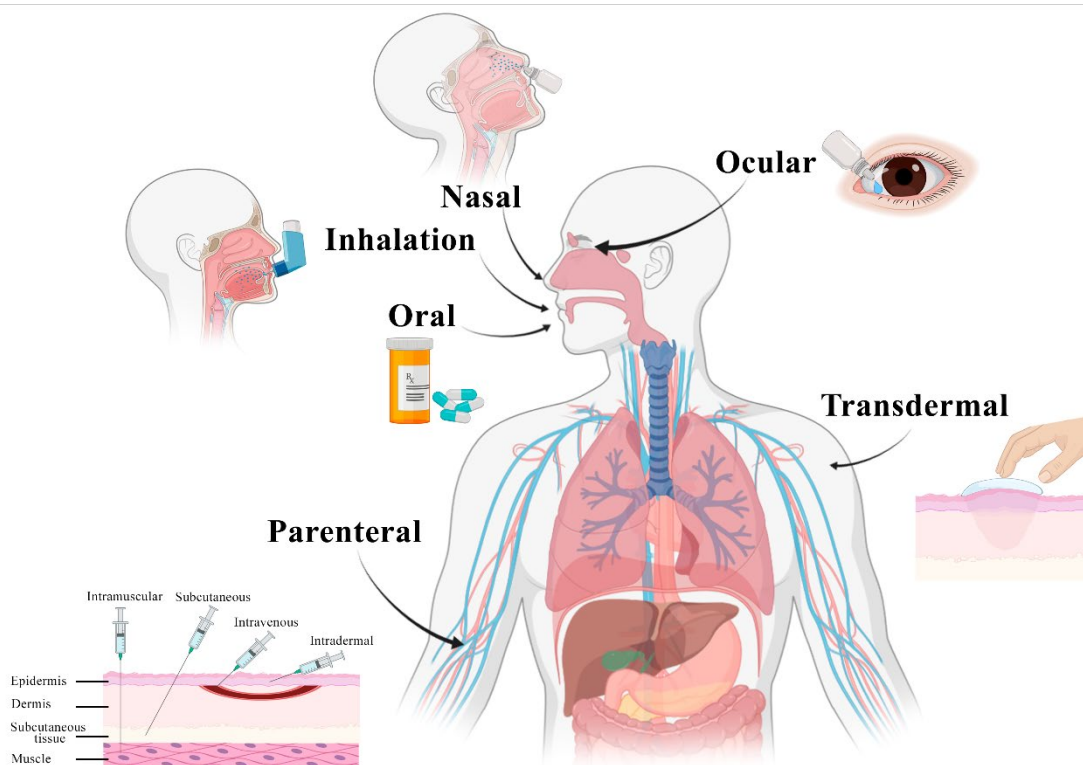


**Figure 11.** Schematic representation of the different administration routes: oral, parenteral, transdermal, nasal, ocular and inhalation.

### 2.2.3 Hydrogels as macroscopic devices for controlled release

New strategies that have been developed to improve the efficiency and effectiveness of macroscopic controlled-release drug systems have been growing in recent years.

Hydrogels are one of the devices that have demonstrated their versatility to release a drug in a local and sustained manner both for large and small molecules, achieving very ambitious objectives such as the development of injectable biodegradable hydrogels able to form the required depot *in situ* [108][109].

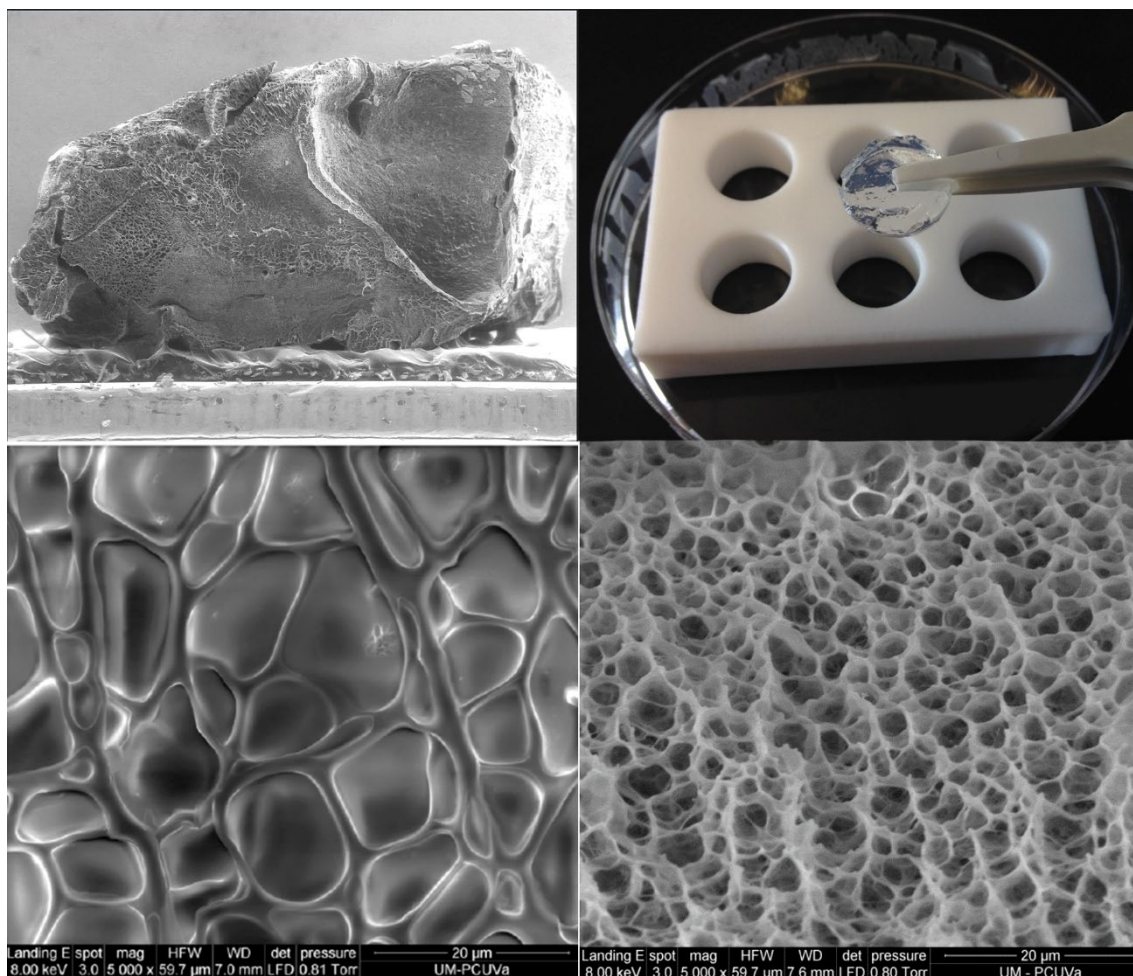


**Figure 12.** ELR hydrogel obtained by click chemistry at a concentration of 50 mg/mL. Hydrogel general SEM image (top left). Detailed SEM image of the hydrogel porous structure at 4°C (bottom left) and at 37°C (bottom right). Reproduced from [110] [111].

Hydrogel is defined as a three-dimensional network of flexible polymeric chains, consisting of elements interconnected in a certain elastomeric way and able to swell in water but do not dissolve (Figure 12). Recent progress in new hydrogels development involving smart devices achieves new features never seen before, such as controlled porosity and swelling behaviour, improved mechanical properties, degradability or stimuli-responsiveness to changes in the environment [112]. In this sense, promising new biomaterials such as ELRs are presently being investigated. Although this field is maturing and growing with a wealth of well-understood methods to improve or provide new functionalities to these devices [113]. Protein-based biopolymers can be synthesized by genetic engineering techniques, which makes it possible to modify their amino acidic

sequence in a simple way to modulate their properties to precisely fit the desired application [114]. Indeed, the porosity or even the pore size can be modified by adjusting certain parameters such as concentration, CO<sub>2</sub> pressure [115], or by using gas-foaming and salt-leaching techniques [116]. In addition, mechanical properties can also be modified by modulating the concentration or crosslinking conditions, [117][118]. As mentioned above, ELRs thermoresponsiveness in an aqueous medium is conditioned by the amino acid host, so by making small changes in the amino acid sequence, different responses to temperature and other different stimuli can be achieved, e.g. pH [119] or ion concentration [120]. One of the disadvantages of ELR-based hydrogels for drug encapsulation is that the hydrogel needs to be produced in an aqueous medium and the drug needs to be dissolved in the same medium, so when hydrophobic drugs are used, the amount of drug that can be loaded into these hydrogels is usually very low [102,103,121].

#### **2.2.4 ELR nanoparticles as devices for controlled drug release**

One of the disadvantages of hydrogel-based devices is that they can only treat the damage when it is well located and can be applied *in situ*, but when simultaneous treatment of different targets is required, the strategy has to be different. Therefore, the drug must be protected from natural barriers and targeted to the specific treatment areas while remaining in the circulatory system. This problem has attracted the attention of biomedicine in the past few years with the use of nanomaterials as smart drug delivery carriers. However, this issue seems to be more problematic than thought tentatively and it is still far from its optimal timing of application [122–124].

Broadly speaking, a nanocarrier is considered as a device that has sufficient drug load, good stability during transport, that reaches its target safely and is able to induce appropriate changes in the cell status [125]. Traditional biomaterials could be capable of

achieving the first two premises, but reaching an effective interaction with the cells in the biological functions they perform is more complicated.

Drugs are incorporated into the nanoparticle structure and when they are targeted to a specific site, the amount of drug is released due to the low drug content in the environment. In contrast, in the latter case, the targeted drugs are directly conjugated to the carrier nanostructure material to facilitate their delivery. In this approach, the timing of the release is critical, as the drug will not reach the target site and dissociate from the carrier very quickly, and conversely, its bioactivity and efficacy will decrease if it is not released from its nanocarrier system at the right time. Drug targeting is another important aspect using nanoparticles or nanoformulations as drug delivery systems and is classified into active and passive. In the case of active targeting, components such as antibodies and peptides are attached to the drug delivery system to tie them to the receptor structures expressed at the target site. In passive targeting, the complex carrier of the formulated drug circulates in the bloodstream and is delivered to the target site by affinity or binding mediated by properties such as pH, temperature, molecular size and shape. Thus, new pathways should be found to effectively coat an active agent to protect it and maintain an adequate drug load.

New approaches have been shown to cope with targeting problems more efficiently by using genetic engineering to custom-design smart biomaterials making them highly specific and effective in their application, and therefore, to develop new devices that can interact with the damaged cells. ELRs are capable of meeting these characteristics and, in addition, when the payload is exhausted, the biodegradation of these protein-based carriers follows the same natural routes as those found for structural proteins so they can be removed by the body itself in a natural way.

Thanks to the heterogeneity of the blocks that compose ELRs and their characteristic transition temperature, it is possible to produce self-assembled nanoparticles, since, for example, an ELR containing a hydrophobic block and another hydrophilic block, in an aqueous medium, will be capable of self-assembling to create a core and an external corona, forming stable micelles or vesicles [126]. Thus, the inner core will be responsible for the stability of the structure itself and the corona will be able to interact with the different actors that are involved in the environment surrounding the nanoparticle. This phenomenon occurs due to the attraction-repulsion forces that are generated between the two blocks and the physiological environment in which it is located, resulting in the formation of spherical particles. Therefore, taking advantage of the different design possibilities that ELRs provide, it is possible to model amphiphilic ELRs that allow us to encapsulate drugs, especially those that are not very soluble in aqueous media. This opens a new horizon for a controlled release system, which at first appears simple, but hides a great potential to deliver drugs and interact with the environment.

### **2.3 Encapsulation of active agents into biomaterials**

The encapsulation could be defined as a technique that allows storing within a shell, surrounded or coated with a continuous film, an active agent to produce particles in the range from nano to micro-scale, in order to protect the active compound from the environmental or physiological conditions and allowing the controlled release of the payload. The encapsulating agent can be from different nature, depending on the application for which the system is designed, e.g. inorganic materials such as thermo-/photo-/magnetic-responsive particles [127], derivatives from lipid-based materials [128], liposomes, polymeric materials (Figure 13) such as poly(lactic acid) (PLA), poly(lactic co-glycolic acid) (PLGA), poly(ethylene glycol) (PEG), poly(caprolactone) (PCL), or

novel protein polymer-type biomaterials [80]. However, the bioactivity and biocompatibility achieved by ELRs provide a great advantage over any of the other carriers most commonly used to encapsulate APIs.

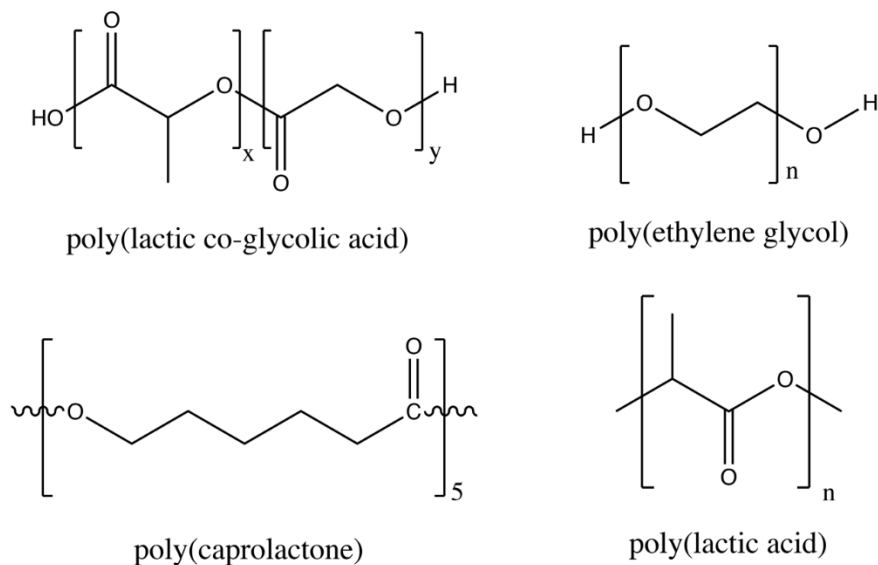


**Figure 13.** Chemical structures of some polymeric materials commonly used as encapsulating agents. Poly(lactic acid) (PLA), poly(lactic co-glycolic acid) (PLGA), poly(ethylene glycol) (PEG) and poly(caprolactone) (PCL).

The encapsulation can be classified according to particle size, where two distinguishes [129] can be made: microparticles, from 3 to 800  $\mu\text{m}$ , and nanoparticles, from 10 to 1000 nm. On this background, two approaches can be considered, top-down and bottom-up synthesis. In a top-down approach, materials produced are processed by tools to obtain smaller particle sizes. However, in the bottom-up approach materials are produced by self-assembly of molecules during the synthesis step. Thus, a large number of alternative methods have been developed, such as emulsification, emulsification-solvent evaporation, precipitation, coacervation, freeze-drying and spray drying [130–132]. While emulsification and emulsification-solvent evaporation are top-down techniques, precipitation, spray drying, and coacervation are bottom-up techniques. Unfortunately, these approaches result in problems related to long and complex processes and in the use

of toxic solvents, or low encapsulation efficiencies. A number of works have shown that this problem can be overcome using supercritical fluids; especially supercritical carbon dioxide (scCO<sub>2</sub>) which has been studied as a sustainable alternative solvent for polymer processing.

## **2.4 Processes with supercritical CO<sub>2</sub>**

Thanks to the moderate temperature and pressure at which the supercritical state is reached (7.38 MPa and 33.1°C), scCO<sub>2</sub> allows polymers to be processed at low temperatures, generally below 50°C, and under an inert atmosphere that is non-flammable, non-corrosive, non-toxic and non-carcinogenic. Furthermore, scCO<sub>2</sub> does not generate waste since it can be recycled and is an excellent green solvent due to its solvent strength [133–137]. The most common processes using scCO<sub>2</sub> to encapsulate APIs are the rapid expansion of supercritical solution (RESS), supercritical antisolvent (SAS), supercritical solvent impregnation (SSI), particles from gas saturated solutions (PGSS) and supercritical fluid extraction of emulsions (SFEEs).

### **2.4.1 Rapid expansion of supercritical solution (RESS)**

Rapid expansion of supercritical solution (RESS) is a process used in the food, cosmetic or pharmaceutical industry in which the solute is dissolved in scCO<sub>2</sub> and used to rapidly expand the supercritical solution through an expansion nozzle. Due to the rapid drop in pressure, a very high supersaturation occurs, resulting in the formation of small particles. This process can also be used to produce composites by dissolving both components in the supercritical solution, but the most important limitation is that both components of the mixture must be soluble in the supercritical solution. This problem has been attempted to be solved by adding certain amounts of organic solvents such as trifluoromethane or

chlorodifluoromethane [138]. Another solution proposed to eliminate the limitation of solubilities, consists of using a liquid antisolvent for one of the components acting as a cosolvent in the mixture and improving the solubility in the supercritical solution. This process variant is known as RESS-non-solvent and has been used to encapsulate drugs or proteins in different polymers such as PEG, PMMA or PLA [139]. Another problem when using this process is that, due to the fact that the precipitation is very fast, the control of the particle size, as well as its morphology or its load, is very complicated, since these parameters are very sensitive when the supersaturation of the mixture occurs, which are very related to the majority of the most important parameters that govern the process [137]. However, this problem can be solved by precipitating the carrier over previously precipitated particles of the active substance, so that both the load and the thickness of the particles can be effectively controlled by varying the feed composition of both compounds [140]. Another possibility that also improves product homogeneity is to perform the RESS precipitation over a fluidized bed of the active particles [141]. By precipitating the coating material in the upper section of the fluidized bed, the homogeneity of the coating is facilitated by the intense mixing of the particles inside the fluidized bed.

### **2.4.2 Supercritical solvent impregnation (SSI)**

This is a technique widely used for the impregnation of active compounds into a porous solid. To this end, the active substance should be soluble in  $\text{scCO}_2$ , so taking advantage of the fact that SCF is able to penetrate easily into the solid matrix thanks to the sorption and solubility of  $\text{scCO}_2$  in some polymers that are considerably high, promoting polymer swelling and changing polymeric mechanical properties by a plasticization effect [142][143][144], therefore it is possible to deposit the active compound into the matrix



of the solid. It is also feasible to enhance either the solubility of the drug or to improve the dispersion of the polymer by adding a co-solvent or a surfactant respectively. By adjusting parameters such as the depressurization step, the impregnation time or by changing the density of the co-solvent by modifying the pressure and temperature of the system, certain characteristics of the final product can be modified, such as the loading of the drug or its penetration into the solid matrix.

### **2.4.3 Particles from gas saturated solutions (PGSS) and PGSS-drying**

PGSS is a particle formation method that consists in saturating a solution that contains the solute of interest, which is achieved by mixing the solute of interest in scCO<sub>2</sub> in a vessel with static agitation. The saturated solution is then very quickly depressurised through a nozzle until it reaches atmospheric pressure, causing instantaneous vaporisation of the CO<sub>2</sub>, promoting the pulverisation of the solution. In addition, the sudden cooling due to the Joule-Thomson effect during the expansion of the CO<sub>2</sub> contributes to the formation of the particles. Both effects guarantee the formation of particles in the microscale range with a narrow size distribution. Different materials of relatively low melting temperatures, such as polymers, waxes or fats can be processed by this technique and are also suitable for incorporating active substances into these particles [145]. This process can also be extended to liquid mixtures containing active compounds by means of spray-drying, which allows satisfactory drying and micronisation of the aqueous solutions at operating temperatures significantly below the minimum temperatures required by conventional spray-drying, making it a particularly suitable technique for the processing of thermosensitive materials, or for materials with very low melting temperatures that would be liquid under the typical operating conditions of spray-drying.

#### **2.4.4 Supercritical fluid extraction of emulsion (SFEE)**

Supercritical fluid extraction of emulsion (SFEE) is a novel particle formation technique where it employs a supercritical fluid (SCF) such as supercritical carbon dioxide (scCO<sub>2</sub>) to rapidly extract the solvent or oil phase of an emulsion. The removal of the solvent leads to the precipitation of the solute resulting in an aqueous suspension containing nanoparticles. Particles can thereafter be recovered from the aqueous suspension by centrifugation and/or by evaporation at room temperature [146]. Particles generated via SFEE have an ordered size and morphology because the emulsification process provides a template and the fast kinetics of the scCO<sub>2</sub> extraction prevents particle agglomeration [147].

This technique was proposed as particularly suitable to produce nano-suspensions of pharmaceutical substances [148] that are slightly soluble or insoluble in water instead of dry particles, which requires additional steps like air drying, vacuum drying or freeze-drying to produce powder-like particles. An advantage of using emulsions for encapsulation is that if the active solution is dissolved in the disperse phase and the carrier in the continuous phase, the emulsion provides a template for the final morphology of the microcapsules. Recently the application of the SFEE technology was used to form particles from different substances, for example, the PLGA/piroxicam system was precipitated from an ethyl acetate in water emulsion for drug delivery purposes in a batch mode [149], and  $\beta$ -carotene was also processed forming a nanosuspension of the carotenoid in water from DCM in water emulsions or application for liquid and solid quercetin formulations [150].

### **2.4.5 Supercritical anti-solvent (SAS) precipitation**

Supercritical Anti-solvent (SAS) is a technique proposed for those substances that are not soluble in  $\text{scCO}_2$ . To successfully perform this technique, two conditions should necessarily be met, (a) the solvent and  $\text{scCO}_2$  must be soluble under the operating conditions, and (b) the solute to be precipitated should be soluble in the solvent and practically near zero soluble in the mixture solvent- $\text{scCO}_2$ . Therefore, the solvent-solute solution is sprayed through a nozzle into a reactor containing  $\text{scCO}_2$  under the right operating conditions, then an instant supersaturation of the micro-droplets leads to a decrease in the solubility of the solute in the mixture that triggers nucleation causing the instantaneous precipitation of the solute of interest. The particle size and morphology of the particles can be controlled by adjusting the process parameters, including  $\text{scCO}_2$  density, which depends on temperature and pressure, solution concentration and flow rate [151]. Another key factor that has an important influence on the SAS process, is the nozzle diameter and its geometry. Reverchon and coworkers investigated these phenomena, finding a correlation between the particle size with the nozzle diameter [152]. When the nozzle diameter was decreased the spray velocity increase enabling smaller droplets during the pulverization which results in a higher mass transfer due to higher surface area. In this sense, in recent years, some modifications have been proposed to the SAS process, such as incorporating an ultrasonic horn placed where the liquid solution is injected, so that, the ultrasonic field generated causes an improvement in the mass transfer, reducing possible agglomerations and promoting the formation of nanoparticles [153].

The Supercritical Antisolvent technique has been widely used for the precipitation and encapsulation of pharmaceutical compounds [154]. However, a fundamental role can be played by the use of Elastin Like Recombinamers specially designed for each application,

which is still practically unexplored with regard to the SAS technique. Thus, becoming a strategic process in the biomedical field, since it may produce composite systems without residues of solvents that are toxic for human health and produce particles in a controlled manner.

## 2.5 REFERENCES

- [1] T. Sahu, Y.K. Ratre, S. Chauhan, L.V.K.S. Bhaskar, M.P. Nair, H.K. Verma, Nanotechnology based drug delivery system: Current strategies and emerging therapeutic potential for medical science, *J. Drug Deliv. Sci. Technol.* 63 (2021) 102487. <https://doi.org/10.1016/j.jddst.2021.102487>.
- [2] J.K. Patra, G. Das, L.F. Fraceto, E.V.R. Campos, M.D.P. Rodriguez-Torres, L.S. Acosta-Torres, L.A. Diaz-Torres, R. Grillo, M.K. Swamy, S. Sharma, S. Habtemariam, H.S. Shin, Nano based drug delivery systems: Recent developments and future prospects 10 *Technology* 1007 *Nanotechnology* 03 *Chemical Sciences* 0306 *Physical Chemistry (incl. Structural)* 03 *Chemical Sciences* 0303 *Macromolecular and Materials Chemistry* 11 *Medical and Health Sciences* 1115 *Pharmacology and Pharmaceutical Sciences* 09 *Engineering* 0903 *Biomedical Engineering Prof Ueli Aebi, Prof Peter Gehr, J. Nanobiotechnology.* 16 (2018) 71. <https://doi.org/10.1186/s12951-018-0392-8>.
- [3] K. Savolainen, U. Backman, D. Brouwer, B. Fadeel, T. Fernandes, T. Kuhlbusch, R. Landsiedel, Nanosafety in Europe 2015-2025: Towards Safe and Sustainable Nanomaterials and Nanotechnology Innovations, 2013. [www.ttl.fi/en/publications/electronic\\_publications/pages/default.aspx](http://www.ttl.fi/en/publications/electronic_publications/pages/default.aspx) (accessed July 5, 2021).
- [4] EUROPEAN SCIENCE FOUNDATION Forward Look on Nanomedicine 2005, 2005.
- [5] Y. Barenholz, Doxil® - The first FDA-approved nano-drug: Lessons learned, *J. Control. Release.* 160 (2012) 117–134. <https://doi.org/10.1016/j.jconrel.2012.03.020>.
- [6] M.R. Green, G.M. Manikhas, S. Orlov, B. Afanasyev, A.M. Makhson, P. Bhar, M.J. Hawkins, Abraxane®, a novel Cremophor®-free, albumin-bound particle form of paclitaxel for the treatment of advanced non-small-cell lung cancer, *Ann. Oncol.* 17 (2006) 1263–1268. <https://doi.org/10.1093/annonc/mdl1104>.
- [7] FDA approves ado-trastuzumab emtansine for early breast cancer | FDA, (n.d.). <https://www.fda.gov/drugs/resources-information-approved-drugs/fda-approves-ado-trastuzumab-emtansine-early-breast-cancer> (accessed July 5, 2021).
- [8] P.C. Schmidt, *Encyclopedia of Pharmaceutical Technology*. Vol. 1 Third Edition, Informa Healthcare USA, Inc., 2007.
- [9] G.M. Barratt, Therapeutic applications of colloidal drug carriers, *Pharm. Sci. Technol. Today.* 3 (2000) 163–171. [https://doi.org/10.1016/S1461-5347\(00\)00255-8](https://doi.org/10.1016/S1461-5347(00)00255-8).
- [10] P. Couvreur, C. Dubernet, F. Puisieux, Controlled drug delivery with nanoparticles: Current possibilities and future trends, *Eur. J. Pharm. Biopharm.* 41 (1995) 2–13.

- 
- [11] M. Santos, S. Serrano-Dúcar, J. González-Valdivieso, R. Vallejo, A. Girotti, P. Cuadrado, F.J. Arias, Genetically Engineered Elastin-based Biomaterials for Biomedical Applications, *Curr. Med. Chem.* 26 (2018) 7117–7146. <https://doi.org/10.2174/0929867325666180508094637>.
- [12] E.M. Pridgen, F. Alexis, O.C. Farokhzad, Polymeric nanoparticle drug delivery technologies for oral delivery applications, *Expert Opin. Drug Deliv.* 12 (2015) 1459–1473. <https://doi.org/10.1517/17425247.2015.1018175>.
- [13] Y.H. Choi, H.K. Han, Nanomedicines: current status and future perspectives in aspect of drug delivery and pharmacokinetics, *J. Pharm. Investig.* 48 (2018) 43–60. <https://doi.org/10.1007/s40005-017-0370-4>.
- [14] A.C. Anselmo, S. Mitragotri, Nanoparticles in the clinic, *Bioeng. Transl. Med.* 1 (2016) 10–29. <https://doi.org/10.1002/btm2.10003>.
- [15] A.C. Anselmo, S. Mitragotri, Nanoparticles in the clinic: An update, *Bioeng. Transl. Med.* 4 (2019) 1–16. <https://doi.org/10.1002/btm2.10143>.
- [16] I. Ahmed Hamed Khalil, I. A. Arida, M. Ahmed, Introductory Chapter: Overview on Nanomedicine Market, in: *Curr. Futur. Asp. Nanomedicine*, IntechOpen, 2020. <https://doi.org/10.5772/intechopen.91890>.
- [17] ClinicalTrials.gov, (n.d.). <http://clinicaltrials.gov/> (accessed May 21, 2021).
- [18] R. Pita, F. Ehmann, M. Papaluca, Nanomedicines in the EU—Regulatory Overview, *AAPS J.* 18 (2016) 1576–1582. <https://doi.org/10.1208/S12248-016-9967-1>.
- [19] V. Wagner, A. Dullaart, A.K. Bock, A. Zweck, The emerging nanomedicine landscape, *Nat. Biotechnol.* 24 (2006) 1211–1217. <https://doi.org/10.1038/NBT1006-1211>.
- [20] W.H. De Jong, P.J.A. Borm, Drug delivery and nanoparticles: Applications and hazards, *Int. J. Nanomedicine.* 3 (2008) 133–149. <https://doi.org/10.2147/ijn.s596>.
- [21] M.C. Garnett, P. Kallinteri, Nanomedicines and nanotoxicology: Some physiological principles, *Occup. Med. (Chic. Ill).* 56 (2006) 307–311. <https://doi.org/10.1093/occmed/kql052>.
- [22] Y. Fan, L. Lin, F. Yin, Y. Zhu, M. Shen, H. Wang, L. Du, S. Mignani, J.P. Majoral, X. Shi, Phosphorus dendrimer-based copper(II) complexes enable ultrasound-enhanced tumor theranostics, *Nano Today.* 33 (2020) 100899. <https://doi.org/10.1016/j.nantod.2020.100899>.
- [23] P. Qiu, J. Yang, W. Jiang, L. Wang, Y. Fan, W. Luo, Interfacial engineering of core-shell structured mesoporous architectures from single-micelle building blocks, *Nano Today.* 35 (2020) 100940. <https://doi.org/10.1016/j.nantod.2020.100940>.
- [24] K. Sen, M. Mandal, Second generation liposomal cancer therapeutics: Transition from laboratory to clinic, *Int. J. Pharm.* 448 (2013) 28–43. <https://doi.org/10.1016/j.ijpharm.2013.03.006>.
- [25] J. Yang, S. He, Z. Hu, Z. Zhang, C. Cao, Z. Cheng, C. Fang, J. Tian, In vivo multifunctional fluorescence imaging using liposome-coated lanthanide nanoparticles in near-infrared-II/IIa/IIb windows, *Nano Today.* 38 (2021) 101120. <https://doi.org/10.1016/j.nantod.2021.101120>.
- [26] P.R. Shankar, D.K. Upadhyay, Book Review: *Pharmacology* by Rang HP, Dale MM, Ritter JM and Moore PK. Fifth Edition Churchill Livingstone, Edinburgh, 2005.
- [27] A.W. Jones, A. Holmgren, F.C. Kugelberg, Concentrations of scheduled prescription drugs in blood of impaired drivers: Considerations for interpreting the results, *Ther. Drug Monit.* 29 (2007) 248–260.
-

- <https://doi.org/10.1097/FTD.0b013e31803d3c04>.
- [28] K.A. Walters, *Dermatological and transdermal formulations*, CRC Press, 2002. <https://doi.org/10.1201/9780824743239>.
- [29] A.A. Noyes, W.R. Whitney, The rate of solution of solid substances in their own solutions, *J. Am. Chem. Soc.* 19 (1897) 930–934. <https://doi.org/10.1021/ja02086a003>.
- [30] T. Higuchi, Rate of release of medicaments from ointment bases containing drugs in suspension, *J. Pharm. Sci.* 50 (1961) 874–875. <https://doi.org/10.1002/jps.2600501018>.
- [31] W.I. Higuchi, Analysis of data on the medicament release from ointments, *J. Pharm. Sci.* 51 (1962) 802–804. <https://doi.org/10.1002/jps.2600510825>.
- [32] T. Higuchi, Mechanism of sustained-action medication. Theoretical analysis of rate of release of solid drugs dispersed in solid matrices, *J. Pharm. Sci.* 52 (1963) 1145–1149. <https://doi.org/10.1002/jps.2600521210>.
- [33] R.W. Korsmeyer, R. Gurny, E. Doelker, P. Buri, N.A. Peppas, Mechanisms of solute release from porous hydrophilic polymers, *Int. J. Pharm.* 15 (1983) 25–35. [https://doi.org/10.1016/0378-5173\(83\)90064-9](https://doi.org/10.1016/0378-5173(83)90064-9).
- [34] W.D. Lindner, B.C. Lippold, Drug Release From Hydrocolloid Embeddings with High or Low Susceptibility to Hydrodynamic Stress, *Pharm. Res. An Off. J. Am. Assoc. Pharm. Sci.* 12 (1995) 1781–1785. <https://doi.org/10.1023/A:1016238427313>.
- [35] P.L. Ritger, N.A. Peppas, A simple equation for description of solute release I. Fickian and non-fickian release from non-swellable devices in the form of slabs, spheres, cylinders or discs, *J. Control. Release.* 5 (1987) 23–36. [https://doi.org/10.1016/0168-3659\(87\)90034-4](https://doi.org/10.1016/0168-3659(87)90034-4).
- [36] N.A. Peppas, J.J. Sahlin, A simple equation for the description of solute release. III. Coupling of diffusion and relaxation, *Int. J. Pharm.* 57 (1989) 169–172. [https://doi.org/10.1016/0378-5173\(89\)90306-2](https://doi.org/10.1016/0378-5173(89)90306-2).
- [37] T. Loftsson, M.E. Brewster, Pharmaceutical applications of cyclodextrins: Basic science and product development, *J. Pharm. Pharmacol.* 62 (2010) 1607–1621. <https://doi.org/10.1111/j.2042-7158.2010.01030.x>.
- [38] J. Hodgson, ADMET - Turning chemicals into drugs. Rapidly resolving the pharmacokinetic and toxicological properties of drug candidates remains a key challenge for drug developers, *Nat. Biotechnol.* 19 (2001) 722–726. <https://doi.org/10.1038/90761>.
- [39] A. Charalabidis, M. Sfouni, C. Bergström, P. Macheras, The Biopharmaceutics Classification System (BCS) and the Biopharmaceutics Drug Disposition Classification System (BDDCS): Beyond guidelines, *Int. J. Pharm.* 566 (2019) 264–281. <https://doi.org/10.1016/j.ijpharm.2019.05.041>.
- [40] G.A. Van Norman, Drugs, Devices, and the FDA: Part 1: An Overview of Approval Processes for Drugs, *JACC Basic to Transl. Sci.* 1 (2016) 170–179. <https://doi.org/10.1016/j.jacbts.2016.03.002>.
- [41] R. Ghadi, N. Dand, BCS class IV drugs: Highly notorious candidates for formulation development, *J. Control. Release.* 248 (2017) 71–95. <https://doi.org/10.1016/j.jconrel.2017.01.014>.
- [42] Y.C. Tham, X. Li, T.Y. Wong, H.A. Quigley, T. Aung, C.Y. Cheng, Global prevalence of glaucoma and projections of glaucoma burden through 2040: A systematic review and meta-analysis, *Ophthalmology.* 121 (2014) 2081–2090. <https://doi.org/10.1016/j.ophtha.2014.05.013>.
- [43] I.P. Kaur, R. Smitha, D. Aggarwal, M. Kapil, Acetazolamide: Future perspective

- in topical glaucoma therapeutics, *Int. J. Pharm.* 248 (2002) 1–14. [https://doi.org/10.1016/S0378-5173\(02\)00438-6](https://doi.org/10.1016/S0378-5173(02)00438-6).
- [44] N.M. Morsi, M.I. Mohamed, H. Refai, H.M. El Sorogy, Nanoemulsion as a novel ophthalmic delivery system for acetazolamide, *Int. J. Pharm. Pharm. Sci.* 6 (2014) 227–236.
- [45] Ficha técnica EDEMOX 250 mg comprimidos, (n.d.). [https://cima.aemps.es/cima/dochtml/ft/24408/FT\\_24408.html#4-4-advertencias-y-precauciones-especiales-de-empleo](https://cima.aemps.es/cima/dochtml/ft/24408/FT_24408.html#4-4-advertencias-y-precauciones-especiales-de-empleo) (accessed June 18, 2021).
- [46] R.M. Heiberger, B. Holland, *Data and Statistics*, (2015) 13–27. [https://doi.org/10.1007/978-1-4939-2122-5\\_2](https://doi.org/10.1007/978-1-4939-2122-5_2).
- [47] L.A. Mucci, K.M. Wilson, E.L. Giovannucci, Epidemiology of prostate cancer, *Pathol. Epidemiol. Cancer.* 10 (2016) 107–125. [https://doi.org/10.1007/978-3-319-35153-7\\_9](https://doi.org/10.1007/978-3-319-35153-7_9).
- [48] F. Bray, J. Ferlay, I. Soerjomataram, R.L. Siegel, L.A. Torre, A. Jemal, Global cancer statistics 2018: GLOBOCAN estimates of incidence and mortality worldwide for 36 cancers in 185 countries, *CA. Cancer J. Clin.* 68 (2018) 394–424. <https://doi.org/10.3322/caac.21492>.
- [49] E. Zhang, R. Xing, S. Liu, P. Li, Current advances in development of new docetaxel formulations, *Expert Opin. Drug Deliv.* 16 (2019) 301–312. <https://doi.org/10.1080/17425247.2019.1583644>.
- [50] T. Ogura, Y. Tanaka, H. Tamaki, M. Harada, Docetaxel induces Bcl-2- and pro-apoptotic caspase-independent death of human prostate cancer DU145 cells, *Int. J. Oncol.* 48 (2016) 2330–2338. <https://doi.org/10.3892/ijo.2016.3482>.
- [51] Innovation.ca, Human Metabolome Database: Showing metabocard for Serylllysine, Show. Metabocard Terbinafine. (n.d.). <https://hmdb.ca/metabolites/HMDB0011111%0Ahttps://hmdb.ca/metabolites/HMDB0014995%0Ahttps://hmdb.ca/metabolites/HMDB0029044> (accessed May 21, 2021).
- [52] H. Zhang, J. Dou, Y. Zhai, A. Liu, G. Zhai, Advances in the formulations of non-injection administration of docetaxel, *J. Drug Target.* 22 (2014) 87–94. <https://doi.org/10.3109/1061186X.2013.839686>.
- [53] B. Pellegrino, D. Boggiani, C. Tommasi, D. Palli, A. Musolino, Nab-paclitaxel after docetaxel hypersensitivity reaction: case report and literature review, *Acta Biomed.* 88 (2017) 329–333. <https://doi.org/10.23750/abm.v88i3.6138>.
- [54] C.N. Frederiks, S.W. Lam, H.J. Guchelaar, E. Boven, Genetic polymorphisms and paclitaxel- or docetaxel-induced toxicities: A systematic review, *Cancer Treat. Rev.* 41 (2015) 935–950. <https://doi.org/10.1016/j.ctrv.2015.10.010>.
- [55] S. Mazzaferro, K. Bouchemal, R. Skanji, C. Gueutin, H. Chacun, G. Ponchel, Intestinal permeation enhancement of docetaxel encapsulated into methyl- $\beta$ -cyclodextrin/poly(isobutylcyanoacrylate) nanoparticles coated with thiolated chitosan, *J. Control. Release.* 162 (2012) 568–574. <https://doi.org/10.1016/j.jconrel.2012.08.005>.
- [56] W. Lorenz, A. Schmal, H. Schult, S. Lang, C. Ohmann, D. Weber, B. Kapp, L. Lüben, A. Doenicke, Histamine release and hypotensive reactions in dogs by solubilizing agents and fatty acids: Analysis of various components in cremophor El and development of a compound with reduced toxicity, *Agents Actions.* 12 (1982) 64–80. <https://doi.org/10.1007/BF01965109>.
- [57] M. Bergh, K. Magnusson, J.L.G. Nilsson, A.T. Karlberg, Contact allergenic activity of Tween® 80 before and after air exposure, *Contact Dermatitis.* 37 (1997) 9–18. <https://doi.org/10.1111/j.1600-0536.1997.tb00368.x>.

- [58] M. Mark, R. Walter, D.O. Meredith, W.H. Reinhart, Commercial taxane formulations induce stomatocytosis and increase blood viscosity, *Br. J. Pharmacol.* 134 (2001) 1207–1214. <https://doi.org/10.1038/sj.bjp.0704387>.
- [59] S.E. Moss, R. Klein, B.E.K. Klein, Prevalance of and risk factors for dry eye syndrome, *Arch. Ophthalmol.* 118 (2000) 1264–1268. <https://doi.org/10.1001/archoph.118.9.1264>.
- [60] S. Barabino, Y. Chen, S. Chauhan, R. Dana, Ocular surface immunity: Homeostatic mechanisms and their disruption in dry eye disease, *Prog. Retin. Eye Res.* 31 (2012) 271–285. <https://doi.org/10.1016/j.preteyeres.2012.02.003>.
- [61] R. Reinoso, M. Calonge, E. Castellanos, M. Martino, I. Fernández, M.E. Stern, A. Corell, Differential cell proliferation, apoptosis, and immune response in healthy and evaporative-type dry eye conjunctival epithelia, *Investig. Ophthalmol. Vis. Sci.* 52 (2011) 4819–4828. <https://doi.org/10.1167/iovs.10-6073>.
- [62] A. Enríquez-de-Salamanca, E. Castellanos, M.E. Stern, I. Fernández, E. Carreño, C. García-Vázquez, J.M. Herreras, M. Calonge, Tear cytokine and chemokine analysis and clinical correlations in evaporative-type dry eye disease, *Mol. Vis.* 16 (2010) 862–873.
- [63] H.M. Garrott, M.J. Walland, Glaucoma from topical corticosteroids to the eyelids [3], *Clin. Exp. Ophthalmol.* 32 (2004) 224–226. <https://doi.org/10.1111/j.1442-9071.2004.00787.x>.
- [64] R. González, I. Ballester, R. López-Posadas, M.D. Suárez, A. Zarzuelo, O. Martínez-Augustin, F. Sánchez de Medina, Effects of flavonoids and other polyphenols on inflammation, *Crit. Rev. Food Sci. Nutr.* 51 (2011) 331–362. <https://doi.org/10.1080/10408390903584094>.
- [65] A. Abengózar-Vela, M. Calonge, M.E. Stern, M.J. González-García, A. Enríquez-De-Salamanca, Quercetin and resveratrol decrease the inflammatory and oxidative responses in human ocular surface epithelial cells, *Investig. Ophthalmol. Vis. Sci.* 56 (2015) 2709–2719. <https://doi.org/10.1167/iovs.15-16595>.
- [66] J.M. Davis, E.A. Murphy, M.D. Carmichael, Effects of the dietary flavonoid quercetin upon performance and health, *Curr. Sports Med. Rep.* 8 (2009) 206–213. <https://doi.org/10.1249/JSR.0b013e3181ae8959>.
- [67] D.X. Hou, T. Kumamoto, Flavonoids as protein kinase inhibitors for cancer chemoprevention: Direct binding and molecular modeling, *Antioxidants Redox Signal.* 13 (2010) 691–719. <https://doi.org/10.1089/ars.2009.2816>.
- [68] F.T.M.C. Vicentini, T. He, Y. Shao, M.J.V. Fonseca, W.A. Verri, G.J. Fisher, Y. Xu, Quercetin inhibits UV irradiation-induced inflammatory cytokine production in primary human keratinocytes by suppressing NF- $\kappa$ B pathway, *J. Dermatol. Sci.* 61 (2011) 162–168. <https://doi.org/10.1016/j.jdermsci.2011.01.002>.
- [69] M.A. Read, Flavonoids: naturally occurring anti-inflammatory agents., *Am. J. Pathol.* 147 (1995) 235–237.
- [70] A. Gupta, K. Birhman, I. Raheja, S.K. Sharma, H.K. Kar, Quercetin: A wonder bioflavonoid with therapeutic potential in disease management, *Asian Pacific J. Trop. Dis.* 6 (2016) 248–252. [https://doi.org/10.1016/S2222-1808\(15\)61024-6](https://doi.org/10.1016/S2222-1808(15)61024-6).
- [71] J.M. Wu, T. chen Hsieh, Resveratrol: A cardioprotective substance, *Ann. N. Y. Acad. Sci.* 1215 (2011) 16–21. <https://doi.org/10.1111/j.1749-6632.2010.05854.x>.
- [72] J. Gusman, H. Malonne, G. Atassi, A reappraisal of the potential chemopreventive and chemotherapeutic properties of resveratrol, *Carcinogenesis.* 22 (2001) 1111–1117. <https://doi.org/10.1093/carcin/22.8.1111>.
- [73] C.A. De La Lastra, I. Villegas, Resveratrol as an anti-inflammatory and anti-aging agent: Mechanisms and clinical implications, *Mol. Nutr. Food Res.* 49 (2005) 405–



430. <https://doi.org/10.1002/mnfr.200500022>.
- [74] K. Srinivas, J.W. King, L.R. Howard, J.K. Monrad, Solubility and solution thermodynamic properties of quercetin and quercetin dihydrate in subcritical water, *J. Food Eng.* 100 (2010) 208–218. <https://doi.org/10.1016/J.JFOODENG.2010.04.001>.
- [75] A. Amri, J.C. Chaumeil, S. Sfar, C. Charrueau, Administration of resveratrol: What formulation solutions to bioavailability limitations?, *J. Control. Release.* 158 (2012) 182–193. <https://doi.org/10.1016/j.jconrel.2011.09.083>.
- [76] K. Madaan, V. Lather, D. Pandita, Evaluation of polyamidoamine dendrimers as potential carriers for quercetin, a versatile flavonoid, *Drug Deliv.* 23 (2016) 254–262. <https://doi.org/10.3109/10717544.2014.910564>.
- [77] A.R. Neves, S. Martins, M.A. Segundo, S. Reis, Nanoscale delivery of resveratrol towards enhancement of supplements and nutraceuticals, *Nutrients.* 8 (2016). <https://doi.org/10.3390/nu8030131>.
- [78] Y. Fang, W. Cao, M. Xia, S. Pan, X. Xu, Study of structure and permeability relationship of flavonoids in caco-2 cells, *Nutrients.* 9 (2017). <https://doi.org/10.3390/nu9121301>.
- [79] A. Abengózar-Vela, C.S. Schaumburg, M.E. Stern, M. Calonge, A. Enríquez-de-Salamanca, M.J. González-García, Topical Quercetin and Resveratrol Protect the Ocular Surface in Experimental Dry Eye Disease, *Ocul. Immunol. Inflamm.* 27 (2019) 1023–1032. <https://doi.org/10.1080/09273948.2018.1497664>.
- [80] J.C. Rodríguez-Cabello, I.G. De Torre, S. Acosta, S. Salinas, M. Herrero, Elastin-like proteins: Molecular design for self-assembling, in: *Self-Assembling Biomater. Mol. Des. Charact. Appl. Biol. Med.*, 2018: pp. 49–78. <https://doi.org/10.1016/B978-0-08-102015-9.00004-6>.
- [81] J.C. Rodríguez-Cabello, F.J. Arias, M.A. Rodrigo, A. Girotti, Elastin-like polypeptides in drug delivery, *Adv. Drug Deliv. Rev.* 97 (2016) 85–100. <https://doi.org/10.1016/j.addr.2015.12.007>.
- [82] J.C. Rodríguez-Cabello, L. Martín, M. Alonso, F.J. Arias, A.M. Testera, “Recombinamers” as advanced materials for the post-oil age, *Polymer (Guildf).* 50 (2009) 5159–5169. <https://doi.org/10.1016/j.polymer.2009.08.032>.
- [83] J.C. Rodríguez-Cabello, L. Martín, A. Girotti, C. García-Arévalo, F.J. Arias, M. Alonso, Emerging applications of multifunctional elastin-like recombinamers, *Nanomedicine.* 6 (2011) 111–122. <https://doi.org/10.2217/nmm.10.141>.
- [84] A. Ibáñez-Fonseca, T.L. Ramos, I. González de Torre, L.I. Sánchez-Abarca, S. Muntión, F.J. Arias, M.C. del Cañizo, M. Alonso, F. Sánchez-Guijo, J.C. Rodríguez-Cabello, Biocompatibility of two model elastin-like recombinamer-based hydrogels formed through physical or chemical cross-linking for various applications in tissue engineering and regenerative medicine, *J. Tissue Eng. Regen. Med.* 12 (2018) e1450–e1460. <https://doi.org/10.1002/term.2562>.
- [85] F. Arias, M. Santos, A. Fernández-Colino, G. Pinedo, A. Girotti, Recent Contributions of Elastin-Like Recombinamers to Biomedicine and Nanotechnology, *Curr. Top. Med. Chem.* 14 (2014) 819–836. <https://doi.org/10.2174/1568026614666140118223412>.
- [86] J.C. Rodríguez-Cabello, A. Girotti, A. Ribeiro, F.J. Arias, Synthesis of genetically engineered protein polymers (recombinamers) as an example of advanced self-assembled smart materials, *Methods Mol. Biol.* 811 (2012) 17–38. [https://doi.org/10.1007/978-1-61779-388-2\\_2](https://doi.org/10.1007/978-1-61779-388-2_2).
- [87] J.C. Rodríguez-Cabello, M. Pierna, A. Fernández-Colino, C. García-Arévalo, F.J. Arias, Recombinamers: Combining molecular complexity with diverse

- bioactivities for advanced biomedical and biotechnological applications, *Adv. Biochem. Eng. Biotechnol.* 125 (2011) 145–179. [https://doi.org/10.1007/10\\_2010\\_94](https://doi.org/10.1007/10_2010_94).
- [88] D.W. Urry, Molecular Machines: How Motion and Other Functions of Living Organisms Can Result from Reversible Chemical Changes, *Angew. Chemie Int. Ed. English.* 32 (1993) 819–841. <https://doi.org/10.1002/anie.199308191>.
- [89] P.L. San Biagio, F. Madonia, T.L. Trapane, D.W. Urry, The overlap of elastomeric polypeptide coils in solution required for single-phase initiation of elastogenesis, *Chem. Phys. Lett.* 145 (1988) 571–574. [https://doi.org/10.1016/0009-2614\(88\)87422-0](https://doi.org/10.1016/0009-2614(88)87422-0).
- [90] G. Pinedo-Martín, M. Santos, A.M. Testera, M. Alonso, J.C. Rodríguez-Cabello, The effect of NaCl on the self-assembly of elastin-like block co-recombinamers: Tuning the size of micelles and vesicles, *Polymer (Guildf).* 55 (2014) 5314–5321. <https://doi.org/10.1016/j.polymer.2014.08.053>.
- [91] A. Girotti, J. Reguera, F.J. Arias, M. Alonso, A.M. Testera, J.C. Rodríguez-Cabello, Influence of the molecular weight on the inverse temperature transition of a model genetically engineered elastin-like pH-responsive polymer, *Macromolecules.* 37 (2004) 3396–3400. <https://doi.org/10.1021/ma035603k>.
- [92] F. Aladini, C. Araman, C.F.W. Becker, Chemical synthesis and characterization of elastin-like polypeptides (ELPs) with variable guest residues, *J. Pept. Sci.* 22 (2016) 334–342. <https://doi.org/10.1002/psc.2871>.
- [93] M. Alonso, V. Reboto, L. Guiscardo, V. Maté, J.C. Rodríguez-Cabello, Novel photoresponsive p-phenylazobenzene derivative of an elastin-like polymer with enhanced control of azobenzene content and without pH sensitiveness, *Macromolecules.* 34 (2001) 8072–8077. <https://doi.org/10.1021/ma010455o>.
- [94] D.E. Meyer, A. Chilkoti, Quantification of the effects of chain length and concentration on the thermal behavior of elastin-like polypeptides, *Biomacromolecules.* 5 (2004) 846–851. <https://doi.org/10.1021/bm034215n>.
- [95] L.A. Ferreira, J.T. Cole, C. Reichardt, N.B. Holland, V.N. Uversky, B.Y. Zaslavsky, Solvent properties of water in aqueous solutions of elastin-like polypeptide, *Int. J. Mol. Sci.* 16 (2015) 13528–13547. <https://doi.org/10.3390/ijms160613528>.
- [96] F. Dehghani, N. Annabi, P. Valtchev, S.M. Mithieux, A.S. Weiss, S.G. Kazarian, F.H. Tay, Effect of dense gas CO<sub>2</sub> on the coacervation of elastin, *Biomacromolecules.* 9 (2008) 1100–1105. <https://doi.org/10.1021/bm700891b>.
- [97] M. Barczyk, S. Carracedo, D. Gullberg, Integrins, *Cell Tissue Res.* 339 (2010) 269–280. <https://doi.org/10.1007/s00441-009-0834-6>.
- [98] D.L. Nettles, A. Chilkoti, L.A. Setton, Applications of elastin-like polypeptides in tissue engineering, *Adv. Drug Deliv. Rev.* 62 (2010) 1479–1485. <https://doi.org/10.1016/j.addr.2010.04.002>.
- [99] S.M. Lippow, P.M. Aha, M.H. Parker, W.J. Blake, B.M. Baynes, D. Lipovšek, Creation of a type IIS restriction endonuclease with a long recognition sequence, *Nucleic Acids Res.* 37 (2009) 3061–3073. <https://doi.org/10.1093/nar/gkp182>.
- [100] D.E. Meyer, A. Chilkoti, Purification of recombinant proteins by fusion with thermally-responsive polypeptides, *Nat. Biotechnol.* 17 (1999) 1112–1115. <https://doi.org/10.1038/15100>.
- [101] R.E. Sallach, W. Cui, F. Balderrama, A.W. Martinez, J. Wen, C.A. Haller, J. V. Taylor, E.R. Wright, R.C. Long, E.L. Chaikof, Long-term biostability of self-assembling protein polymers in the absence of covalent crosslinking, *Biomaterials.* 31 (2010) 779–791. <https://doi.org/10.1016/j.biomaterials.2009.09.082>.

- [102] A. Fernández-Colino, J.M. Bermudez, F.J. Arias, D. Quinteros, E. Gonzo, Development of a mechanism and an accurate and simple mathematical model for the description of drug release: Application to a relevant example of acetazolamide-controlled release from a bio-inspired elastin-based hydrogel, *Mater. Sci. Eng. C.* 61 (2016) 286–292. <https://doi.org/10.1016/j.msec.2015.12.050>.
- [103] A. Fernández-Colino, D.A. Quinteros, D.A. Allemandi, A. Girotti, S.D. Palma, F.J. Arias, Self-Assembling Elastin-Like Hydrogels for Timolol Delivery: Development of an Ophthalmic Formulation Against Glaucoma, *Mol. Pharm.* 14 (2017) 4498–4508. <https://doi.org/10.1021/acs.molpharmaceut.7b00615>.
- [104] J.S. Ryu, D. Raucher, Anti-tumor efficacy of a therapeutic peptide based on thermo-responsive elastin-like polypeptide in combination with gemcitabine, *Cancer Lett.* 348 (2014) 177–184. <https://doi.org/10.1016/j.canlet.2014.03.021>.
- [105] W. Wang, J. Despanie, P. Shi, M.C. Edman, Y.A. Lin, H. Cui, M. Heur, M.E. Fini, S.F. Hamm-Alvarez, J.A. Mackay, Lacritin-mediated regeneration of the corneal epithelia by protein polymer nanoparticles, *J. Mater. Chem. B.* 2 (2014) 8131–8141. <https://doi.org/10.1039/c4tb00979g>.
- [106] J.F. Nawroth, J.R. McDaniel, A. Chilkoti, R. Jordan, R. Luxenhofer, Maleimide-Functionalized Poly(2-Oxazoline)s and Their Conjugation to Elastin-Like Polypeptides, *Macromol. Biosci.* 16 (2016) 322–333. <https://doi.org/10.1002/mabi.201500376>.
- [107] J. Hu, L. Xie, W. Zhao, M. Sun, X. Liu, W. Gao, Design of tumor-homing and pH-responsive polypeptide-doxorubicin nanoparticles with enhanced anticancer efficacy and reduced side effects, *Chem. Commun.* 51 (2015) 11405–11408. <https://doi.org/10.1039/c5cc04035c>.
- [108] S. Mitragotri, P.A. Burke, R. Langer, Overcoming the challenges in administering biopharmaceuticals: Formulation and delivery strategies, *Nat. Rev. Drug Discov.* 13 (2014) 655–672. <https://doi.org/10.1038/nrd4363>.
- [109] A. Hatefi, B. Amsden, Biodegradable injectable in situ forming drug delivery systems, *J. Control. Release.* 80 (2002) 9–28. [https://doi.org/10.1016/S0168-3659\(02\)00008-1](https://doi.org/10.1016/S0168-3659(02)00008-1).
- [110] R. Vallejo Vicente, J. Míguez Perez, Desarrollo de “click hidrogel” basados en ELRs (Elastin-Like Recombinamers) para aplicaciones avanzadas en biomedicina, Universidad de Valladolid, 2014.
- [111] A.M. Testera, A. Girotti, I.G. de Torre, L. Quintanilla, M. Santos, M. Alonso, J.C. Rodríguez-Cabello, Biocompatible elastin-like click gels: design, synthesis and characterization, *J. Mater. Sci. Mater. Med.* 26 (2015). <https://doi.org/10.1007/s10856-015-5435-1>.
- [112] M.C. Koetting, J.T. Peters, S.D. Steichen, N.A. Peppas, Stimulus-responsive hydrogels: Theory, modern advances, and applications, *Mater. Sci. Eng. R Reports.* 93 (2015) 1–49. <https://doi.org/10.1016/j.mser.2015.04.001>.
- [113] A. Ibáñez Fonseca, Novel Hydrogel-forming elastin-like recombinamers for biomedical applications, Universidad de Valladolid, 2017. <https://doi.org/10.35376/10324/29460>.
- [114] J.E. Gagner, W. Kim, E.L. Chaikof, Designing protein-based biomaterials for medical applications, *Acta Biomater.* 10 (2014) 1542–1557. <https://doi.org/10.1016/j.actbio.2013.10.001>.
- [115] N. Annabi, S.M. Mithieux, E.A. Boughton, A.J. Ruys, A.S. Weiss, F. Dehghani, Synthesis of highly porous crosslinked elastin hydrogels and their interaction with fibroblasts in vitro, *Biomaterials.* 30 (2009) 4550–4557.

- <https://doi.org/10.1016/j.biomaterials.2009.05.014>.
- [116] L. Martín, M. Alonso, A. Girotti, F.J. Arias, J.C. Rodríguez-Cabello, Synthesis and characterization of macroporous thermosensitive hydrogels from recombinant elastin-like polymers, *Biomacromolecules*. 10 (2009) 3015–3022. <https://doi.org/10.1021/bm900560a>.
- [117] S. Moreno-Estar, S. Serrano, M. Arévalo-Martínez, P. Ciudad, J.R. López-López, M. Santos, M.T. Pérez-García, F.J. Arias, Elastin-like recombinamer-based devices releasing Kv1.3 blockers for the prevention of intimal hyperplasia: An in vitro and in vivo study, *Acta Biomater.* 115 (2020) 264–274. <https://doi.org/10.1016/j.actbio.2020.07.053>.
- [118] Y.N. Zhang, R.K. Avery, Q. Vallmajo-Martin, A. Assmann, A. Vegh, A. Memic, B.D. Olsen, N. Annabi, A. Khademhosseini, A Highly Elastic and Rapidly Crosslinkable Elastin-Like Polypeptide-Based Hydrogel for Biomedical Applications, *Adv. Funct. Mater.* 25 (2015) 4814–4826. <https://doi.org/10.1002/adfm.201501489>.
- [119] A. Ribeiro, F.J. Arias, J. Reguera, M. Alonso, J.C. Rodríguez-Cabello, Influence of the amino-acid sequence on the inverse temperature transition of elastin-like polymers, *Biophys. J.* 97 (2009) 312–320. <https://doi.org/10.1016/j.bpj.2009.03.030>.
- [120] J. Reguera, D.W. Urry, T.M. Parker, D.T. McPherson, J.C. Rodríguez-Cabello, Effect of NaCl on the exothermic and endothermic components of the inverse temperature transition of a model elastin-like polymer, *Biomacromolecules*. 8 (2007) 354–358. <https://doi.org/10.1021/bm060936l>.
- [121] S. Serrano-Dúcar, Development of advanced modular molecules for innovative devices in delivery of therapeutic agents, Universidad de Valladolid, 2021.
- [122] J.A. Hubbell, A. Chilkoti, Nanomaterials for drug delivery, *Science (80-. )*. 337 (2012) 303–305. <https://doi.org/10.1126/science.1219657>.
- [123] H. Zou, Z. Wang, M. Feng, Nanocarriers with tunable surface properties to unblock bottlenecks in systemic drug and gene delivery, *J. Control. Release*. 214 (2015) 121–133. <https://doi.org/10.1016/j.jconrel.2015.07.014>.
- [124] Y. Zhang, H.F. Chan, K.W. Leong, Advanced materials and processing for drug delivery: The past and the future, *Adv. Drug Deliv. Rev.* 65 (2013) 104–120. <https://doi.org/10.1016/j.addr.2012.10.003>.
- [125] R. Lin, H. Cui, Supramolecular nanostructures as drug carriers, *Curr. Opin. Chem. Eng.* 7 (2015) 75–83. <https://doi.org/10.1016/j.coche.2014.11.005>.
- [126] L. Martín, E. Castro, A. Ribeiro, M. Alonso, J.C. Rodríguez-Cabello, Temperature-triggered self-assembly of elastin-like block co-recombinamers: The controlled formation of micelles and vesicles in an aqueous medium, *Biomacromolecules*. 13 (2012) 293–298. <https://doi.org/10.1021/bm201436y>.
- [127] E.C. Dreaden, A.M. Alkilany, X. Huang, C.J. Murphy, M.A. El-Sayed, The golden age: Gold nanoparticles for biomedicine, *Chem. Soc. Rev.* 41 (2012) 2740–2779. <https://doi.org/10.1039/c1cs15237h>.
- [128] R. Couto, V. Alvarez, F. Temelli, Encapsulation of Vitamin B2 in solid lipid nanoparticles using supercritical CO<sub>2</sub>, *J. Supercrit. Fluids*. 120 (2017) 432–442. <https://doi.org/10.1016/j.supflu.2016.05.036>.
- [129] Y.N. Konan, R. Gurny, E. Allémann, Preparation and characterization of sterile and freeze-dried sub-200 nm nanoparticles, *Int. J. Pharm.* 233 (2002) 239–252. [https://doi.org/10.1016/S0378-5173\(01\)00944-9](https://doi.org/10.1016/S0378-5173(01)00944-9).
- [130] P. Chattopadhyay, R.B. Gupta, Protein Nanoparticles Formation by Supercritical Antisolvent with Enhanced Mass Transfer, *AIChE J.* 48 (2002) 235–244.

- <https://doi.org/10.1002/aic.690480207>.
- [131] K.A. Black, D. Priftis, S.L. Perry, J. Yip, W.Y. Byun, M. Tirrell, Protein encapsulation via polypeptide complex coacervation, *ACS Macro Lett.* 3 (2014) 1088–1091. <https://doi.org/10.1021/mz500529v>.
- [132] P.N. Ezhilarasi, P. Karthik, N. Chhanwal, C. Anandharamakrishnan, Nanoencapsulation Techniques for Food Bioactive Components: A Review, *Food Bioprocess Technol.* 6 (2013) 628–647. <https://doi.org/10.1007/s11947-012-0944-0>.
- [133] E. Reverchon, Supercritical-assisted atomization to produce micro- and/or nanoparticles of controlled size and distribution, *Ind. Eng. Chem. Res.* 41 (2002) 2405–2411. <https://doi.org/10.1021/ie010943k>.
- [134] D.T. Santos, M.A.A. Meireles, Micronization and encapsulation of functional pigments using supercritical carbon dioxide, *J. Food Process Eng.* 36 (2013) 36–49. <https://doi.org/10.1111/j.1745-4530.2011.00651.x>.
- [135] H. Zheng, J. Zhang, J. Yan, L. Zheng, An industrial scale multiple supercritical carbon dioxide apparatus and its eco-friendly dyeing production, *J. CO2 Util.* 16 (2016) 272–281. <https://doi.org/10.1016/j.jcou.2016.08.002>.
- [136] R. Campardelli, L. Baldino, E. Reverchon, Supercritical fluids applications in nanomedicine, *J. Supercrit. Fluids.* 101 (2015) 193–214. <https://doi.org/10.1016/j.supflu.2015.01.030>.
- [137] M.J. Cocero, Á. Martín, F. Mattea, S. Varona, Encapsulation and co-precipitation processes with supercritical fluids: Fundamentals and applications, *J. Supercrit. Fluids.* 47 (2009) 546–555. <https://doi.org/10.1016/j.supflu.2008.08.015>.
- [138] M. Charoenchaitrakool, F. Dehghani, N.R. Foster, H.K. Chan, Micronization by rapid expansion of supercritical solutions to enhance the dissolution rates of poorly water-soluble pharmaceuticals, in: *Ind. Eng. Chem. Res.*, 2000: pp. 4794–4802. <https://doi.org/10.1021/ie000151a>.
- [139] K. Mishima, K. Matsuyama, D. Tanabe, S. Yamauchi, T.J. Young, K.P. Johnston, Microencapsulation of proteins by rapid expansion of supercritical solution with a nonsolvent, *AIChE J.* 46 (2000) 857–865. <https://doi.org/10.1002/aic.690460418>.
- [140] K. Mishima, K. Matsuyama, Method for preparing composite fine particles, 2006.
- [141] S. Rodríguez-Rojo, N. López-Valdezate, M.J. Cocero, Residence time distribution studies of high pressure fluidized bed of microparticles, *J. Supercrit. Fluids.* 44 (2008) 433–440. <https://doi.org/10.1016/j.supflu.2007.09.008>.
- [142] O.S. Fleming, S.G. Kazarian, Polymer Processing with Supercritical Fluids, in: *Supercrit. Carbon Dioxide Polym. React. Eng.*, 2006: pp. 205–238. <https://doi.org/10.1002/3527606726.ch10>.
- [143] I. Kikic, F. Vecchione, Supercritical impregnation of polymers, *Curr. Opin. Solid State Mater. Sci.* 7 (2003) 399–405. <https://doi.org/10.1016/j.cossms.2003.09.001>.
- [144] O.S. Fleming, S.G. Kazarian, Polymer Processing with Supercritical Fluids, *Supercrit. Carbon Dioxide Polym. React. Eng.* (2006) 205–238. <https://doi.org/10.1002/3527606726.ch10>.
- [145] E. Weidner, M. Petermann, Z. Knez, Multifunctional composites by high-pressure spray processes, *Curr. Opin. Solid State Mater. Sci.* 7 (2003) 385–390. <https://doi.org/10.1016/j.cossms.2003.09.002>.
- [146] J.P. Rao, K.E. Geckeler, Polymer nanoparticles: Preparation techniques and size-control parameters, *Prog. Polym. Sci.* 36 (2011) 887–913. <https://doi.org/10.1016/j.progpolymsci.2011.01.001>.
- [147] C. Prieto, L. Calvo, Supercritical fluid extraction of emulsions to nanoencapsulate vitamin E in polycaprolactone, *J. Supercrit. Fluids.* 119 (2017) 274–282.

- <https://doi.org/10.1016/j.supflu.2016.10.004>.
- [148] P. Chattopadhyay, R. Huff, B.Y. Shekunov, Drug encapsulation using supercritical fluid extraction of emulsions, *J. Pharm. Sci.* 95 (2006) 667–679. <https://doi.org/10.1002/jps.20555>.
- [149] G. Della Porta, E. Reverchon, Nanostructured microspheres produced by supercritical fluid extraction of emulsions, *Biotechnol. Bioeng.* 100 (2008) 1020–1033. <https://doi.org/10.1002/bit.21845>.
- [150] G. Levai, Bioproducts processing by Sfee: application for liquid and solid Quercetin formulations, (2016). <https://dialnet.unirioja.es/servlet/tesis?codigo=155412&info=resumen&idioma=SPA> (accessed May 21, 2021).
- [151] M. Kalani, R. Yunus, Application of supercritical antisolvent method in drug encapsulation: a review., *Int. J. Nanomedicine.* 6 (2011) 1429–1442. <https://doi.org/10.2147/ijn.s19021>.
- [152] E. Reverchon, G. Caputo, I. De Marco, Role of Phase Behavior and Atomization in the Supercritical Antisolvent Precipitation, *Ind. Eng. Chem. Res.* 42 (2003) 6406–6414. <https://doi.org/10.1021/ie0302138>.
- [153] A.J. Thote, R.B. Gupta, Formation of nanoparticles of a hydrophilic drug using supercritical carbon dioxide and microencapsulation for sustained release, *Nanomedicine Nanotechnology, Biol. Med.* 1 (2005) 85–90. <https://doi.org/10.1016/j.nano.2004.12.001>.
- [154] P. Franco, I. De Marco, Supercritical antisolvent process for pharmaceutical applications: A review, *Processes.* 8 (2020). <https://doi.org/10.3390/PR8080938>.

**HYPOTHESIS**  
**&**  
**OBJECTIVES**





### 3. HYPOTHESIS

It is hypothesised that using the Supercritical antisolvent (SAS) technique with supercritical CO<sub>2</sub> enables the encapsulation of highly hydrophobic drugs with Elastin-Like Recombinamers (ELRs) that mimic physiological conditions suitable for biomedical applications. This would improve control over the rate of release, control over the location of release, reduction of dosage and side effects, resulting in a more precise, bioactive and biocompatible release system.

### 4. OBJECTIVES

The main objective of this Thesis is to develop a release system for the sustained, controlled and targeted delivery of hydrophobic active agents. For this purpose, Supercritical Antisolvent (SAS) technique with CO<sub>2</sub> in a supercritical state will be used in order to encapsulate these hydrophobic compounds in amphiphilic biopolymers such as ELRs.

- First, the encapsulation of different therapeutic agents such as acetazolamide (Chapter 1), docetaxel (Chapter 2), resveratrol and quercetin (Chapter 3) will be studied using environmentally friendly solvents such as DMSO and ethanol/water mixtures.
- Secondly, this work aims to improve the design of a precipitation vessel, the pulverization of the solution with a coaxial nozzle and the particle recovery system to operate at high pressure with CO<sub>2</sub> in the supercritical state and to establish the optimal operating conditions to the specific use of ELRs, reducing as much as possible, without compromising the yield of the process, the amount of residual solvent in the final product (Chapter 2).
- Thirdly, identify by <sup>1</sup>H-NMR that the structure of the ELR in the final product obtained and that its smart behaviour has not been affected by the SAS technique (Chapter 1, 2 and 3), as well as to perform a study on the encapsulation by means of <sup>1</sup>H-NMR, to determine if the drug is effectively inside the carrier (Chapter 2).
- Fourthly, physically characterise the final product obtained, as well as model the *in vitro* release profiles in each case (Chapter 1, 2 and 3).

Finally, thanks to collaborations with experts in fields such as biotechnology, biology and pharmacy it will be tested *ex vivo* and *in vivo* the different encapsulated therapeutic agents to determine their effectiveness.

**MATERIALS**  
**&**  
**METHODS**



## 4. MATERIALS

### 4.1. Reagents

The reagents used during the progress of this thesis can be found in Table 1.

| Reagent  | Supplier                    |
|--|-----------------------------|
| Acetazolamide purity $\geq 99\%$   | Sigma Aldrich               |
| Carbon dioxide (CO <sub>2</sub> ) purity of 99.95%                             | Carbueros<br>Metálicos S.A. |
| Deuterium oxide (D <sub>2</sub> O) purity of 99.9 atom % D                     | Sigma Aldrich               |
| Dimethyl sulfoxide (DMSO) purity of $\geq 99.7\%$                              | Sigma Aldrich               |
| Dimethyl sulfoxide-d <sub>6</sub> (DMSO-d <sub>6</sub> ) purity 99.96 atom % D | Sigma-Aldrich               |
| Docetaxel (DTX) purity of 99%  | Apollo Scientific           |
| Dulbecco's phosphate-buffered saline DPBS                                      | Invitrogen                  |
| E. coli BLR (DE3) strain   | Merck                       |
| Ethanol absolute 99% no marked   | Scharlau                    |
| Fluoresceinyl Glycine Amide (5-(Aminoacetamido)Fluorescein)                    | Invitrogen                  |
| Minimum Essential Medium (MEM)   | Invitrogen                  |
| Nile red for microscopy  | Sigma Aldrich               |
| Penicillin/streptomycin solution   | Invitrogen                  |
| Quercetin purity $>98\%$   | Sigma Aldrich               |
| Resveratrol purity 99%   | acros organics              |
| Rhodamine B for fluorescence   | Sigma Aldrich               |
| Trypsin-EDTA   | Invitrogen                  |

**Table 1.** List of Reagents used in the framework of this PhD thesis

All disposable plastic material (pipette tips, pipettes, centrifuge tubes, microcentrifuge tubes, etc.) were obtained sterile or autoclaved (Autotester E-75) at 121°C and 0.1 MPa of pressure for 20 minutes. The glass material (glasses, flasks, pipettes, etc.) was properly washed for use and sterilized in the same way, if necessary.

#### 4.2. Elastin-like Recombinamers (ELRs)

The ELRs used in the framework of this PhD thesis are described in Table 2, and a scheme of them is presented in Figure 14.

| ELR      | Abbreviated amino acid sequence   | Molecular weight (kDa) |
|----------|---|------------------------|
| (EI)2    | MESLLP-[[ $(\text{VPGVG})_2$ VPGE $(\text{VPGVG})_2$ ] <sub>10</sub> -(VGIPG) <sub>60</sub> ] <sub>2</sub> -V   | 92.90                  |
| (EI)2RGD | MESLLP-[[ $(\text{VPGVG})_2$ VPGE $(\text{VPGVG})_2$ ] <sub>10</sub> -(VGIPG) <sub>60</sub> ] <sub>2</sub> -VG-<br>[(VPGIG) <sub>10</sub> -AVTGRGDSPASS-<br>$(\text{VPGIG})_{10}$ ] <sub>2</sub> -V | 112.27                 |

**Table 2.** ELRs used in this thesis, obtained in the G.I.R. BIOFORGE laboratories of the University of Valladolid.

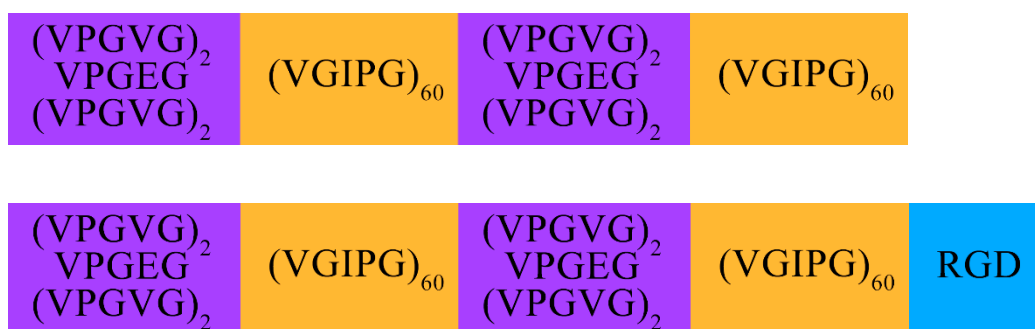


**Figure 14.** Scheme of (EI)2 and (EI)2RGD recombinamers. Non-scaled scheme

## 5. METHODS

### 5.1. ELRs synthesis

All the genes encoding the ELRs used in this work have been obtained using genetic engineering techniques described in the bibliography [1,2]. The genes encoding the different polypeptides, both ELR and bioactive sequences/other proteins, are synthesised by an external service (NZYTech) and cloned into the pDriveAll plasmid, obtained from various modifications of the pDrive plasmid (Qiagen), as described above [3]. The restriction enzymes used for "seamless cloning" are EarI and SapI (Thermo Scientific), two IIS-type restriction enzymes that have endonuclease activity on a sequence adjacent to the recognition sequence and are therefore optimal for this type of cloning. Once the final gene construction is obtained, it is extracted from the cloning plasmid and a subcloning is performed on the pET7 expression plasmid, the result of different modifications on the commercial pET-25b(+) vector (Novagen). Subsequently, this plasmid is used to transform expression strains of *Escherichia coli*, specifically BLR(DE3) (Novagen), which are cultivated in a 15 L bioreactor (Applikon Biotechnology) under controlled pH, temperature, agitation and O<sub>2</sub> concentration conditions, thus achieving the bioproduction of the different ELRs. Subsequently, after the mechanical rupture of the cell wall and the bacterial membrane by disruption (model TS 0.75KW, Constant Systems), the ELRs are purified by taking advantage of their thermosensitivity feature by means of successive cooling and heating cycles (known as "Inverse Transition Cycling", ITC), followed by centrifugation at each step [4]. Finally, Endotoxins were removed from the ELR by means of additional NaCl and NaOH treatments [5], the polymer was then dialyzed against ultrapure water type I, sterilized by filtration (0.22 µm filters, Nalgene) and then the pure product is freeze-dried (FreeZone

1, LABCONCO) prior to storage. Depending on the protein being produced, the overall production yield can fluctuate between 150 to 300 mg/L of culture media.

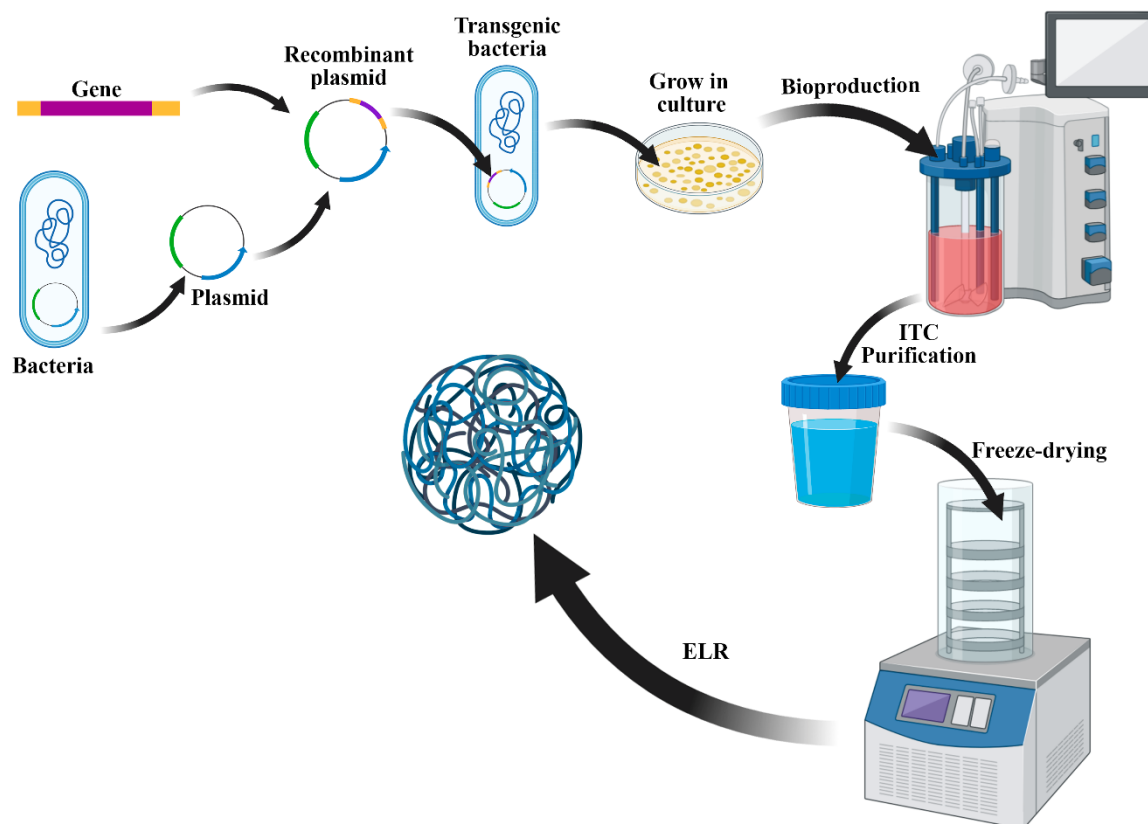


**Figure 15.** Schematic representation of the ELR synthesis

## 5.2. Supercritical Antisolvent (SAS) pilot plan description.

Due to the specific application that will be given to this installation during the progress of this thesis, a new reactor was designed. 316L steel was chosen for its manufacture, as it is austenitic stainless steel that contains between 16-18% chrome, 10-14% nickel, 2-3% molybdenum and a maximum of 0.03% carbon, which provides high resistance to corrosion, pitting and resistance to acids. This allows us to perform cleaning and disinfection operations in the reactor to avoid contaminations.



The reactor is a 16 mm thick cylinder designed to withstand pressures of up to 35MPa and mirror polished inside to make it difficult for the precipitated product to adhere to the walls of the reactor. To control the temperature inside, the reactor has a 3.2 L capacity jacket through which water circulates to maintain the desired temperature. The reactor is sealed by two 25 mm thick covers (upper and lower) with Teflon O-rings to ensure the reactor is leak-proof. The upper cover contains 4 GAS ¼" inlets through which the devices that transmit the pressure and temperature inside are installed, as well as the inlet for the entry of both the solution and the scCO<sub>2</sub>. The lower cover contains a GAS 3/8" outlet connexion and was designed with a conical shape to promote the formation of the vortex at the outlet of the reactor that would drag the precipitated product. All blueprints and dimensions can be found in annexe I.

The installation is composed of the reactor described above, which is equipped with a Pt-100 thermoresistance with an accuracy of 0.1°C and a membrane digital pressure meter with an accuracy of 0.5 bar to measure the operating conditions. The CO<sub>2</sub> is taken from a gas cylinder, cooled down and pumped at a predetermined flowrate using a diaphragm pump (Dosapro Milton Roy). The mass flow was measured by a Coriolis flowmeter (Micro Motion, Emerson) and the pressure was controlled using a back-pressure valve (model BP-66, GO, Spartan-burg, SC). The solution is pumped into the reactor using an HPLC pump (Gilson 305) and the final product is recovered from a porous metal in-line filter with a screen size of 1 µm placed out of the reactor.

Figure 16 show a schematic flow diagram of the SAS pilot plant, using a non-coaxial 1/6" ID nozzle and introducing the scCO<sub>2</sub> into the reactor through one of the holes adjacent to that of the solution. The organic solvent used to perform the experiments in Chapters 1 and 2 was DMSO, and in chapter 3 the solvent used was a mixture of ethanol-water. The working pressure and temperature were established in the one phase area by studying the

corresponding solubility diagrams found in the literature [6] [7]. The final product was dried with fresh scCO<sub>2</sub> for 2h to remove as much residual solvent as possible.

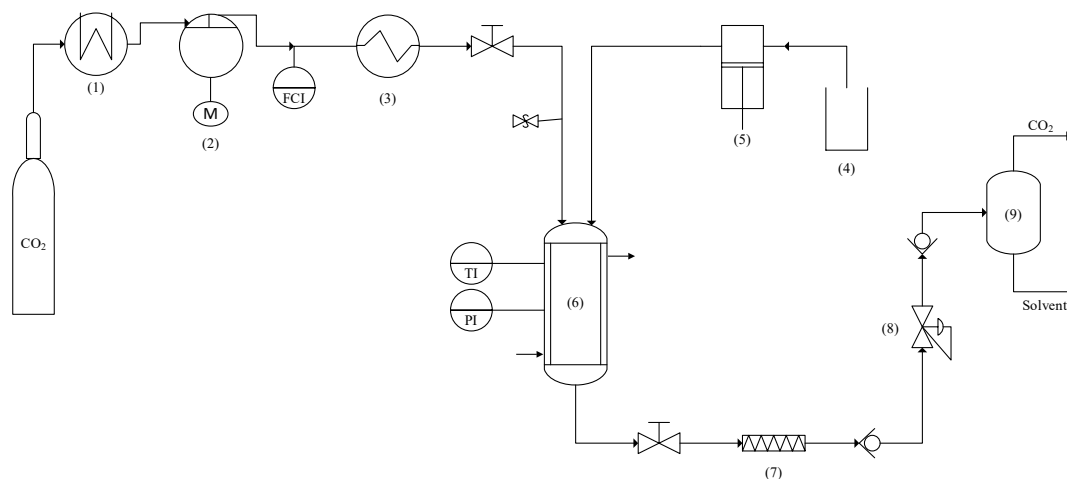


**Figure 16.** Schematic flow diagram of the SAS pilot plant. (1) cooler, (2) CO<sub>2</sub> pump, (3) heater, (5) liquid pump, (4) solution, (6) precipitator vessel, (7) filter, (8) back-pressure valve, (9) separator

### 5.3. Particle characterization

#### 5.3.1. Proton Nuclear Magnetic Resonance <sup>1</sup>H-NMR

Nuclear magnetic resonance is a spectroscopic technique developed to study the nuclei of atoms and can be used for the structural determination of organic compounds. However, it can only be used to study atomic nuclei with an odd number of protons or neutrons (or both). When a sample is placed in a magnetic field, the nuclei with positive spin are oriented in the same direction of the field, while the nuclei with negative spin are oriented in the opposite direction of the magnetic field. The relaxation of these nuclei, when the external magnetic field is no longer active, depends on the molecular structure and is therefore different for each molecule, and a "fingerprint" can be obtained from them, even for those that give place to complex spectra, such as proteins, specifically ELRs. In this work, the proton NMR spectra (<sup>1</sup>H-NMR) have been obtained for ELRs

characterization and for the determination of the proportions of each chemical species present in the particles obtained by the SAS technique with the NMR 500MHz and 400MHz equipments (Agilent Technologies) of Instrumental Techniques Laboratory from University of Valladolid [8]. All spectra were analysed using MestreNova v 9.0.1

### **5.3.2. Mass spectrometry (MALDI-TOF)**

Matrix-assisted laser desorption/ionization–Time-of-flight (MALDI-TOF) is a soft ionization technique used in mass spectrometry to determine molecular weight excellent accuracy. It is a highly sensitive and high-resolution capacity technique that allows the analysis of proteins, peptides and large organic molecules, such as polymers or dendrimers. The analysis of the ELRs produced during this thesis were analysed using this technique with a MALDI-TOF Voyager STR team (Applied Biosystems) equipment in the Instrumental Techniques Laboratory from the University of Valladolid [9].

### **5.3.3. Fourier transform infrared spectroscopy (FTIR)**

Infrared spectroscopy (IR) is based on the fact that most molecules absorb light in the infrared range of the electromagnetic spectrum and this energy is converted into molecular vibration. This absorption is specific to the bonds between the atoms present in the molecule. Using a spectrometer, this absorption of infrared light through the sample material is measured as a function of the wavelength. The result is a spectrum that provides a "molecular fingerprint" characteristic with which samples can be examined, scanned and identified for many different organic and inorganic components.

Instead of checking the absorption of the sample one after the other with individual (dispersive) wavelengths, FT-IR spectroscopy allows recording all spectral information simultaneously. This produces an interferogram, a raw signal representing the intensity of light as a function of the position of the mirror. This signal first needs to be transformed into Fourier (FT) to produce the known IR representation of intensity against the wavenumber.

Fourier Transform Infrared (FTIR) spectroscopy was performed by attenuated total reflectance equipment (ATR-FTIR) using a Bruker Tensor27. For baseline correction and data acquisition, 256 scans were performed with a  $4\text{ cm}^{-1}$  resolution. Briefly, the freeze-dried sample is placed in the ATR equipment and compressed against the ATR crystal, until a good signal-to-noise ratio was achieved [10].

### **5.3.4. Differential scanning calorimetry (DSC)**

DSC is a thermo-analytical technique that evaluates the effect of temperature on the variation of the heat capacity ( $C_p$ ) of a material. A sample is taken from a known mass and it is heated or cooled down in a controlled temperature cycle, recording the heat flow required to determine changes in its heat capacity. This allows the detection of transitions such as melting points, glass transitions or phase changes. In our case, it is used to measure the  $T_t$  of ELRs, since, when a phase change or transition occurs, the amount of heat that will be necessary to provide to the ELR solution to increase the temperature will be greater than for the reference (solvent without ELR), since it is an endothermic process and part of the energy provided to the system during the transition will be consumed. Mettler Toledo 822e (USA) equipment with liquid nitrogen cooling was used for this purpose. Samples were dissolved overnight (O/N) at  $50\text{ mg/mL}$  and pH 7 in ultrapure deionized water below  $T_t$  ( $4\text{ }^\circ\text{C}$ ) The heating program for DSC experiments included an

initial isothermal stage (5 min at 0 °C for stabilization of the temperature), followed by heating at 5 °C/min from 0 to 60 °C [11].

### **5.3.5. Dynamic light scattering and zeta potential**

Dynamic light scattering (DLS), sometimes referred to as quasi-elastic light scattering (QELS), is a well-established, non-invasive technique for measuring the size and size distribution of molecules and particles. The sample is illuminated with a laser light source and a photodetector detects fluctuations in the scattered light at a known scattering angle. The particles scatter the light and as such, "print" information about their movement. By analysing the fluctuations of the scattered light, the size of the particles is obtained.

The zeta potential ( $\zeta$ -Potential) is a measure of the magnitude of the repulsion or electrostatic (or charge) attraction between particles that exist in the particle cutting plane, with a short distance from the surface, and is one of the fundamental parameters known to affect stability. Its measurement provides detailed information about the causes of dispersion, aggregation or flocculation.

$\zeta$ -Potential and particle size distribution in aqueous solution were measured using a Zetasizer Nano ZS (Malvern Instruments Ltd., UK). Samples involving pure ELR were dissolved at 1 mg/mL in ultrapure deionized water below Tt (4 °C) overnight (O/N), then the temperature was raised above Tt at 37 °C for 15 min. However, the samples obtained after the SAS process were dispersed in PBS at 37°C for 15 minutes when measuring particle size, and in ultrapure deionized water when measuring  $\zeta$ -Potential with the same procedure. All samples were adjusted to neutral pH with NaOH 0.5 M at room temperature and filtered through a 0.45  $\mu$ m nylon filter to avoid the presence of dust before measuring. Three measurements were taken per sample.

### **5.3.6. Scanning electron microscopy (SEM)**

Particle morphology was studied by scanning electron microscopy (SEM) at the Advanced Microscopy Laboratory (Parque Científico, University of Valladolid) using an ESEM QUANTA 200 FEG instrument. The powder obtained after SAS process of representative samples was placed under an argon atmosphere at room temperature before examination of different magnifications for comparison. The voltage used in each SEM analysis was 1 kV, which provided a sufficient resolution and did not produce any changes in the samples. The particles in the photomicrographs were measured using a Carl Zeiss GmbH microscope and the 2011 ZEN 2.3 (blue edition) software [8].

### **5.3.7. Transmission Electron microscopy (TEM)**

Particle morphology and the amphiphilic behaviour of the biopolymer and particles obtained after SAS process in aqueous media were observed by TEM using a JEOL JEM-1011 HR instrument equipped with a ES1000W (4000x2672 pixels) CCD camera (GATAN, UK) Parque Científico, University of Valladolid. Samples were prepared at a concentration of 1 mg/mL in ultrapure deionized water with negative staining at neutral pH and room temperature. The particles in the photomicrographs were measured using a Carl Zeiss GmbH microscope and the 2011 ZEN 2.3 (blue edition) software [8].

### 5.3.8. Atomic force microscopy (AFM)

AFM imaging was performed with a MFP-3D Asylum AFM (Oxford Instruments, Scotts Valley, CA) at the Laboratory of Instrumental Techniques (University of Valladolid), Spain. To image the desiccated nanoparticles, OLYMPUS OMCL-AC probe, designed for AC mode AFM in air, with a stiffness constant  $k = 26 \text{ N/m}$  was used. To image hydrated nanoparticles, Asylum Research BL-AC40TS probe, with  $k = 0.09 \text{ N/m}$  was used. Images were captured using tapping mode, with sizes of  $256 \times 256$  pixels and  $512 \times 512$  pixels. Areas of  $20 \mu\text{m}^2$ ,  $10 \mu\text{m}^2$ ,  $5 \mu\text{m}^2$ ,  $2 \mu\text{m}^2$  and  $1 \mu\text{m}^2$  were scanned on all samples. Images were processed and analysed using AR v.16.10.208 and Gwyddion v.2.56. The protocol followed to obtain AFM images is described below.

The epoxy adhesive was used to firmly attach a mica disk to an AFM magnetic stainless-steel specimen disk (Ted Pella, AFM/STM Metal Specimen Discs,  $\text{Ø}15 \text{ mm}$ ). Mica disc where flesh cleaved attaching an adhesive tape to the top surface and then peeling it off to remove a layer of material. In addition, nanoparticles were immobilized to improve the imaging acquisition [12]. Mica substrates were modified to have a positive charge, using a  $\text{NiCl}_2$  treatment. However, the same electrostatic forces that immobilize the nanoparticles on the surface may also alter their shape [13]. The process followed for the preparation of the samples is detailed below:

1. At room temperature,  $100 \mu\text{L}$  of  $10 \text{ mM NiCl}_2$  solution was placed on the top mica surface for  $10 \text{ s}$ , which modifies the surface charge from negative to positive. Hereafter, the  $\text{NiCl}_2$  solution was blotted with a lint-free wipe and then the mica surface was washed three times with deionized water, dried with a stream of dry nitrogen and placed in a petri dish.
2.  $100 \mu\text{L}$  of the nanoparticles sample solution were deposited on the surface-modified mica.

3. With the lid of the petri dish on and sealed with a paraffin film to reduce sample evaporation; the samples were incubated for 12h at room temperature.
4. After incubation, 80–90% of the sample was aspirated without disturbing the surface. At this point, the nanoparticles were electrostatically immobilized on the mica substrate.
5. Before imaging hydrated nanoparticles, the surface was rinsed three times with deionized water, taking care to keep the sample hydrated throughout the rinsing process.
6. Hereafter, 80%–90% of liquid was removed, and 40  $\mu$ L of fresh deionized water was placed to cover the sample.
7. When imaging the desiccated nanoparticles, the same abovementioned sample preparation is carried out and, finally, the substrate was rinsed three times with deionized water, and after removing as much liquid as possible without touching the surface, the remainder, was dried with nitrogen.

### **5.3.9. Confocal microscopy**

Confocal microscopy works with one or more lasers, light detectors, photomultipliers and a physical barrier, pinhole, which blocks light from other levels of the detector. The principle on which this technique is based is to avoid light reaching the detector from different levels of the focus, which allows us to obtain higher quality images by means of spatial filtering techniques. Confocal microscopy images were acquired by Dr Juan Gonzalez Valdivieso Smart Devices for NanoMedicine Group, University of Valladolid) and can be found described in [11] and images were taken using a Leica TCS SP8 X confocal microscope at the Laboratory of Instrumental Techniques (University of Valladolid) [11].



### **5.3.10. Fluorescence microscopy**

Fluorescence microscopy is a special type of optic microscopy that uses the capacity of fluorochromes to emit light after being excited with light at a certain wavelength. The image observed is the result of electromagnetic radiation emitted by the molecules that have absorbed the primary excitation and re-emitted light with a higher wavelength. Fluorescence microscopy images were acquired by Dr Juan Gonzalez Valdivieso (Smart Devices for NanoMedicine Group, University of Valladolid) and can be found described in [11] and images were taken using a Nikon eclipse Ti-SR (Japan) fluorescence microscope.

## **5.4. *In vitro* release studies**

The methodology used to obtain the cell viability, cell proliferation and apoptosis/necrosis Assay results involving DTX were performed by Dr Juan Gonzalez Valdivieso (Smart Devices for NanoMedicine Group, University of Valladolid) and can be found described in his Doctoral Thesis [11].

### **5.4.1. Experimental procedure to acquire the drug-delivery profiles**

Acetazolamide delivery assays were performed in a modified Franz diffusion assembly at  $35.0 \pm 0.5^\circ\text{C}$ . The cell, made of acrylic plastic, consisted of donor and receiving receptor compartments (of volumes 1.0 and 4.0 mL, respectively). A semi-permeable acetate cellulose membrane (Sigma® MWCO 12 kDa) was introduced between the donor and receptor compartments, and nanocapsule suspensions (1 mL) were placed in the donor compartment, while sodium chloride, monobasic sodium phosphate and dibasic

sodium phosphate (pH 7.2) were put in the receptor compartment. The receptor solution was aerated with a mixture of 95% O<sub>2</sub> and 5% CO<sub>2</sub>, in order to maintain agitation in the medium. At selected times, the 1mL aliquots were removed and replaced with the same volume of the receptor medium. Data were corrected for dilution, and the amount released was determined by UV spectroscopy (278 nm). Each sample was assayed in triplicate (n = 3). Experiments involving acetazolamide were conducted by Dra. Daniela A. Quinteros (Unidad de Investigación y Desarrollo en Tecnología Farmacéutica (UNITEFA), CONICET and Departamento de Ciencias Farmacéuticas, Facultad de Ciencias Químicas, Universidad Nacional de Córdoba

Drug-delivery experiments containing DTX formulations usually involve mixtures with polysorbate 80. Since surfactants could affect the amphiphilic behaviour of the ELR in aqueous solution, the assays were performed by using the dialysis method and avoiding the use of surfactants as described elsewhere [14], 1 mg of (EI)x<sub>2</sub>+DTX particles in 1 mL of 7:3 (v/v) water/ethanol release medium were dispersed, to contain 0.6 mg of encapsulated DTX, at 37°C and in triplicate. Previously activated dialysis bags (MWCO 12 kDa) were filled with this solution and sealed at both ends. These bags were then immersed in 30 mL glass vials, previously filled with 20 mL of release medium. The content of these vials was stirred at 80 rpm and 37°C in an incubator throughout the experiment. A 2 mL sample was withdrawn from the release medium at predetermined time intervals and the same volume of fresh medium was added to maintain sink conditions. As a control, the drug delivery assay was carried out with pure DTX (0.6 mg), also in triplicate. The amount of DTX released with time was determined by UV-vis spectrometry (UV-Vis NanoDrop 2000, Thermo Scientific) following the Lambert-Beer law, at a wavelength of 234 nm. A calibration curve was plotted beforehand using

solutions of DTX dissolved in a 7:3 (v/v) water/ethanol at a concentration between 62.5 and 0.98 mg/mL.

Release experiments involving quercetin and resveratrol were performed in triplicate in an incubator at 37°C using the dialysis method, dispersing the different formulations at a concentration of 100mM and using PBS as the release medium. Dialysis membranes (MWCO 12 kDa) were pre-activated and filled with 1 mL of each formulation and sealed at the ends. These bags were placed in 30 mL vials that had been pre-filled with 20 mL of dispersant medium. The vials were then kept at 37°C and 80 rpm in an incubator for the duration of the release experiment. At each of the stipulated times, 2 mL of sample dispersant medium was removed and the same volume was refilled with fresh medium to maintain sink conditions. As a control, the same release assay was performed under the same conditions with both quercetin and pure resveratrol, also in triplicate. The amount of quercetin released, as well as the amount of resveratrol released, were determined by UV-vis spectroscopy (Lambda 25 UV-vis spectrometer, Perkin Elmer) following the Lambert-Beer law, at a wavelength of 258nm for quercetin and 310nm for resveratrol. The calibration curve was previously plotted at a concentration between 0.012 and 0.0006 mg/mL.

#### **5.4.2. Modelling of the drug delivery profiles**

The study of the release kinetics of a drug is of considerable importance in the development of new release systems since it allows the calculation of parameters that provide very useful information related to the mechanism by which the release process occurs.

For the study of the release profiles obtained throughout this thesis, two mathematical models have been used. The Peppas-Sahlin model (Eq.7) and the Lindner-Lippold model (Eq.5) are the ones that best meet the properties and characteristics of the formulations that have been used.

### **5.5. Anti-glaucoma activity of AZM formulations**

#### **5.5.1. Determination of the pH and osmolality**

Determination of the pH and osmolality in the samples that comprised acetazolamide were conducted in collaboration with Dra. Daniela A. Quinteros (Unidad de Investigación y Desarrollo en Tecnología Farmacéutica (UNITEFA), CONICET and Departamento de Ciencias Farmacéuticas, Facultad de Ciencias Químicas, Universidad Nacional de Córdoba, Argentina.

Each formulation involving acetazolamide after SAS process were acquired using a potentiometer (Mettler Toledo, Seven Multi) and an osmometer (VAPRO, model 5600), with dextrose used as a reference (300 mmol/kg). Each sample was assayed in triplicate ( $n = 3$ ). The quantification of Acetazolamide was carried out by using a UV spectrophotometer (Thermo electron Corporation®) used at 278 nm. A stock solution of

concentration  $1,722 \times 10^{-3} \text{M}$  was prepared and successive dilutions were made from this stock. Performed in triplicate and both PBS.

## **5.6. *Ex vivo* assays**

*Ex vivo* assays were conducted by Dra. Daniela A. Quinteros (Unidad de Investigación y Desarrollo en Tecnología Farmacéutica (UNITEFA), CONICET and Departamento de Ciencias Farmacéuticas, Facultad de Ciencias Químicas, Universidad Nacional de Córdoba).

### **5.6.1. Transcorneal Permeation studies of acetazolamide**

Permeation studies have been performed using Franz diffusion cells. In this case, a cornea was placed between the donor and receptor compartments. The rabbits were anaesthetized with phenobarbital and euthanized with a mixture of 10% O<sub>2</sub> and 90% CO<sub>2</sub> in an acrylic hermetic chamber. Then, the corneas, with a 2mm ring of the sclera, were immediately excised and mounted in the diffusion cells.

The behaviour of the different acetazolamide formulations (1:1, 1:2 and 1:3) and of pure AZM solution at 1 mg/mL, was determined and analysed. For that purpose, a 4mL aliquot of the receptor solution was added to the endothelial face, while 1.0 mL of each formulation was added to the epithelial face. The receptor solution was made up of sodium chloride, monobasic sodium phosphate, and dibasic sodium phosphate (pH 7.2), with the temperature in the diffusion chamber being maintained at  $35.0 \text{ }^\circ\text{C} \pm 0.5 \text{ }^\circ\text{C}$  by means of a thermostatic water bath. Sample aliquots from the receptor cell were withdrawn at 0.25, 0.5, 0.75, 1, 2, 3, 4, 5, 6 and 7 h and immediately replaced by the same volume of previously aerated fresh receptor medium. Samples were filtered through a

0.45  $\mu\text{m}$  microporous membrane and kept at 4°C until being analysed by UV. The area available for permeation in the cell was 0.785  $\text{cm}^2$ .

A linear regression analysis of the pseudo-steady-state diffusion data allowed the steady-state flux ( $J$ , given by  $\Delta Q/\Delta t$ ) to be calculated, where  $Q$  is the amount of acetazolamide diffused across the area  $A$  at time  $t$ . The apparent permeability coefficient ( $P_{app}$ ) was calculated using the relationship:

$$P_{app} = \frac{J}{C_i} \text{ (Eq. 8)}$$

where  $C_i$  is the initial drug concentration in the donor phase. The lag times for drug absorption (the time required so that the drug can saturate the cornea and reach the receiver compartment) were calculated from the interception of the x-axis with the regression lines.

### **5.7. In-vivo assays**

All the experiments involving acetazolamide were conducted in accordance with the procedures of the Association for Research in Vision and Ophthalmology resolution on the use of animals in research, the European Communities Council Directive (86/609/EEC), and the Institutional Care and Use Committee (CICUAL) of the School of Medicine Sciences, the National University of Cordoba (Res. 44/17.).

All efforts were made to reduce the number of animals used.

*In vivo* assays involving acetazolamide formulations were conducted by Dra. Daniela A. Quinteros (Unidad de Investigación y Desarrollo en Tecnología Farmacéutica

(UNITEFA), CONICET and Departamento de Ciencias Farmacéuticas, Facultad de Ciencias Químicas, Universidad Nacional de Córdoba.

### **5.7.1. Hypotensive efficacy studies in vivo: IOP determinations**

Experiments were performed in both eyes of non-sedated female Hypertensive of New Zealand white rabbits (2–2.5 kg). The hypertensive ocular model was obtained by the application of intracameral injections of alpha-chymotrypsin (C425-250 mg Sigma laboratory) in the right eye (RE) of rabbits [15]. The left eye was not intervened with the main purpose of not compromising the welfare of the animal. IOP was measured with a Tonovet rebound tonometer (Tiolat, Helsinki, Finland), which allows us to measure IOP without the requirement of topical anaesthesia on the animals. Each formulation was evaluated in 8 rabbits and for every eye, the IOP was set at 100% by taking two basal readings immediately after installation and 30 min later. 40µL drop of the acetazolamide formulations at 1:1, 1:2 and 1:3 ratios with a concentration of acetazolamide of 1mg/mL were placed in the cul-de-sac of the right eye of 48 rabbits with glaucoma for each formulation, and IOPs were measured at 0.5, 1, 2, 4, 6, 7 hours. At each point, the average pressure (in mmHg) of 6 consecutive measurements was recorded. In the other 4 hypertensive rabbits, the same procedure was performed placing one drop of free acetazolamide solution at the same concentration.

### 5.7.2. Ocular irritation test

The potential ocular irritancy and/or damaging effects of the formulations under test were evaluated using a modified version of the Draize test [16]. Twelve rabbits were divided into five groups of three rabbits each, to which 40  $\mu$ L of each formulation was administered in both eyes as described below.

Group 1: sodium chloride 0.9% (negative control)

Group 2: sodium lauryl sulphate 2% (positive control)

Group 3: (EI)2:AZM (1:1)

Group 4: (EI)2:AZM(1:2)

Group 5: (EI)2:AZM (1:3)

The clinical signs of damage in the anterior and posterior segments in response to the treatments were evaluated using a slit-lamp (Huvitz HIS5000-Sud Korea) by an experienced ophthalmologist. Furthermore, the integrity of the corneal epithelium was checked by fluorescein staining. All observations were made at predefined times: 1, 2, 4, and 7 hours after the administration of the formulations. The final irritation value was obtained from the sum of the individual values according to Table 3 and the score values obtained were classified as, no irritation, mild irritation, moderate irritation and serious irritation with values between 0-2, 3-7, 8-12 and 12-20, respectively.



| <b>Ocular irritation test with slit-lamp bio-microscopy</b>                 |   |
|---|---|
| <b>Cornea</b>   |   |
| Without opacity or keratitis  | 0 |
| Diffuse opacity or keratitis, clearly visible iris details                  | 1 |
| Easily discernible translucent areas slightly darkened iris details         | 2 |
| Opalescent areas, no visible iris details, barely discernible pupil size    | 3 |
| Opaque cornea, iris not discernible through opacity                         | 4 |
| <b>Corneal area involved</b>  |   |
| A quarter (or less) but not zero  | 1 |
| Greater than a quarter and less than a half                                 | 2 |
| Greater than half and less than three-quarters                              | 3 |
| Greater than three-quarters of the entire area                              | 4 |
| <b>Iris</b>   |   |
| Normal (clean camera)   | 0 |
| Turbidity of aqueous humour   | 4 |
| Crypt deepening and/or iris congestion and oedema with pericarp injection   | 6 |
| Haemorrhage, destruction of the iris, pupil, or pupil not reactive to light | 8 |
| <b>Conjunctiva</b>  |   |
| Normal blood vessels  | 0 |
| Some hyperemic blood vessels (conjunctival injection)                       | 1 |
| Diffuse redness, blood vessels not easily discernible                       | 2 |
| Red eye   | 3 |
| Chemosis  | 4 |

**Table 3.** Scores assignation to different eye tissue symptoms for determination of score of eye irritation

## 5.8. REFERENCES

- [1] J.C. Rodríguez-Cabello, A. Girotti, A. Ribeiro, F.J. Arias, Synthesis of genetically engineered protein polymers (recombinamers) as an example of advanced self-assembled smart materials, *Methods Mol. Biol.* 811 (2012) 17–38. [https://doi.org/10.1007/978-1-61779-388-2\\_2](https://doi.org/10.1007/978-1-61779-388-2_2).
- [2] M. Yamato, *Nanotechnology in regenerative medicine*, Humana Press, 2006. <https://doi.org/10.2745/dds.21.623>.
- [3] A. Girotti, *Desarrollo de una plataforma biotecnológica para la obtención de polímeros rocombinantes tipo elastina*, Universidad de Valladolid, 2007.
- [4] D.E. Meyer, A. Chilkoti, Protein Purification by Inverse Transition Cycling, in: P. Golemis, E. Adams (Ed.), *Protein–Protein Interact. A Mol. Cloning Man.*, 2002nd ed., Cold Spring Harbor Laboratory Press, 2002: pp. 329–344.
- [5] R.E. Sallach, W. Cui, F. Balderrama, A.W. Martinez, J. Wen, C.A. Haller, J. V. Taylor, E.R. Wright, R.C. Long, E.L. Chaikof, Long-term biostability of self-assembling protein polymers in the absence of covalent crosslinking, *Biomaterials.* 31 (2010) 779–791. <https://doi.org/10.1016/j.biomaterials.2009.09.082>.
- [6] A.E. Andreatta, L.J. Florusse, S.B. Bottini, C.J. Peters, Phase equilibria of dimethyl sulfoxide (DMSO) + carbon dioxide, and DMSO + carbon dioxide + water mixtures, *J. Supercrit. Fluids.* 42 (2007) 60–68. <https://doi.org/10.1016/j.supflu.2006.12.015>.
- [7] M.L. Gilbert, M.E. Paulaitis, Gas-liquid equilibrium for ethanol-water-carbon dioxide mixtures at elevated pressures, *J. Chem. Eng. Data.* 31 (2002) 296–298. <https://doi.org/10.1021/JE00045A012>.
- [8] R. Vallejo, J. Gonzalez-Valdivieso, M. Santos, S. Rodriguez-Rojo, F.J. Arias, Production of elastin-like recombinamer-based nanoparticles for docetaxel encapsulation and use as smart drug-delivery systems using a supercritical anti-solvent process, *J. Ind. Eng. Chem.* 93 (2021) 361–374. <https://doi.org/10.1016/j.jiec.2020.10.013>.
- [9] L. Martín, F.J. Arias, M. Alonso, C. García-Arévalo, J.C. Rodríguez-Cabello, Rapid micropatterning by temperature-triggered reversible gelation of a recombinant smart elastin-like tetrablock-copolymer, *Soft Matter.* 6 (2010) 1121–1124. <https://doi.org/10.1039/b923684h>.
- [10] T. Flora, *Bioengineered dynamic systems based on elastin-like recombinamers*, Universidad de Valladolid, 2019. <https://doi.org/10.35376/10324/38770>.
- [11] J. Gonzalez-Valdivieso, *Advanced nanodevices based on Elastin-like Recombinamers as smart drug delivery systems for biomedical applications*, Universidad de Valladolid, 2020. <https://doi.org/10.35376/10324/43317>.
- [12] R. Louise Meyer, X. Zhou, L. Tang, A. Arpanaei, P. Kingshott, F. Besenbacher, Immobilisation of living bacteria for AFM imaging under physiological conditions, *Ultramicroscopy.* 110 (2010) 1349–1357. <https://doi.org/10.1016/j.ultramic.2010.06.010>.
- [13] M. Skliar, V.S. Chernyshev, Imaging of extracellular vesicles by atomic force microscopy, *J. Vis. Exp.* 2019 (2019). <https://doi.org/10.3791/59254>.
- [14] S. Akhtartavan, M. Karimi, K. Karimian, N. Azarpira, M. Khatami, H. Heli, Evaluation of a self-nanoemulsifying docetaxel delivery system, *Biomed. Pharmacother.* 109 (2019) 2427–2433. <https://doi.org/10.1016/j.biopha.2018.11.110>.

- [15] N. Angel Aillegas, L.I. Tártara, G. Caballero, V. Campana, D.A. Allemandi, S.D. Palma, Antioxidant status in rabbit aqueous humor after instillation of ascorbyl laurate-based nanostructures, *Pharmacol. Reports.* 71 (2019) 794–797. <https://doi.org/10.1016/j.pharep.2019.04.014>.
- [16] Methods for the Study of Irritation and Toxicity of Substances Applied Topically To the Skin and Mucous Membranes, *J. Pharmacol. Exp. Ther.* 82 (1944).



**RESULTS**

**&**

**DISCUSSION**



**CHAPTER 1:**

**ACETAZOLAMIDE**

**ENCAPSULATION WITH**

**ELASTIN LIKE**

**RECOMBINAMERS BY**

**SUPERCritical**

**ANTISOLVENT (SAS) PROCESS**

**FOR GLAUCOMA TREATMENT**





## **CHAPTER 1: ACETAZOLAMIDE ENCAPSULATION WITH ELASTIN LIKE RECOMBINAMERS BY SUPERCRITICAL ANTISOLVENT (SAS) PROCESS FOR GLAUCOMA TREATMENT.**

In this chapter, a new controlled release system based on elastin-like recombinamers (ELRs) has been developed using the Supercritical Antisolvent (SAS) technique employing supercritical CO<sub>2</sub> in a one-step process. The particulate system has been satisfactorily encapsulated in different ratios and has been characterized physically and chemically, finding the proportions of each compound, the stability of the particulate system in aqueous media and the topography of the particles. Drug release assays have been performed and they have provided valuable information about the solute transport mechanism. Finally, thanks to the collaboration with the Unidad de Investigación y Desarrollo en Tecnología Farmacéutica of the Universidad Nacional de Córdoba, Argentina, it has been possible to perform both *ex vivo* and *in vivo* assays of the formulations developed in this chapter.

## 6. RESULTS & DISCUSSION

### 6.1. Microencapsulation of ELR with acetazolamide

One of the most important factors when working with supercritical fluids is the correct choice of operating conditions, more specifically the choice of pressure and temperature. The study of the solubility curves of scCO<sub>2</sub>-solvent provides crucial information to select the experimental region of the diagram where both components are miscible and, therefore, stay in the single-phase area.

In this case, DMSO was chosen, a very versatile and powerful aprotic polar solvent classified by the European Medicines Agency (EMA) guidelines as a class 3 solvent [1] with low toxic potential and no health-based exposure limits. In addition, DMSO achieves high solubility of both ELRs and acetazolamide (AZM) (200 mg/mL and 100 mg/mL [2], respectively). Therefore, the study of the scCO<sub>2</sub>-DMSO solubility curves will be decisive for choosing the right pressure and temperature to carry out the experiments.

The scCO<sub>2</sub>-DMSO phase equilibria diagram for different temperatures was obtained from a bibliographic study (Figure 17 reproduced from [3]). In our case, we select a temperature of 308 K because it is moderate, easy to reach and maintain stable in the reactor. In the case of pressure, we should guarantee that we are above the solubility curve that marks the limit between the single-phase and two-phase areas. Therefore, a pressure of 11 MPa was chosen, so that possible pressure fluctuations in the system would not affect the solubility between scCO<sub>2</sub> and the DMSO.

The mass flow of scCO<sub>2</sub> was set at 2 kg/h and the solution flow at 0.5mL/min to ensure that there is a continuous supply of fresh CO<sub>2</sub> in the reactor. In addition, in order to remove as much residual DMSO as possible from the final product, after pumping the solution into the reactor, the particles retained in the filter were dried with fresh scCO<sub>2</sub> at a mass flow rate of 3kg/h during 2h.

To study the effect of the drug loading in the formulations in the ex vivo and in vivo

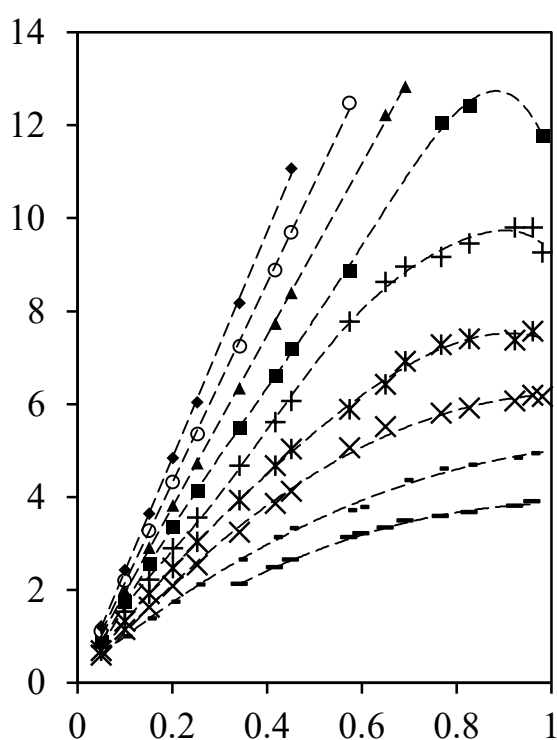


**Figure 17.** Isothermal P, x diagrams derived from the measured phase equilibrium isopleths. From lower to higher pressures the isotherms correspond to 278, 288, 298, 308, 318, 328, 338, 348 and 358 K. Reproduced from [2].

weight of (EI)2 and acetazolamide dissolved in DMSO in relation to the amount by weight of sample collected in the filter after SAS process. As it can be seen in Table 4 a slight increase in process yield was found when the AZM ratio increases with respect to

experiments, three different ratios of (EI)2:AZM (w/w) (1:1, 1:2 and 1:3) were tested. The corresponding amount of (EI)2 and AZM was dissolved in DMSO under magnetic stirring (1000 rpm) until the complete solution. As polymer production is limited, 600 mg was used in each experiment. Therefore, 20 mL of DMSO were finally used, resulting in final acetazolamide concentrations of 30, 60 and 90 mg/mL respectively.

The samples produced from each formulation were collected in the SAS pilot plant filter. The yield was calculated based on the amount by

(EI)2. This is due to the fact that there is a greater quantity in weight in each formulation and therefore it is possible to recover a greater quantity in each successive experiment.

| Formulation (EI)2:AZM | Concentration of AZM (mg/mL) | Yield (%) | DMSO (%) | AZM (%) | Average size ( $\mu\text{m}$ ) |
|-----------------------|------------------------------|-----------|----------|---------|--------------------------------|
| Control 1:0           | -                            | 46        | 7        | -       | 22 $\pm$ 12                    |
| 1:1                   | 30                           | 52        | 9        | 41      | 35 $\pm$ 8                     |
| 1:2                   | 60                           | 55        | 11       | 59      | 71 $\pm$ 16                    |
| 1:3                   | 90                           | 62        | 12       | 65      | 96 $\pm$ 26                    |

**Table 4.** Formulations of (EI)2 and AZM produced by SAS process under the selected experimental conditions. DMSO and AZM composition (% (w/w)) in each formulation was determined by NMR and power average size was analysed by SEM deviation by Mean  $\pm$ SD.

## 6.2. $^1\text{H-NMR}$ study for acetazolamide and ELR-Acetazolamide mixture.

In order to find the proportions of each component present in the final product obtained after the SAS technique, a  $^1\text{H-NMR}$  spectrum in  $\text{D}_2\text{O}$  was carried out for each sample. Firstly, we should know which are the signals in the spectrum that identify each compound and which are perfectly distinguishable from the rest of the compounds, so that we can quantify each component by the integral of the area under the corresponding signal. To do this, we use MestReNova to simulate the  $^1\text{H-NMR}$  spectrum of the acetazolamide molecule in  $\text{D}_2\text{O}$ .

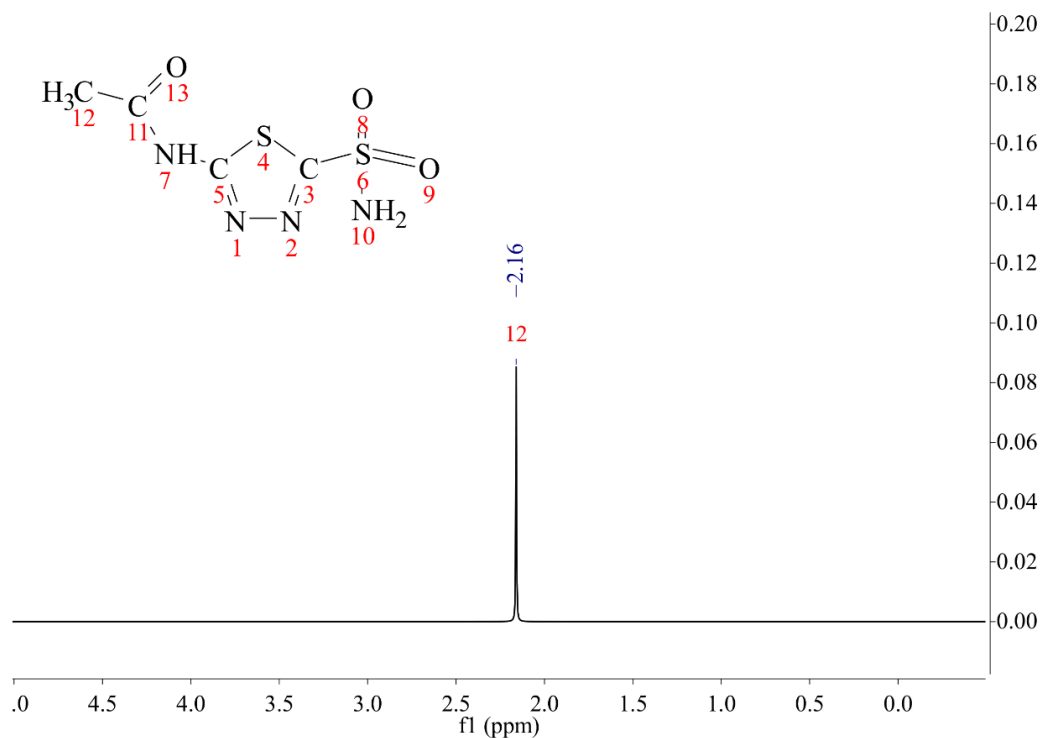


**Figure 18.**  $^1\text{H}$ -NMR predicted spectrum for acetazolamide in  $\text{D}_2\text{O}$ .

As it can be observed in Figure 18, one peak can be identified corresponding to the methyl group  $-\text{CH}_3$  (12) at 2.16 ppm. In order to identify acetazolamide in the final product, we should analyse the spectrum of the ELR (EI)2 used in this chapter in  $\text{D}_2\text{O}$  and superpose it with the acetazolamide predicted spectrum to check if there is any signal overlapping.

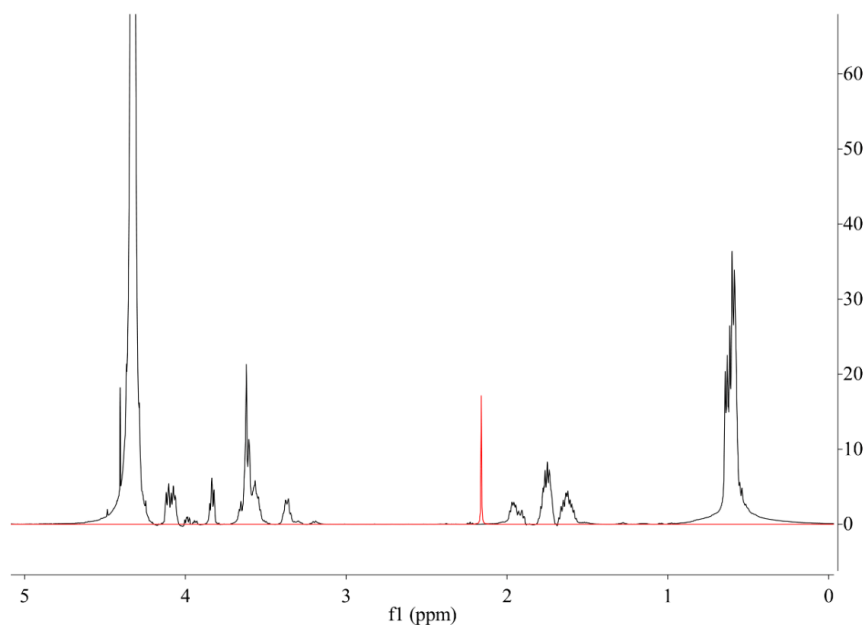


**Figure 19.**  $^1\text{H}$ NMR superposition spectra for (EI)2 (black) and acetazolamide prediction (red) in  $\text{D}_2\text{O}$ .

As we can see in Figure 19 the signal belonging to the methyl group that appears at 2.16 ppm corresponding to acetazolamide can be clearly differentiated from the rest of the ELR signals and thus its quantification is possible.

The samples obtained were analysed by  $^1\text{H}$ -NMR following the procedure described in the methods section 2.3.1. The signal belonging to the methyl groups of the ELR, whose integral value is known and corresponds to 2544 hydrogen protons, was taken as a reference. With the value of the integrals of the signals of each component obtained from the  $^1\text{H}$ NMR spectra of Figure 20, and knowing both the number of hydrogens involved in each signal and the molecular weight of each compound, proportions were calculated and values are shown in Table 4. An increase in residual DMSO is also observed as the concentration of AZM increases in each formulation. This fact suggests that, as the concentration is increased, the viscosity and surface tension of the solution is enhanced producing larger droplets [4]. These effects, together with the low volatility of DMSO, make it more difficult for  $\text{scCO}_2$  to remove the solvent completely because the mass transfer is lower when larger droplets are produced.

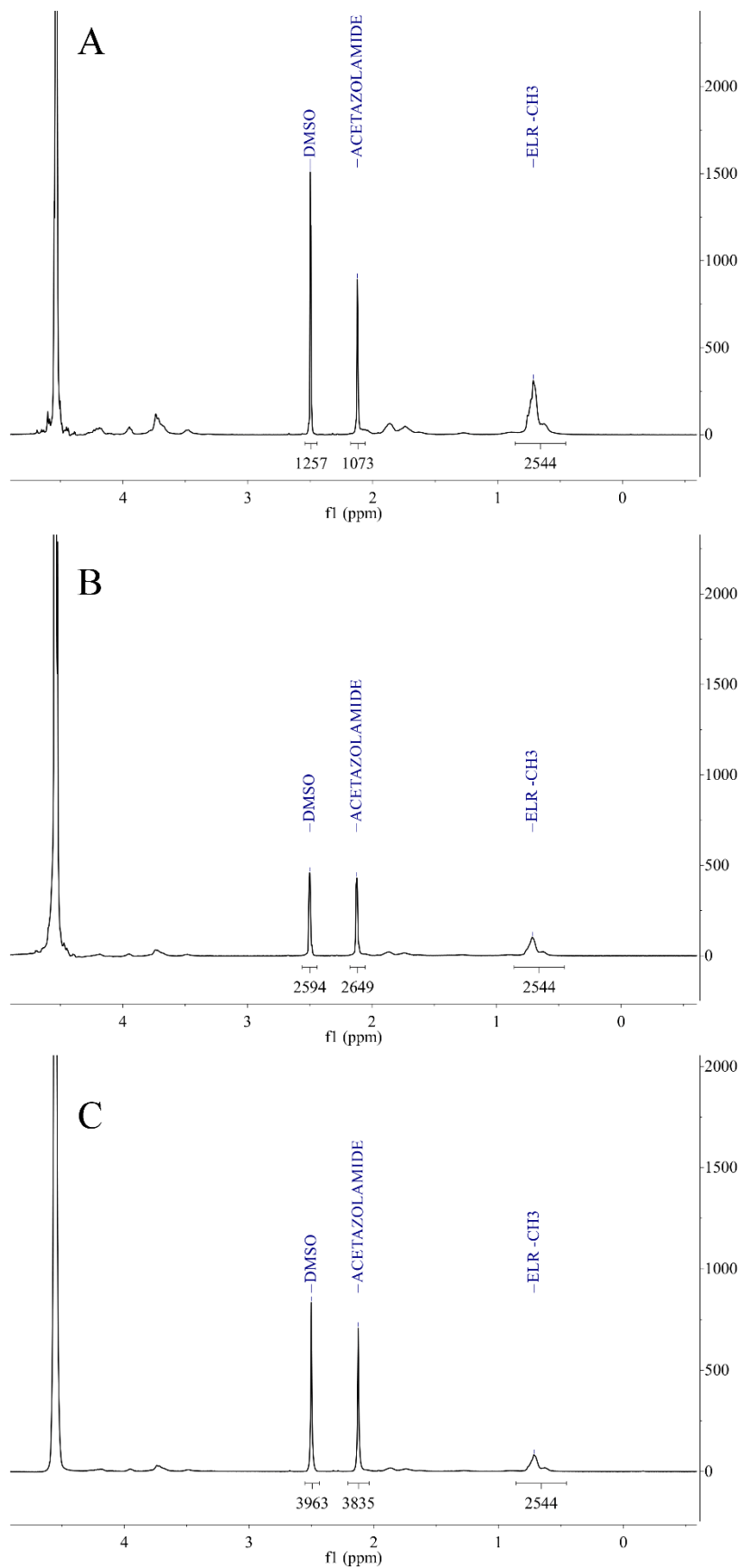


**Figure 20.**  $^1\text{H-NMR}$  of the samples after SAS process at different (EI)<sub>2</sub>:AZM ratios. A 1:1 ratio, B, 1:2 ratios, C 1:3 ratios.

### **6.3. Macroscopic characterization**

The powder collected after the SAS process was analysed by SEM. As it can be seen in Figure 21, in the general images reported, microspherical particles with no important aggregates have been found in the different formulations. An increase in size has been observed as the concentration of acetazolamide and therefore the ratio (EI)<sub>2</sub>:AZM increases (Table 4). This is due, as previously mentioned, to the increase in concentration that enhances viscosity and surface tension of the organic solution, but in addition, this increased concentration triggers an earlier supersaturation which results in faster nucleation, which reveals the influence of the on the initial concentration on the degree of supersaturation [5], [6], leading to produce larger droplets and, therefore, large particles as reported in Table 4. From a closer inspection in Figure 21, in the higher magnification photos, it can be observed a rough or crackled surface.



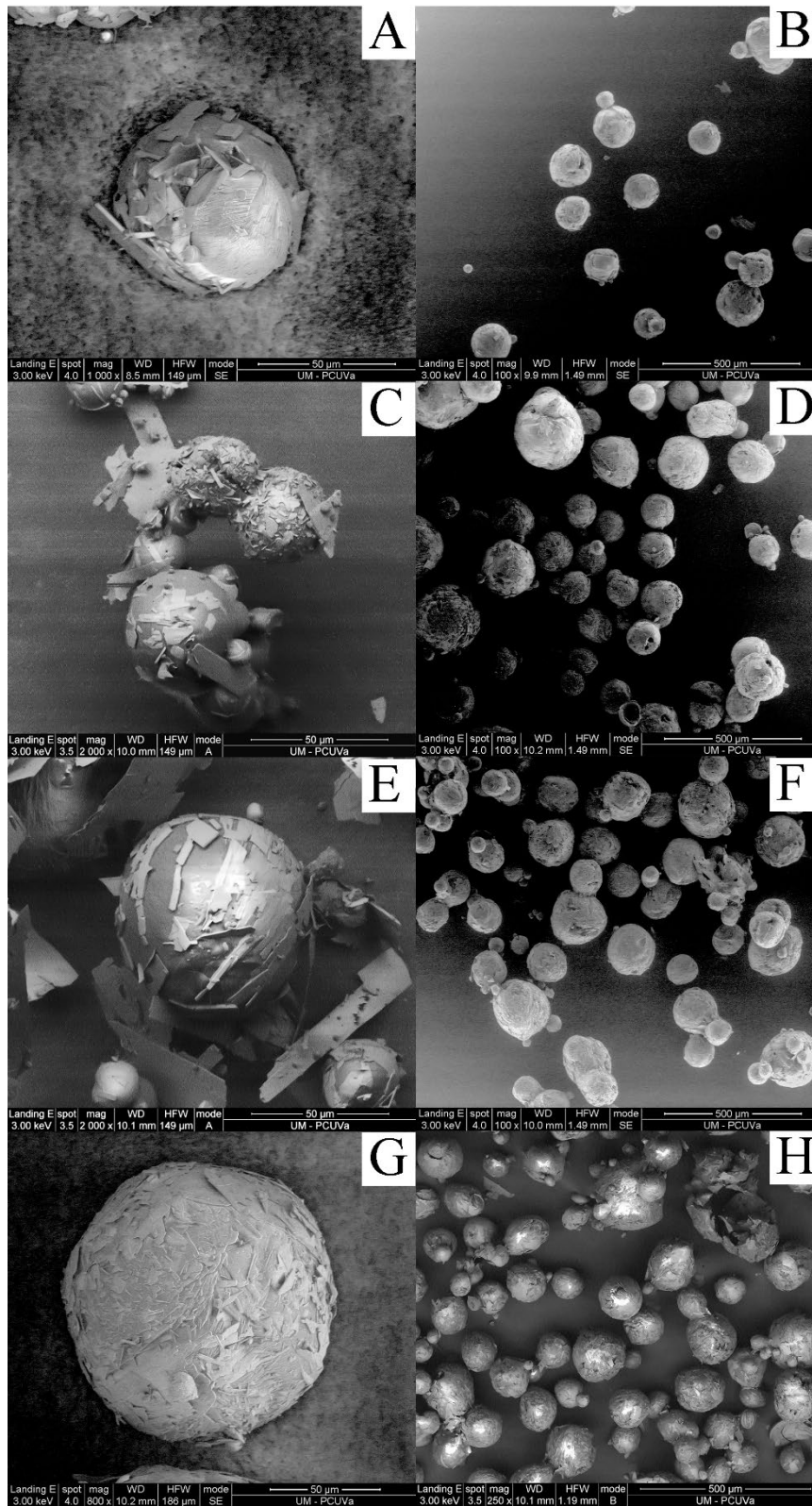


**Figure 21.** SEM Photomicrographs showing general (scale bar 500 $\mu\text{m}$ ; magnification x100 B, D F and x250 H) and detailed views (scale bar 50 $\mu\text{m}$ ; magnification x1000 A, x2000 C, E, and x800 G) from the formulations 1:0 A, B; 1:1 C, D; 1:2 E, F and 1:3 G, H.

#### **6.4. Behaviour in aqueous solution**

Once the macroscopic analysis of the different formulations obtained after the SAS process has been assessed, their behaviour in an aqueous solution is analysed. For this purpose, the particle size was measured by means of DLS during 30 days, as well as the surface charge ( $\zeta$ -potential) and the polydispersity index (PDI), in order to evaluate the stability of the particles. Table 2 shows  $\zeta$  -potential values, as well as the PDI and the particle size in percentage of intensity as D(0.5) value which represents the diameter where 50% of the distribution is below and 50% is above this value. As it can be seen from Table 2, aqueous suspensions of each formulation produce nearly monodisperse distributions since the PDI value is between 0.12 and 0.18, which means that the particle size distribution can be considered as monodisperse [7]. Regarding the  $\zeta$  -potential, this is maintained at values of -34mV during the 30 days of the assay, suggesting that the stability of the particles is guaranteed since the surface charge is high enough, as shown in Table 5, for the particle size to remain stable for 30 days.

| <b>Control (1:0)</b>   |                    |             |                         |                              |
|------------------------|--------------------|-------------|-------------------------|------------------------------|
| <b>Day</b>             | <b>D(0.5) (nm)</b> | <b>PDI</b>  | <b>ζ-Potential (mV)</b> | <b>TEM average size (nm)</b> |
| 0                      | 41±2               | 0.132±0.004 | -33±2                   | 27±2                         |
| 7                      | 42±1               | 0.138±0.003 | -34±1                   |                              |
| 30                     | 36±2               | 0.126±0.005 | -34±1                   |                              |
| <b>Formulation 1:1</b> |                    |             |                         |                              |
| 0                      | 42±1               | 0.155±0.008 | -33±1                   | 28±5                         |
| 7                      | 39±1               | 0.141±0.006 | -33±1                   |                              |
| 30                     | 41±1               | 0.146±0.013 | -33±1                   |                              |
| <b>Formulation 1:2</b> |                    |             |                         |                              |
| 0                      | 43±1               | 0.122±0.007 | -32±2                   | 32±5                         |
| 7                      | 44±1               | 0.133±0.006 | -33±2                   |                              |
| 0                      | 44±1               | 0.145±0.005 | -33±2                   |                              |
| <b>Formulation 1:3</b> |                    |             |                         |                              |
| 0                      | 43±2               | 0.122±0.004 | -34±1                   | 28±4                         |
| 7                      | 42±1               | 0.127±0.004 | -34±0                   |                              |
| 30                     | 41±2               | 0.180±0.007 | -34±1                   |                              |

**Table 5.** Values of the D(0.5), PDI, ζ –potential of the different formulations analysed and control sample during 30 days of stability assay at 37°C in PBS and neutral pH and TEM average size with deviation by Mean ±SD.

In order to check the results obtained by means of DLS, the different formulations were examined by transmission electron microscopy (TEM) (Figure 22). The TEM particle size reported in Table 5 for each formulation is in agreement with the results observed by DLS with small variations that may be due to the fact that two different techniques are being used and that the TEM measurement corresponds to a single day. It can also be seen in Figure 22 the non-formation of large aggregates which is in accordance with the PDIs reported in Table 5, which supports the stability of the particles in aqueous media.

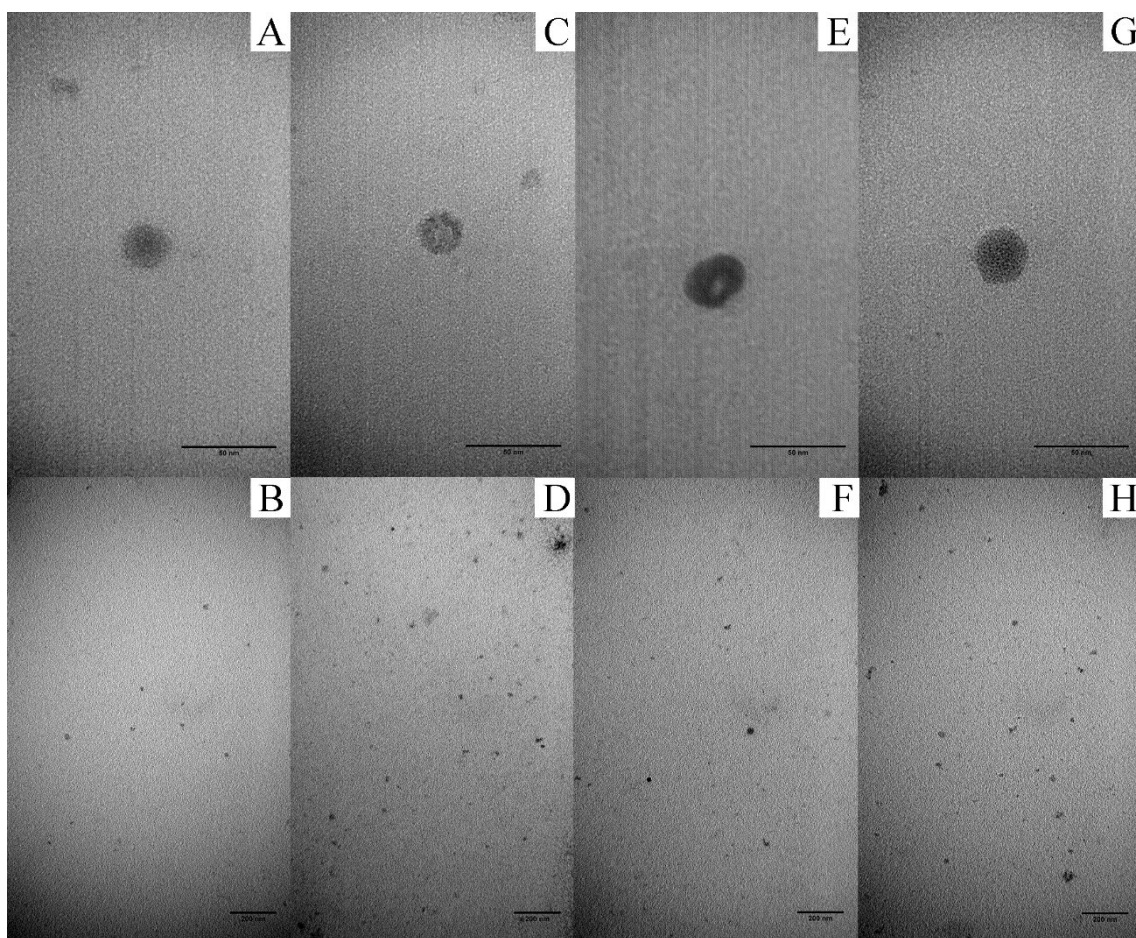


**Figure 22.** TEM photomicrographs of the formulations 1:0 (A, B), 1:1 (C, D), 1:2 (E, F), 1:3 (G, H) prepared at a concentration of 1 mg/mL in ultrapure deionized water with negative staining at neutral pH and room temperature (Scale bar: 50 nm A, C, E, G and 200 nm B, D, F, H).

## 6.5. Characterization of the formulations by Atomic Force Microscopy

In order to analyse the topography of the particles once dispersed in an aqueous medium and analysed dry and hydrated, we have used the AFM technique, which allows us to analyse the size of the particles with high resolution, obtaining images in the X, Y and Z axes (Figure 23 and Figure 24). In our case, as particles have a negative surface charge, as already verified by the Z-potential measurements, a positively charged NiCl<sub>2</sub> substrate was used to fix the particles following the method described in Materials and Methods section 5.3.8.

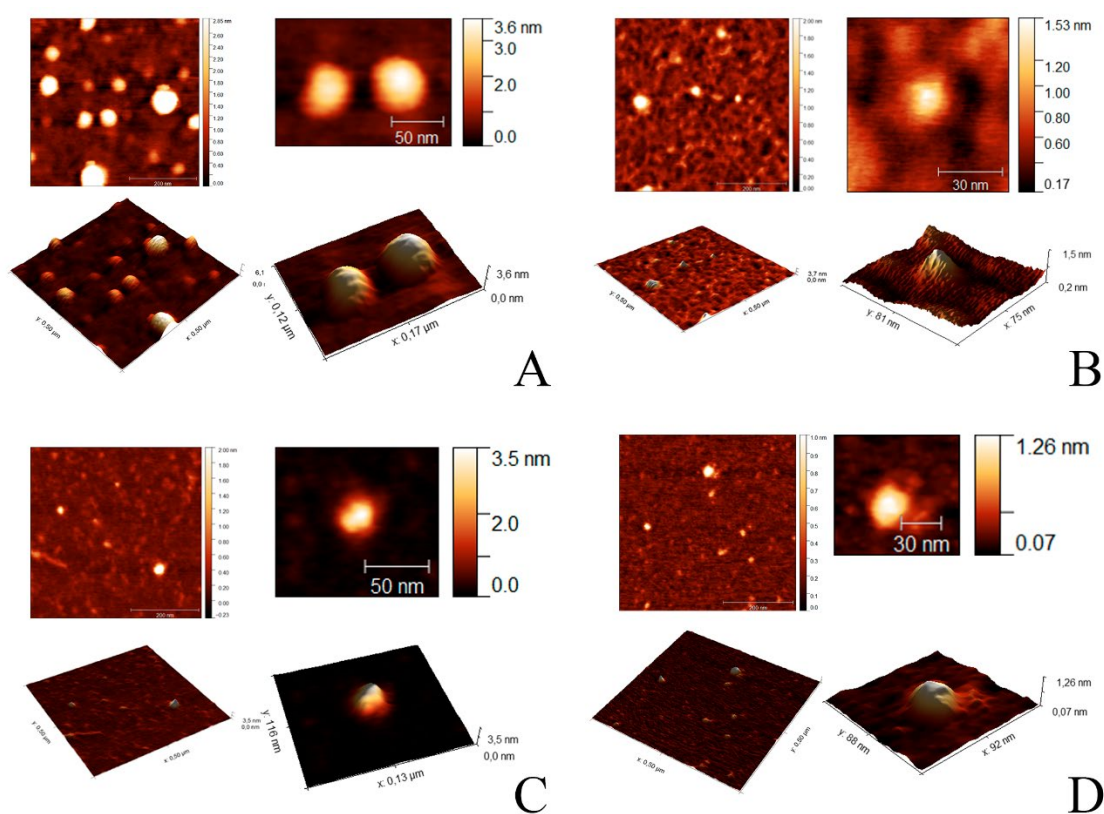


**Figure 23.** Images of the topography of the samples analysed by AFM at 512x512 pixels, scale bar for the general images correspond to 200nm. A control; B (EI)2:AZM 1:1, C (EI)2:AZM 2:1 D (EI)2:AZM 3:1

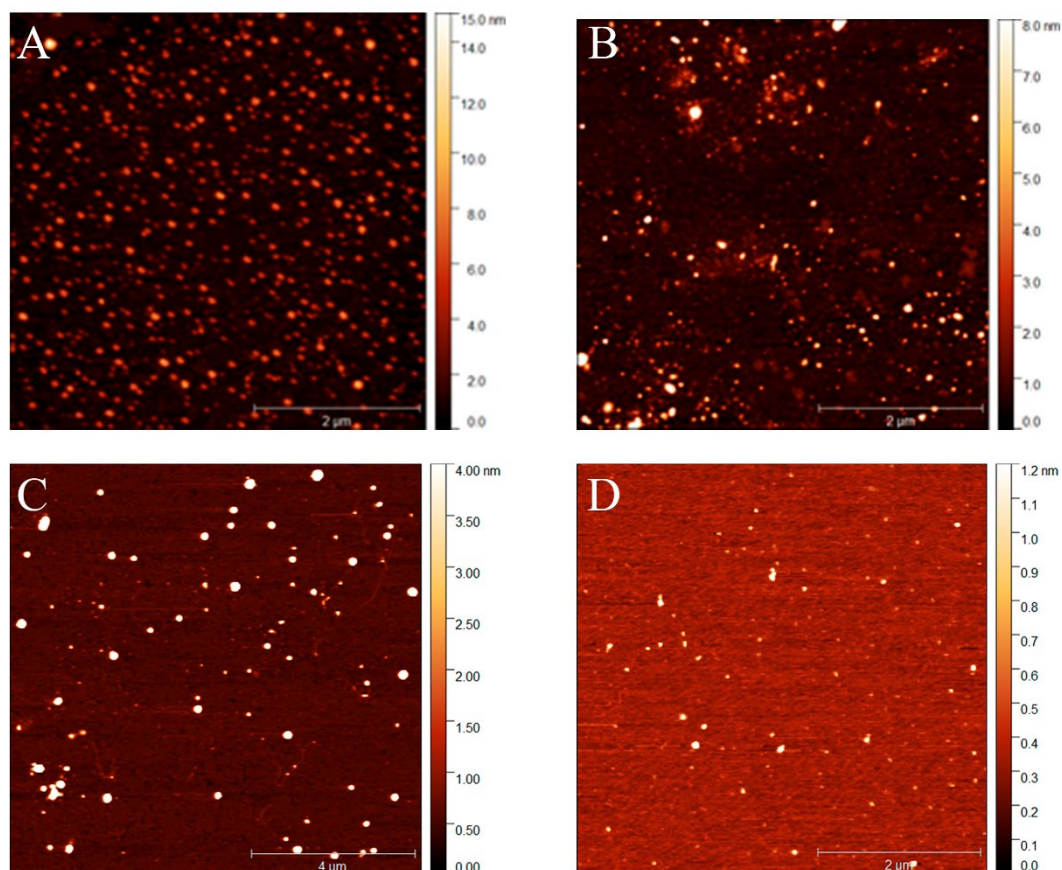


**Figure 24.** Images of the samples analysed by AFM at 512x512 pixels. A control, scale bar 2 $\mu$ m; B (EI)2:AZM 1:1, scale bar 2 $\mu$ m; C (EI)2:AZM 2:1, scale bar 4 $\mu$ m; D (EI)2:AZM 3:1, scale bar 2 $\mu$ m

Once the results have been collected (Table 6), there are two considerations. The first one concerns the values obtained on the Z-axis. These are the values measured in height and shown as D(0.5) or median of the distribution, in which values between 4 and 1 nm are observed. This is due to the fact that when the particles are deposited on the substrate and the liquid evaporates, the spherical particles are flattened as described in [8], decreasing their diameter along the Z-axis. The second consideration is a consequence of the first one, as the diameter in the Z-axis decreases and as a result of the flattening of the particles against the substrate, the diameter in the X- and Y-axis increases [8] [9]. In addition, the AFM tip that runs along the particle is not able to measure the edges perfectly, further

increasing the diameter in the X and Y axis [9]. This effect is observed in the values obtained for the equivalent square side (Table 6), which corresponds to the side of the square with the same projected area as the grain.

|                 | <b>X-Y axis values</b>             | <b>Z-axis values</b> |
|-----------------|------------------------------------|----------------------|
| <b>Sample</b>   | <b>Equivalent square side (nm)</b> | <b>D(0.5) (nm)</b>   |
| Control 1:0     | 60 ± 22                            | 4.4 ± 0.8            |
| Formulation 1:1 | 46 ± 24                            | 4.1 ± 1.4            |
| Formulation 1:2 | 61 ± 45                            | 3.4 ± 2.8            |
| Formulation 1:3 | 36 ± 13                            | 1.3 ± 0.3            |

**Table 6.** Particle size measured by AFM and analysed by Gwyddion 2.56 of the samples Control; Formulation 1:1; Formulation 1:2 and Formulation 1:3.

In addition, we observe how the values of the deviation of the equivalent square side are significantly high, which is due to a pile-up effect of the particles or due to high concentrations of particulate in some locations. For this reason, high deviation values are obtained, but if we examine the graphs showing the number of particles analysed according to their size (Figure 25), we can appreciate that the majority are located between 30 and 50 nm with tails in the distribution of regions of between 80 -150 nm, which means that even though these particles are in the minority, they increase the deviation of the total of the measurements.

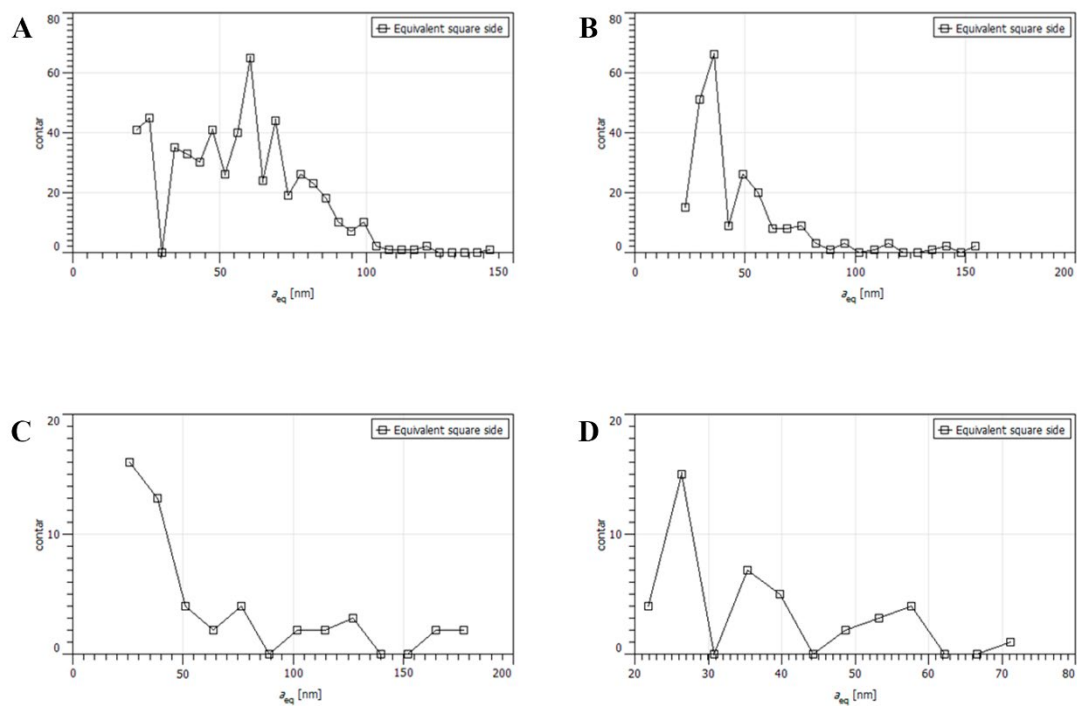


**Figure 25.** Size distribution of the particles counted in the AFM images analysed using Gwyddion 2.56 software. A, Control (1:0); B, (EI)2:AZM (1:1); C (EI)2:AZM (1:2) and D, (EI)2:AZM (1:3)

Thanks to the versatility of the AFM microscope, the different formulations were analysed in a hydrated state following the protocol described in Materials and Methods section 2.3.8. Figure 26 shows the images obtained for each of the formulations. Table 7 shows the results obtained, which show slightly smaller sizes than those obtained in the analysis of the dry samples and closer to the sizes observed by TEM.



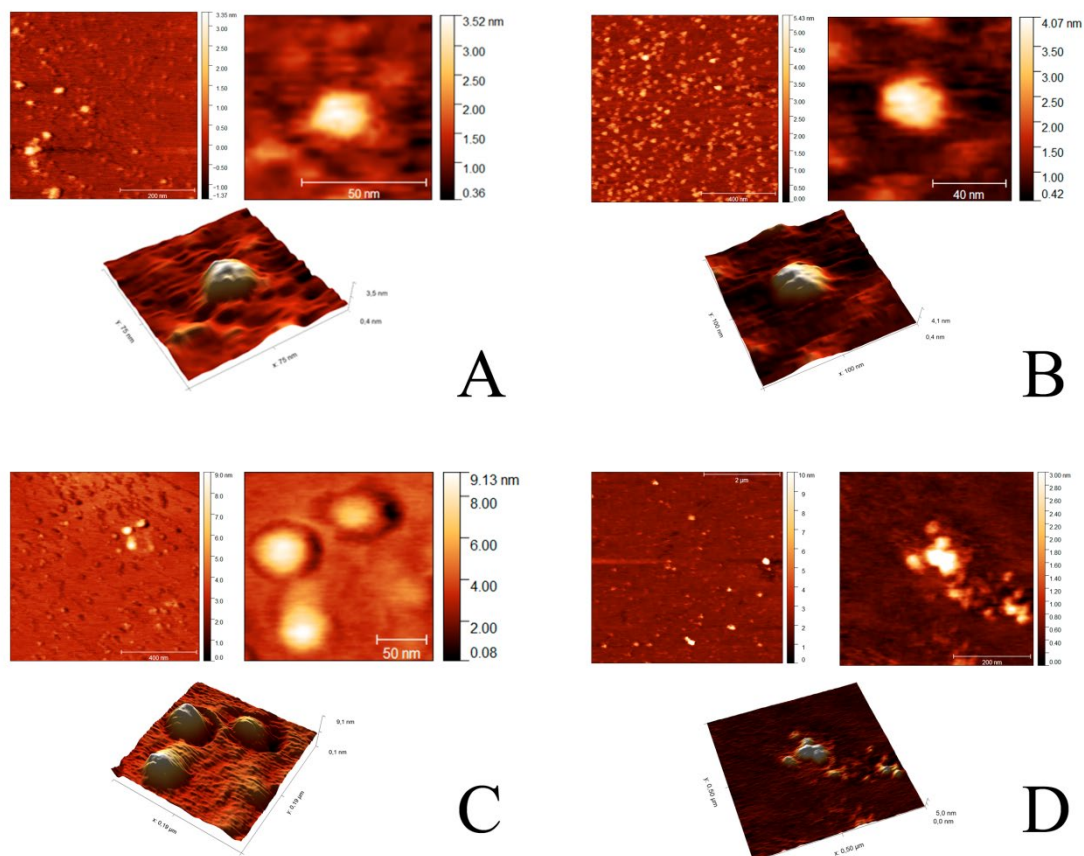


**Figure 26.** Images of the samples analysed by AFM in a hydrated state at 512x512 pixels. A control, general image scale bar 200nm, detailed image scale bar 50nm; B (EI)2:AZM 1:1, general image scale bar 400nm, detailed image scale bar 40nm, C (EI)2:AZM 1:2, general image scale bar 400nm, detailed image scale bar 50nm; D (EI)2:AZM 1:3, general image scale bar 2 $\mu$ m, detailed image scale bar 200nm.

| Sample      | X-Y axis values             |  | Z-axis values |
|-------------|-----------------------------|--|---------------|
|             | Equivalent square side (nm) |  | D(0.5) (nm)   |
| Control 1:0 | 38 $\pm$ 14                 |  | 0.9 $\pm$ 0.1 |
| (EI)2 1:1   | 28 $\pm$ 6                  |  | 6.9 $\pm$ 0.1 |
| (EI)2 1:2   | 47 $\pm$ 5                  |  | 6.2 $\pm$ 0.4 |
| (EI)2 1:3   | 52 $\pm$ 39                 |  | 4.6 $\pm$ 1.2 |

**Table 7.** Particle size measured by AFM and analysed by Gwyddion 2.56 of the samples Control; Formulation 1:1; Formulation 1:2 and Formulation 1:3.

This is due to the fact that when the particles are deposited on the substrate they undergo less flattening, these changes being observed in the height of the particles, which in this case is higher. However, high deviations are observed in the control sample and the 3:1 formulation due to particle agglomeration, causing the size distribution to widen. In spite of these phenomena, we can see in Figure 26 completely defined and clear topographies that constitute the different samples analysed, confirming that the formulations analysed comprise a monodisperse system of nanoparticles.

### **6.6. Drug delivery studies**

The formulations obtained using the SAS technique at the different ratios of (EI)2:AZM were tested for drug release over a period of 7h in PBS at a controlled temperature of 35°C. All formulations were standardised to an acetazolamide concentration of 1 mg/mL, as well as free acetazolamide.

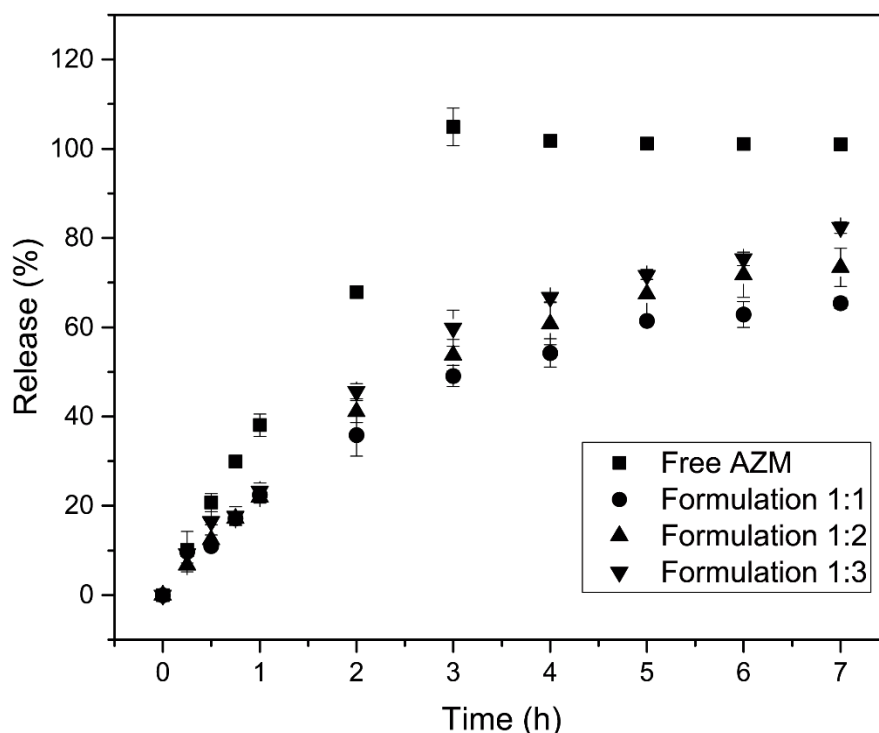


**Figure 27.** In vitro release profile of the free AZM (■) and (EI)2:AZM formulations 1:1 (●), 1:2 (▲), 1:3 (▼) in PBS at 35°C at a normalized concentration in AZM of 1 mg/mL. Results of the triplicate assay in each time point are presented as (Mean ±SD).

The release profiles in all the formulations studied (Figure 27) show how AZM is released in a prolonged manner for a period of 7 hours while a free AZM solution is completely solubilized in 3h. The % release is the same at the beginning of the experiment, but after two hours the % release is greater for the formulation with the higher AZM concentration (1:3). This trend is maintained until the end of the experiment; the % release for each formulation after 7 hours is 60, 75, and 80% (1:1, 1:2 and 1:3 respectively). This can be understood because when the ratio of AZM in the particles is lower, the drug has to cross more distance to reach the dispersing medium and therefore the mass transfer is lower, since the solute flow depends on the concentration gradient. Therefore, in more concentrated formulations, when the thickness of the polymer layer surrounding the drug is thinner, the mass transfer increases, achieving higher concentrations in the medium for the same period of time. Furthermore, we observe in the formulation analysed a release

profile with an ascending slope during the first 3h, which indicates that we have a controlled and prolonged release over time.

The release profiles corresponding to Figure 27 were fitted using the Peppas-Sahlin and Lindner-Lippold mathematical models described in the introduction (Eq 5 and Eq 7). As can be seen in Table 8, both models fit satisfactorily ( $R^2 > 0.980$ ), being slightly better for the Peppas-Sahlin model ( $R^2 > 0.994$ ).

| Formulation | Peppas-Sahlin model |       |      |       | Lindner-Lippold model |      |      |       |
|-------------|---------------------|-------|------|-------|-----------------------|------|------|-------|
|             | $k_1$               | $k_2$ | $n$  | $R^2$ | $k_1$                 | $b$  | $n$  | $R^2$ |
| 1:1         | 24.4                | -2.3  | 0.85 | 0.997 | 25.7                  | -2.3 | 0.53 | 0.982 |
| 1:2         | 30.2                | -2.9  | 0.82 | 0.998 | 31.6                  | -3.2 | 0.52 | 0.981 |
| 1:3         | 28.5                | -2.5  | 0.86 | 0.994 | 30.5                  | -3.2 | 0.55 | 0.981 |

**Table 8.** Fitting of the release profiles, for the (EI)2:AZM formulations 1:1, 1:2 and 1:3 for in vitro assays, to the Peppas-Sahlin and Lindner-Lippold equation.

Furthermore, we can see that the coefficient  $n$  of the Peppas-Sahlin equation takes values between  $0.43 < n < 0.85$ , which suggests an anomalous release mechanism in which the delivery process is governed by Fickian diffusion since ' $k_1$ ' is the parameter that has more weight in the equation for all the adjusted formulations. In addition, the values of ' $n$ ' were found to correspond to spheres geometry, which is in agreement with the particles observed by TEM (**Figure 22**) and AFM (Figure 23, Figure 24, Figure 26). If we look at the Lindner-Lippold adjustment, we can observe that the value of parameter  $b$  (burst effect) takes negative values, indicating that the drug is encapsulated inside the particles.

### 6.7. *Ex vivo* studies of the acetazolamide formulations

*Ex vivo* studies were conducted by Dra. Daniela A. Quinteros at the Unidad de Investigación y Desarrollo de Tecnología Farmacéutica (UNITEFA) of the Universidad Nacional de Córdoba, Argentina.

### 6.7.1. Transcorneal permeation study

The transcorneal permeation of the drug through the cornea of *ex vivo* rabbits is studied for the different formulations obtained in this chapter, as well as for the free AZM used as a control. All formulations, as well as the control, were dispersed in PBS at 35°C at a standardised acetazolamide concentration of 1 mg/mL.

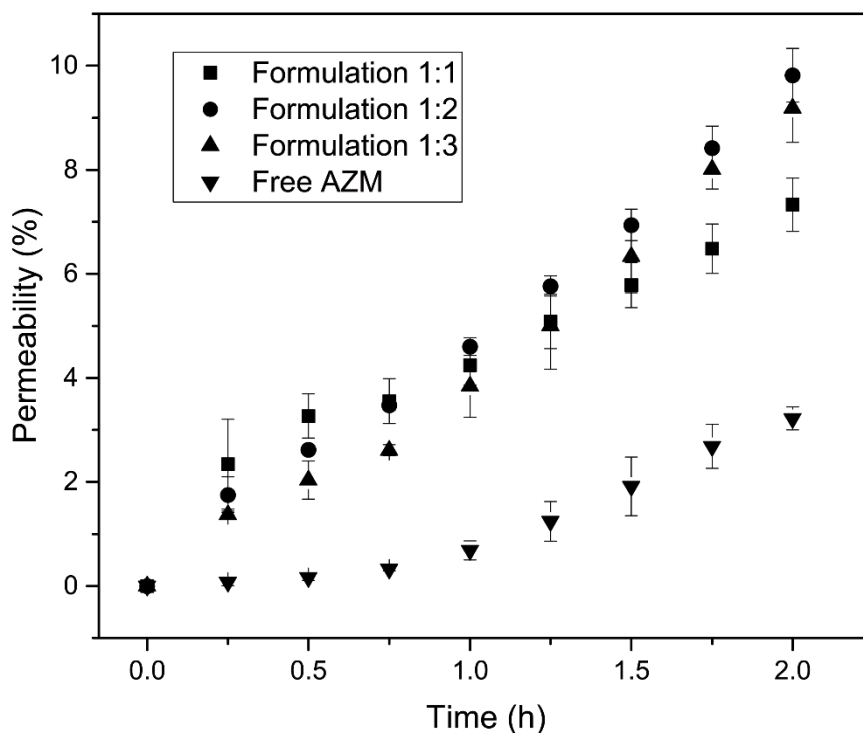


**Figure 28.** Ex vivo permeability profile for AZM from the formulations analysed (E1)2:AZM 1:1 (■); 1:2 (●); 1:3 (▲) and free AZM (▼) in PBS at 35°C and at a normalized concentration of acetazolamide of 1 mg/mL. Results of the triplicate assay in each time point are presented as (Mean  $\pm$ SD). Reproduced from [10]

Figure 28 shows the results of the transcorneal permeation test, in which, it can be observed that all the formulations evaluated show a level of permeation through the cornea about 10% higher than the acetazolamide solution used as control, reaching a difference of more than 30% after 2h. Furthermore, Table 9 shows that the flow rate is about 3 times higher for the different formulations when compared to the control solution. On the other hand, the same trend was found when analysing the apparent coefficient of

permeability ( $P_{aap}$ ) values, which is higher for the 1:2 and 1:3 formulations. This result indicates that (EI)2 biopolymer not only increases the solubility of the drug but also acts as an absorption promoter.

|               | Flow (J)        | Apparent Permeability coef. ( $P_{aap}$ ) $\times 10^{-04}$ | permeated AZM( $\mu$ g) (2h) |
|---------------|-----------------|---|------------------------------|
| (EI)2:AZM 1:1 | $0.59 \pm 0.02$ | $5.9 \pm 0.2$   | $73 \pm 5$                   |
| (EI)2:AZM 1:2 | $0.98 \pm 0.04$ | $9.8 \pm 0.4$   | $92 \pm 7$                   |
| (EI)2:AZM 1:3 | $0.98 \pm 0.06$ | $9.8 \pm 0.6$   | $98 \pm 5$                   |
| Free AZM      | $0.45 \pm 0.06$ | $4.5 \pm 0.6$   | $32 \pm 2$                   |

**Table 9.** Flow, apparent permeability coefficient and permeated AZM for the formulations of (EI)2-AZM at 1:1, 1:2 and 1:3 ratios and for the free AZM solution at a normalized concentration of 1 mg/mL in AZM. Reproduced from [10]

## 6.8. *In vivo* studies of the acetazolamide formulations

*In vivo* studies were conducted by Dra. Daniela A. Quinteros at the Unidad de Investigación y Desarrollo de Tecnología Farmacéutica (UNITEFA) of the Universidad Nacional de Córdoba, Argentina

### 6.8.1. Intraocular pressure *in vivo* assay

Intraocular pressure-lowering studies were performed in a hypertensive ocular model in rabbits, to evaluate the *in vivo* performance of EI2:AZM. The effect of the AZM formulations described in this study was compared using three parameters reported in Table 10: -the maximum hypotensive effect of the drug (% compared to baseline), -the area under the  $\Delta$ PIO curve (%) as a function of time (h) from 0 to 7 hours (AUC) and - the average duration of the effect obtained. In relation to this, all the formulations described in this work showed the ability to decrease more markedly and sustainably the IOP compared to the free drug solution, reaching a maximum IOP reduction of  $42 \pm 7$  %

for (EI)2: AZM 1:1. Conversely, AZM solution reached a maximum IOP reduction of  $25 \pm 7\%$ .

| Formulations   | Average duration of the effect (h) | Max reduction IOP. % | AUC%               |
|----------------|------------------------------------|----------------------|--------------------|
| Free AZM       | 4.5                                | $25.15 \pm 7.48$     | $89.95 \pm 29.70$  |
| (EI)2: AZM 1:1 | 6.0                                | $42.00 \pm 5.16$     | $178.80 \pm 26.03$ |
| (EI)2: AZM 1:2 | 6.0                                | $40.20 \pm 3.13$     | $162.21 \pm 12.82$ |
| (EI)2: AZM 1:3 | 6.0                                | $37.60 \pm 2.30$     | $145.83 \pm 14.84$ |

**Table 10.** Average duration of the effect, Maximum reduction IOP. ( $\% \pm SD$ ), and the area under the  $\Delta$ PIO curve (AUC) ( $\% \pm SD$ ) for each test formulation (EI)2: AZM 1:1, 1:2 and 1:3 and Free AZM at a normalized concentration of 1 mg/mL in AZM. Reproduced from [10]

The area under the curve (AUC) values were greater (practically two times more for the more effective formulation, (EI)2: AZM 1:1) for the three systems evaluated compared to the AZM solution. Figure 29 shows a greater hypotensive effect in absolute values in the formulations studied in the first 7 hours. As seen in the release profiles, 65% of AZM free is released at 2h, but only 3% is permeated. Whereas in the formulations analysed, after 2 hours, 40% is released, but 10% of the active compound is permeated. Therefore, the controlled release system allows AZM to be released slowly, permeating a greater amount of the active compound thanks to the interaction between the polymer and the biological membrane; Thus, a higher drug bioavailability allows decreasing more effectively IOP during the 7 hours of the experiment.

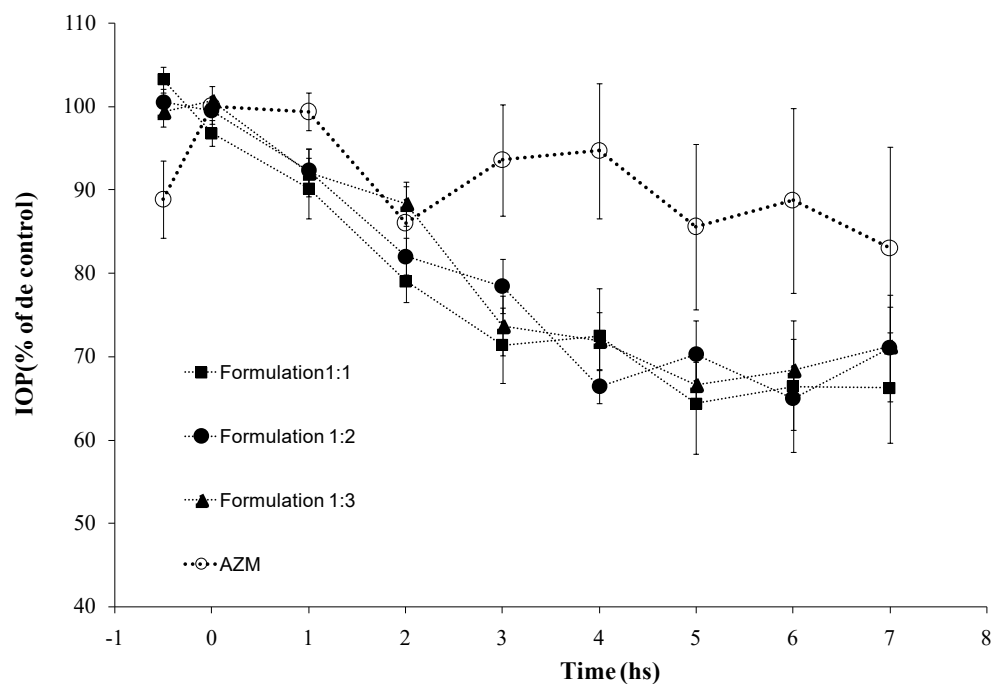


**Figure 29.** IOP profiles of the hypertensive ocular model in rabbits treated by (EI)2:AZM 1:1 (■). 1:2 (●). 1:3 (▲). Free AZM (○) at a normalized concentration of 1 mg/mL in acetazolamide. Reproduced from [10]

Currently, treatment to reduce IOP is performed using Diamox [11], the active ingredient of which is acetazolamide, in 125 and 250 mg tablets. Depending on the initial IOP, a reduction of 20-30% is achieved and the maximum IOP reduction is reached with oral administration of 250 mg four times a day or 500 mg twice a day. These high amounts of active agents are associated with the side effects caused by the treatment. However, the significant reduction in IOP found in the formulations evaluated in this work suggests that this new ELR-based controlled release system produced by SAS and administered topically is, a priori, more effective.

### 6.8.2. Ocular irritation tests

The eye is constantly exposed to the environment and is therefore vulnerable to any physical or chemical agent that may cause alterations, damage or loss of vision depending on the degree of severity it causes. For these reasons, it is essential to estimate as



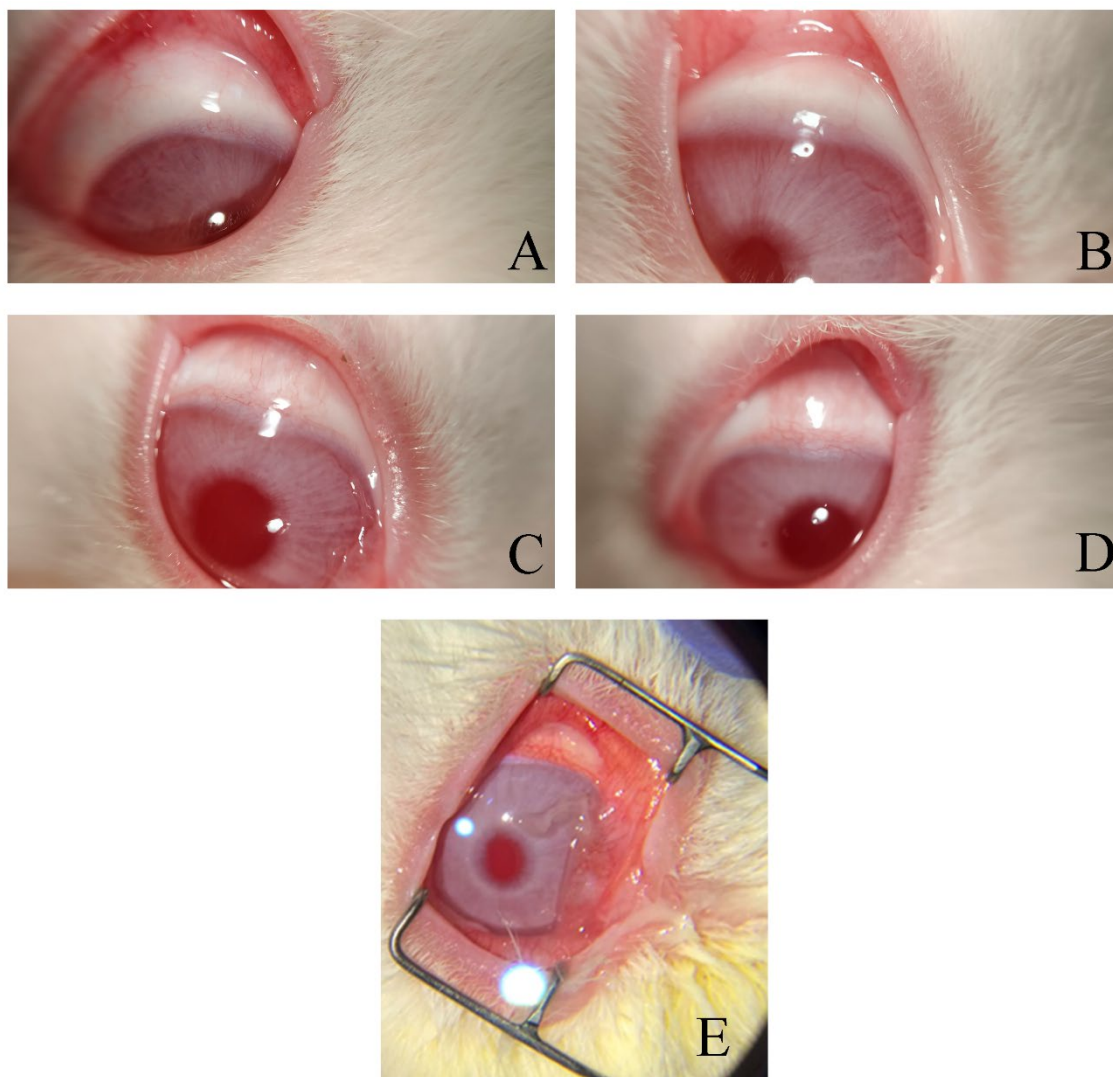
rigorously as possible the irritant potential of any compound that may come into contact with the eye and its adjacent structures. Therefore, the preferred scenario occurs when the lowest level of irritation is induced when a new formulation is applied to the eye. In this sense, and in order to meet this requirement, the new formulations, when applied topically, should have a pH close to neutral or iso-osmotic as well as the tear fluid. In our case, as it can be seen in Table 7, the formulations obtained in this work have a pH close tear fluid (pH 6.5 to 7.6) [12], [13], and osmolarity (304 to 310 Osmol) [14] which, in a first approximation, leads us to think that the irritant effect that may be caused in contact with the eye will be practically negligible.

Table 11 shows the results of the irritation test during the 7h exposure of the different formulations. The sum of the values established for each symptom observed during the test shows the score value obtained in each measurement. Sodium lauryl sulphate (SLS 2%) has been used as a positive control as it is a well-known anionic surfactant mainly used in hygiene and cosmetic products and is known to cause eye irritation [15] (Figure 30E) which reveals redness and oedema of the bulbar and palpebral conjunctiva, with increased mucous secretion.

| Formulation (EI)2 :AZM | pH          | Osmolality (Osmol/kg) | Evaluation of irritation (time h) |   |   |   |
|------------------------|-------------|-----------------------|-----------------------------------|---|---|---|
|                        |             |                       | 1                                 | 2 | 4 | 7 |
| 1:1                    | 7.25 ± 0.08 | 300 ± 1               | 1                                 | 0 | 0 | 0 |
| 1:2                    | 7.37 ± 0.19 | 277 ± 4               | 0                                 | 1 | 0 | 0 |
| 1:3                    | 7.34 ± 0.04 | 304 ± 2               | 0                                 | 1 | 1 | 0 |
| NaCl (0.9%)            | 6.82 ± 0.02 | 298 ± 1               | 1                                 | 0 | 0 | 0 |
| SLS (2%)               | -           | -                     | 8                                 | 8 | 3 | 2 |

**Table 11.** Osmolality and Ocular irritation after 7h of exposure of the formulations (EI)2 :AZM (1:1;1:2 and 1:3) at a normalized concentration of 1mg/mL of acetazolamide, NaCl (0.9%) and sodium lauryl sulfate (SLS 2%). . Reproduced from [10]

Nevertheless, all the formulations have scored values between 0 and 2, which implies that can be considered as non-irritant. This suggests, on the one hand, that the formulations will not cause ocular alterations or damage (Figure 30) and, on the other hand, that the small amount of residual DMSO present in the formulations has no adverse effects on the ocular surface, which makes these devices safe for topical administration.



**Figure 30.** Photographs illustrating the absence of eye irritation in rabbits evaluated within the first hour of treatment. A NaCl (0.9%) B EI2: AZM 1:1, C EI2: AZM 1:2, D EI2: AZM 1:3, at a normalized concentration of 1mg/mL in AZM, E sodium lauryl sulfate (SLS 2%). Reproduced from [10]

## 6.9. Final remarks

A hydrophobic drug such as acetazolamide, used in the treatment of glaucoma, was successfully encapsulated using the SAS technique and supercritical CO<sub>2</sub> in a one-step process, maintaining safe levels of residual solvent in accordance with current EMA and FDA regulations [1]. In addition, it has been possible to encapsulate different drug ratios, which has allowed us to analyse a wide range of doses. As a result of the physical characterisation, it has been found that the release system is stable over time and shows a controlled release of AZM governed by Fick diffusion, with no burst release demonstrating that the drug is encapsulated inside the particles.

After characterisation of the particles based on ELRs, a transcorneal permeation study was performed where it has been found that the apparent permeation coefficient increases for the release system compared to a simple drug solution, indicating that the biopolymer acts as an adsorption promoter. Furthermore, the effect on intraocular pressure was tested *in vivo* in hypertensive rabbits where it has been found a higher ocular bioavailability and a higher hypotensive effect in terms of maximum IOP reduction and also in terms of drug bioavailability (expressed as AUC<sub>(0-12)</sub>) compared to the control solution, resulting in a decrease in IOP of almost double compared to the control solution, as well as sustained over time. Finally, the ocular irritation test shows that the formulations analysed in this work do not cause ocular irritation, indicating, that the release system does not produce any alterations or damage to the ocular surface. Therefore, this new release system produced by the SAS technique, and based on ELRs, has been applied for the treatment of glaucoma and has successfully shown to be efficient in reducing IOP and to be safe for topical administration.

**6.10. REFERENCES**

- [1] EMA, “ICH Q3C (R6) Residual solvents | European Medicines Agency,” 2013. <https://www.ema.europa.eu/en/ich-q3c-r6-residual-solvents>.
- [2] Lawrence H. Keith and Douglas B. Walters, *National Toxicology Program’s Chemical Solubility Compendium*, 1<sup>o</sup> edition. CRC Press, 1991.
- [3] A. E. Andreatta, L. J. Florusse, S. B. Bottini, and C. J. Peters, “Phase equilibria of dimethyl sulfoxide (DMSO) + carbon dioxide, and DMSO + carbon dioxide + water mixtures,” *J. Supercrit. Fluids*, vol. 42, no. 1, pp. 60–68, 2007, doi: 10.1016/j.supflu.2006.12.015.
- [4] M. Kalani and R. Yunus, “Application of supercritical antisolvent method in drug encapsulation: a review.,” *International journal of nanomedicine*, vol. 6. pp. 1429–1442, 2011, doi: 10.2147/ijn.s19021.
- [5] F. Miguel, A. Martín, T. Gamse, and M. J. Cocero, “Supercritical anti solvent precipitation of lycopene: Effect of the operating parameters,” *J. Supercrit. Fluids*, vol. 36, no. 3, pp. 225–235, Jan. 2006, doi: 10.1016/j.supflu.2005.06.009.
- [6] A. Z. Chen *et al.*, “Application of organic nonsolvent in the process of solution-enhanced dispersion by supercritical CO<sub>2</sub> to prepare puerarin fine particles,” *J. Supercrit. Fluids*, vol. 49, no. 3, pp. 394–402, Jul. 2009, doi: 10.1016/j.supflu.2009.02.004.
- [7] J. Stetefeld, S. A. McKenna, and T. R. Patel, “Dynamic light scattering: a practical guide and applications in biomedical sciences,” *Biophysical Reviews*, vol. 8, no. 4. pp. 409–427, 2016, doi: 10.1007/s12551-016-0218-6.
- [8] M. Skliar and V. S. Chernyshev, “Imaging of extracellular vesicles by atomic force microscopy,” *J. Vis. Exp.*, vol. 2019, no. 151, 2019, doi: 10.3791/59254.
- [9] Y. G. Kuznetsov and A. McPherson, “Atomic Force Microscopy in Imaging of Viruses and Virus-Infected Cells,” *Microbiol. Mol. Biol. Rev.*, vol. 75, no. 2, pp. 268–285, Jun. 2011, doi: 10.1128/membr.00041-10.
- [10] R. Vallejo, D. A. Quinteros, S. Rodriguez-Rojo, M. Santos Garcia, S. D. Palma, and F. J. Arias Vallejo, “acetazolamide encapsulation with elastin like recombinamers by supercritical antisolvent (sas) process for glaucoma treatment (to be submitted to International Journal of Nanomedicine).”
- [11] I. P. Kaur, R. Smitha, D. Aggarwal, and M. Kapil, “Acetazolamide: Future perspective in topical glaucoma therapeutics,” *International Journal of Pharmaceutics*, vol. 248, no. 1–2. Elsevier, pp. 1–14, Nov. 06, 2002, doi: 10.1016/S0378-5173(02)00438-6.
- [12] S. Ligório Fialho and A. da Silva-Cunha, “New vehicle based on a microemulsion for topical ocular administration of dexamethasone,” *Clin. Exp. Ophthalmol.*, vol. 32, no. 6, pp. 626–632, 2004, doi: 10.1111/j.1442-9071.2004.00914.x.
- [13] M. Ahuja, A. S. Dhake, S. K. Sharma, and D. K. Majumdar, “Topical ocular delivery of NSAIDs,” *AAPS Journal*, vol. 10, no. 2. pp. 229–241, 2008, doi: 10.1208/s12248-008-9024-9.
- [14] A. Tomlinson, S. Khanal, K. Ramaesh, C. Diaper, and A. McFadyen, “Tear film osmolarity: determination of a referent for dry eye diagnosis,” *Invest. Ophthalmol. Vis. Sci.*, vol. 47, no. 10, pp. 4309–4315, Oct. 2006, doi: 10.1167/IOVS.05-1504.
- [15] C. A. M. Bondi, J. L. Marks, L. B. Wroblewski, H. S. Raatikainen, S. R. Lenox, and K. E. Gebhardt, “Human and Environmental Toxicity of Sodium Lauryl Sulfate (SLS): Evidence for Safe Use in Household Cleaning Products,” *Environ. Health Insights*, vol. 9, p. 27, 2015, doi: 10.4137/EHL.S31765.

**CHAPTER 2:  
PRODUCTION OF ELASTIN-  
LIKE RECOMBINAMERS-  
BASED NANOPARTICLES FOR  
DOCETAXEL  
ENCAPSULATION AND USE AS  
SMART DRUG-DELIVERY  
SYSTEMS USING A  
SUPERCRITICAL ANTI-  
SOLVENT PROCESS.**



## **CHAPTER 2: PRODUCTION OF ELASTIN-LIKE RECOMBINAMERS-BASED NANOPARTICLES FOR DOCETAXEL ENCAPSULATION AND USE AS SMART DRUG-DELIVERY SYSTEMS USING A SUPERCRITICAL ANTI-SOLVENT PROCESS.**

In this chapter, DTX has been successfully encapsulated in ELR microparticles by SAS using DSMO as solvent. In this work, the SAS equipment has been modified and a co-axial nozzle has been implemented to reduce the residual solvent, without compromising the precipitation yield. Therefore, a series of experiments have been carried out to set up the installation with the new modifications in order to find the most suitable operating conditions. The results obtained show a stable nanoparticulate system suitable for use as a controlled release device. Finally, thanks to the collaboration with Dr Juan González Valdivieso, Smart Devices for NanoMedicine Group, Universidad de Valladolid *in vitro* cell assays have been performed.

## 7. RESULTS & DISCUSSION

### 7.1. Optimization of the supercritical antisolvent process (SAS)

A schematic representation of the supercritical antisolvent process pilot plant, and its modifications (red lines), used to encapsulate docetaxel in ELRs is shown in Figure 31.

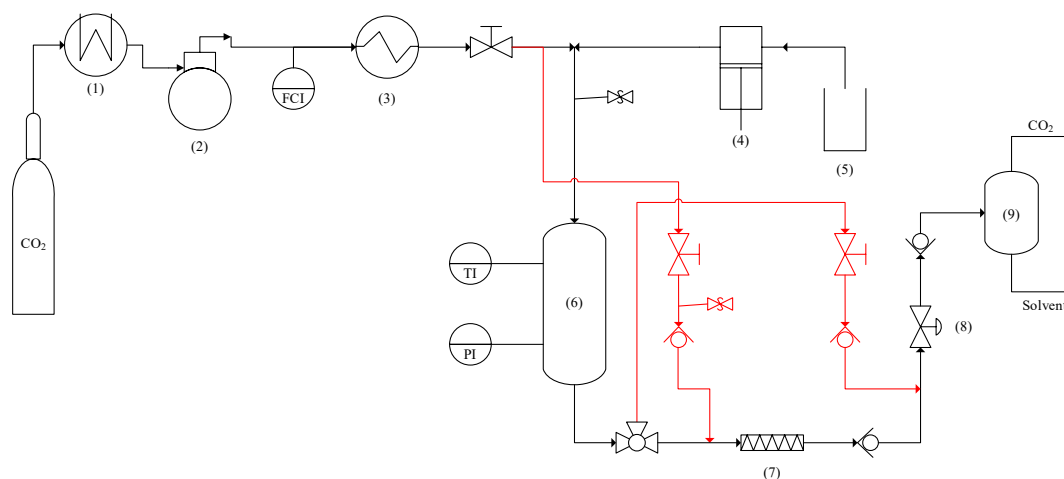


**Figure 31.** Schematic flow diagram of the SAS pilot plant. (1) cooler, (2) CO<sub>2</sub> pump, (3) heater, (4) chromatographic pump, (5) solution, (6) precipitator vessel, (7) filter, (8) back-pressure valve, (9) separator. Red lines represent the bypass modification implemented in the pilot plant according to method 2.

The installation was modified in order to reduce the drying times and to decrease the amount of residual solvent. To this end, a bypass line was implemented to dry the precipitated product directly on the filter (Figure 31) and a coaxial nozzle was designed to allow the solution to be sprayed into the reactor with smaller droplet size.

Nozzles for specific high-pressure processes are currently designed to allow high flows due to their industrial applications (painting, high-pressure washing, etc.). The SAS pilot plant was originally equipped with a non-coaxial nozzle, which basically comprised a 1/16" pipe with 0.020" ID (Figure 32A); the scCO<sub>2</sub> was pumped into the vessel through a small opening of 1/4". To improve the spraying process, the solution of drug and polymer is typically pumped through a coaxial nozzle [1]–[3] in order to generate smaller particle sizes and to enhance mass transfer [4] between the solution and the scCO<sub>2</sub>. As such, a new nozzle was designed with features more appropriate for the characteristics of



the process. To that end, fused deposition modelling (FDM) 3D printing was selected as the manufacturing technique since it allows pieces to be prototyped more cheaply and easily than other techniques, such as CNC machining, and, in addition, allows complex geometries to be manufactured. Furthermore, design improvements can be made in a short period of time. Polyoxymethylene (POM) was chosen to manufacture the nozzle since this material allows a wide range of working temperatures (between  $-40$  and  $90$  °C), has high mechanical strength, rigidity and hardness, as well as high shock resistance, excellent dimensional stability, and can be purchased cheaply.

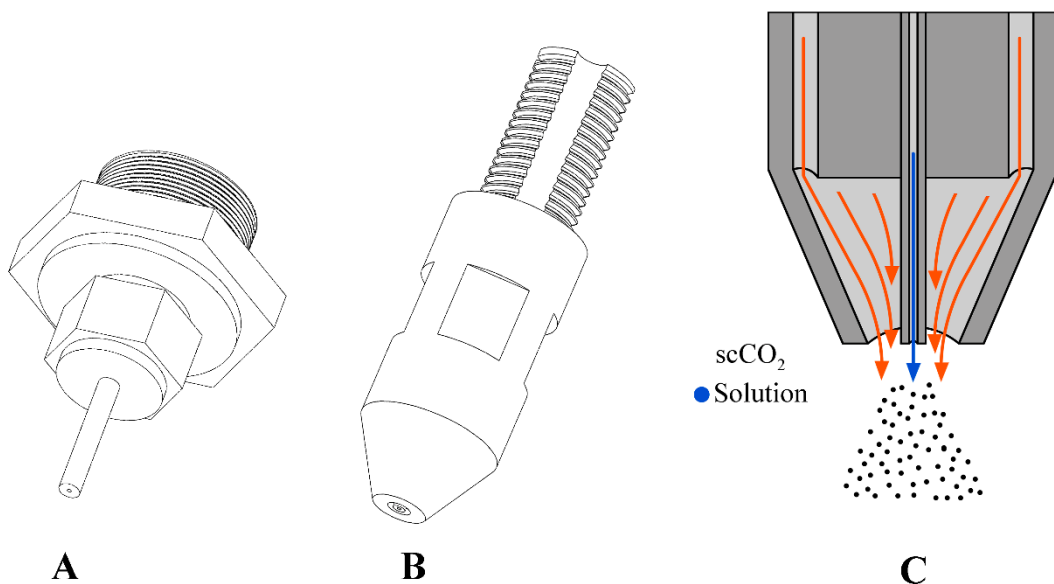


**Figure 32.** Representation of the different nozzles used in this thesis: A: non-coaxial nozzle (Chapter 1), B: Coaxial nozzle (Chapters 2 & 3) and C: Representation of operation mode with the coaxial nozzle.

The new nozzle (Figure 32 B, C and blueprints and dimensions in Annex I) contains four grooves around a central cylinder that can be threaded into the top cover of the reactor, and a central hole through which a 1/16" stainless steel 0.020" ID pipe is inserted, which can be interchanged with another one of higher or lower ID. In this way, the scCO<sub>2</sub> at the

desired flow produces the spray of the pumped solution, which always encounters fresh scCO<sub>2</sub> at the tip of the nozzle.

The procedure was optimized with (EI)2 ELR (400 mg in each experiment) to determine the appropriate nozzle design (coaxial or non-coaxial; Figure 32) and drying process. The influence of pressure (9.5-11.0 MPa) and ELR concentration (15-40 mg/mL of (EI)2) was also studied. Three **drying methods** were employed: In method 1, particles were dried in the reactor at 2 kg/h scCO<sub>2</sub> mass flow for 2 h; in method 2, a bypass line was implemented (Figure 31 red lines) and the particles kept in the filter were dried for 15 min at 2 kg/h scCO<sub>2</sub> mass flow; and in method 3, the reactor was flushed for 45 min at 2 kg/h scCO<sub>2</sub> mass flow, and then the particles retained by the filter were dried for 15 min at the same scCO<sub>2</sub> mass flow.

The ELR concentration was fixed originally at 30 mg/mL and the operating temperature was established as 308K since this moderate temperature does not induce thermal degradation and is above the transition temperature for the ELR, in addition to being easy to reach and maintain. In the initial experiments (1-6, Table 12), the pressure was fixed at 11 MPa to remain in the single-phase area according to the DMSO:scCO<sub>2</sub> solubility diagram [5] established in Chapter 1.

| Exp. | Drying Method | (EI)2 (mg/mL) | Nozzle Design | Drying Bypass | P (MPa) | DMSO (%)        | Yield (%)   | SEM Average size ( $\mu\text{m}$ ) |
|------|---------------|---------------|---------------|---------------|---------|-----------------|-------------|------------------------------------|
| 1    | 1             | 30            | No coaxial    | No            | 11.0    | *16.0 $\pm$ 1.4 | *39 $\pm$ 6 | 18 $\pm$ 14                        |
| 2    | 1             | 30            | Coaxial       | No            | 11.0    | *6.0 $\pm$ 1.0  | *56 $\pm$ 2 | n/d                                |
| 3    | 2             | 30            | Coaxial       | Yes           | 11.0    | 1.0             | 35          | n/d                                |
| 4    | 3             | 30            | Coaxial       | Yes           | 11.0    | *2.4 $\pm$ 1.2  | *69 $\pm$ 1 | 10 $\pm$ 5                         |
| 5    | 3             | 15            | Coaxial       | Yes           | 11.0    | 3.0             | 53          | 13 $\pm$ 8                         |
| 6    | 3             | 40            | Coaxial       | Yes           | 11.0    | 3.0             | 18          | 10 $\pm$ 5                         |
| 7    | 3             | 30            | Coaxial       | Yes           | 9.5     | 3.0             | 46          | 9 $\pm$ 4                          |

**Table 12.** Screening experiments to select operating conditions for the SAS process. Experimental conditions, final \*DMSO composition (% (w/w)  $\pm$ SD) in the powder obtained (determined by NMR), SEM average size ( $\mu\text{m}$   $\pm$  SD) and process \*yield (%  $\pm$  SD); n/d: not determined

The effect of using a simple or co-axial nozzle was analysed in experiments 1 and 2 under the conditions of drying method 1, as previously described. Thus, the use of the new coaxial nozzle results in a decrease in the amount of residual DMSO from 16% to 6%, as well as an increase in the yield from 39% to 56%. This could be explained because the coaxial nozzle enhances spraying by generating smaller droplets, thereby improving the mass transfer between  $\text{scCO}_2$  and the solution and meaning that supersaturation is greater and is reached faster and more evenly.

To reduce the amount of residual DMSO as much as possible, an improvement in the pilot plant was done in experiment 3 by including a new stream (red line in Figure 31) to dry the precipitated powder retained by the filter with fresh  $\text{scCO}_2$  according to method 2. The amount of DMSO was reduced to 1%, although the process yield was seriously compromised. This may be because most of the particles were not dragged down during the process and were not retained by the filter as expected. To solve this problem, experiment 4 included a step of flushing the reactor with fresh  $\text{scCO}_2$  after pumping the solution (drying method 3). As can be seen from Table 12, residual DMSO only increased

to 2.4% and the process yield was not compromised, as found for experiment 3. After considering these results, and to study the repeatability of the process, experiments 1, 2 and 4 were performed in triplicate. As can be seen from Table 12, in terms of yield, the results show good reproducibility, with deviations of less than 3% when the coaxial nozzle was employed. However, the deviation for the residual DMSO content in experiment 4 is high (50%), although the maximum DMSO content is well below that achieved with experiment 2.

To check the effect of ELR concentration on the process, experiments 5 and 6 (method 3), in which less concentrated and more concentrated solutions were studied, respectively, were performed. As shown in Table 12, values are not different taking into account the deviation of the measurements. In the case of experiment 6, a marked decrease in process yield was also observed upon increasing the concentration. The effect of pressure was determined in experiment 7 using the conditions of experiment 4 but operating at 9.5 MPa. As can be seen from Table 12, the process yield was lower than in experiment 4 and the quantity of residual DMSO was higher. This could be because this operating point is close to the solubility curve of the scCO<sub>2</sub>-DMSO phase diagram and the precipitation process is limited by the mass transfer of CO<sub>2</sub> into DMSO. In this case, the supersaturation of the solute is reached slowly, which results in higher residual DMSO content. In the case of higher pressure, saturation occurs very rapidly and mass transfer is enhanced, thus resulting in lower DMSO content [6].

In summary, we can conclude that the best-operating conditions for this process are 11 MPa, 308K, solution concentration of 30 mg/mL, coaxial nozzle and drying method 3.

## **7.2.Characterization of the particles obtained after SAS process**

### **7.2.1. Characterization of the particles by SEM**

The powder obtained in experiments 1, 4, 5, 6 and 7 were analysed by SEM. The images from experiments 1 and 4 can be seen in Figure 33, which shows that the particles produced during these experiments do not exhibit any marked aggregation and have a smooth surface with many small particles stuck to them, thus resulting in a broad particle-size distribution (Table 12).

When compared with experiment 4, the only notable changes in particle size and dispersity were observed for the non-coaxial nozzle used in experiment 1 (Table 12, Figure 33 A and B). The former produces smaller particle size and dispersity thanks to the use of the coaxial nozzle, which enhances the spraying homogeneity, thereby producing smaller droplets of the solution inside the reactor and allowing greater mass transfer between the scCO<sub>2</sub> and the solvent, thus meaning that supersaturation is greater and is reached faster and more evenly.

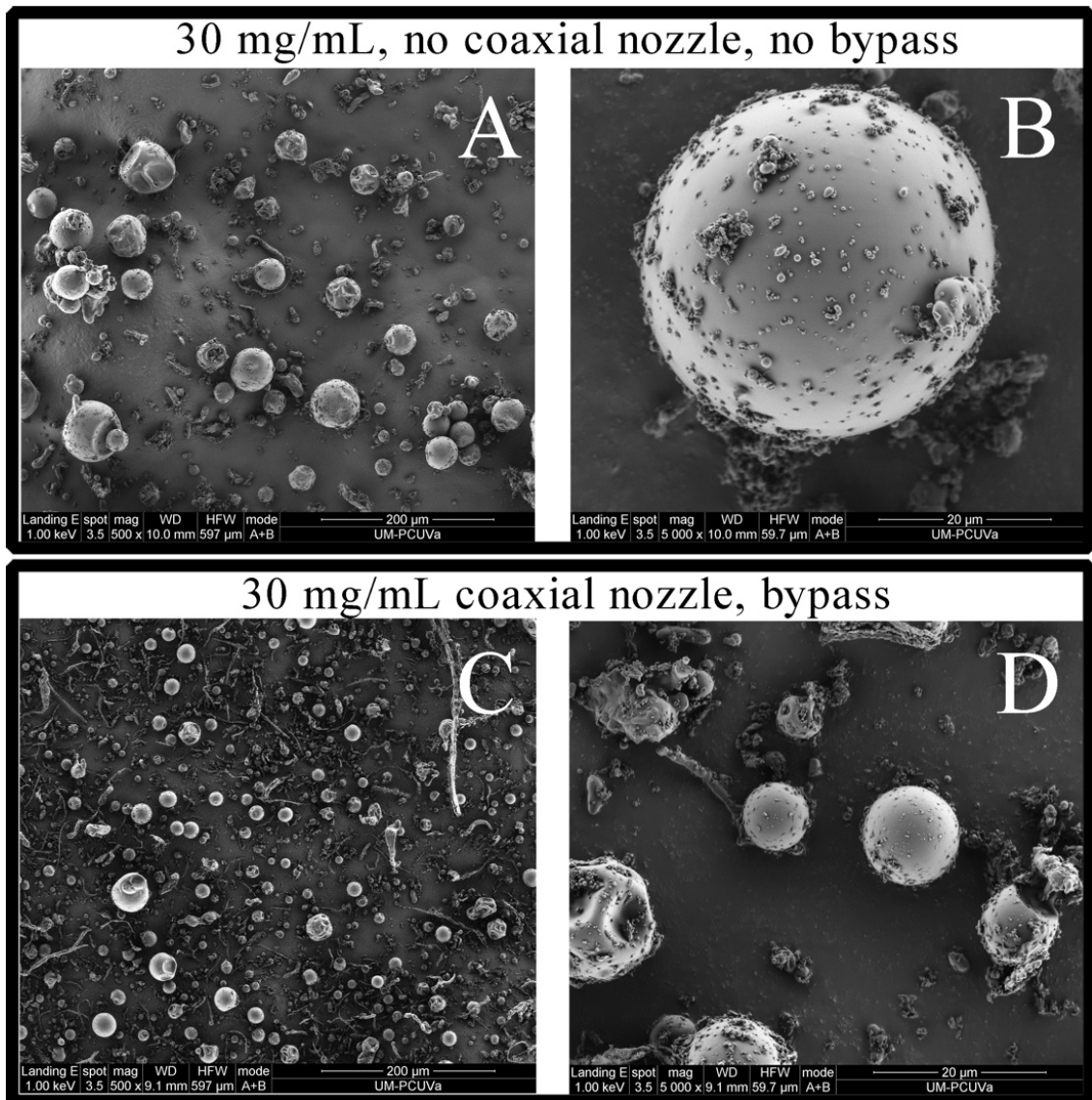


**Figure 33.** SEM Photomicrographs showing general (scale bar: 200  $\mu$ m; magnification: x500; A, C) and detailed views (scale bar: 20  $\mu$ m; magnification: x5000; B, D) for the powder obtained in experiment 1 (A and B) with no coaxial nozzle and using method 1, and experiment 4 (C and D) with coaxial nozzle and using drying method 3

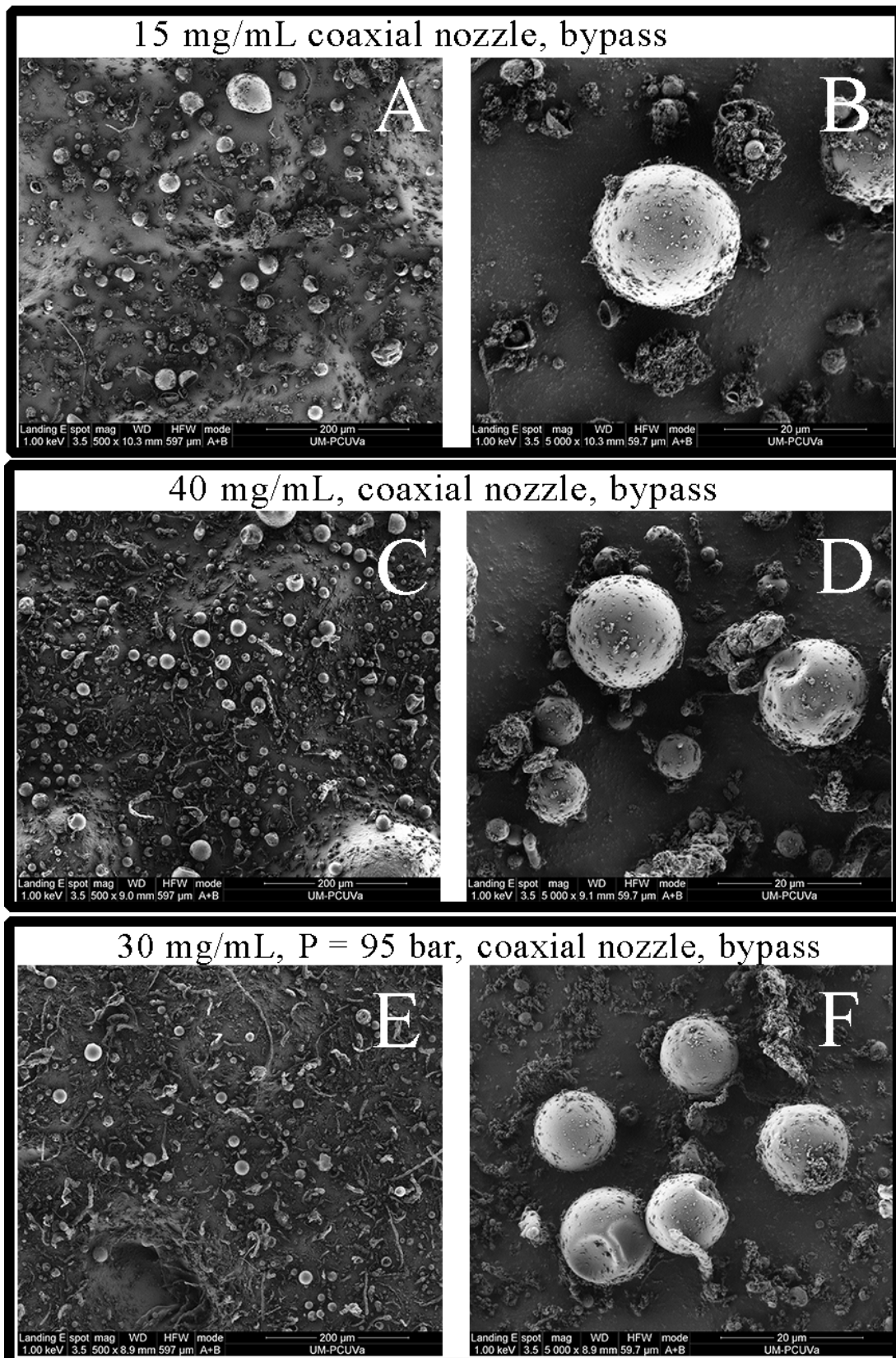


**Figure 34.** SEM Photomicrographs showing general (scale bar: 200μm; magnification: x500; A, C, E) and detailed views (scale bar: 20μm; magnification: x5000; B, D, F) views from experiments 5, 6 and 7

Once the coaxial nozzle and drying method had been established, it was found that, upon decreasing the concentration (experiment 5, Table 12, Figure 34 A, B), higher particle size was found compared with experiments 4 and 6 (Figure 34 C, D). This effect can be explained by the fact that the higher concentration enhances supersaturation, thus causing faster and more homogenous nucleation, which results in smaller particle sizes and therefore a more uniform particle size.

The effect of pressure was analysed in experiment 7 (Table 12, Figure 34 E, F), with no significant changes in particle size compared to experiment 4 being found even though a decrease in pressure has been reported to produce bigger particles due to a decrease in scCO<sub>2</sub> density [7]. Particles with a similar size to those in experiment 4 were found, with an average particle size of 10 µm for the samples produced using the coaxial nozzle and high concentration.

### **7.2.2. Behaviour in aqueous solution**

The self-assembling nature of ELR molecules in an aqueous solution above  $T_t$  is governed by the hydrophobic-hydrophilic balance of the block copolymer structure in a bottom-up process, from molecular size to nanosize. Similarly, ELRs from SAS-microparticles should undergo a temperature-driven process to generate particles in an aqueous solution. The microparticles obtained after the SAS process (Table 12) were dispersed at 37°C, as described in the Materials and Methods section, and analysed by dynamic light scattering (DLS; Table 13). The resulting values were then compared with those obtained for the unprocessed (EI)<sub>2</sub>, which was solubilized at 4°C and then incubated at 37°C, to determine whether the SAS process has any effect on the behaviour of the ELRs.



| Experiment | D(0.5) (nm) | PDI           | $\zeta$ -Potential (mV) |
|------------|-------------|---------------|-------------------------|
| 1          | 43 ± 14     | 0.100 ± 0.009 | -34.6 ± 0.4             |
| 2          | 44 ± 18     | 0.113 ± 0.003 | -33.4 ± 0.7             |
| 3          | 51 ± 21     | 0.147 ± 0.003 | -33.1 ± 1.6             |
| 4          | 44 ± 18     | 0.128 ± 0.005 | -34.2 ± 0.8             |
| 5          | 43 ± 14     | 0.120 ± 0.005 | -35.1 ± 1.7             |
| 6          | 40 ± 15     | 0.134 ± 0.003 | -33.6 ± 0.6             |
| 7          | 37 ± 12     | 0.119 ± 0.004 | -32.8 ± 0.4             |
| (EI)2      | 41 ± 6      | 0.030 ± 0.003 | -35.4 ± 1.4             |

**Table 13.** Values for the diameter D (0.5) and polydispersity index (PDI), determined from the intensity vs. measured size data obtained by DLS, and  $\zeta$ -potential for samples derived from each experiment described in Table 12. (EI)2 corresponds to the ELR solution with no SAS processing.

As shown in Table 13, the sizes of each sample are quite similar, which implies that the SAS process does not affect the structure or behaviour of the polymer in an aqueous medium above  $T_t$  and there are no marked differences between the transition temperatures (Table 14, Figure 35) for the processed samples and the unprocessed ELR even when comparing experiments 1 and 4 (the product of experiment 1 contains around three times more residual DMSO than that from experiment 4). As such, it is clear that neither processing with  $scCO_2$  or the quantity of residual DMSO found in the samples affects the thermal behaviour of the ELRs.

| Sample | pH   | $\Delta H$ (J·g <sup>-1</sup> ) | $T_t$ (°C) |
|--------|------|---------------------------------|------------|
| Exp. 1 | 7.22 | -8.92                           | 16.52      |
| Exp. 4 | 6.92 | -8.62                           | 16.56      |
| (EI)2  | 7.49 | -8.76                           | 16.50      |

**Table 14.** Transition temperatures and enthalpy for the processed ELR from experiments 1 and 4 and (EI)2 without SCF processing, as measured by DSC.

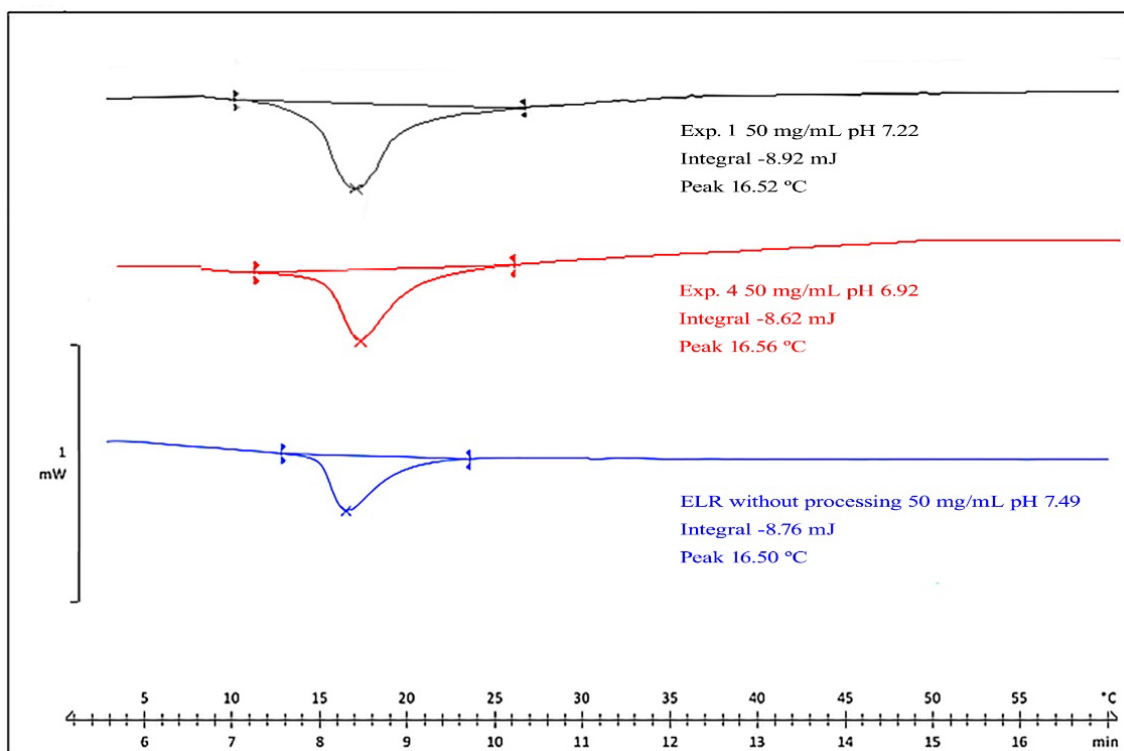


**Figure 35.** DSC thermograms for heating cycle (5°C/min from 0°C to 60°C) for unprocessed (blue), (EI)2 from experiment 1 (black) and experiment 4 (red) at 50 mg/mL and pH 7.

As can be seen from Table 13, aqueous suspensions of the processed particles always produced nearly monodisperse distributions since the PDI value is between 0.1 and 0.7 [8] but clearly higher than the value for (EI)2 without SAS processing (PDI 0.030). This may occur because the nanoparticle formation process starts from microscale structure and goes from higher to lower scale giving a little more heterogeneous sizes instead of the bottom-up process of the molecular self-assembling. As such, the process gives better homogeneous associations when the process starts from a molecular structure thereby giving lower PDIs. Moreover, the  $\zeta$ -potential results show that ELRs produced using the SAS process have a similar charge to their unprocessed counterparts since scCO<sub>2</sub> creates an inert atmosphere that does not interact chemically with the polymer to change its properties. A surface charge higher than -30 mV means that all particles have sufficient charge to form a stable particle system. This fact demonstrates that the process is governed by a hydrophobic-hydrophilic balance of the polymer, with the isoleucine block

defining the hydrophobic core and the glutamic acid block defining the corona, which has a negative  $\zeta$ -potential because of the deprotonated carboxylic group in the side chain.

To gain insight into the self-assembling behaviour in an aqueous medium, a  $^1\text{H}$  NMR spectroscopic study of SAS-microparticles in  $\text{D}_2\text{O}$  was carried out and the results compared with those for non-processed (EI)2 under the same conditions. Firstly, a solution of (EI)2 in  $\text{D}_2\text{O}$ , at a concentration of 1 mg/ml and pH 7, was studied by  $^1\text{H}$  NMR spectroscopy at both 5 and 37°C (Figure 36 A and B). The  $^1\text{H}$  NMR spectrum for (EI)2 at 5°C (Figure 36 A) shows the signals for protons at 0.6 ppm, corresponding to the methyl groups of valine and isoleucine, 0.8 and 1.2 ppm (two signals integrating for 117 and 123 protons, respectively, and corresponding to the methylene group from isoleucine), 1.5-2.0 ppm (signals corresponding to methylene groups from proline and the methine groups from valine and isoleucine) and 3.2-4.4 ppm (signals corresponding to the methine and methylene groups from the main amino acid chain). The values for the signals and integrals are in agreement with those predicted for (EI)2, with the presence of signals for the hydrophobic and hydrophilic blocks indicating a non-aggregated conformation for the biopolymer (Figure 36 A).

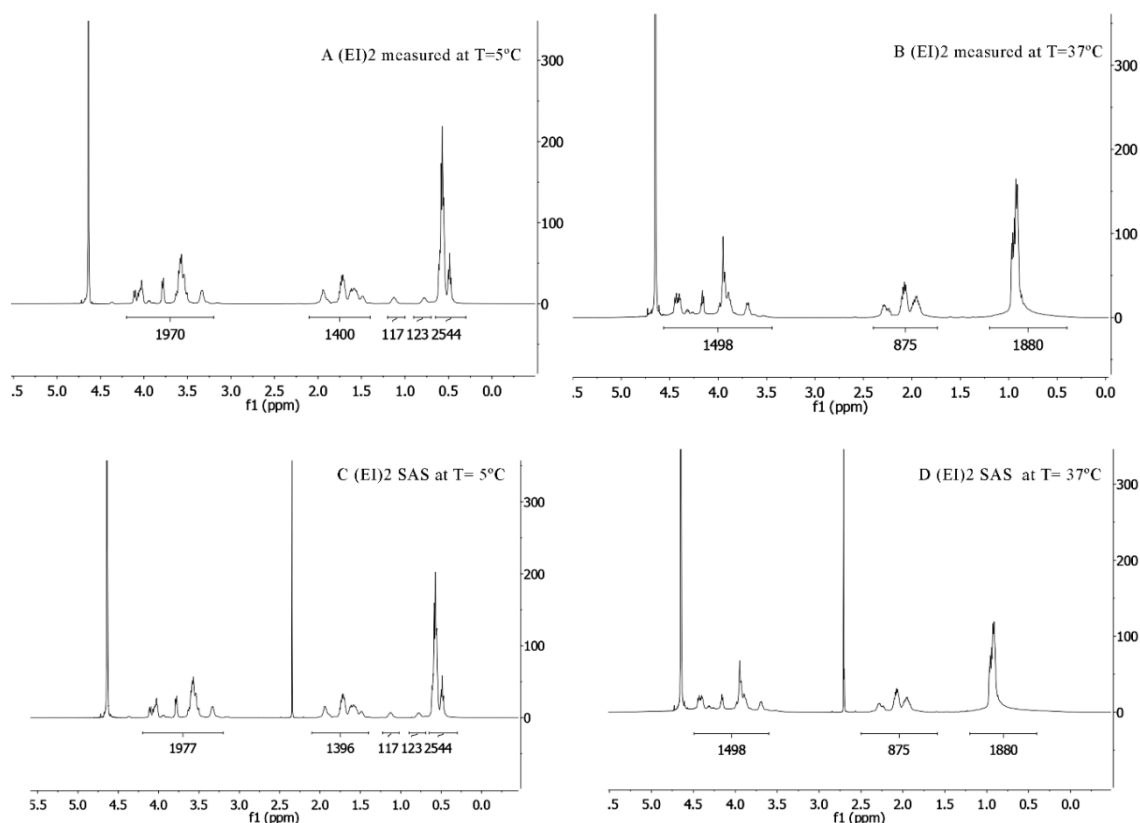


**Figure 36.**  $^1\text{H}$  NMR spectrum of pure (EI)2 at 5 (A) and 37°C (B) and (EI)2 after the SAS process from experiment 4 (Table 12) at 5 (C) and 37°C (D).

However, the spectrum for (EI)2 at 37°C (Figure 36 B) shows the absence of the signals at 0.8 and 1.2 ppm corresponding to the isoleucine residues from the hydrophobic block. Moreover, a general reduction in the other signals is observed, and the residual integrals are in agreement with those for the hydrophilic block, i.e., 1880 protons for the methyl groups of valine at 0.6 ppm, 875 protons for the methylene groups of proline and the methine groups of valine at 1.5-2.0 ppm, and 1498 protons for the main amino acid chain at 3.2-4.4 ppm. The lack of signals for the hydrophobic block is in agreement with the aggregation of the biopolymer into nanoparticles, in which the hydrophobic block at the core is not detectable using this technique and the hydrophilic block is exposed at the corona, at this temperature (above  $T_t$ ). This finding agrees with that for the nanoparticles analysed in the DLS assay for (EI)2 and their negative  $\zeta$ -potential value (Table 13).

The same procedure was performed with the powder obtained after processing (EI)2 using the SAS technique. The  $^1\text{H}$  NMR spectrum was found to be identical to that for (EI)2 at the same temperatures (Figure 36 C and D), except for the signal for residual DMSO at 2.49 ppm. Indeed, the spectrum recorded at 37°C (Figure 36 D) shows the signals and integrals corresponding exclusively to the hydrophilic block, with no signals corresponding to the apolar block, in accordance with the formation of nanoparticles with a hydrophobic core.

The  $^1\text{H}$  NMR spectrum of (EI)2-SAS solution at 5°C (Figure 36 C) shows identical signals and integrals to those for (EI)2 (Figure 36 A) at the same temperature. The presence of signals for both blocks again indicates a non-aggregated conformation for the biopolymer.

A comparison of the  $^1\text{H}$  NMR spectra recorded under the same conditions showed similar behaviour for (EI)2-SAS microparticles and unprocessed (EI)2 biopolymer in an aqueous solution (Figure 37), thus demonstrating that the SAS technique does not alter the ELR transition and that the self-assembly of ELRs into stable nanoparticles can be achieved with (EI)2 microparticles processed using the SAS technique in a top-down approach involving reorganization in aqueous solution at 37°C.

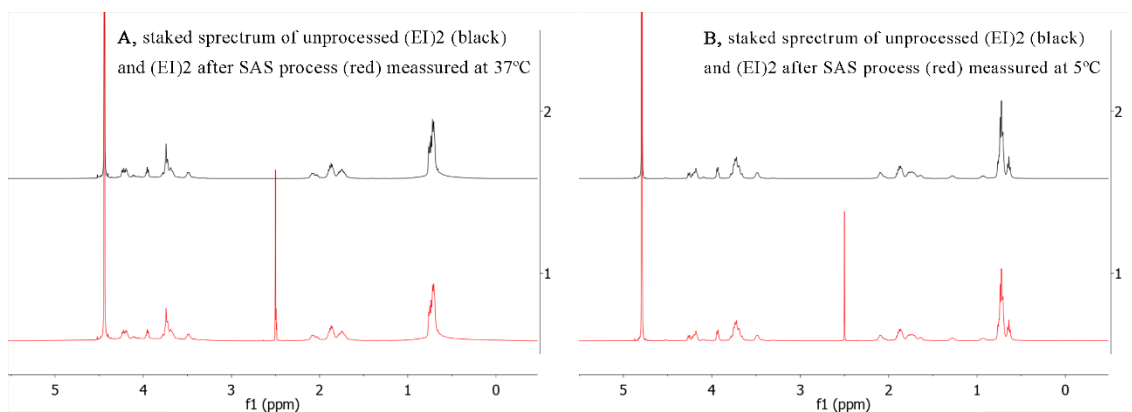


**Figure 37.** A: Staked spectrums of unprocessed (EI)2 (black) and (EI)2 after SAS process (red) at 37°C. B: staked spectrums of unprocessed (EI)2 (black) and (EI)2 after SAS process (red) at 5°C.

### 7.2.3. <sup>1</sup>H NMR study for Docetaxel and ELR-Docetaxel mixture.

In order to find the proportions of each component present in the final product obtained after SAS technique, we should know which are the signals that identify each compound and which are perfectly distinguishable from the rest of the compounds, so that we can quantify each component. To do this, we use MestReNova to simulate the <sup>1</sup>H NMR spectrum of the docetaxel molecule in D<sub>2</sub>O (Figure 38).

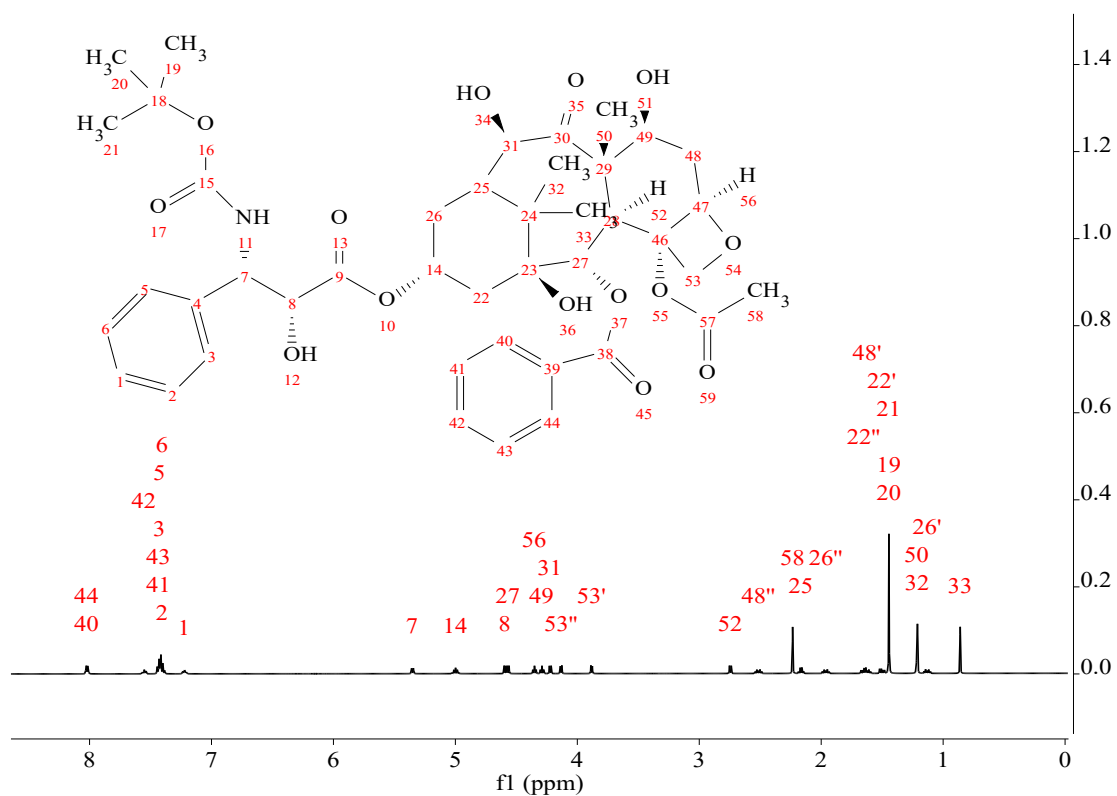


**Figure 38.**  $^1\text{H}$ NMR predicted spectra for docetaxel in  $\text{D}_2\text{O}$ .

In order to identify docetaxel in the final product, we should analyse the spectrum of the ELR (EI)2 used in this chapter in  $\text{D}_2\text{O}$  and superpose with the docetaxel predicted spectra to check if there is any signal overlapping (Figure 39).

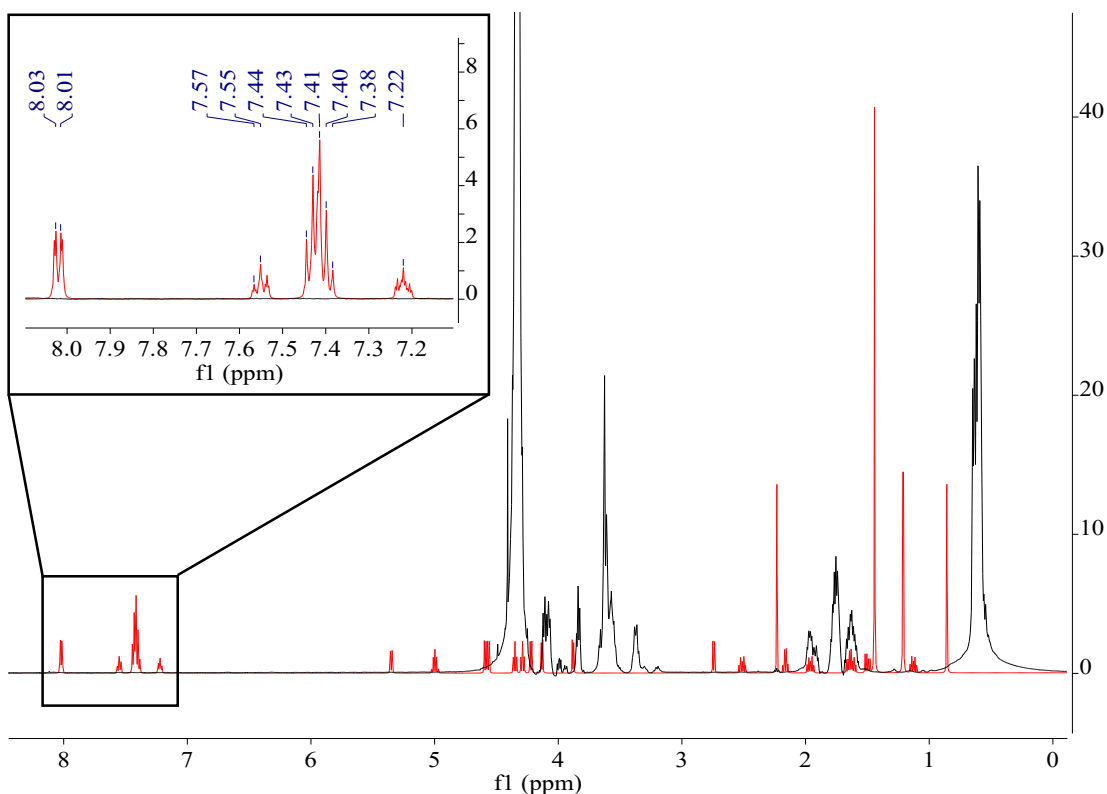


**Figure 39,**  $^1\text{H}$ NMR superposition spectra for (EI)2 (black) and docetaxel prediction (red) in  $\text{D}_2\text{O}$ .

As we see in Figure 39 there are a lot of signals that overlap or could be difficult to identify. However, there is a group of signals between 7.22-8.03 ppm that correspond to 10 hydrogen protons that are separated from the rest of the signals that are within the ELR and are therefore easily identifiable and integrated which will be the signals used to analyse the DTX proportions in the encapsulated particles.

### 7.3. Encapsulation of DTX by ELRs

For the DTX encapsulation experiments, two polymers were used: (EI)2 and the same polymer with the inclusion of the RGD peptide (EI)2RGD), since it and have been well studied therapeutically for cancer treatment, because it binds peripherally to  $\alpha_v\beta_3$  and  $\alpha_v\beta_5$  heterodimers and becomes an excellent candidate for use as a model for controlled drug delivery as it allows internalization into cancer cells [16]



Experiments were carried out under previously established experimental conditions (30 mg/mL, 35°C, 11 MPa, coaxial nozzle and drying method 3) with a biopolymer:drug ratio of 1:1 (w/w). Experiments with (EI)2 and (EI)2RGD were also carried out in the absence of DTX, using each as a control in subsequent cell assays.

Due to the low solubility of docetaxel in water and in order to ensure that all the docetaxel present in the final product obtained after the SAS technique is detected, the samples are analysed in D<sub>2</sub>O and DMSO d<sub>6</sub>, so that, to obtain the proportions of each compound in the final product a relationship can be established between the signals for protons at 0.6 ppm, corresponding to the methyl groups of valine and isoleucine of the polymer, the DMSO at 2.49 ppm and the characteristic signals of the docetaxel between 7.22-8.03 ppm in D<sub>2</sub>O and DMSO d<sub>6</sub>, respectively. So, we obtain a system of 2 equations with 2 unknowns that will give us the proportions of each component.

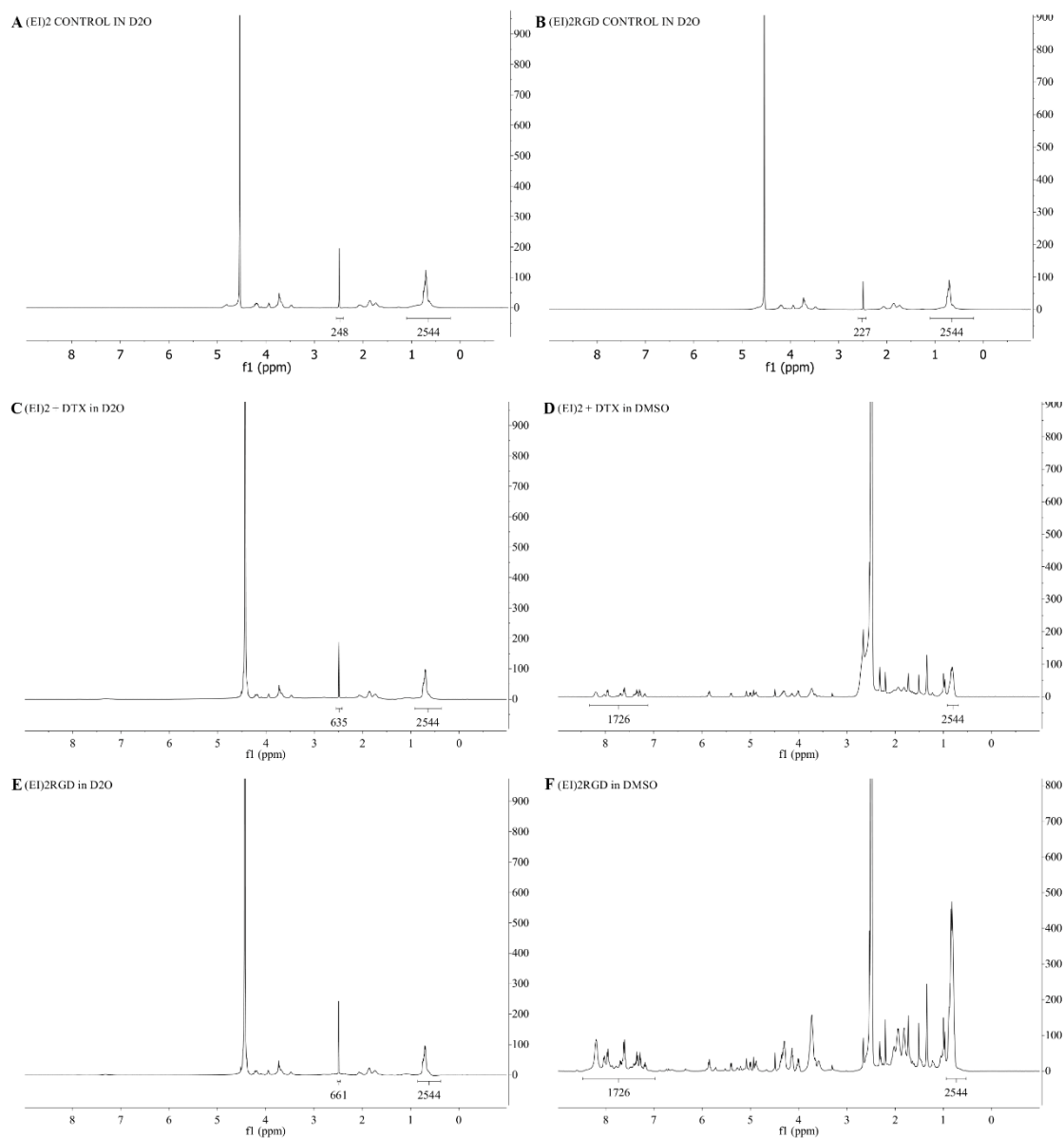


**Figure 40.**  $^1\text{H}$ NMR of the samples after SAS process. A (EI)2 control in D<sub>2</sub>O, B (EI)2RGD in D<sub>2</sub>O, C (EI)2 + DTX in D<sub>2</sub>O, D (EI)2 + DTX in DMSO, E (EI)2RDG + DTX in D<sub>2</sub>O, F (EI)2RDG + DTX in DMSO.

The amount of residual DMSO in the microparticles was similar to that obtained for experiment 4 (Table 12) under the operating conditions selected (3.4% and 3.1% for (EI)2 and (EI)2RGD lacking DTX, respectively). For the SAS experiments with DTX, the initial 1:1 (w/w) ELR:DTX ratio used was not maintained in the resulting microparticles, which exhibited a final ratio of 1:1.5, with the presence of 57.9% and 57.8% DTX and 3.5% and 3.7% residual DMSO for (EI)2 and (EI)2RGD, respectively. This change in the

mass ratio is probably due to the ELR forming stronger hydrogen bonds with DMSO and some ELR not precipitating, thus suggesting that a higher affinity for DMSO reduces the antisolvent effect of the scCO<sub>2</sub>. This new ratio was taken into consideration in subsequent cell assays.

(EI)2/DTX microparticles were also analysed by SEM (Figure 41 A), although no marked difference in particle size compared to the experiments reported previously was observed. It is striking that the small fibres seen in the SEM images (Figure 33) for pure (EI)2 are not present in Figure 41. This effect could be explained because the drug facilitates the nucleation of the polymer around it, thus avoiding the formation of small fibres, by precipitating first.

### **7.3.1. Behaviour in an aqueous solution of the encapsulated DTX in ELRs**

Particle sizes were measured by DLS using aqueous solutions of the DTX-containing particles at neutral pH, 37°C and a concentration of 1 mg/mL. The stability was followed over a period of 5 days. Table 15 shows the values for D(0.5), PDI and ζ-potential and, as expected, the ELRs controls have similar values to those found in Table 13, with a D(0.5) of around 40 nm, PDIs of less than 0.2 and a ζ-potential of around -30 mV. During the stability assay, (EI)2+DTX and (EI)2RGD+DTX maintain similar values within a small range of variation (Table 15) thus clearly indicating that these systems are stable over time.

| Sample         | Day 0       |                       |                  | Day 3       |                       |                  | Day 5       |                       |                  |
|----------------|-------------|-----------------------|------------------|-------------|-----------------------|------------------|-------------|-----------------------|------------------|
|                | D(0.5) (nm) | PDI                   | ζ-Potential (mV) | D(0.5) (nm) | PDI                   | ζ-Potential (mV) | D(0.5) (nm) | PDI                   | ζ-Potential (mV) |
| (EI)2          | 43 ± 10     | 0.17<br>0 ± 0.00<br>2 | -28.8 ± 3.1      | 32 ± 11     | 0.18<br>5 ± 0.00<br>8 | -32.3 ± 3.2      | 38 ± 15     | 0.06<br>3 ± 0.00<br>5 | -29.8 ± 4.2      |
| (EI)2RGD       | 36 ± 12     | 0.18<br>4 ± 0.00<br>7 | -29.5 ± 2.5      | 40 ± 15     | 0.07<br>2 ± 0.00<br>6 | -30.5 ± 2.6      | 37 ± 10     | 0.09<br>2 ± 0.00<br>3 | -31.6 ± 1.3      |
| (EI)2 + DTX    | 45 ± 14     | 0.19<br>4 ± 0.00<br>6 | -31.1 ± 2.2      | 42 ± 15     | 0.06<br>9 ± 0.00<br>3 | -28.4 ± 1.8      | 35 ± 11     | 0.16<br>5 ± 0.00<br>4 | -30.3 ± 20.1     |
| (EI)2RGD + DTX | 40 ± 12     | 0.17<br>4 ± 0.00<br>5 | -30.4 ± 4.1      | 37 ± 16     | 0.12<br>8 ± 0.00<br>7 | -34.6 ± 2.2      | 41 ± 16     | 0.13<br>6 ± 0.00<br>4 | -33.7 ± 4.1      |

**Table 15.** Values for the diameter, PDI and ζ-potential at different times during the stability assay (37°C and neutral pH).

Transmission electron microscopy (TEM) was used to confirm the results obtained by DLS. Figure 41 B shows nanoparticles with an average size of  $27.9 \pm 4.4$  nm, similar to those reported in Table 15, which form due to the amphiphilic nature and self-assembly behaviour of the biopolymer. It can be also seen that there is no tendency to form large agglomerations, in accordance with the PDI values obtained from the DLS results.

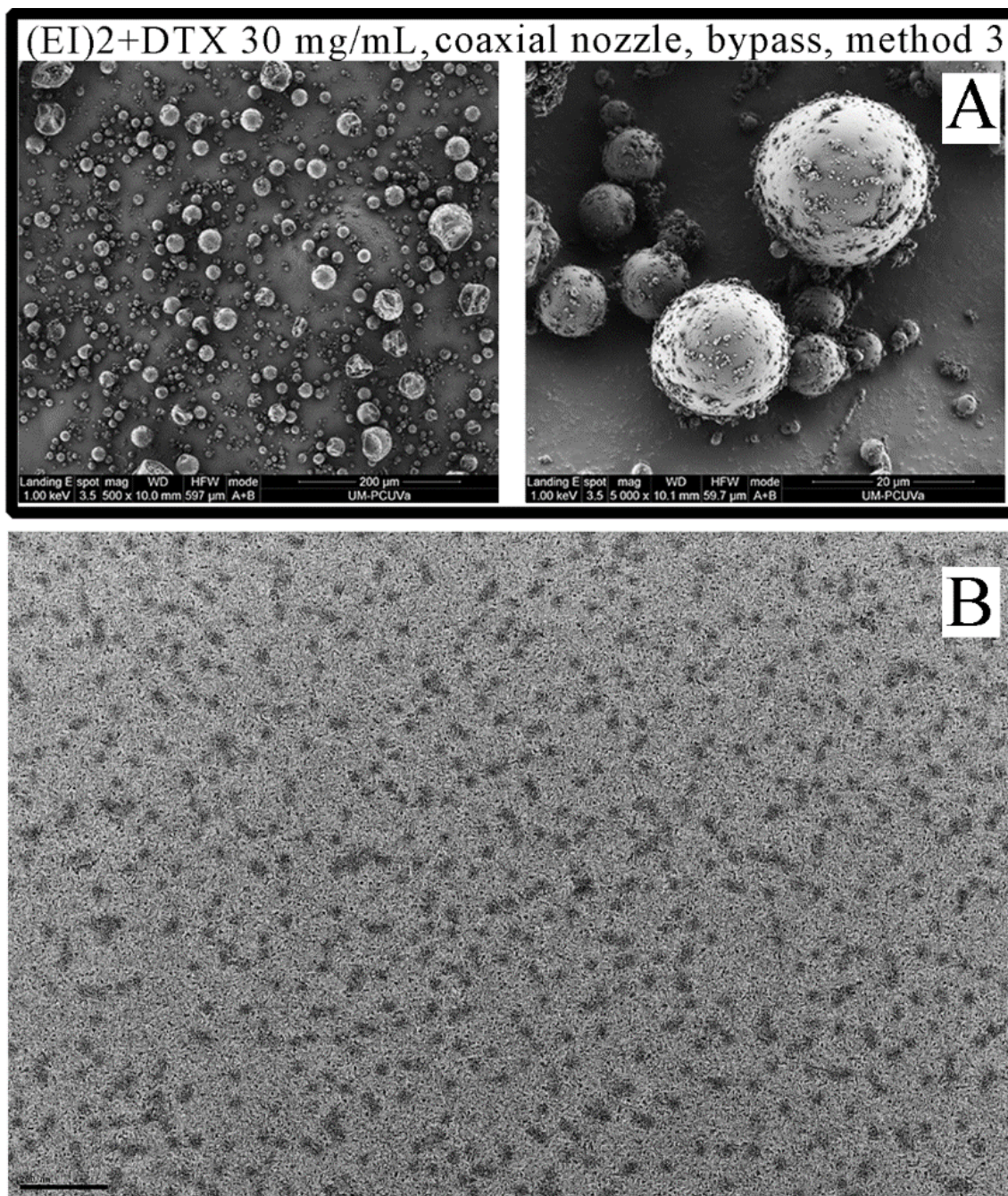


**Figure 41.** A) SEM Photomicrographs showing general (scale bar: 200  $\mu\text{m}$ ; magnification: x500) and detailed views (scale bar: 20  $\mu\text{m}$ ; magnification: x5000) of (EI)2+DTX microparticles. B) TEM photomicrograph of (EI)2+DTX prepared at a concentration of 1 mg/mL in ultrapure deionized water, at neutral pH and room temperature, with negative staining (scale bar: 200 nm).

Also, it should be noted that the stability test was carried out with a DTX concentration of 0.6 mg/mL resulting from the starting SAS-microparticle solution (concentration of 1 mg/mL concentration), which implies that, as a result of the ELRs used to co-precipitate DTX in the SAS process, it is possible to increase the solubility of DTX in an aqueous medium by approximately fifty orders of magnitude. This result would allow the use of solvents and surfactants such as ethanol and polysorbate 80, respectively in conventional treatments with this drug to be avoided [9].

The encapsulation of DTX into the nanoparticles was studied by  $^1\text{H}$  NMR spectroscopy by recording the spectrum of an aqueous solution of (EI)2+DTX microparticles from the SAS process in  $\text{D}_2\text{O}$  (1 mg/mL, pH 7 and  $37^\circ\text{C}$ ) as in the DLS assay (Table 15).

The spectrum obtained at  $37^\circ\text{C}$  (Figure 42 A) is similar to that obtained for (EI)2 microparticles (Figure 36 B and D) and shows the same signals and integrals for the hydrophilic glutamic acid block. The only difference compared to the Figure 36 spectra is the appearance of very small and broad signals in the range 6.7-7.7 ppm and at around 1 ppm that could correspond to DTX molecules present in small quantities on the surface of the core. As such, this result is in accordance with the formation of nanoparticles with a hydrophobic core and with results from DLS or TEM (Table 15 and Figure 41 B). Thus, the almost complete absence of DTX signals could allow us to conclude that a correct encapsulation of the DTX drug has been achieved.

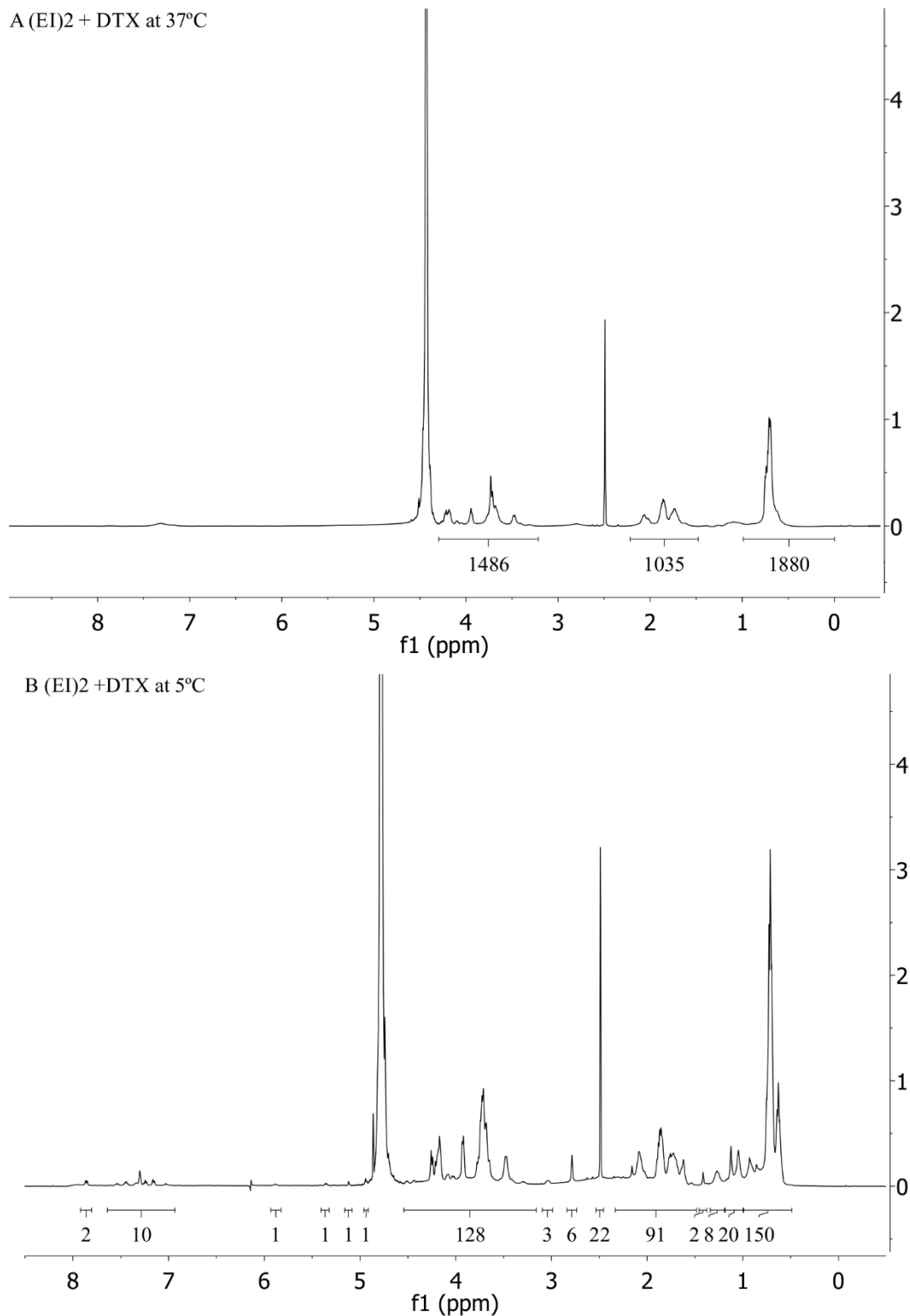


**Figure 42.**  $^1\text{H}$  NMR spectrum in  $\text{D}_2\text{O}$  of (EI)2+DTX encapsulated at 37°C (A) and 5°C (B).

When the sample was cooled to 5°C (Figure 42 B), the spectrum showed the signals from the (EI)2 biopolymer in a non-aggregated conformation, as can be deduced from the

signals for the methyl groups of valine and isoleucine at 0.6 ppm and the signals for the methylene groups of isoleucine at 1.2 ppm. The presence of signals in the range 6.7-7.7 ppm due to the protons of DTX should also be noted. This result shows that DTX was delivered from the core of the nanoparticles and confirms that the drug was encapsulated inside those nanoparticles.

When this sample was again heated to 37°C, the NMR spectrum obtained (Figure 43) was found to be identical to that shown in Figure 42 A. The spectrum shows a similar absence of DTX signals to that found after nanoparticle formation, thus meaning that DTX is embedded in the hydrophobic core. Consequently, we can conclude that DTX is trapped inside the ELR particles during the SAS process and that the solubility thereof is improved, probably due to a non-covalent interaction with the ELR. In this respect, the ability of the SAS technique to bring the ELR closer to the hydrophobic drug allows interaction between them and also contributes to subsequent encapsulation.



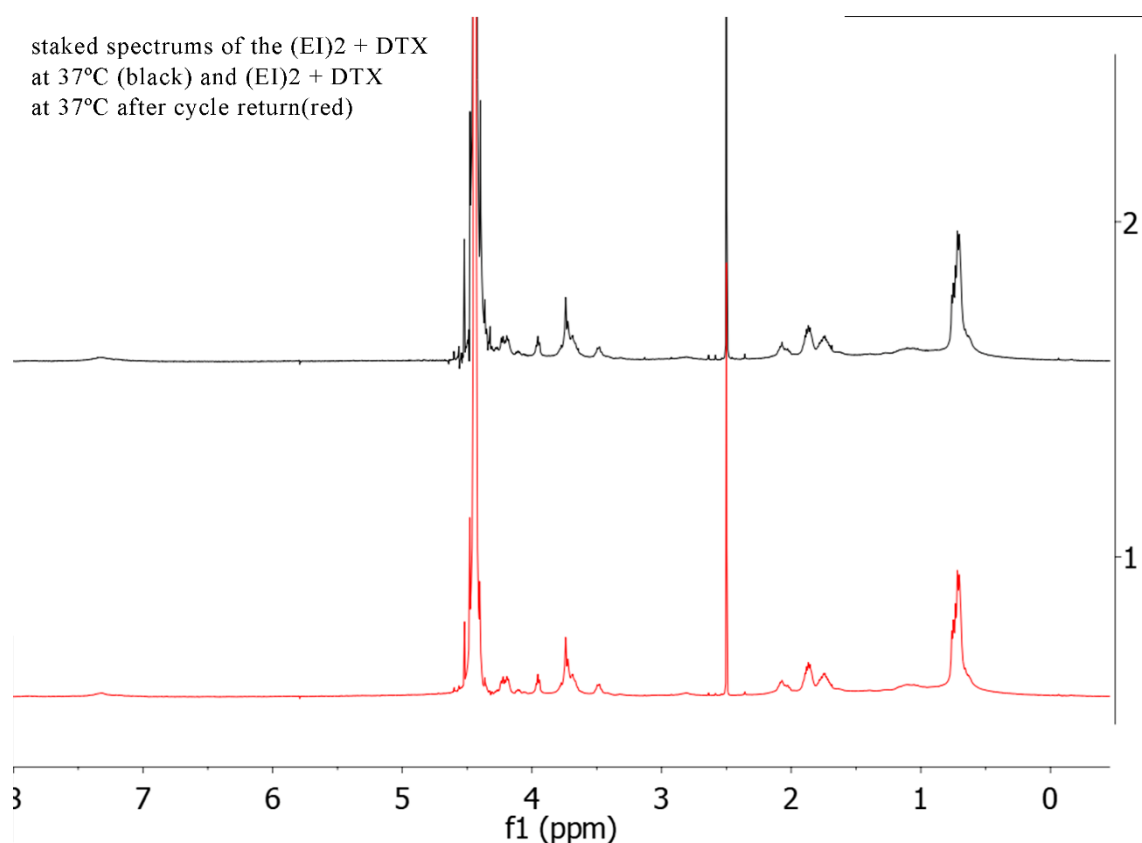


**Figure 43.** Staked  $^1\text{H}$  NMR spectra in  $\text{D}_2\text{O}$  of the (EI)2+DTX at 37°C (black) and (EI)2+DTX at 37°C after cycle return (red).

As a control, a mixture of unprocessed (EI)2 polymer and DTX, at the same weight ratio as in the previous assays, was prepared and the NMR spectrum was acquired (Figure 44). The spectrum recorded at 37°C showed identical signals and integrals to those shown above for (EI)2 (Figure 36 C) or (EI)2+DTX (Figure 42 A) using the SAS technique, in accordance with the formation of nanoparticles with a hydrophobic core. Upon cooling the sample to 5°C, the NMR spectrum showed the presence of non-aggregated (EI)2 biopolymer, with the presence of DTX being practically negligible (Figure 44 B). This finding is in accordance with the absence of DTX inside the hydrophobic core of the nanoparticle at 37°C, thereby confirming the need for SAS-type processing to enable this hydrophobic drug (DTX) to be embedded into the core of the (EI)2 nanoparticle.

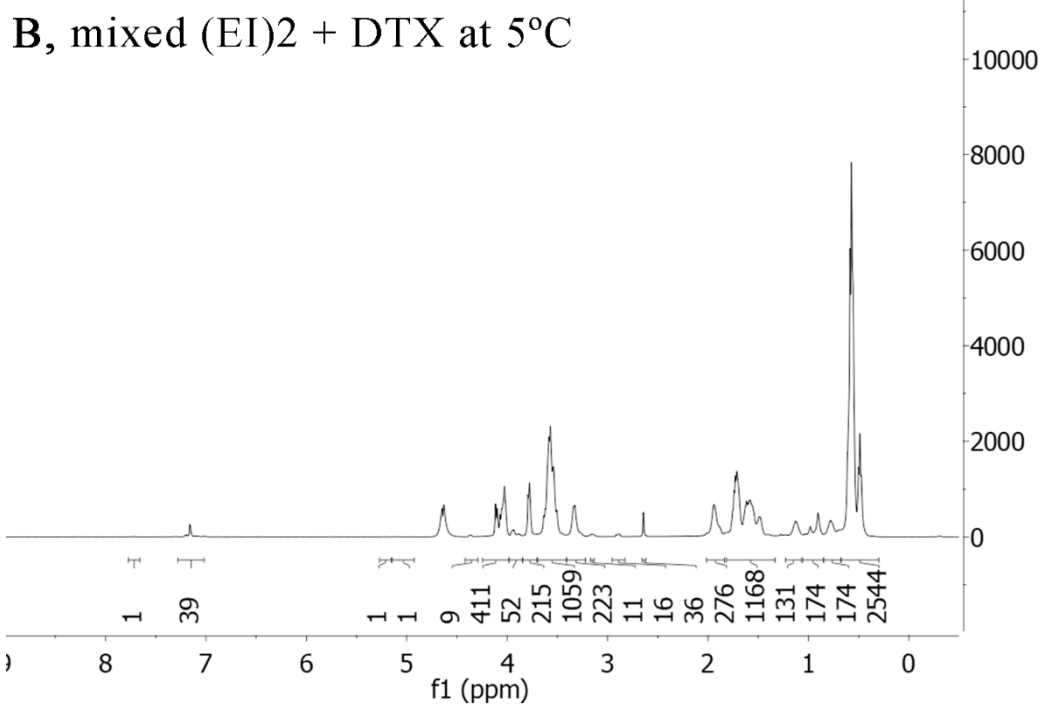
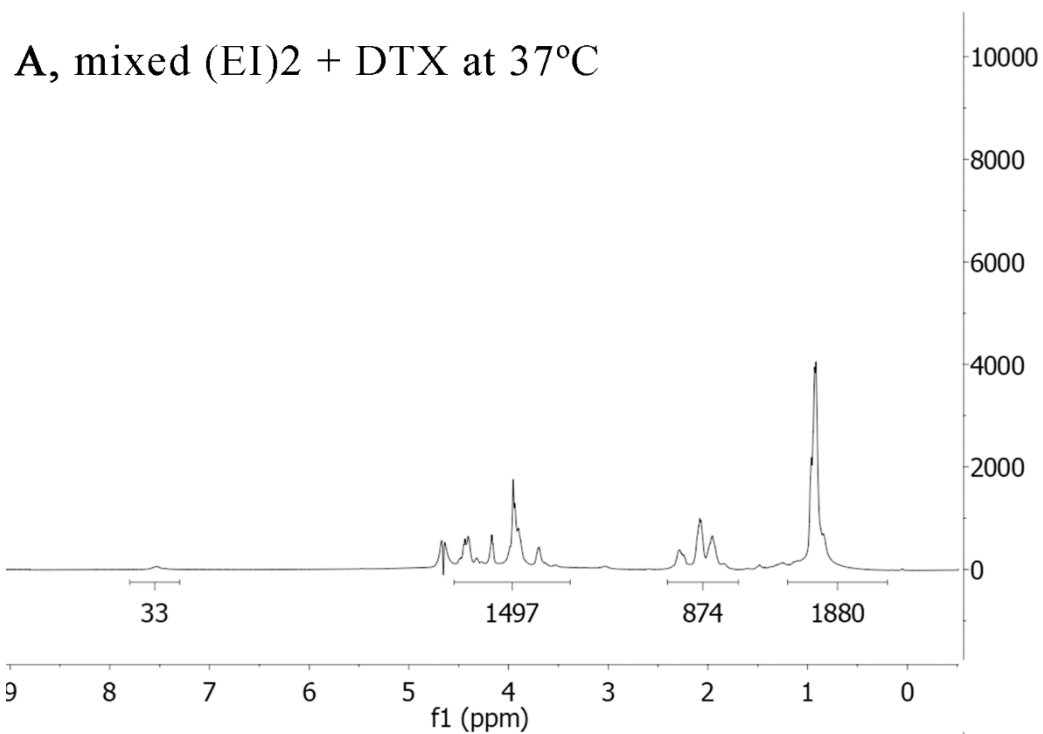


**Figure 44.**  $^1\text{H}$  NMR spectrum in  $\text{D}_2\text{O}$  of A: the mixture of (EI)2 and DTX (1:1 w/w) at  $37^\circ\text{C}$ ; and B: mixed (EI)2 and DTX (1:1 w/w) at  $5^\circ\text{C}$ .

### 7.3.2. Drug-release study

A kinetic release study was performed by comparing (EI)2+DTX with pure DTX to determine the quantity of drug delivered at each time point. Figure 45 shows the percentage of drugs released from the (EI)2+DTX particles and the percentage of drugs released from the control samples, in both cases for an experimental time of 96 hours. Each point represents the result of an analysis in triplicate, with the standard deviation represented in the error bars. As can be seen for the (EI)2+DTX particles,  $55 \pm 11\%$  of the drug is released in the first 10 hours of the experiment, with the release velocity subsequently decreasing until total release at 96 hours. However, in the control sample,  $53 \pm 2\%$  is released in the first 2 hours, with all the drugs having been released after 24 hours. These results show a clear delay in the delivery of the drug from the co-precipitated (EI)2+DTX particles as it must cross the polymer barrier to reach the release medium, which could prove useful for sustained release purposes.

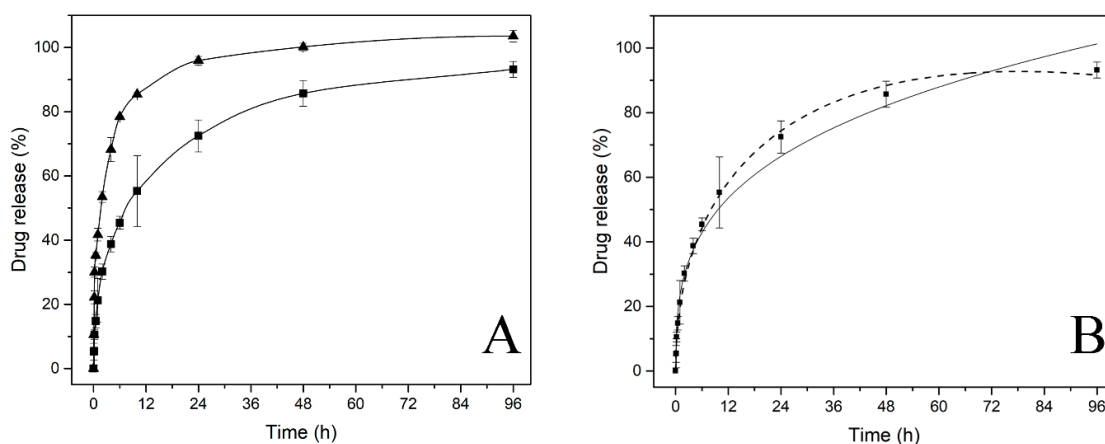


**Figure 45.** A) Study of drug release from (EI)2+DTX and free DTX control sample vs. time (h) at a normalized DTX concentration of 0.6 mg/mL in water:ethanol (7:3) release medium. Each point represents the result of an analysis in triplicate, with the standard deviation represented in the error bars. ■: (EI)2 + DTX ▲: Free DTX control. Lines are used to guiding the eye. B) Graphical fitting of the different mathematical models used to describe the release of DTX from (EI)2 + DTX (■). Dashed line: Peppas–Sahlin fitting; solid line: Lindner–Lippold fitting.

To understand the drug-delivery process, the experimental profile was mathematically fitted using the models described in materials and methods. To get a more accurate description of the process, three-time frames were defined (Table 16 and Figure 45 B). Both models fit satisfactorily, ( $R^2 > 0.980$ ), with the fit being slightly better for the Peppas–Sahlin equation. As can be seen from Table 16, the coefficient  $n$  from the Peppas–Sahlin equation has values of  $0.5 < n < 1$  in the three-time periods, which suggests anomalous transport due to the slow rearrangement of polymeric chains and the diffusion process occurring simultaneously, thus resulting in time-dependent anomalous effects. However, between 0 and 24 hours,  $n$  has a value of close to 0.5, thus indicating that release depends on diffusion of the fraction of docetaxel occluded in the material and close to its surface through the polymer matrix. Between 0 and 96 hours, the diffusion process becomes slower as DTX must diffuse through the nanoparticle to reach the release medium.

Furthermore, the Peppas–Sahlin equation shows that the coefficient  $k_1$  predominates in all stages, thus meaning that the process is clearly governed by the Fickian diffusion mechanism. These results are in agreement with those reported in the literature with the same ELR in a hydrogel configuration [10] [11]. Likewise, the coefficient  $b$  (burst effect) in the Lindner-Lippold equation is small and negative, thus indicating that the quantity of DTX present on the surface of the particles is practically negligible, in agreement with the conclusions for the solution behaviour of SAS-processed (EI)<sub>2</sub>+DTX particles from the NMR spectroscopy study.

| Model  | Peppas–Sahlin  |                |               |       | Lindner–Lippold    |               |                |       |
|--------|----------------|----------------|---------------|-------|--------------------|---------------|----------------|-------|
|        | Time frame (h) | k1             | k2            | n     | COD R <sup>2</sup> | k1            | n              | b     |
| 0 - 1  | 0.263 ± 0.030  | -0.050 ± 0.031 | 0.615 ± 0.054 | 0.999 | 0.221 ± 0.005      | 0.529 ± 0.026 | -0.001 ± 0.004 | 0.999 |
| 0- 24  | 0.226 ± 0.003  | -0.016 ± 0.001 | 0.503 ± 0.014 | 0.999 | 0.240 ± 0.020      | 0.367 ± 0.023 | -0.022 ± 0.018 | 0.994 |
| 0 - 96 | 0.228 ± 0.05   | -0.014 ± 0.001 | 0.464 ± 0.008 | 0.999 | 0.295 ± 0.047      | 0.281 ± 0.030 | -0.055 ± 0.044 | 0.980 |

**Table 16.** Fitting of the profiles for release of DTX from (EI)2+DTX processed using the SAS technique to the Peppas–Sahlin and Lindner–Lippold equations using samples prepared at a normalized concentration of 0.6 mg/mL during the different time frames.

#### 7.4. *In vitro* cell assays

Once the solid microparticles and their behaviour in aqueous media as nanoparticles had been completely characterized, their therapeutical effectivity was determined by Dr Juan Gonzalez Valdivieso in his PhD thesis [12] and further published in [13]. A selection of the most relevant results obtained thanks to his collaboration is summarized below.

Two different human cell lines were used, namely MDA-MB-231 breast cancer cells and human endothelial HUVEC cells. These cell lines were used because they do not have the same high expression on the surface of integrin receptors [14], which are implicated in a broad number of cancer diseases [15].

Three different concentrations of free DTX (0.1, 1 and 10  $\mu$ M) and the same amount of DTX were used for the formulations with both types of ELRs. As a control, ELRs without drugs were used to determine the effect of the carrier on the cells and the internalization process. DTX concentrations were chosen on the basis of the standards used in the literature [17], [18].

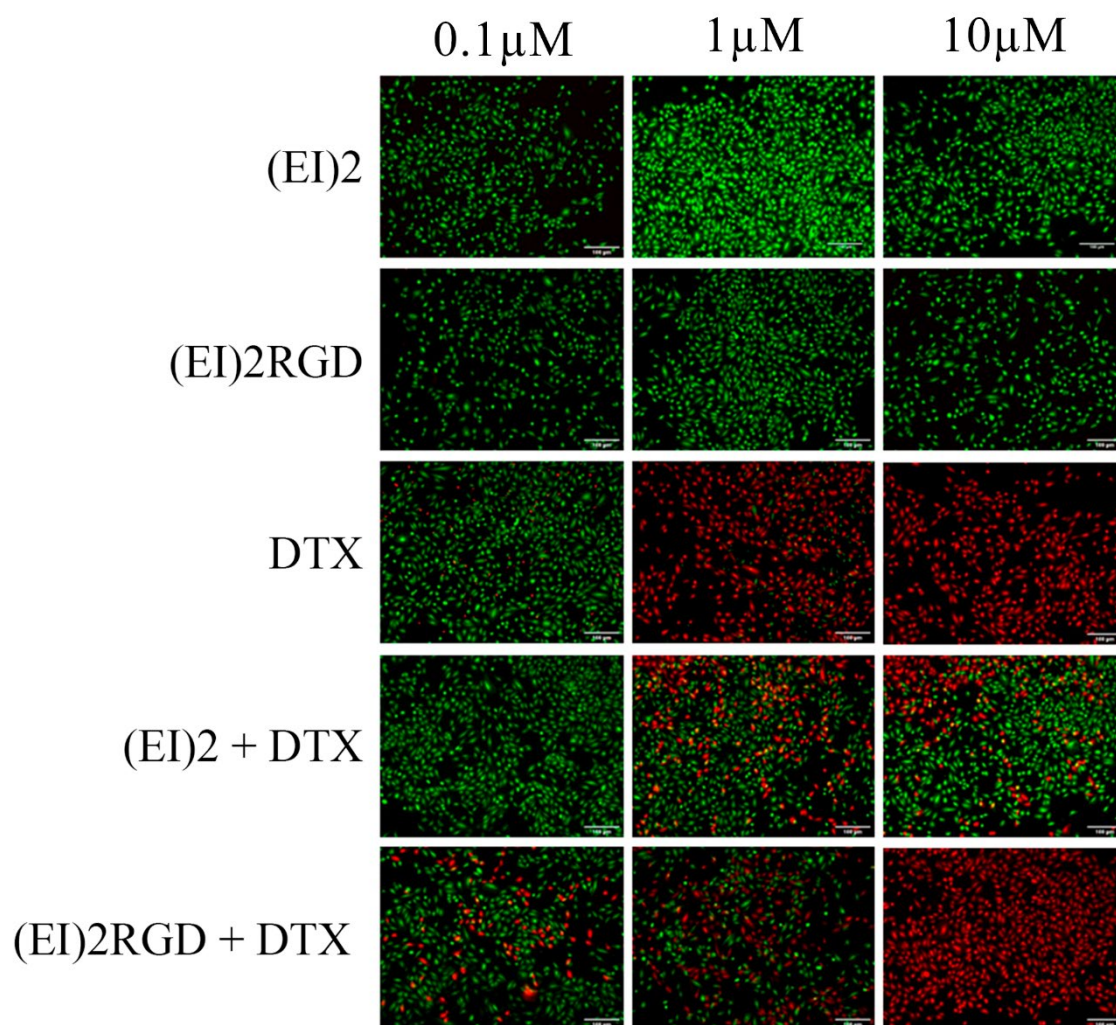


**Figure 46.** Representative fluorescence microscopy images for HUVEC cells after incubation with free DTX at three concentrations or encapsulated DTX within ELR nanoparticles at the corresponding concentrations for 24 hours. Cell viability was measured using the LIVE/DEAD Assay kit. Scale bars: 100  $\mu$ m. Reproduced from [13].

Incubation with empty control nanoparticles, either containing the RGD sequence or not, did not significantly affect the viability of either cell line (Figure 46 and Figure 47). Indeed, our results showed no differences between three different concentrations, thereby corroborating previous studies from this group in which ELR-based biopolymers with and without the RGD peptide were characterized and showed no cytotoxicity [10], [19].

Regarding the effect of free DTX, it can be observed that after incubation of the cells at the highest concentration, a remarkable toxic effect is produced, decreasing cell viability up to 3-5%. However, when the lowest concentration of free DTX is used, cell viability

is practically not affected, while with the intermediate concentration it decreases up to 23-29%. Furthermore, it can be seen that there is no difference between the two cell lines regardless of the concentration, which means that DTX does not differentiate between cancerous and non-cancerous cells. Furthermore, an interesting effect is observed when DTX is encapsulated with (EI)2, lacking the RGD peptide, as it can be seen that the therapeutic effect of DTX on both cell lines is not enhanced, despite the concentration. However, when the formulations contain the RGD peptide, cancer cells are much more affected than those treated with free DTX, and this effect is not observed in HUVEC cells (Figure 46), which show higher levels of viability compared to free DTX.

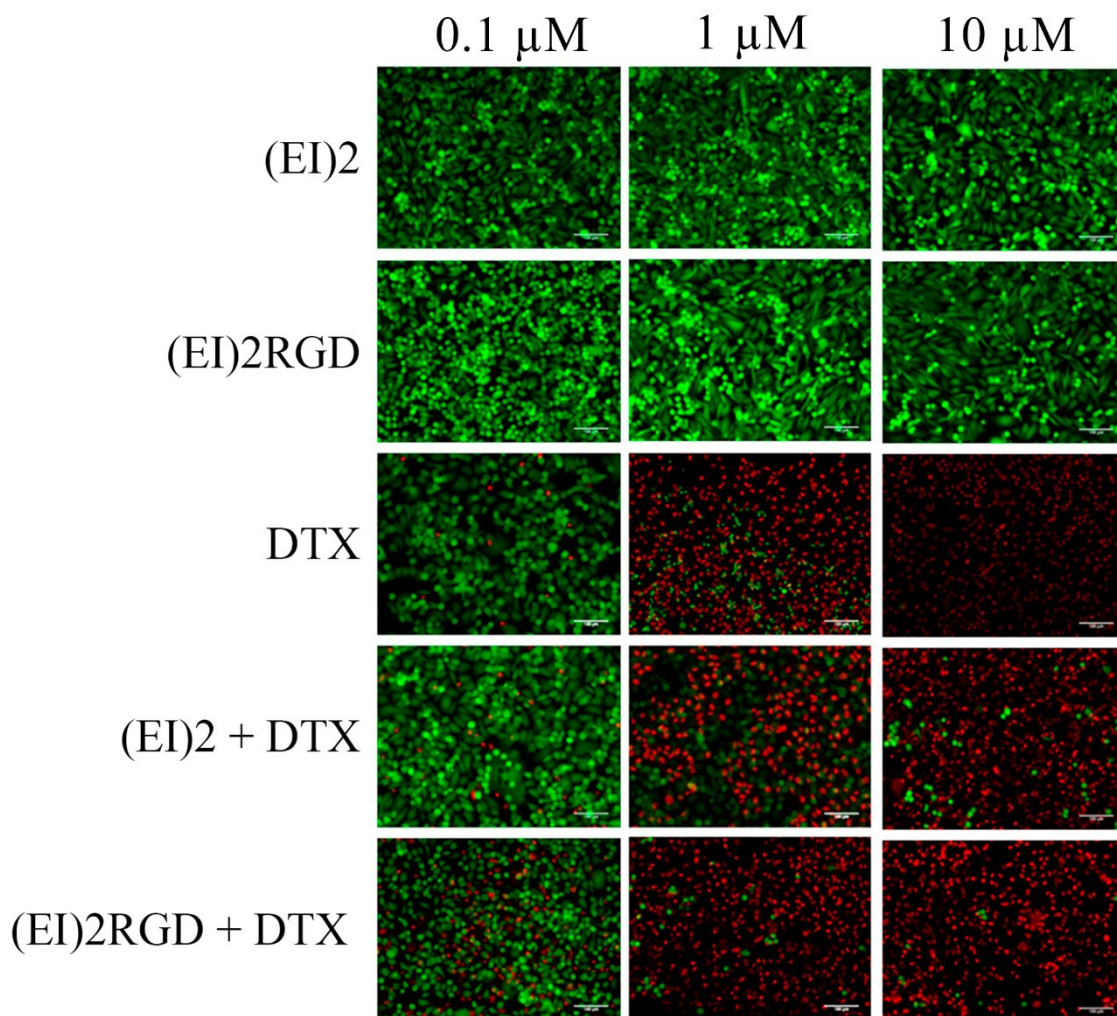


**Figure 47.** Representative fluorescence microscopy images for MDA-MB-231 cells after incubation with free DTX at three concentrations or encapsulated DTX within ELR nanoparticles at the corresponding concentrations for 24 hours. Cell viability was measured using the LIVE/DEAD Assay kit. Scale bars: 100  $\mu\text{m}$ . Reproduced from [13].

In order to observe cell internalisation, rhodamine was encapsulated with the ELR containing the RGD peptide using the SAS technique and the results were verified by confocal spectroscopy (Figure 48) that the nanoparticles have been able to enter the cells and are mainly located in the perinuclear zone of the cytoplasm.



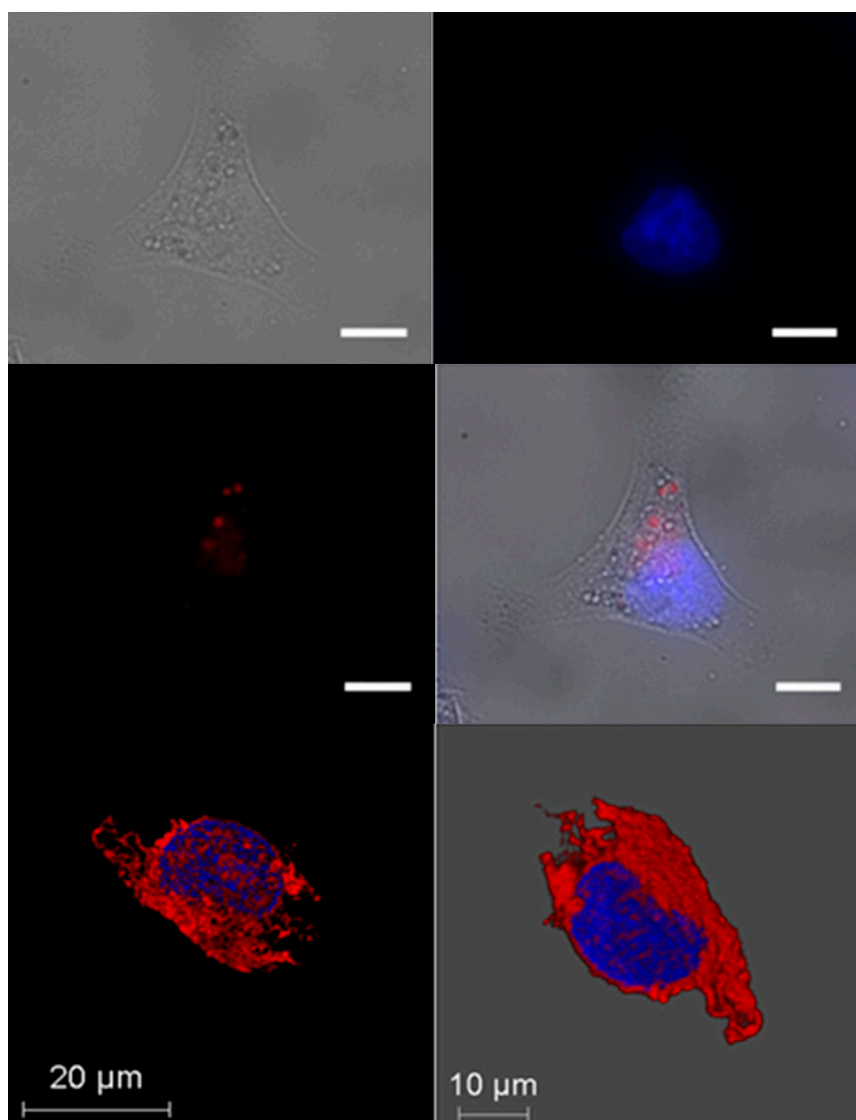


**Figure 48.** Fluorescence (Top panel) and confocal (Bottom panel) microscopy image of MDA-MB-231 cells treated with (EI)2RGD nanoparticles with encapsulated rhodamine. Cell nuclei were stained with DAPI. Scale bars: 10  $\mu\text{m}$ . Reproduced from ([13]).

Regarding cell proliferation results [12], it has been found that when a  $1\mu\text{M}$  concentration of free DTX is used, cell proliferation stops after 12h of treatment and remains in this condition until 72h of the assay, which supports the results previously found on cell viability, since this was established at 25% after 24h of incubation. The same effect has been found in cancer cells when DTX is encapsulated with (EI)2 at a concentration of  $1\mu\text{M}$  in DTX, although this formulation slightly improves cell proliferation compared to free DTX [13]. Finally, when cancer cells were treated with the same amount of

encapsulated DTX but with the ELR containing the RGD peptide, cell proliferation was completely stopped and lower values were found compared to cells treated with free DTX. Therefore, not only is DTX causing cell death but also the surviving cells are unable to proliferate, probably entering a senescent state.

### **7.5. Final remarks**

The operating conditions for producing docetaxel-loaded ELR microparticles using a supercritical antisolvent process have been established. This is a one-step process that avoids post-processing steps. The coaxial nozzle designed to improve the jet-spray inside the reactor managed to reduce the amount of residual solvent from 16% to 2.4% while still achieving high SAS process yields. As a result of the amphiphilic nature of the biopolymer. The particles obtained exhibit sizes of approximately 10 $\mu$ m displaying smooth surface without remarkable aggregation, although with very small particle sizes stuck to their surface, which resulted in a wide range of particle sizes. According to their behaviour in aqueous media, nanoparticles were found to be very stable for 5 days thanks to a  $\zeta$  -potential of -30mV and particle sizes close to 40nm. Notably, the aqueous solubility of the drug increased by five orders of magnitude. Furthermore, it was verified by NMR that the formulations retained the smart behaviour and it was possible to verify by the same technique that the drug is encapsulated inside the ELR. In addition, release assays showed a sustained release of the drug in the formulations tested, a process which is governed by Fick diffusion.

After characterization of the ELR-based nanoparticles, their effect was measured *in vitro* in human endothelial and breast cancer cells. The results showed that encapsulation of the chemotherapeutic drug in ELR nanoparticles lacking the RGD cancer-targeting

sequence diminished the cell toxicity of DTX and, also, that breast cancer cells treated with DTX-loaded nanoparticles carrying the RGD sequence were more affected and showed lower cell viability than cells treated with free DTX. In contrast, this effect was not seen in HUVEC endothelial cells. As such, we have developed a novel drug-delivery system that is more accurate than the non-selective chemotherapeutic drug DTX alone and shows an enhanced effect in breast cancer cells compared to healthy endothelial cells, which would come into contact with such nanoparticles after systemic administration. Consequently, this smart ELR polymer could be a useful approach for drug-delivery purposes due to its ability to encapsulate highly hydrophobic drugs and incorporate different bioactive peptides or sequences as targeting systems to achieve a more advanced tool for cancer treatment than current non-specific chemotherapeutic agents.

## 7.6. REFERENCES

- [1] O. R. Davies, A. L. Lewis, M. J. Whitaker, H. Tai, K. M. Shakesheff, and S. M. Howdle, "Applications of supercritical CO<sub>2</sub> in the fabrication of polymer systems for drug delivery and tissue engineering," *Advanced Drug Delivery Reviews*, vol. 60, no. 3, pp. 373–387, 2008, doi: 10.1016/j.addr.2006.12.001.
- [2] S. Bristow, T. Shekunov, B. Y. Shekunov, and P. York, "Analysis of the supersaturation and precipitation process with supercritical CO<sub>2</sub>," *J. Supercrit. Fluids*, vol. 21, no. 3, pp. 257–271, 2001, doi: 10.1016/S0896-8446(01)00100-0.
- [3] C. G. Kalogiannis, E. Pavlidou, and C. G. Panayiotou, "Production of amoxicillin microparticles by supercritical antisolvent precipitation," *Ind. Eng. Chem. Res.*, vol. 44, no. 24, pp. 9339–9346, 2005, doi: 10.1021/ie050654m.
- [4] K. Mishima, "Biodegradable particle formation for drug and gene delivery using supercritical fluid and dense gas," *Advanced Drug Delivery Reviews*, vol. 60, no. 3, pp. 411–432, 2008, doi: 10.1016/j.addr.2007.02.003.
- [5] A. E. Andreatta, L. J. Florusse, S. B. Bottini, and C. J. Peters, "Phase equilibria of dimethyl sulfoxide (DMSO) + carbon dioxide, and DMSO + carbon dioxide + water mixtures," *J. Supercrit. Fluids*, vol. 42, no. 1, pp. 60–68, 2007, doi: 10.1016/j.supflu.2006.12.015.
- [6] F. Liebner, E. Haimer, M. Wendland, A. Potthast, and T. Rosenau, "Precipitation of hemicelluloses from DMSO/water mixtures using carbon dioxide as an antisolvent," *J. Nanomater.*, vol. 2008, no. 1, 2008, doi: 10.1155/2008/826974.

- [7] M. Kalani and R. Yunus, “Application of supercritical antisolvent method in drug encapsulation: a review.,” *International journal of nanomedicine*, vol. 6, pp. 1429–1442, 2011, doi: 10.2147/ijn.s19021.
- [8] J. Stetefeld, S. A. McKenna, and T. R. Patel, “Dynamic light scattering: a practical guide and applications in biomedical sciences,” *Biophysical Reviews*, vol. 8, no. 4, pp. 409–427, 2016, doi: 10.1007/s12551-016-0218-6.
- [9] European Medicines Agency, “Taxotere product information,” 2008. [https://www.ema.europa.eu/en/documents/product-information/taxotere-epar-product-information\\_es.pdf](https://www.ema.europa.eu/en/documents/product-information/taxotere-epar-product-information_es.pdf).
- [10] A. Fernández-Colino, J. M. Bermudez, F. J. Arias, D. Quinteros, and E. Gonzo, “Development of a mechanism and an accurate and simple mathematical model for the description of drug release: Application to a relevant example of acetazolamide-controlled release from a bio-inspired elastin-based hydrogel,” *Mater. Sci. Eng. C*, vol. 61, pp. 286–292, 2016, doi: 10.1016/j.msec.2015.12.050.
- [11] A. Fernández-Colino, D. A. Quinteros, D. A. Allemandi, A. Girotti, S. D. Palma, and F. J. Arias, “Self-Assembling Elastin-Like Hydrogels for Timolol Delivery: Development of an Ophthalmic Formulation Against Glaucoma,” *Mol. Pharm.*, vol. 14, no. 12, pp. 4498–4508, Dec. 2017, doi: 10.1021/acs.molpharmaceut.7b00615.
- [12] J. González Valdivieso, “Advanced nanodevices based on Elastin-like Recombinamers as smart drug delivery systems for biomedical applications,” Universidad de Valladolid, 2020.
- [13] R. Vallejo, J. Gonzalez-Valdivieso, M. Santos, S. Rodriguez-Rojo, and F. J. Arias, “Production of elastin-like recombinamer-based nanoparticles for docetaxel encapsulation and use as smart drug-delivery systems using a supercritical antisolvent process,” *J. Ind. Eng. Chem.*, vol. 93, pp. 361–374, 2021, doi: 10.1016/j.jiec.2020.10.013.
- [14] T. Meyer, J. F. Marshall, and I. R. Hart, “Expression of  $\alpha$ v integrins and vitronectin receptor identity in breast cancer cells,” *Br. J. Cancer*, vol. 77, no. 4, pp. 530–536, 1998, doi: 10.1038/bjc.1998.86.
- [15] S. L. Goodman, H. J. Grote, and C. Wilm, “Matched rabbit monoclonal antibodies against  $\alpha$ v-series integrins reveal a novel  $\alpha$ v $\beta$ 3-LIBS epitope, and permit routine staining of archival paraffin samples of human tumors,” *Biol. Open*, vol. 1, no. 4, pp. 329–340, 2012, doi: 10.1242/bio.2012364.
- [16] F. F. Lang *et al.*, “Phase I study of DNX-2401 (delta-24-RGD) oncolytic adenovirus: replication and immunotherapeutic effects in recurrent malignant glioma,” *J. Clin. Oncol.*, vol. 36, no. 14, pp. 1419–1427, 2018, doi: 10.1200/JCO.2017.75.8219.
- [17] P. E. Saw, M. Yu, M. Choi, E. Lee, S. Jon, and O. C. Farokhzad, “Hyper-cell-permeable micelles as a drug delivery carrier for effective cancer therapy,” *Biomaterials*, vol. 123, pp. 118–126, 2017, doi: 10.1016/j.biomaterials.2017.01.040.
- [18] G. Battogtokh *et al.*, “Triphenylphosphine-docetaxel conjugate-incorporated albumin nanoparticles for cancer treatment,” *Nanomedicine*, vol. 13, no. 3, pp. 325–338, 2018, doi: 10.2217/nnm-2017-0274.
- [19] D. Pescador *et al.*, “Regeneration of hyaline cartilage promoted by xenogeneic mesenchymal stromal cells embedded within elastin-like recombinamer-based bioactive hydrogels,” *J. Mater. Sci. Mater. Med.*, vol. 28, no. 8, 2017, doi: 10.1007/s10856-017-5928-1.

**CHAPTER 3:**  
**Quercetin and resveratrol**  
**encapsulation in a single drug**  
**delivery system with elastin-like**  
**recombinamers by Supercritical**  
**antisolvent process (SAS)**



### **CHAPTER 3: Quercetin and resveratrol encapsulation in a single drug delivery system with elastin-like recombinamers by Supercritical antisolvent process (SAS)**

In this chapter, ELR particles have been produced by combining two hydrophobic drugs, quercetin (QCT), a phenolic compound of the flavonoid family with neuroprotective and anti-cancer benefits, and resveratrol (RES), a stilbene belonging to the phenolic compounds with antioxidant and anti-inflammatory properties. In this case, a mixture of ethanol and water has been used as a solvent in the SAS plant. First, a range of experiments has been carried out to set up the plant and to establish the new operating conditions to obtain an adequate yield. The new formulations obtained have been physically and chemically characterised; Besides the release profiles of both drugs have been measured and mathematically modelled. Finally, thanks to the collaboration with the Instituto Universitario de Oftalmobiología Aplicada (IOBA) of the Universidad de Valladolid, Spain, it has been proposed to carry out *in vitro* and *ex vivo* tests of the formulations developed in this chapter.

## 8. RESULTS & DISCUSSION

In the first two chapters of this thesis we have used DMSO as a solvent to work with the SAS technique, however, in certain cases, although both compounds, polymer/drug, show high solubility in DMSO, it is not desirable to use it because of the possible residues that may remain in the final product. To overcome this setback, more suitable solvents, such as ethanol, can be used. The limiting factor that exists with this solvent, is that ELRs are not soluble in ethanol, however, adding a certain amount of water, the resulting mixture is a possible solvent for ELR as for the drugs used. At this point, as the number of solvents increases when using the SAS technique, the complexity of finding the appropriate operating conditions increases, as we now have a three-phase diagram, as shown in Figure 49. Regarding the drugs used in this chapter, both quercetin and resveratrol are soluble in ethanol (2 mg/mL [1] and 50 mg/mL [2]) and would not constitute a solubility problem. Although there are examples in the literature in which the solutions of both the carrier and the solutes are prepared independently and mixed before being co-precipitated [3], in this case, the objective is to take advantage of the pulverisation capacity of the coaxial nozzle designed in previous chapters, therefore, an ethanol-water mixture that is capable of dissolving both the ELR and both drugs could be adequate to achieve the desired objectives.

### 8.1. Optimization of the operational conditions for ethanol-water-scCO<sub>2</sub> encapsulation with ELRs.

As in previous chapters, pressure and temperature were set at 11MPa and 308K. From the bibliographic study of the ethanol-water-scCO<sub>2</sub> ternary diagram for these operating conditions[4], the solubility curve is shown in Figure 49.

The experiments were started at P1 Figure 49, taking as a reference the results obtained in [5], where two independent solutions of ethanol and water were mixed before being



sprayed into the precipitation vessel. In our case, a unique solution using ethanol/water as solvent was used and the pulverisation was performed using a coaxial nozzle. Nevertheless, we have taken as a starting point the conditions established in [5] as this is where the highest yield and the lowest percentage of residual ethanol by weight in the final product are found.

Therefore, to carry out the encapsulation experiments of resveratrol (RES) and quercetin (QCT), as well as their combination, we started conducting basic solubility tests with ELR in ethanol-water at different v/v ratios of the ethanol/water mixture and also including QCT and RES, as they have water solubility limitations. A 90/10 v/v ratio was found to be successful in solubilising the ELR and QCT and RES at the desired concentrations. in the mixture. The operating conditions in the SAS plant were established at a CO<sub>2</sub> flow of 0.5 kg/h and solution flow pumping in the reactor of 10.8 mL/min.

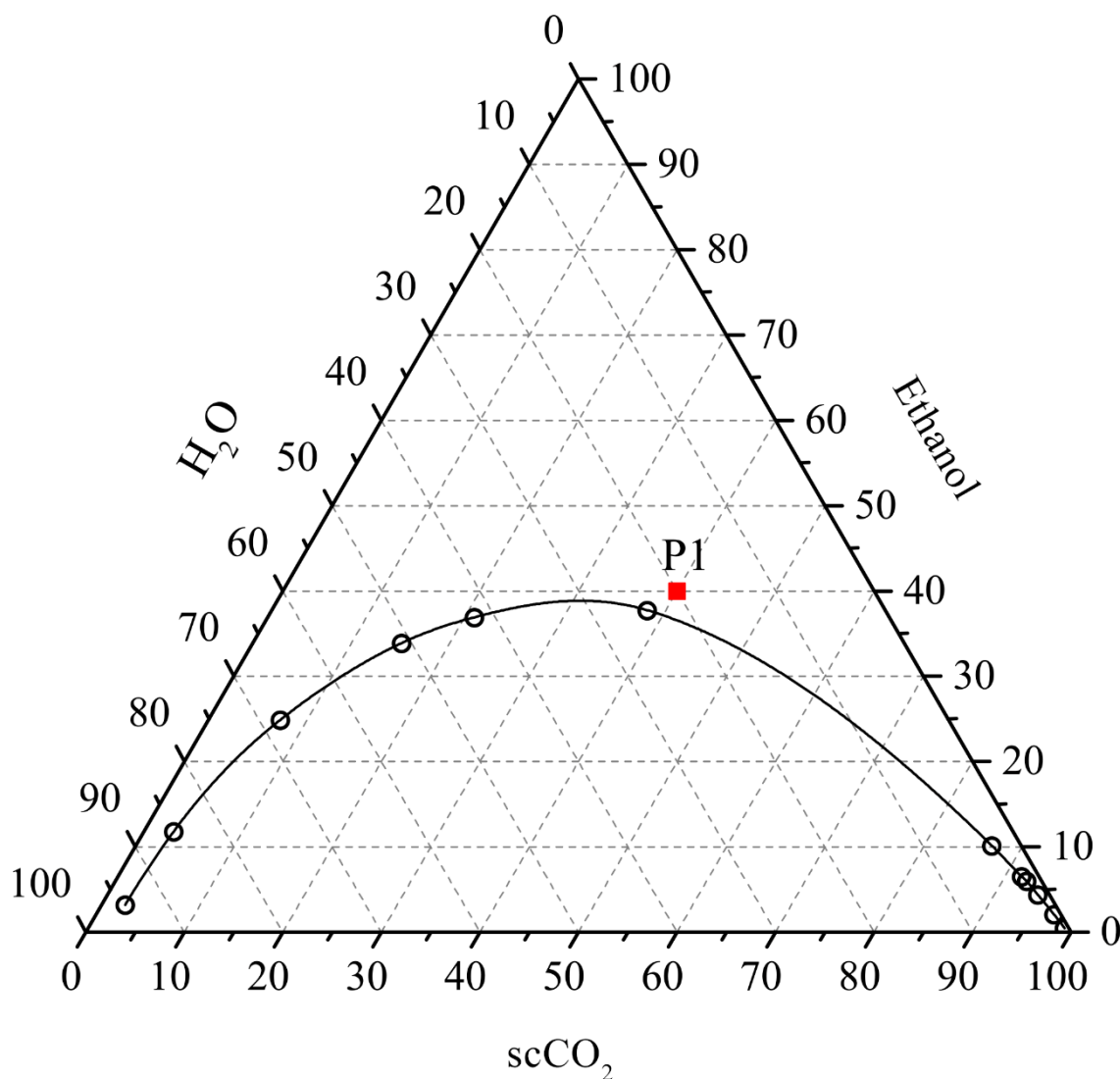


**Figure 49.** Mole fraction phase diagram of the system (ethanol-water-scCO<sub>2</sub>) at 11 MPa and 308K, P1 represents the operating conditions of 0.5 kg/h CO<sub>2</sub> flow rate and 10.8 mL/min solution flow rate. The solubility curve values were reproduced from [6]

Two ratios (ELR:drug) of 3:1 and 6:1 (w/w) were established to initiate the encapsulation tests in which the ELR concentration was set at 15 mg/mL and the drug concentration at 5 mg/mL. In the case where the two drugs are combined (quercetin and resveratrol), a molar ratio of 1:1 is established between them and 6:1 (w/w) for ELR (ELR: (QUER:RES), resulting in an ELR:QCT:RES ratio of 13.95:1.32:1 (w/w). The drug and polymer solutions were prepared in separate vials. Over the weighed drug mass, 18 mL of pure non-denatured ethanol is added and kept under magnetic stirring at 700 rpm until

completely dissolved (approximately 10 min), then the ethanol/drug solution was pipetted over the previously weighed polymer mass, and 2 mL of ultrapure deionised water was added to achieve a 90/10 (v/v) ethanol/water ratio and was kept under magnetic stirring at 700 rpm until completely dissolved (approximately 10 min). The first experiments under P1 conditions (Figure 49 are shown in Table 17 (experiments 1-5)) where we can observe low yields in the final product obtained as well as the appearance of the film in the samples that comprises QCT with a greater amount of ELR. In all cases, the collection of the final powder required a complicated procedure, as it remained stuck to the walls of the reactor and, even in the experiment with the lowest yield (experiment 3) no powder was found in the filter placed out of the reactor. Furthermore, we observed that when we have ELR:drug ratios of 3:1 the yield obtained drops considerably compared to the yield obtained with a 6:1 ratio. These results confirm that the variation of the ratio and, therefore, of the ELR concentration in the solution, has a significant influence on the yield of the process. Hence, all subsequent experiments were carried out with a 6:1 ratio to maintain a high concentration of polymer and achieve higher yields.

| Exp. | (EI) <sub>2</sub> : Drug | CO <sub>2</sub> mass flow rate (kg/h) | Solution flow rate (mL/min) | Drug    | (EI) <sub>2</sub> (mg/mL) | Drug (mg/mL) | Yield (%) (w/w) | Final appearance |
|------|--------------------------|---------------------------------------|-----------------------------|---------|---------------------------|--------------|-----------------|------------------|
| 1    | 3:1                      | 0.5                                   | 10.8                        | QCT     | 15                        | 5            | 13              | powder           |
| 2    | 6:1                      | 0.5                                   | 10.8                        | QCT     | 30                        | 5            | 53              | Powder + film    |
| 3    | 3:1                      | 0.5                                   | 10.8                        | RES     | 15                        | 5            | 3               | powder           |
| 4    | 6:1                      | 0.5                                   | 10.8                        | RES     | 30                        | 5            | 41              | powder           |
| 5    | 6:1*                     | 0.5                                   | 10.8                        | QCT+RES | 30                        | 5            | 35              | film             |
| 6    | 6:1                      | 2                                     | 2                           | QCT     | 30                        | 5            | 62              | powder           |
| 7    | 6:1                      | 2                                     | 2                           | RES     | 30                        | 5            | 68              | powder           |
| 8    | 6:1*                     | 2                                     | 2                           | QCT+RES | 30                        | 5            | 65              | powder           |
| 9    | 6:1*                     | 2                                     | 2                           | QCT+RES | 30                        | 5            | 61              | powder           |

**Table 17.** Screening experiments for the SAS process performed with (EI)<sub>2</sub>, quercetin (QCT), resveratrol (RES) at 11MPa, 308 K. \*1:1 Molar ratio between quercetin and resveratrol.

## CONCLUSIONS

---

Looking at the three-phase diagram shown in Figure 49, it can be observed that previously described operating conditions are located above the solubility curve and, therefore, in the miscible area of the diagram (ethanol-water-scCO<sub>2</sub>) but, analysing the coaxial nozzle outflow velocities of both fluids (Table 18), it can be noticed that the difference between them is very high. This results in a failure to produce the desired turbulence for the desired pulverisation of the ethanol-water-ELR-drug solution with scCO<sub>2</sub>. As can be seen in Table 18, in operating condition A, the differences between the outlet velocities of the two fluids are very different, and even if the scCO<sub>2</sub> mass flow rate is increased (operating condition B), this difference in velocities is not sufficiently reduced, which makes it impossible for the scCO<sub>2</sub> to pulverise the solution. Neither is this result achieved when the volume flow of the solution is decreased while maintaining the scCO<sub>2</sub> mass flow rate at 0.5 kg/h as observed in operating condition C. However, when the CO<sub>2</sub> mass flow rate is increased to 2kg/h and solution volumetric flow was reduced to 2 mL/min the outflow velocity of the scCO<sub>2</sub> through the nozzle increases, matching the outflow velocity of the solution through the inner coaxial nozzle pipe and thus enabling the scCO<sub>2</sub> to generate an aerosol from the liquid solution [7].

| <b>Operating condition</b> | <b>scCO<sub>2</sub> mass flow (kg/h)</b> | <b>Solution volumetric flow (mL/min)</b> | <b>CO<sub>2</sub> velocity (m/s)</b> | <b>Solution velocity (m/s)</b> |
|----------------------------|--|--|--------------------------------------|--------------------------------|
| A (P1)                     | 0.5                                      | 10.8                                     | 0.0366                               | 0.8881                         |
| B                          | 2  | 10.8                                     | 0.1464                               | 0.8881                         |
| C                          | 0.5                                      | 2  | 0.0366                               | 0.1645                         |
| D (P2)                     | 2  | 2  | 0.1464                               | 0.1645                         |

**Table 18.** CO<sub>2</sub> and solution outflow velocities through the coaxial nozzle calculated according to the geometry of the nozzle, see annexe I

Due to the modification of the CO<sub>2</sub> and solution flows, the location in the three-phase diagram changes, placing it in the zone shown in Figure 50, which is still located in the single-phase miscible zone. With these new operating conditions (P2; Figure 50), the

yields improved considerably as shown in Table 17 (experiments 5-9) where the final product obtained was a homogeneous fine powder that did not stick to the reactor walls, which facilitated its recovery.

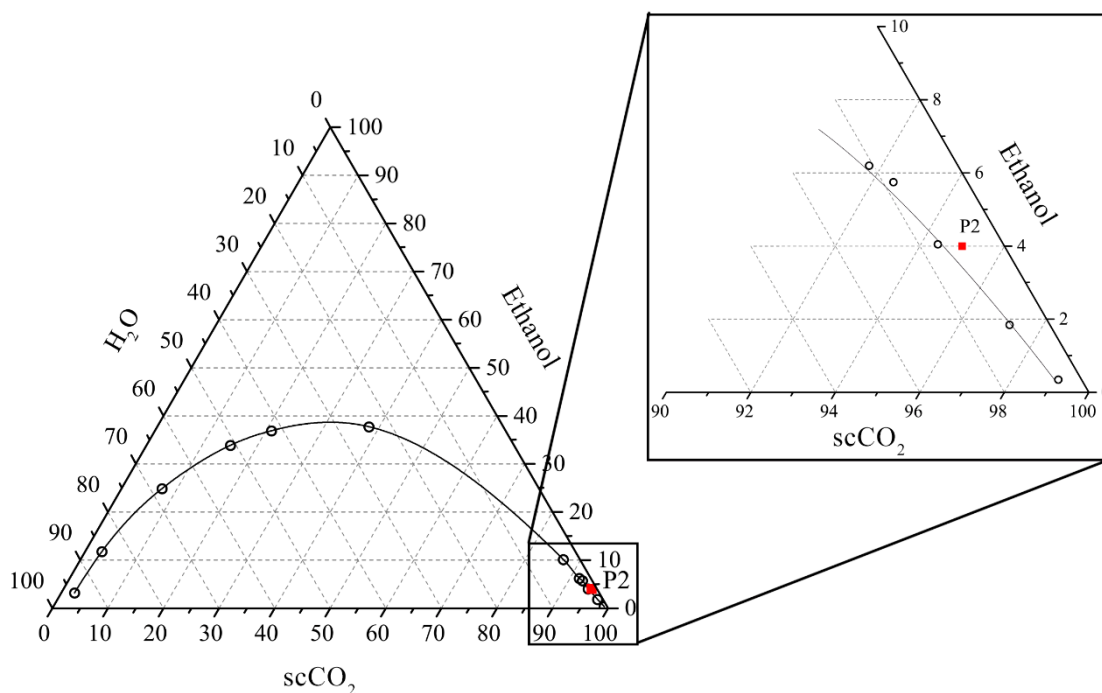


**Figure 50.** Mole fraction phase diagram of the system (scCO<sub>2</sub> - ethanol - water) at 11MPa and 308K. P2 represents the operating conditions of 2 kg/h CO<sub>2</sub> flow rate and 2 mL/min solution flow rate. The solubility curve values were reproduced from [6].

## 8.2. Particle characterization

### 8.2.1. NMR study for quercetin, resveratrol and their mixture with ELRs.

In order to find the proportions of each component present in the final product obtained after the SAS technique, we should know which are the signals that identify each compound and which are perfectly distinguishable from the rest of the compounds, so that we can quantify each component by the integral of the area under the corresponding signal.

In order to identify quercetin and resveratrol by NMR, a previous simulation is performed in MEstReNova v 9.0.1 using deuterated DMSO as a solvent, Figure 51. From both

## CONCLUSIONS

spectra, the signals that will not interfere with the signals provided by the NMR spectrum corresponding to the ELR are taken. Thus, for quercetin, the signals that refer to the CH groups of carbons 6 and 2 (6.4 and 6.2 ppm, respectively) are taken. In the same way, for resveratrol, the CH group corresponding to carbon 14, at 6.13 ppm, is taken as a reference, Figure 51. In both cases, the signals were identified in the commercial compounds.

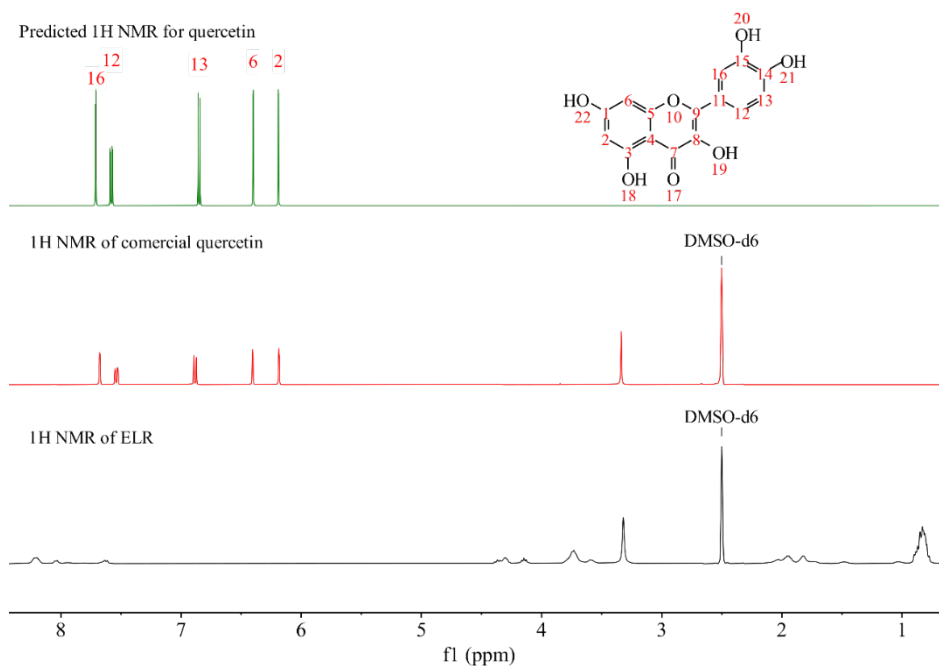


**Figure 51.** Stacked <sup>1</sup>H-NMR spectra of the predicted quercetin (green), <sup>1</sup>H-NMR spectrum corresponding to the commercial quercetin used in this chapter (red) and <sup>1</sup>H-NMR spectrum of the ELR (EI)2 (black).

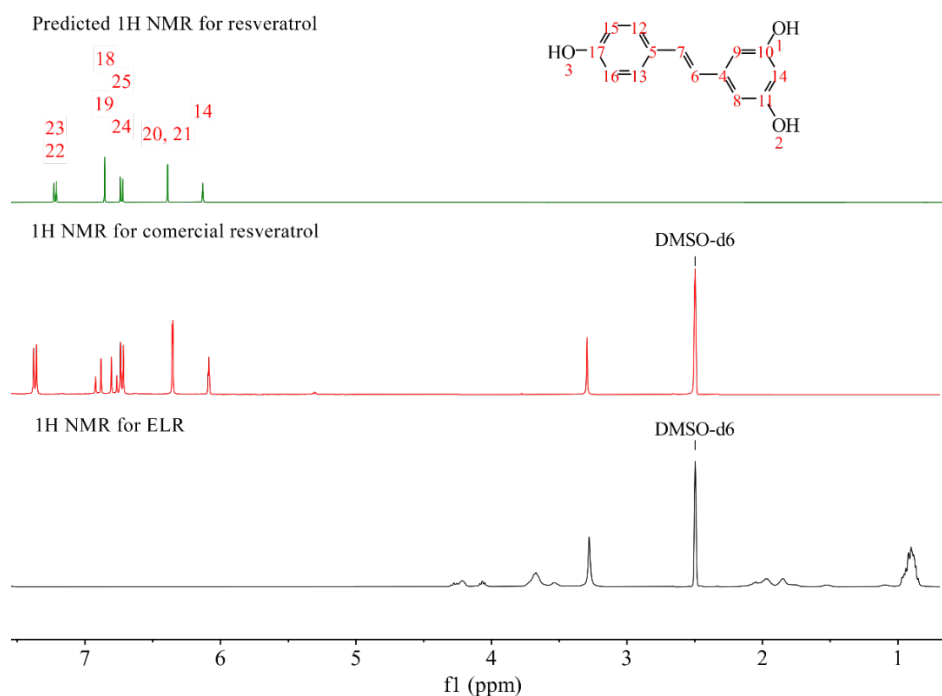


**Figure 52.** Stacked <sup>1</sup>H NMR spectra of the predicted resveratrol (green), <sup>1</sup>H NMR spectrum corresponding to the commercial resveratrol used in this chapter (red) and <sup>1</sup>H NMR spectrum of the ELR (EI)2 (black).

The samples obtained in experiments 1-9 (Table 17) were analysed following the protocol described in the Materials and Methods section 2.3.1. In all cases, except in experiment 1, the initial ELR:drug ratio was maintained (Table 19), and we can also observe the low amount of residual ethanol in the final product, which is very low, indicating that the formulations have high purity and no residues, as can be seen in Figure 54 corresponding to experiments 5-9, where the peak that identifies the ethanol (at 1.20 ppm) in the samples has a very low intensity.

## CONCLUSIONS

| Exp. | final ratio (ELR:drug) | ELR % | QCT % | RES % | ethanol % | SEM D(3.2) (µm) | SEM D(0.5) (µm) |
|------|------------------------|-------|-------|-------|-----------|-----------------|-----------------|
| 1    | 4:1                    | 81.0  | 18.6  | -     | 0.1       | N/D             | N/D             |
| 2    | 6:1                    | 86.1  | 13.8  | -     | 0.1       |                 |                 |
| 3    | 3:1                    | N/D   | -     | N/D   | N/D       |                 |                 |
| 4    | 6:1                    | 85.0  | -     | 14.9  | 0.1       |                 |                 |
| 5    | 6:1                    | 86.6  | 7.3   | 5.9   | 0.2       |                 |                 |
| 6    | 6:1                    | 86.1  | 13.8  | -     | 0.1       | 16.7            | 5.9             |
| 7    | 6:1                    | 84.6  | -     | 15.1  | 0.3       | 8.6             | 2.6             |
| 8    | 6:1                    | 85.4  | 7.8   | 6.3   | 0.5       | 16.2            | 3.7             |
| 9    | 6:1                    | 85.4  | 7.8   | 6.1   | 0.4       | N/D             | N/D             |

**Table 19.** Final ratios and proportions of the different compounds obtained in % (w/w) and determined by <sup>1</sup>H-NMR corresponding to the screening of experiments made for the setting up of the SAS plant., D (3.2) or Mean Sauter Diameter is the diameter of a sphere that has the same volume/surface area ratio as the particle size distribution (). and D (0.5), is determined from the images obtained by SEM (n>200) -. N/D not determined

In samples comprising both quercetin and resveratrol, we should be able to distinguish the signals of the two compounds clearly. Figure 53 shows the combined <sup>1</sup>H NMR spectra of both commercial compounds overlaid on top of each other. As we can see there are overlapping signals between the two compounds, but we can distinguish two signals that appear in the peaks at 6.18 ppm and 6.09 ppm, which, although they are very close, are easily identifiable and correspond to the CH group number 2 of quercetin (Figure 51) and the CH group number 14 of resveratrol (Figure 52).



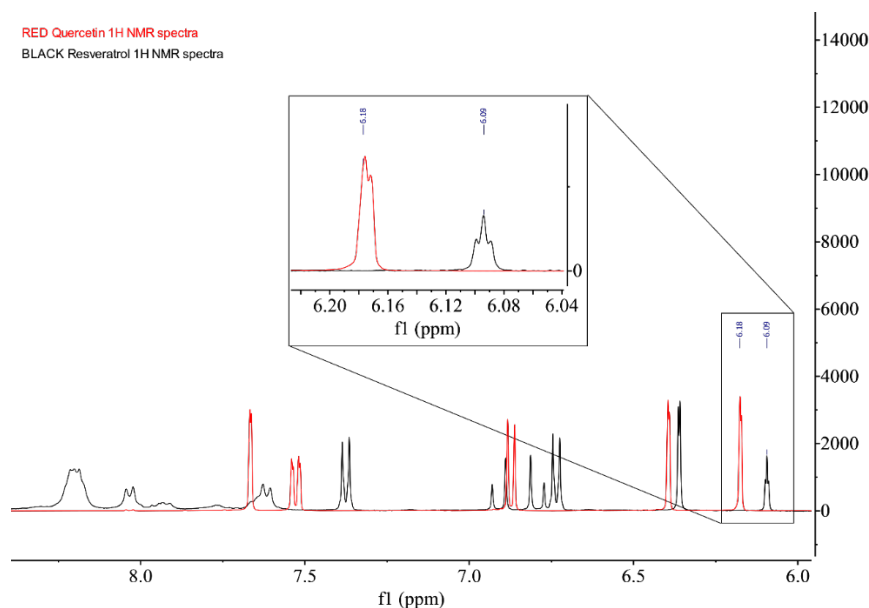


**Figure 53.** Overlapped  $^1\text{H}$ -NMR spectra of commercial quercetin (red) and commercial resveratrol (black)

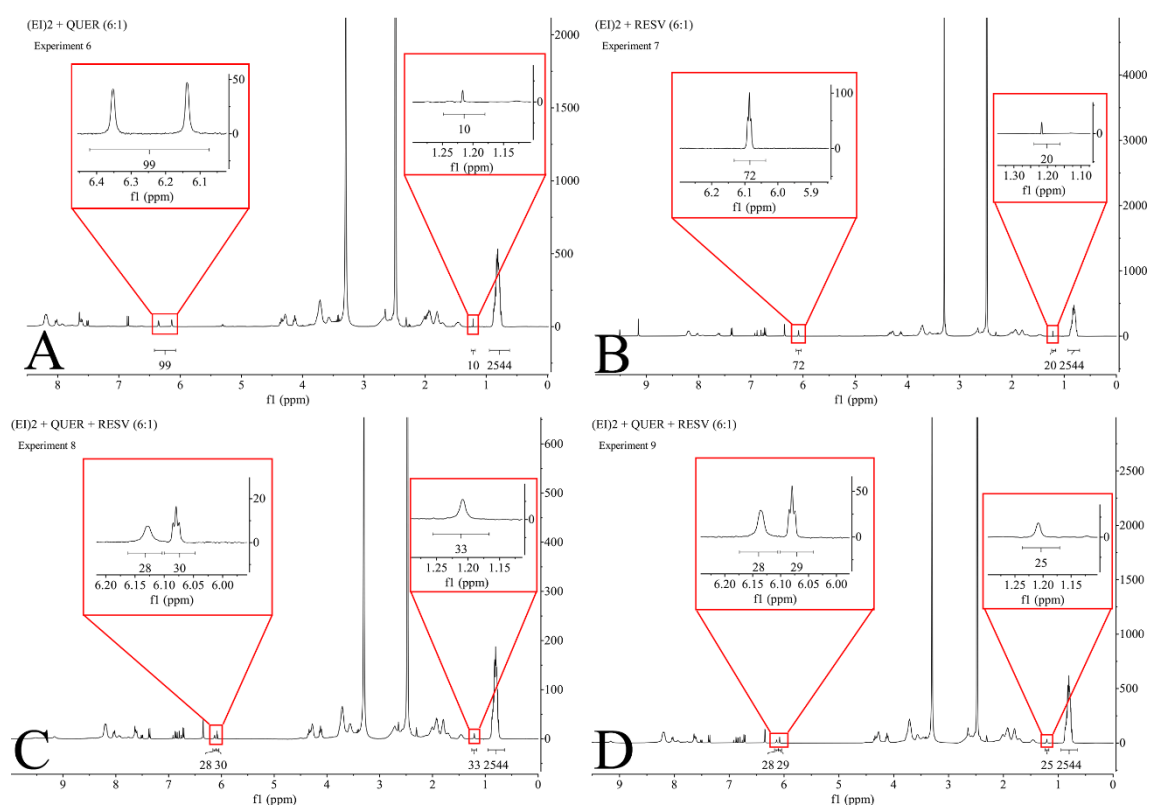


**Figure 54.**  $^1\text{H}$  NMR spectra and value of the integrals measured on the distinctive peaks of each compound of the samples used for further analysis. A (EI)2 + QCT (6:1); B (EI)2 + RES; C (EI)2 + QCT + RES (6:1) and D (EI)2 + QCT + RES (6:1). Magnifications in the spectra: A between 6.4-6.1 ppm for QCT signal and 1.25-1.15 ppm for ethanol signals, B between 6.2-5.9 ppm for RES signals and 1.3-1.10 ppm for ethanol signals, C between 6.2-6 ppm for RES signals and 1.25-1.15 ppm for ethanol signals and D between 6.2-6 ppm for RES signals and 1.25-1.15 ppm for ethanol signals.

### **8.2.2. Particle analysis by SEM**

The particles obtained in the experiments with an ELR:drug ratio of 6:1 were analysed by SEM in order to check the geometry of the powder obtained after encapsulation by SAS. As can be seen in Figure 55 the samples do not show significant aggregation, however, a wide range of sizes can be seen, from very small particles to particles twice or three times the size of the earlier mentioned ones.

This may be due to two reasons, the first is related to the fluid outlet velocities through the coaxial nozzle. In previous chapters, this difference in velocities was much greater ( $\text{CO}_2$  outflow velocity  $\gg$  solution outflow velocity), resulting in a more homogeneous pulverisation of the solution containing the ELR and the drug, giving place to microdroplets where very fast nucleation and more homogeneous sizes are produced. In this case, the outflow velocities of both fluids (Table 18) is very close, which may cause the pulverisation to be less homogeneous, leading to microdroplets of different sizes, and consequently to more heterogeneous nucleation. The second reason is related to the concentration of the active agent. Low supersaturation in the SAS technique [8] causes slower nucleation and results in more heterogeneous particles.

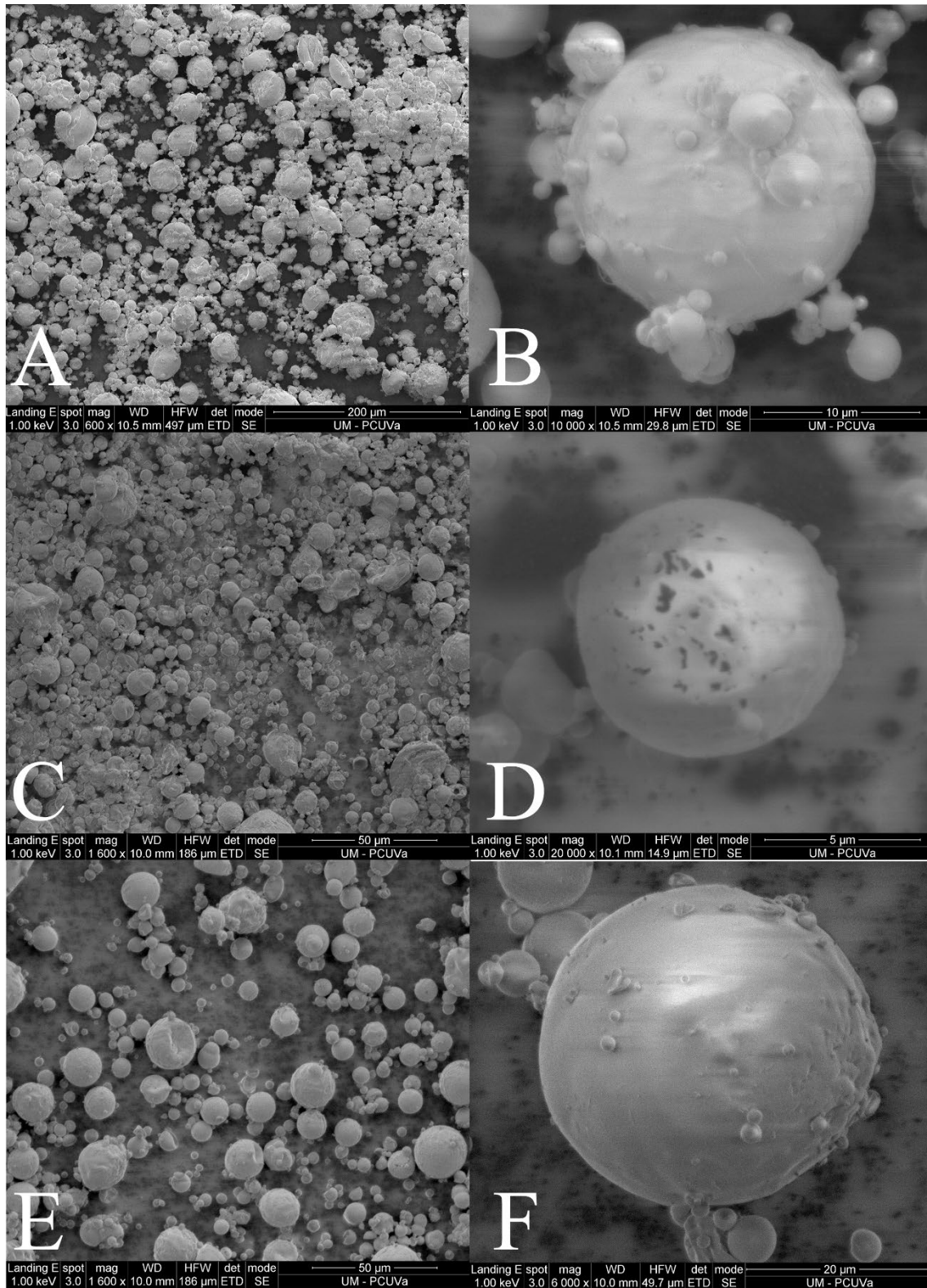


**Figure 55.** SEM Photomicrographs showing general (A, scale bar: 200  $\mu\text{m}$ ; magnification: x600; C and E scale bar: 50  $\mu\text{m}$  magnification x1600). Detailed views (B, scale bar: 10  $\mu\text{m}$ ; magnification: x10000; D, scale bar: 5  $\mu\text{m}$ ; magnification: x20000; F, scale bar: 20  $\mu\text{m}$ ; magnification: x6000) for the powder obtained in experiment 6 (A and B), experiment 7 (C and D) and experiment 8 (E and F)

### 8.2.3. Behaviour in aqueous solution

It is of vital importance that the particles are stable over time, i.e. that they do not tend to form agglomerations, establishing a heterogeneous dispersion in the medium in which they are found. For this purpose, the particles obtained by SAS corresponding to experiments 6-8 (Table 17), were dispersed in an aqueous medium at 37°C, as described in the Materials and Methods section 2.3.5, and the particle size was monitored for 5 days, preserving the samples in an incubator at 37°C during the measurements.

| Exp. | Day 0      |               |                  | Day 3      |               |                  | Day 5      |               |                  |
|------|------------|---------------|------------------|------------|---------------|------------------|------------|---------------|------------------|
|      | D(0.5)     | PDI           | ζ-Potential (mV) | D(0.5)     | PDI           | ζ-Potential (mV) | D(0.5)     | PDI           | ζ-Potential (mV) |
| 6    | 56.7 ± 1.0 | 0.072 ± 0.007 | -30.2 ± 3.2      | 57.9 ± 2.6 | 0.080 ± 0.005 | -31.2 ± 1.8      | 56.3 ± 1.6 | 0.067 ± 0.007 | -31.7 ± 2.1      |
| 7    | 58.6 ± 2.2 | 0.094 ± 0.010 | -32.6 ± 3.95     | 61.2 ± 2.2 | 0.098 ± 0.011 | -34.5 ± 2.3      | 57.6 ± 1.7 | 0.098 ± 0.004 | -33.1 ± 3.3      |
| 8    | 61.5 ± 2.6 | 0.115 ± 0.004 | -33.1 ± 2.8      | 64.5 ± 2.6 | 0.119 ± 0.012 | -31.1 ± 1.9      | 59.9 ± 2.3 | 0.113 ± 0.006 | -32.4 ± 1.8      |

**Table 20.** Values for the diameter, PDI and ζ-potential at different times during the stability assay (37°C and neutral pH). Deviation presented by Mean ±SD

The results obtained are shown in Table 20 where we can observe particle sizes between 56 and 61 nm with a PDI of 0.1 or below, maintaining these values without significant variations during the rest of the measurements. These results, supported by a ζ- Potential above -30mV, confirm that the particle dispersion in the aqueous medium remains stable, not giving place to the formation of aggregates thanks to the fact that the ζ- potential is high enough to maintain a homogeneous particle dispersion as it is proved by the low PDI values in all the measurements.

### 8.3. Drug delivery study

A release kinetic study was carried out comparing the pure drugs with the prepared formulations (EI)<sub>2</sub>+QCT; (EI)<sub>2</sub>+RES and (EI)<sub>2</sub>+QCT+RES in order to determine the amount of drug released at each time point. In this case, the formulation containing both drugs have been analysed separately, i.e. the amount of quercetin released ((EI)<sub>2</sub> + QCT + RES (QCT)) on the one hand and the amount of resveratrol released ((EI) + QCT + RES (RES)) in order to determine the amount of each compound released over time when they are combined in the same formulation at a concentration of 0.012 mg/mL of both drugs. Figure 56, shows the percentage of the compounds released by each of the formulations analysed in a total time of 24 hours. Each of the time points represents the result of the analysis in triplicate, with the standard deviation represented by the error bars.

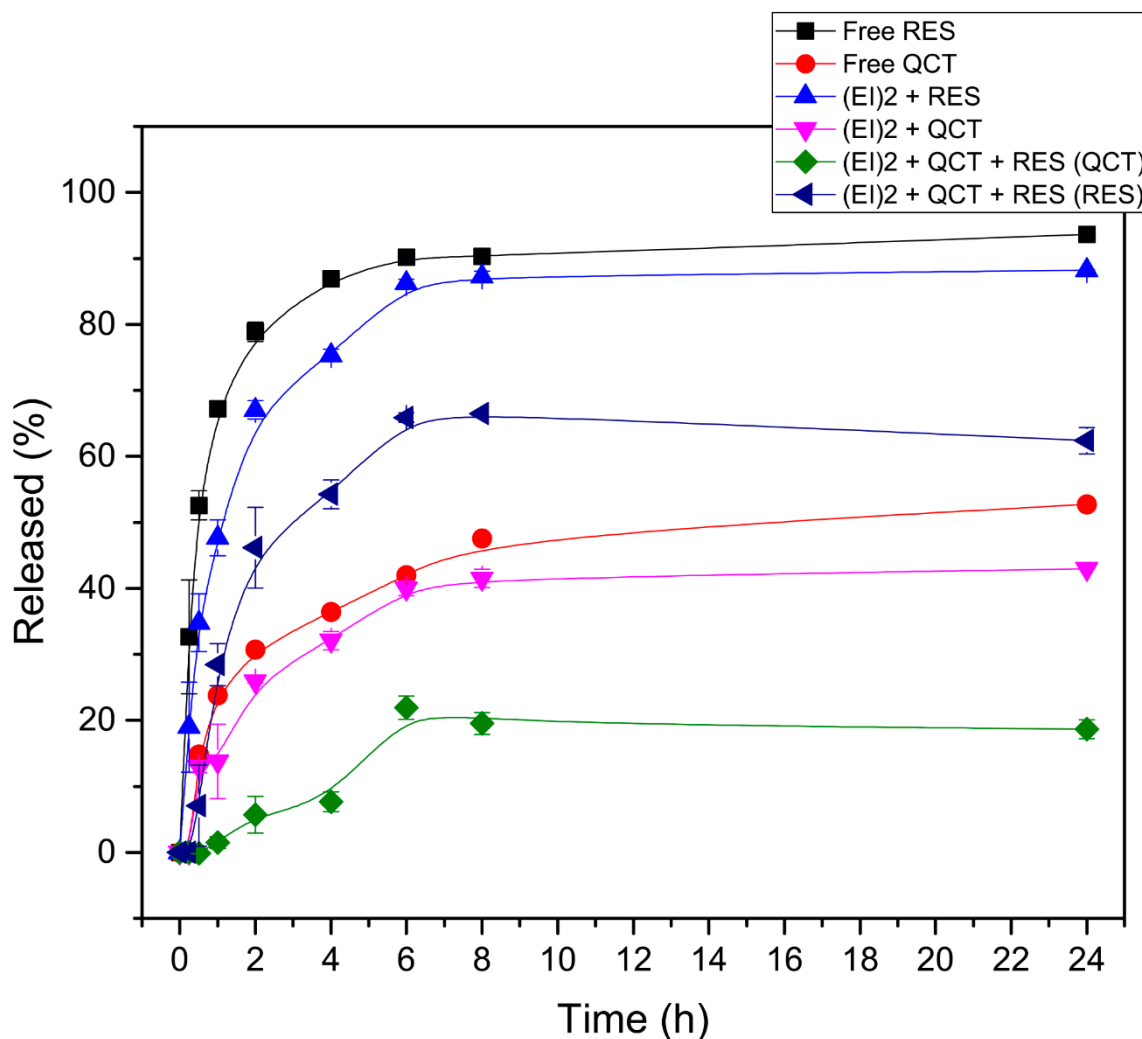


**Figure 56.** Drug delivery profiles of the samples comprising quercetin and resveratrol and free resveratrol and quercetin control samples vs. time (h) at a normalized QCT and RES concentration of 100mM in PBS release medium at 37°C. ■: Free Resveratrol; ●: Free Quercetin; ▲: (EI)2 + Resveratrol; ▼: (EI)2 + Quercetin; ◆: (EI)2 + Quercetin + Resveratrol (Quercetin); ◀: (EI)2 + Quercetin + Resveratrol (Resveratrol). (Lines are used to guiding the eye).

As can be seen for both the (EI)2 + RES and (EI)2 + QCT profiles, there is a clear delay in the release of each compound, reaching 48 % and almost 15 % respectively after 1 hour of the assay with respect of the free molecules that reach 68% and 22 for the free RES and QCT respectively. Furthermore, it can be seen how there is a clear difference in the release between both compounds, being almost double for RES than for QCT; This may be due to the difference in solubility of each of the compounds since in the case of RES the solubility 10 folds higher that of QCT (0.03 and 0.003 mg/mL respectively [9,10]),

this is a fact that we also observed in the free compounds (Free RES and Free QCT) establishing a difference in the release behaviour of both compounds when they are contained in independent formulations. However, the differences are more pronounced when both compounds are incorporated in the same formulation ((EI)2 + RES + QCT)), in this case, 50% of the release is reached after 4 hours for RES and only about 10% for QCT for the same period of time. In this situation, there are some interesting observations: on the one hand, when both drugs are part of the same formulation, the release of both compounds is even more delayed compared to the other two formulations ((EI)2 +RES and (EI)2 + QCT), which implies that the release is more sustained over time. But, on the other hand, we see how the release profile of QCT when released from the formulation (EI)2 + RES + QCT is very erratic, this may be due to the fact that quercetin is very easily degraded in the medium, as has been reported in literature [5,6]:Thus hypothesising a scenario where QCT is being released into the medium and there is a part that is degraded and cannot be measured and there is another part that has been released in a short period

of time and is the one that has actually been analysed resulting in the profile shown in the Figure 56.

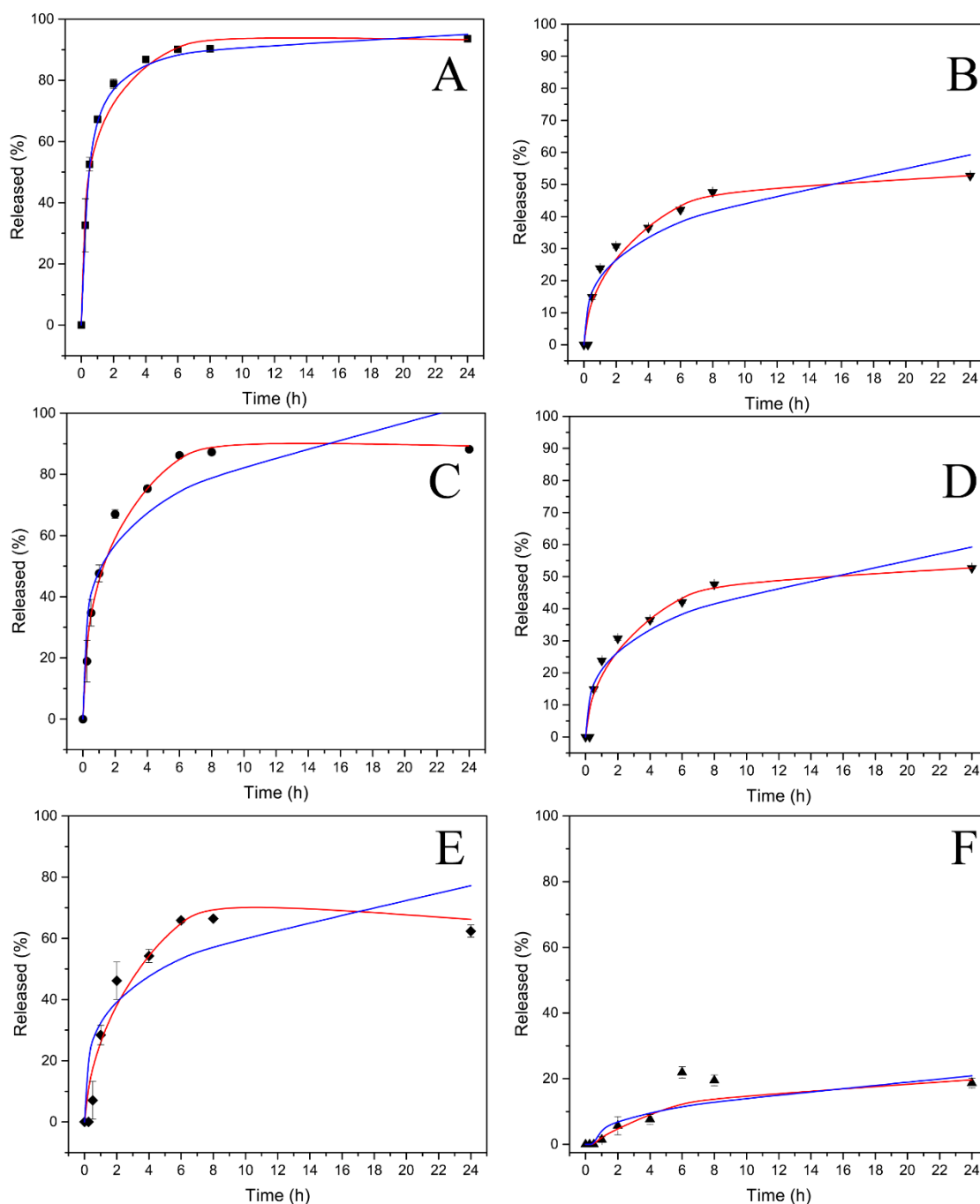


**Figure 57.** Mathematical fitting of release profiles to Peppas-Sahlin (red) and Lindner-Lippold (blue) models. A) ■ Free Resveratrol; B) ▼: Free Quercetin; C) ●: (EI)2 + Resveratrol; D) ◄: (EI)2 + Quercetin; E) ◆: (EI)2 + Quercetin + Resveratrol (Quercetin); F) ▲: (EI)2 + Quercetin + Resveratrol (Resveratrol).



In order to have a better understanding of the release process, the experimental profiles shown in Figure 56, have been mathematically fitted to the most appropriate mathematical models described in the Introduction. The results of these fits are shown graphically in Figure 57 and the values of the constants which define these models can be seen in Table 21. In all cases, the Peppas-Sahlin model fits the release profiles properly with  $R^2 > 0.96$ , except in the case of the profile of the quercetin released in the formulation containing quercetin and resveratrol (EI)<sub>2</sub> + QCT + RES (QCT)) and that being such an erratic profile as discussed above, the mathematical fit is very poor, due to the fact that for achieving an optimal fitting, data of at least 60% released must be obtained, in this case, no more than 22% released is reached, which severely compromises the fit. As for the coefficient 'n' of the Peppas-Sahlin equation, values between  $0.5 < n < 0.85$  were found, which indicates that we are dealing with a case of anomalous transport in the form of spheres and a process governed by a Fick-type diffusion, as can be seen in Table 21, since in all cases the coefficient 'k1', which is the constant related to the contribution to the Fick-type mechanism, has the most weight in the equation. However, a particular case is the one involving the formulation (EI)<sub>2</sub> + QCT + RES (QCT) where we observe an  $n > 1$ , this could indicate a case of super case II transport, but it occurs that 60% of the release is not reached and therefore the fit is unreliable even more when the  $R^2$  value is 0.82.

| Model                                  | Peppas-Sahlin fitting |                 |                |                       | Lindner-Lippold fitting |                  |                |                       |
|--|-----------------------|-----------------|----------------|-----------------------|-------------------------|------------------|----------------|-----------------------|
| Coefficient<br>Sample                  | k <sub>1</sub>        | k <sub>2</sub>  | n              | COD<br>R <sup>2</sup> | k <sub>1</sub>          | b                | n              | COD<br>R <sup>2</sup> |
| Free QCT                               | 21.59 ±<br>3.01       | -2.12 ±<br>0.66 | 0.57 ±<br>0.07 | 0.95                  | 25.03 ±<br>7.58         | -3.67 ±<br>0.69  | 0.29 ±<br>0.07 | 0.90                  |
| Free RES                               | 52.14 ±<br>0.168      | -6.63 ±<br>0.04 | 0.45 ±<br>0.04 | 0.99                  | -32.72<br>± 2.58        | 101.08<br>± 2.04 | 0.53 ±<br>0.04 | 0.99                  |
| (EI) <sub>2</sub> + QCT                | 16.54 ±<br>2.21       | -1.39 ±<br>0.43 | 0.65 ±<br>0.07 | 0.97                  | 21.55 ±<br>7.73         | -3.75 ±<br>0.70  | 0.29 ±<br>0.09 | 0.87                  |
| (EI) <sub>2</sub> + RES                | 53.91 ±<br>3.03       | -7.55 ±<br>0.97 | 0.48 ±<br>0.03 | 0.98                  | 52.93 ±<br>13.11        | -3.99 ±<br>1.18  | 0.22 ±<br>0.06 | 0.89                  |
| (EI) <sub>2</sub> + QCT +<br>RES (QCT) | 2.399 ±<br>0.43       | -0.05 ±<br>0.02 | 1.13 ±<br>0.08 | 0.83                  | 6.24 ±<br>0.61          | -1.21 ±<br>0.55  | 0.40 ±<br>0.27 | 0.82                  |
| (EI) <sub>2</sub> + QCT +<br>RES (RES) | 29.28 ±<br>4.58       | 2.80 ±<br>1.01  | 0.63 ±<br>0.08 | 0.96                  | 36.50 ±<br>1.51         | -3.61 ±<br>1.37  | 0.24 ±<br>0.10 | 0.80                  |

**Table 21.** Fitting of the profiles for release Free Resveratrol; Free Quercetin; (EI)<sub>2</sub> + Resveratrol; (EI)<sub>2</sub> + Quercetin; (EI)<sub>2</sub> + Quercetin + Resveratrol (Quercetin); (EI)<sub>2</sub> + Quercetin + Resveratrol (Resveratrol) processed using the SAS technique to the Peppas–Sahlin and Lindner–Lippold equations.

Analysing the values obtained by the Lindner-Lippold adjustment, parameter ‘b’ (burst effect) it can be seen that in all cases it takes negative values, indicating that the drug is inside the particles and is released by diffusion towards the dispersant medium in a sustained manner. As regards the values obtained in the coefficient 'b' (burst effect) corresponding to the free resveratrol (Free RES) adjustment, we can see that it has a very high value, indicating that the release process occurs at a very high speed, as expected. Another case to highlight is that of free quercetin (Free QCT), which shows a negative value of the 'b' coefficient. In this case, this parameter cannot be adequately evaluated since part of the quercetin degrades over time and in this situation the quercetin analysed is probably lower than that actually released at each time point and therefore the profile actually has a much greater slope and consequently a value of 'b' above 0.

#### **8.4.Final remarks**

Two highly hydrophobic drugs such as quercetin and resveratrol used for the treatment of dry eye disease have been successfully encapsulated using the SAS technique with CO<sub>2</sub> in a supercritical state in a one-step process, maintaining negligible levels of residual ethanol (0.1-0.5%). Operating conditions were established to have satisfactory precipitation yield (mean value) and a high load of the active compounds. As a result, high added value formulations have been obtained which, as shown in the SEM images shown, do not present significant aggregation. Moreover, the analysis of the formulations in an aqueous medium shows a particle system with a size of approximately 60 nm with PDIs close to 0.1 and thanks to a sufficiently high  $\zeta$ -potential that remains stable over time. On the other hand, the analysis of the release profiles shows a sustained and controlled release over time compared to the controls analysed of free quercetin and resveratrol, although it is also worth noting the difficulty in analysing the quercetin released, as its rapid degradation makes it difficult to analyse the amount released into the medium. Furthermore, analysis of the release profile fittings shows that the process is governed by a Fick-type diffusion from spherical particles. Consequently, a new controlled release system has been produced that is stable over time in aqueous media, capable of releasing two highly hydrophobic drugs. Finally, and thanks to the collaboration with PhD. Luna Kristic from the Instituto Universitario de Oftalmobiología Aplicada (IOBA), the formulations obtained in this chapter are being validated in vitro by cell viability, antioxidant activity in corneal epithelial cell lines (HCE cells) and permeation assays in the same cell line and finally ex vivo ocular permeation assays on pig eyes.

**8.5. REFERENCES**

- [1] D. Lide, G.W.A. Milne, Handbook of data on organic compounds, 3rd ed., CRC Press, Boca Raton Fla., 1994. <https://books.google.com/books?id=-dJ2re4p22gC> (accessed November 27, 2021).
- [2] Resveratrol | 501-36-0, (n.d). [https://www.chemicalbook.com/ChemicalProductProperty\\_EN\\_cb7325012.htm](https://www.chemicalbook.com/ChemicalProductProperty_EN_cb7325012.htm) (accessed November 27, 2021).
- [3] M.J. Cocero, Á. Martín, F. Mattea, S. Varona, Encapsulation and co-precipitation processes with supercritical fluids: Fundamentals and applications, *J. Supercrit. Fluids.* 47 (2009) 546–555. <https://doi.org/10.1016/j.supflu.2008.08.015>.
- [4] J.S. Lim, Y.Y. Lee, H.S. Chun, Phase equilibria for carbon dioxide-ethanol-water system at elevated pressures, *J. Supercrit. Fluids.* 7 (1994) 219–230. [https://doi.org/10.1016/0896-8446\(94\)90009-4](https://doi.org/10.1016/0896-8446(94)90009-4).
- [5] W. Cuervo-Paez, S. Rodriguez-Rojo, M. Salgado, S. Lobos-Garcia, A. Cubero, F. Menegotto, M. Simarro-Grande, M.A. Bratos, A. Orduña, M.J. Cocero, rotein Encapsulation in PolyVinyl Alcohol (PVA) - Inulin Microparticles from Aqueous Solutions by Supercritical Antisolvent, in: Belgrade, 2013.
- [6] M.L. Gilbert, M.E. Paulaitis, Gas-liquid equilibrium for ethanol-water-carbon dioxide mixtures at elevated pressures, *J. Chem. Eng. Data.* 31 (2002) 296–298. <https://doi.org/10.1021/JE00045A012>.
- [7] P.D. Hede, P. Bach, A.D. Jensen, Two-fluid spray atomisation and pneumatic nozzles for fluid bed coating/agglomeration purposes: A review, *Chem. Eng. Sci.* 63 (2008) 3821–3842. <https://doi.org/10.1016/J.CES.2008.04.014>.
- [8] M. Kalani, R. Yunus, Application of supercritical antisolvent method in drug encapsulation: a review., *Int. J. Nanomedicine.* 6 (2011) 1429–1442. <https://doi.org/10.2147/ijn.s19021>.
- [9] K. Srinivas, J.W. King, L.R. Howard, J.K. Monrad, Solubility and solution thermodynamic properties of quercetin and quercetin dihydrate in subcritical water, *J. Food Eng.* 100 (2010) 208–218. <https://doi.org/10.1016/J.JFOODENG.2010.04.001>.
- [10] A. Amri, J.C. Chaumeil, S. Sfar, C. Charrueau, Administration of resveratrol: What formulation solutions to bioavailability limitations?, *J. Control. Release.* 158 (2012) 182–193. <https://doi.org/10.1016/j.jconrel.2011.09.083>.

# CONCLUSIONS



## 9. CONCLUSIONS

- Different hydrophobic drugs, such as acetazolamide (Chapter 1), docetaxel (Chapter 2), quercetin and resveratrol (Chapter 3), have been successfully encapsulated with ELR using the SAS technique, establishing a new working methodology with solvents such as DMSO (Chapters 1 and 2) and ethanol/water mixtures (Chapter 3). where the powder obtained after performing the SAS technique showed no significant differences in morphology as verified by SEM. Moreover, the encapsulation ratios were not affected as verified by  $^1\text{H-NMR}$ .
- The SAS plant has been successfully modified by a new reactor in which the cover seals were modified by toric seals and the lower cover was designed with a conical shape and a new scheme where the filter, which collects the encapsulates, is located outside the vessel itself, thus simplifying the recovery of the high added value final product. In addition, a new coaxial nozzle has been designed and manufactured, which has allowed us to reduce the final quantities of residual solvent maintaining adequate values (55-70%) of process yields (Chapter 2).
- All the drugs used in this thesis were properly encapsulated without significant differences in their morphology, as it has been verified by different microscopy techniques, such as TEM, and AFM. Moreover, all the formulations show a stable behaviour and do not exhibit a tendency to aggregate thanks to the low PDIs found and the negative surface charge (Z-potential) provided by the ELR coating (Chapters 1, 2 and 3).

- An exhaustive  $^1\text{H-NMR}$  analysis of the final product obtained was performed (Chapter 2), where the smart behaviour of the polymer was demonstrated by temperature changes and the consequent modification of its characteristic signals, which also showed that the SAS technique did not affect its smart behaviour. Furthermore, it was demonstrated how the drug was encapsulated inside the ELR by studying the spectra at different temperatures.
- The *in vitro* drug release assays have allowed us to demonstrate that the drugs used in this thesis are released following a fick diffusion release mechanism, obtaining a sustained and controlled release over time (Chapters 1, 2 and 3).
- Finally, and thanks to the collaborations established during this thesis, it has been possible to conduct different *in vitro*, *ex vivo* and *in vivo* assays with the formulations obtained (Chapters 1 and 2). In these analyses, the nanodevices have demonstrated an appropriate cellular specificity, their therapeutic functionality, and excellent biocompatibility to be considered as potential candidates for systemic and topical treatment delivery systems.



# ABBREVIATIONS



---

**10.ABBREVIATIONS**

|                          |  |
|--------------------------|--|
| <b><sup>1</sup>H-NMR</b> | Proton nuclear magnetic resonance                          |
| <b>AFM</b>               | Atomic force microscopy                                    |
| <b>API</b>               | Active Pharmaceutical Ingredient                           |
| <b>AUC</b>               | Area under the curve                                       |
| <b>AZM</b>               | Acetazolamide  |
| <b>BCS</b>               | Biopharmaceutics Classification System                     |
| <b>CAI</b>               | Carbonic anhydrase inhibitors                              |
| <b>CMC</b>               | Critical Micellar concentration                            |
| <b>Da</b>                | Daltons  |
| <b>DAPI</b>              | Diamino-2-phenylindole-dyhydrochloride                     |
| <b>DED</b>               | Dry eye disease  |
| <b>DLS</b>               | Dynamic light scattering                                   |
| <b>DMSO</b>              | Dimethyl sulphoxide  |
| <b>DSC</b>               | Differential scanning calorimetry                          |
| <b>DTX</b>               | Docetaxel  |
| <b><i>E. coli</i></b>    | <i>Escherichia coli</i>                                    |
| <b>ELR</b>               | Elastin like recombinamer                                  |
| <b>EMA</b>               | European Medicine Agency                                   |
| <b>FDA</b>               | Frood and Drug Administration                              |
| <b>FTIR</b>              | Fourier transform infrared spectroscopy                    |
| <b>HLB</b>               | Hydrophilicity-lipophilicity balance                       |
| <b>HUVEC</b>             | Human umbilical vein endothelial cells                     |
| <b>ITT</b>               | Inverse transition temperature                             |
| <b>MALDI-TOF</b>         | Matrix-assisted laser desorption/ionization–Time-of-flight |
| <b>MTD</b>               | Maximum Tolerated Dose                                     |
| <b>MW</b>                | Molecular weight   |
| <b>NDA</b>               | New Drug Application                                       |
| <b>nm</b>                | Nanometers   |
| <b>PBS</b>               | Phosphate buffered saline                                  |
| <b>PCL</b>               | Poly(caprolactone)   |
| <b>PDI</b>               | Polidispersity index                                       |
| <b>PEG</b>               | Poly(ethylene glycol)                                      |
| <b>PGSS</b>              | Particles from gas saturated solutions                     |
| <b>PIO</b>               | Intraocular pressure                                       |
| <b>PLA</b>               | Poly(lactic acid)  |
| <b>PLGA</b>              | Poly(lactic co-glycolic acid)                              |
| <b>PMDA</b>              | Japan Pharmaceuticals and Medical Devices Agency           |
| <b>QCT</b>               | Quercetina   |
| <b>RES</b>               | Resveratrol  |
| <b>RESS</b>              | Rapid expansion of supercritical solution                  |

## ABBREVIATIONS

---

|                         |   |
|-------------------------|---|
| <b>SAS</b>              | Supercritical antisolvent                   |
| <b>scCO<sub>2</sub></b> | Supercritical CO <sub>2</sub>               |
| <b>SCFs</b>             | Supercritical fluids                        |
| <b>SD</b>               | Standard deviation                          |
| <b>SEM</b>              | Scanning electron microscopy                |
| <b>SFEs</b>             | Supercritical fluid extraction of emulsions |
| <b>SSI</b>              | Supercritical solvent impregnation          |
| <b>TEM</b>              | Transmission Electron microscopy            |
| <b>Uv</b>               | Ultraviolet                                 |
| <b>v/v</b>              | Volume/volume                               |
| <b>w/w</b>              | Weight/weight                               |

# ANNEX I



## Chemical modification of polymer (EI)2 with fluorescein

To prepare amine-reactive esters of carboxylate groups for chemical crosslinking. Carboxylate groups (-COOH) from glutamic acid belonging to the (EI)2 may be reacted to N-hydroxysuccinimide (NHS) in the presence of a carbodiimide such as 1-Ethyl-3-(3-dimethylaminopropyl)carbodiimide (EDC), resulting in a semi-stable N-Hydroxysuccinimide ester (NHS), which may then be reacted with primary amines (-NH<sub>2</sub>) to form amide crosslinks (Figure 1). The protocol for the modification is detailed below:

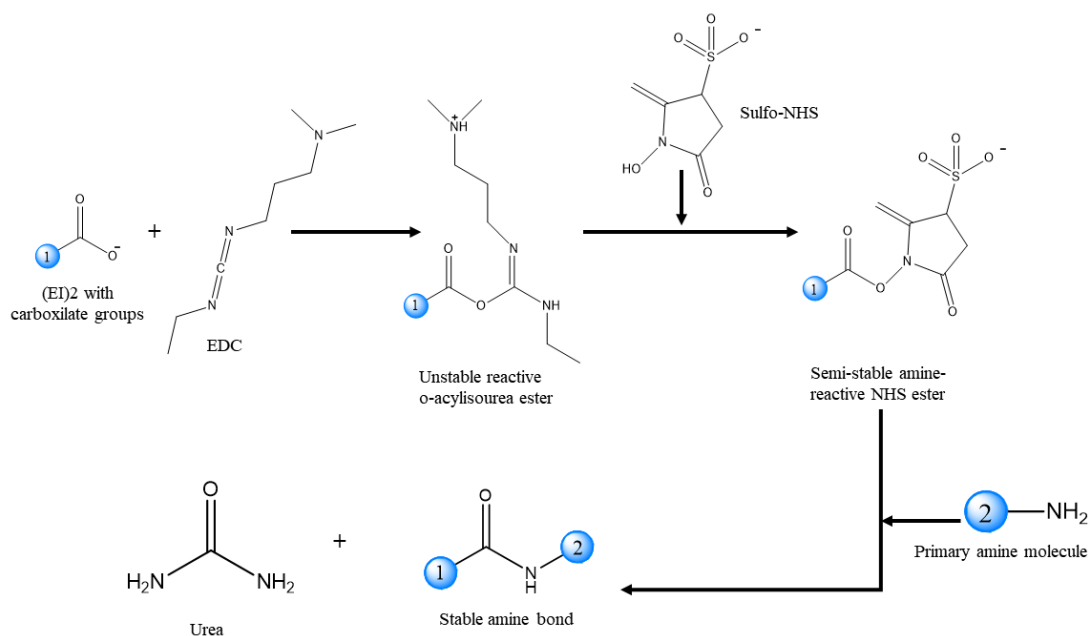


**Figure 1.** The chemical reaction pathway followed to obtain fluorescein-modified (EI)2, where 1, represents the chemical bond to the glutamic acid belonging to the (EI)2, and 2, represents the chemical bond to the fluorescein.

One (EI)2 polymer equivalent is dissolved in 2-ethane sulphonic acid (MES buffer) under magnetic stirring overnight in a cold chamber. Afterwards, 10 EDC equivalents dissolved in the same buffer are added. Subsequently, 10 equivalents of NHS are added on top of the previous solution and left to react under magnetic stirring for 3 hours at 4°C. Then the pH of the reaction is adjusted above 7 using concentrated PBS, followed by the addition of 5 Fluorescein Glycine Amide equivalents to the solution and allowed to react under

magnetic stirring overnight. The pellet is discarded after centrifugation at 8000g and 4°C. Finally, the solution is dialysed in dialysis bags (cut-off 14 kDa) over 25L of pure deionised water overnight and then lyophilised prior to storage.

**<sup>1</sup>H-NMR determination of the presence of fluorescein in the modified polymer.**

The <sup>1</sup>H-NMR analysis was performed following the methodology described in Materials and Methods section 5.3.1, in figure 2 we can observe the stacked spectra of the unmodified (EI)2, the (EI)2 modified with fluorescein and the commercial fluorescein. In red, we can see the signals identifying fluorescein in (EI)2-fluorescein, confirming the presence of this fluorophore in the modified polymer. It is certain that the signals do not have a wide amplitude in the modified polymer ((EI)2-fluorescein), but this is because the degree of modification of the glutamic acids that constitute the (EI)2 polymer is not complete, since only one glutamic acid per molecule was modified to affect as little as possible the formation of nano-particles due to the amphiphilic character.



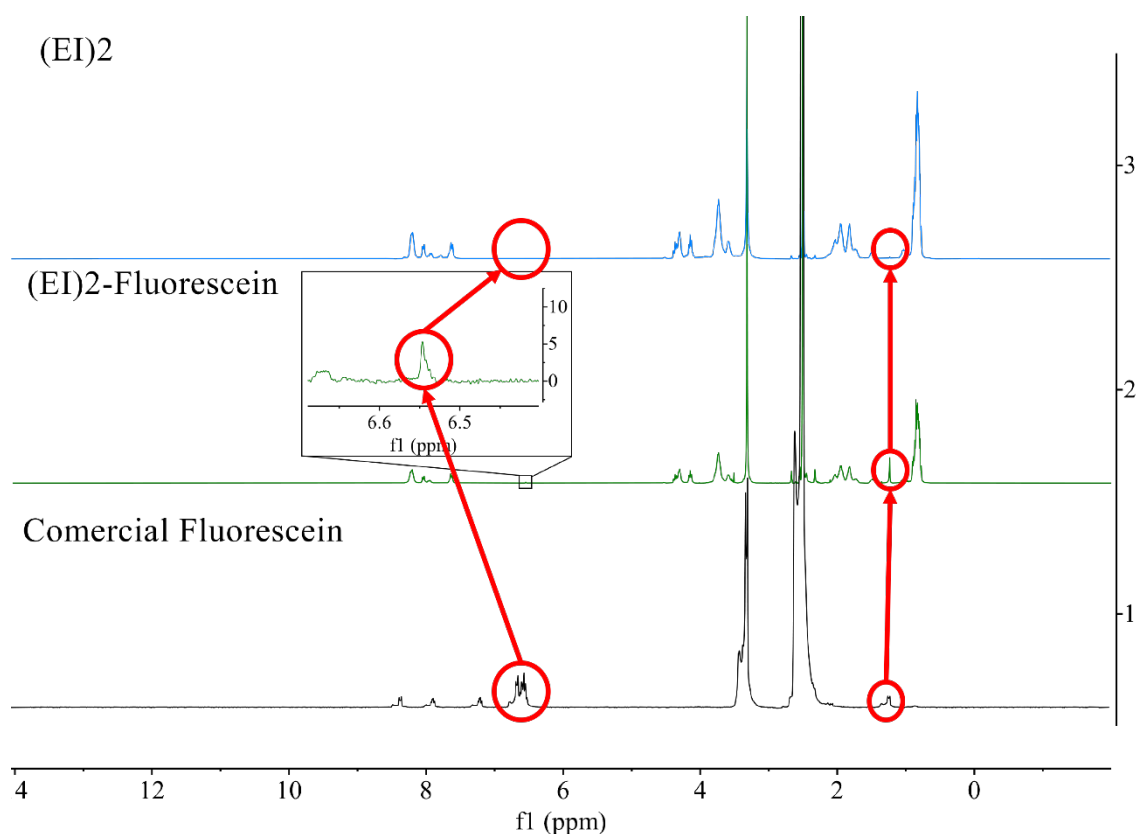


**Figure 2.** Stacked  $^1\text{H-NMR}$  spectra corresponding to the unmodified (EI)2 polymer (1), the (EI)2 polymer modified with fluorescein (2) and the commercial fluorescein (3) used for the chemical modification.

### **Encapsulation of Nile Red with fluorescein-modified (EI)2 by SAS.**

Nile Red (NR) has been encapsulated with fluorescein-modified (EI)2 by SAS technique using the methodology presented in Chapter 3 of this thesis, in order to be able to follow the polymer and the encapsulating agent in future fluorescence microscopy analyses. Unfortunately, it was not possible to confirm by  $^1\text{H-NMR}$  analysis the presence of Nile Red in the final product, because a small amount of this compound was encapsulated, to facilitate its tracking through the fluorescence microscope and not to saturate the detector during the analysis. However, the final product obtained did show the characteristic colouring produced by Nile Red.

**Behaviour in aqueous media**

The fluorescein modified (EI)2 polymer and the SAS encapsulated Nile Red formulation were analysed by DLS for testing their behaviour in aqueous media following the methodology described in Materials and Methods section 5.3.5. Table 1 summarises the results obtained after particle size analysis. Where we can observe particle sizes that are in the range of sizes observed in previous chapters of this Thesis, as well as very low PDIs of 0.1 or lower, combined with  $\zeta$ -Potential of -30mV, which suggests, on the one hand, that the behaviour in aqueous media of the (EI)2 polymer modified with fluorescein has not been affected after the incorporation of the fluorophore to its structure and, in addition, both samples present results that indicate that the system is stable in time and monodisperse.

| <b>Sample</b>          | <b>D (0.5) (nm)</b> | <b>PDI</b>        | <b><math>\zeta</math>-Potential (mv)</b> |
|------------------------|---------------------|-------------------|--|
| (EI)2-Fluorescein      | 50.6 $\pm$ 2.9      | 0.126 $\pm$ 0.005 | -32.6 $\pm$ 1.3                          |
| (EI)2-Fluorescein + NR | 45.9 $\pm$ 2.0      | 0.056 $\pm$ 0.007 | -31.0 $\pm$ 0.8                          |

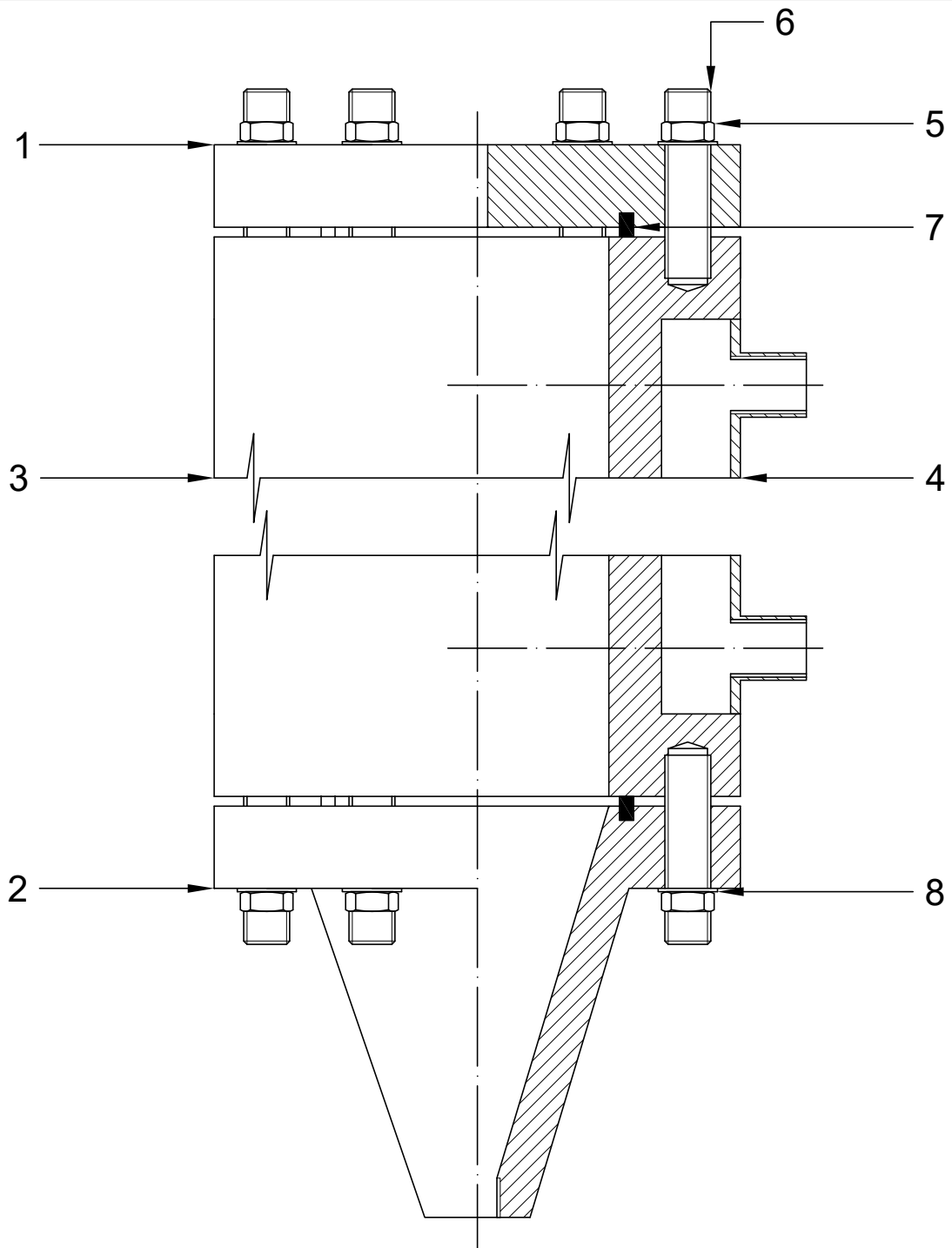
**Table 1.** Values for the diameter, PDI and  $\zeta$ -potential at 37°C and neutral pH for fluorescein modified (EI)2 and Nile Red encapsulated with fluorescein modified (EI)2.

**Final remarks**

It has been possible to chemically modify the (EI)2 polymer with a fluorophore such as fluorescein by modifying the carboxylate groups belonging to the glutamic acids that compose the structure of the polymer, without compromising the behaviour of the polymer in aqueous media. Furthermore, it has been possible to encapsulate Nile Red with (EI)2 modified with fluorescein by means of the SAS technique, obtaining a final product that will allow us to track with the fluorescence microscope, not only the polymer, but also the encapsulated agent.

# ANNEX II

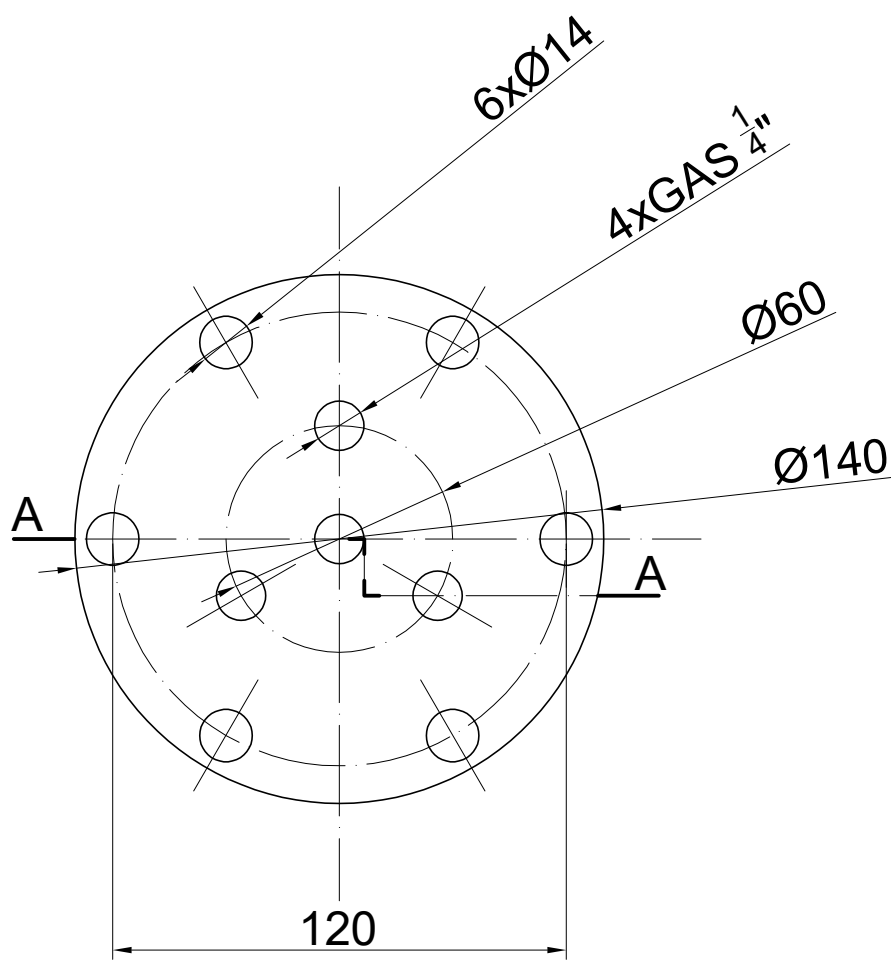




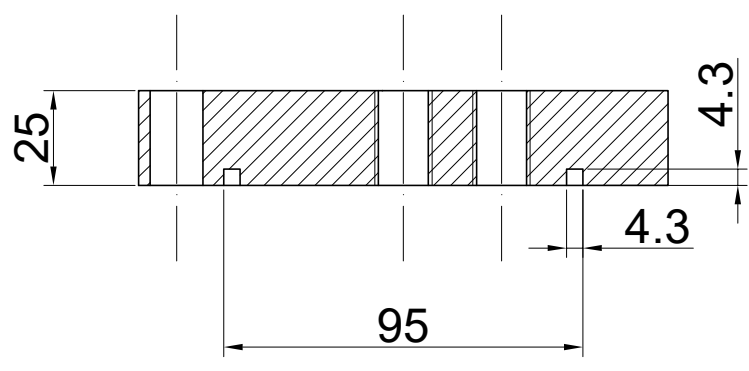
|              |                      |       |            |
|--------------|----------------------|-------|------------|
| 1            | Tapa superior        | 1     | acero 316L |
| 1            | Tapa inferior        | 2     | acero 316L |
| 1            | Cuerpo del reactor   | 3     | acero 316L |
| 1            | Encamisado           | 4     | acero 316L |
| 12           | Tuerca hexagonal M12 | 5     | acero 316  |
| 12           | Perno M12            | 6     | acero 316  |
| 2            | Junta torica         | 7     | teflón     |
| 12           | Arandela M12         | 8     | acero 316  |
| Nº de piezas | Denominación         | Marca | Material   |

|               |                               |                          |       |                                |
|---------------|-------------------------------|--------------------------|-------|--------------------------------|
| SIS. REP.     | FECHA                         | NOMBRE                   | FIRMA | TESIS REINALDO VALLEJO VICENTE |
|               |                               | REINALDO VALLEJO VICENTE |       |                                |
| ESCALA<br>1:2 | CONJUNTO REACTOR ALTA PRESIÓN |                          |       |                                |





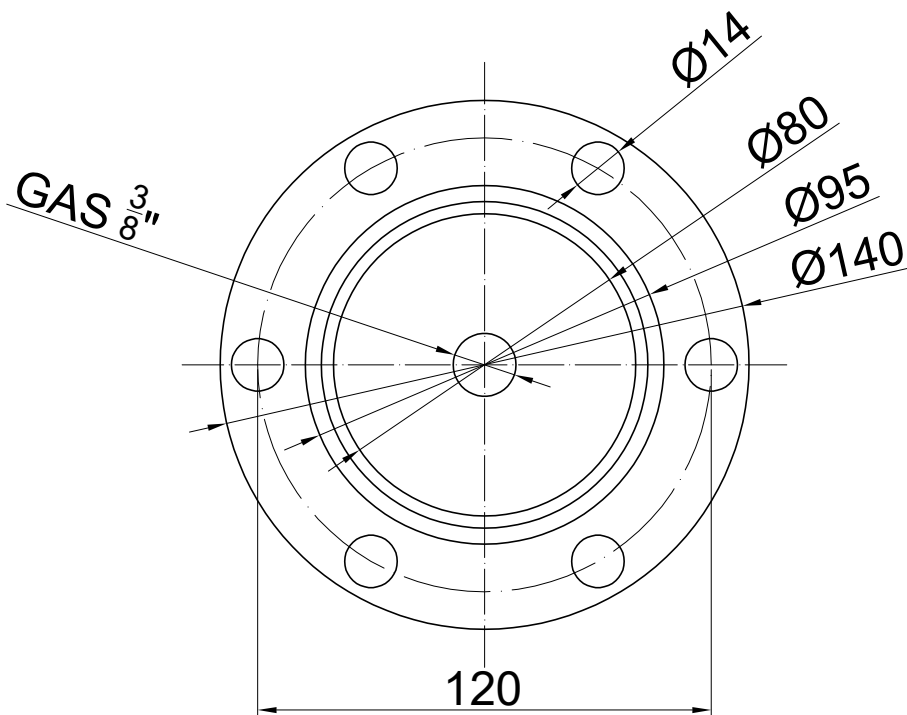
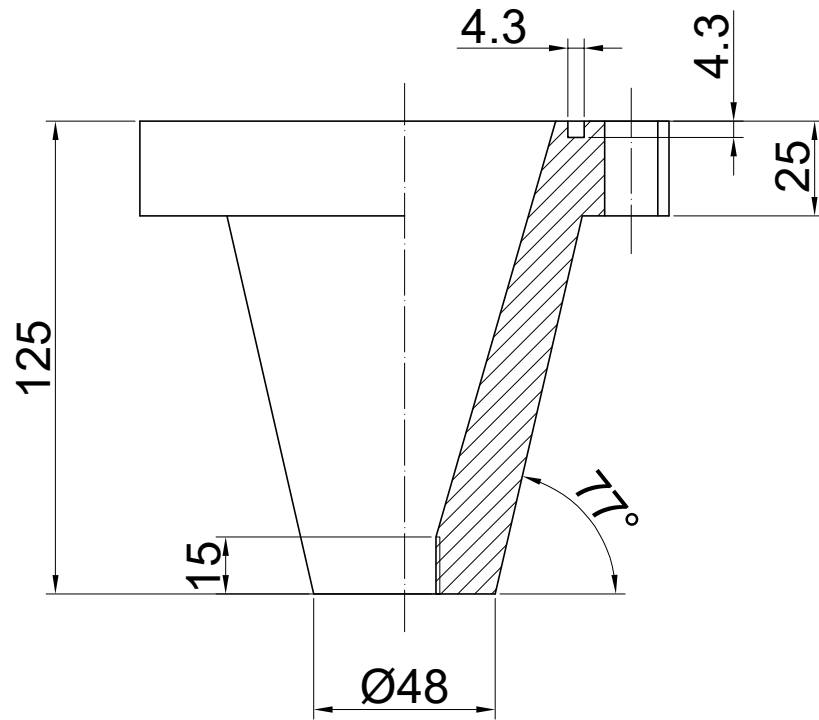
CORTE A-A

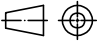


|               |               |                          |       |                                |
|---------------|---------------|--------------------------|-------|--------------------------------|
| SIS. REP.     | FECHA         | NOMBRE                   | FIRMA | TESIS REINALDO VALLEJO VICENTE |
|               |               | REINALDO VALLEJO VICENTE |       |                                |
| ESCALA<br>1:2 | TAPA SUPERIOR |                          |       | PLANO NÚMERO: 1<br>MARCA: 1    |

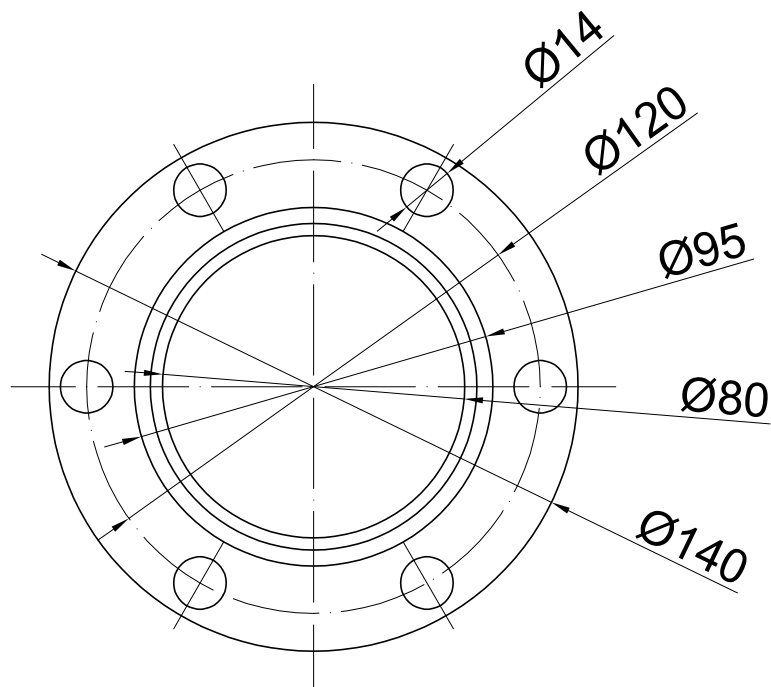
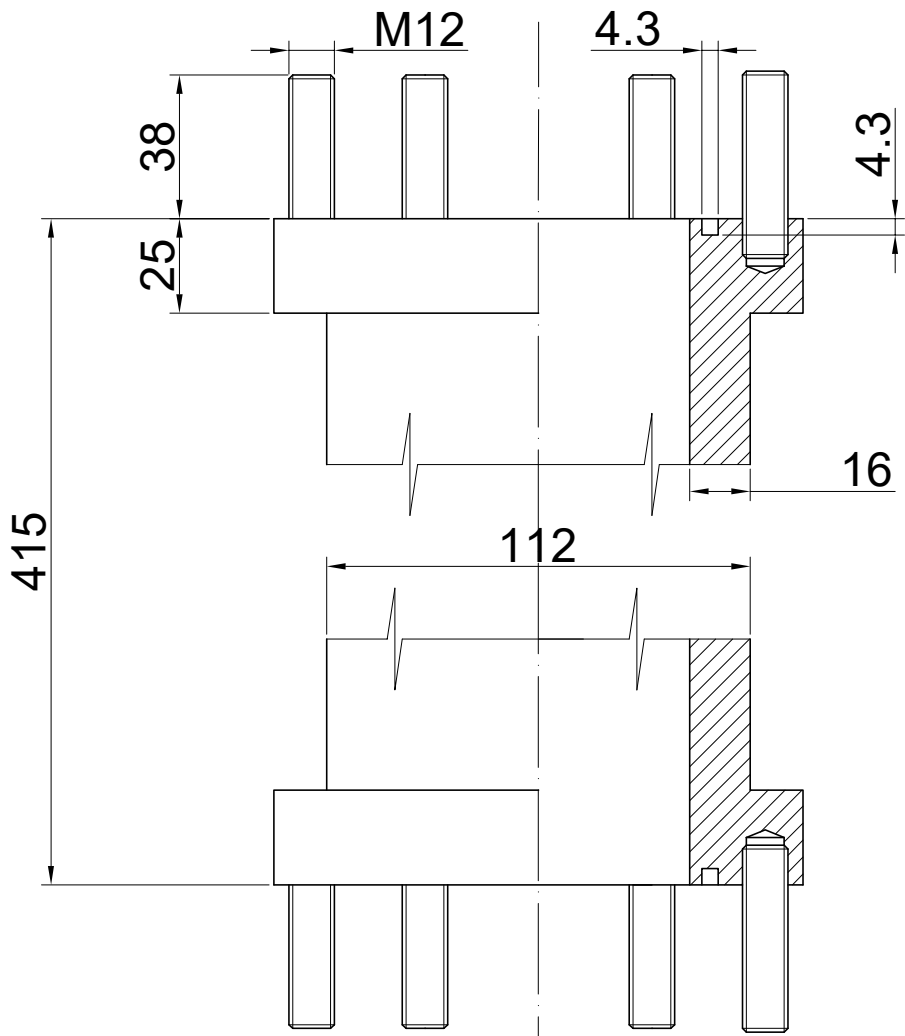


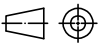




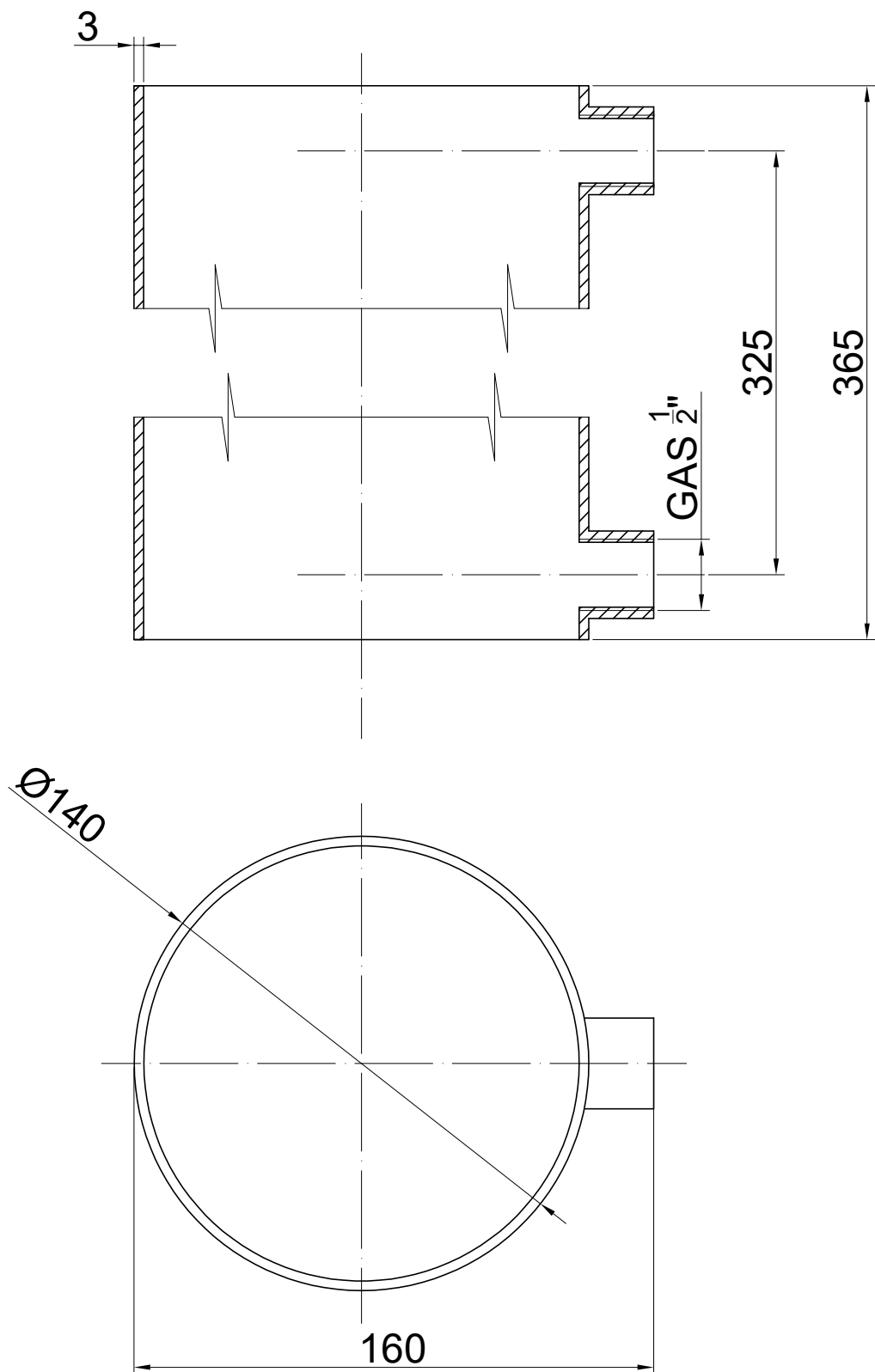
| SIS. REP.   | FECHA         | NOMBRE                   | FIRMA |                                |
|---|---------------|--------------------------|-------|--------------------------------|
|  |               | REINALDO VALLEJO VICENTE |       | TESIS REINALDO VALLEJO VICENTE |
| ESCALA<br>1:2   | TAPA INFERIOR |                          |       | PLANO NÚMERO: 2<br>MARCA: 2    |

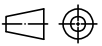




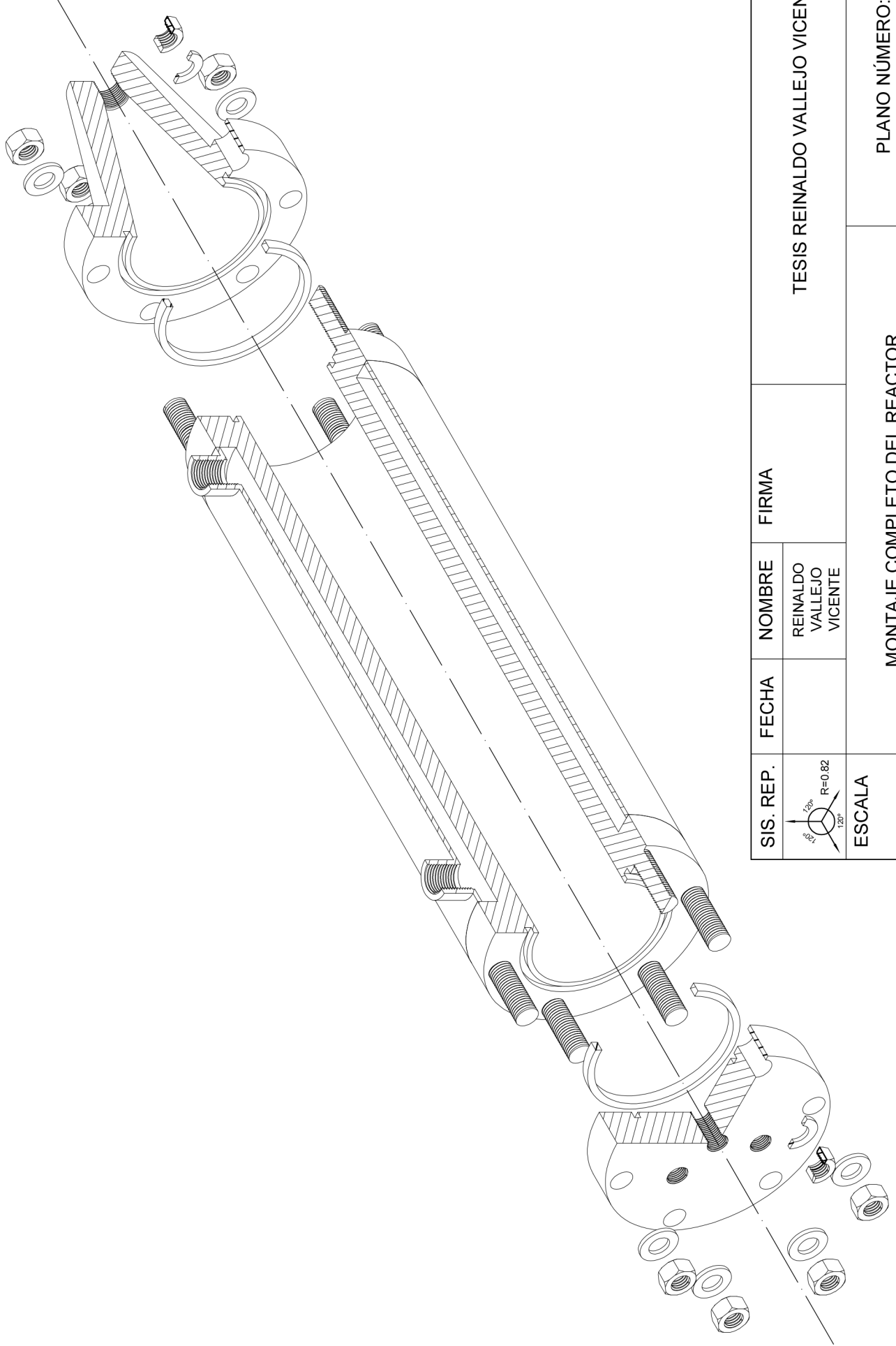
| SIS. REP.   | FECHA              | NOMBRE                   | FIRMA | TESIS REINALDO VALLEJO VICENTE |
|---|--------------------|--------------------------|-------|--------------------------------|
|  |                    | REINALDO VALLEJO VICENTE |       |                                |
| ESCALA<br>1:2   | CUERPO DEL REACTOR |                          |       | PLANO NÚMERO: 3<br>MARCA: 3    |






|   |            |                          |       |                                |
|---|------------|--------------------------|-------|--------------------------------|
| SIS. REP.   | FECHA      | NOMBRE                   | FIRMA | TESIS REINALDO VALLEJO VICENTE |
|  |            | REINALDO VALLEJO VICENTE |       |                                |
| ESCALA  | ENCAMISADO |                          |       | PLANO NÚMERO: 4                |
| 1:2   |            |                          |       | MARCA: 4                       |

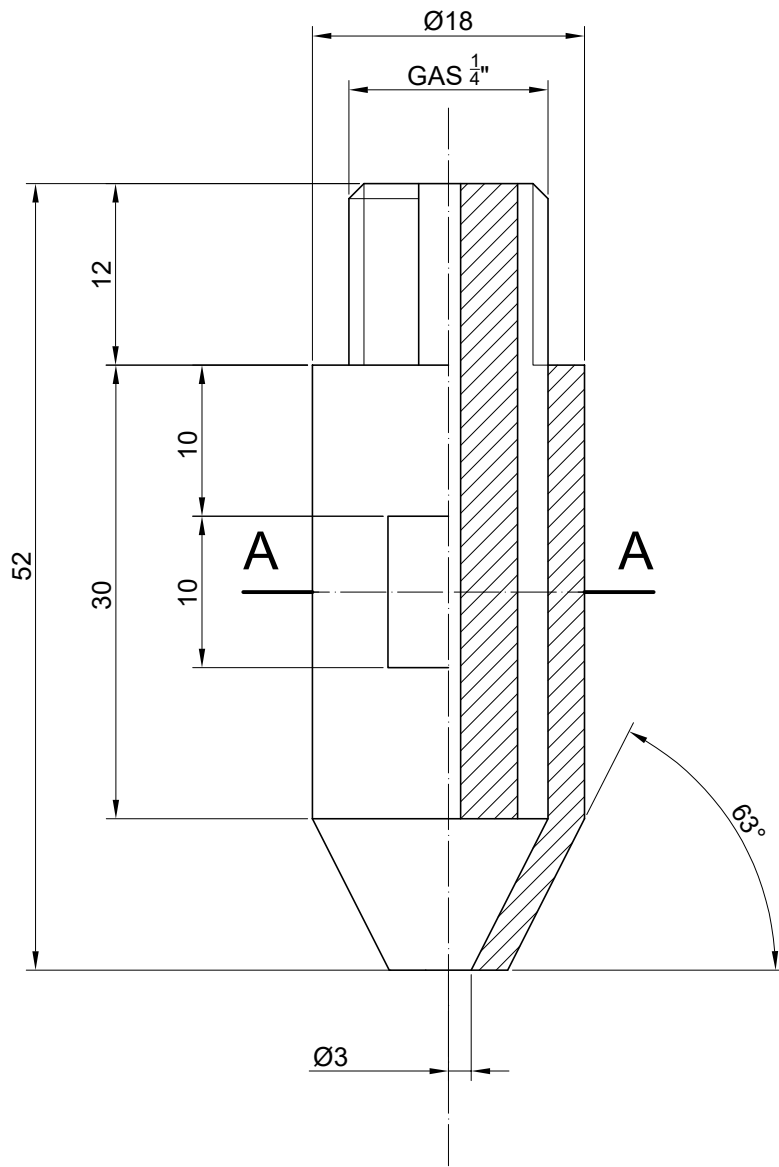




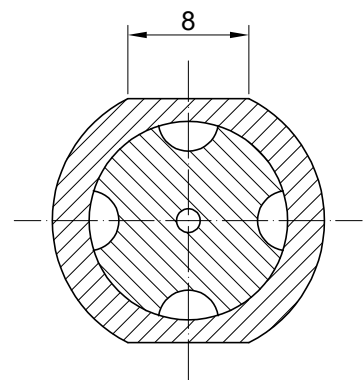
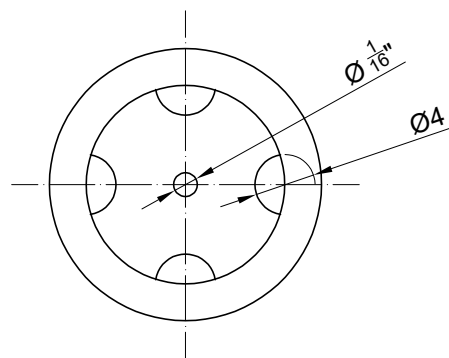
|  |                              |                          |       |                                |
|--|------------------------------|--------------------------|-------|--------------------------------|
| SIS. REP.<br> | FECHA                        | NOMBRE                   | FIRMA | TESIS REINALDO VALLEJO VICENTE |
|  |                              | REINALDO VALLEJO VICENTE |       |                                |
| ESCALA<br>1:3  | MONTAJE COMPLETO DEL REACTOR |                          |       | PLANO NÚMERO: 5                |

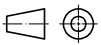




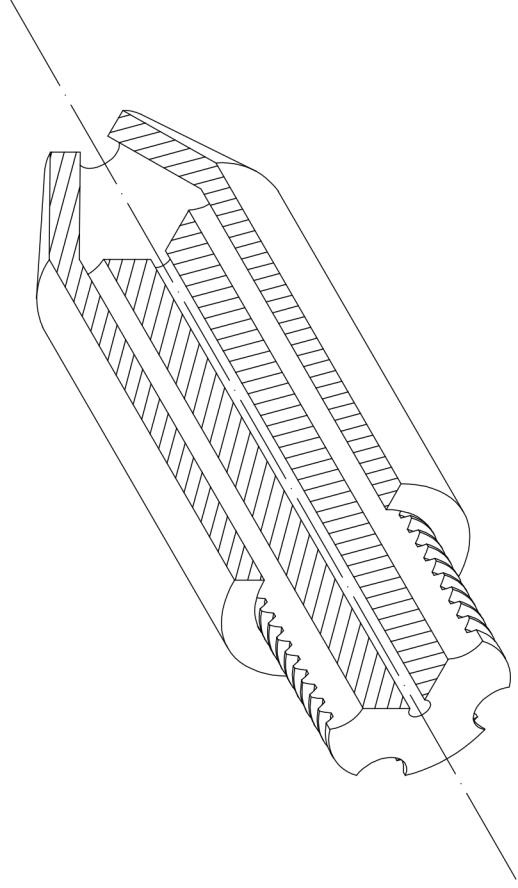


CORTE A-A



|   |                  |                          |                 |                                |
|---|------------------|--------------------------|-----------------|--------------------------------|
| SIS. REP.   | FECHA            | NOMBRE                   | FIRMA           | TESIS REINALDO VALLEJO VICENTE |
|  |                  | REINALDO VALLEJO VICENTE |                 |                                |
| ESCALA  | BOQUILLA COAXIAL |                          | PLANO NÚMERO: 6 |                                |
| 2:1   |                  |                          |                 |                                |





| SIS. REP. | FECHA            | NOMBRE                   | FIRMA | TEMA                           |
|-----------|------------------|--------------------------|-------|--------------------------------|
|           |                  | REINALDO VALLEJO VICENTE |       | TESIS REINALDO VALLEJO VICENTE |
| ESCALA    | BOQUILLA COAXIAL |                          |       | PLANO NÚMERO: 7                |
| 2:1       |                  |                          |       |                                |



## ABOUT THE AUTHOR

Reinaldo Vallejo Vicente, Technical Industrial Engineering specialized in Industrial Chemistry, obtained his degree in 2014 at the University of Valladolid with an honorary degree in the final project; its subject was the characterization of hydrogels based on elastin-like recombinamers for advanced applications in biomedicine, part of this work was awarded the third prize in the summer residences organized by the “Fundación Parque Científico” of the University of Valladolid in 2013. Afterwards, in 2015 obtained his Master’s degree in Fluid Thermodynamic Engineering at the University of Valladolid with an average grade of 9.25 and with honourable mention in his master thesis; its subject was the encapsulation of hydrophobic drugs for the treatment of glaucoma with elastin-like recombinamers by supercritical antisolvent technique (SAS). In 2016, he started to work at the Instituto Murciano de Investigación Agrario-Alimentario (IMIDA) (Region of Murcia) in the R&D project "Nanotechnology applied to the formulation of essential oils for aphid control in horticultural crops". In 2017, he started his PhD at the Chemical and Environmental Engineering PhD program at the University of Valladolid, whose topic is about the development of advanced controlled release systems based on elastin-like recombinamers by supercritical fluids for applications in biomedicine.

### Scientific contributions

**Scientific article:** R. Vallejo; J. Gonzalez-Valdivieso; M. Santos; S. Rodriguez-Rojo; F.J. Arias. 2021. Production of elastin-like recombinamer-based nanoparticles for docetaxel encapsulation and use as smart drug-delivery systems using a supercritical antisolvent process. *Journal of Industrial and Engineering Chemistry*. Elsevier. 93, pp.361-374. JIF: 5.278; 21/143; Q1 Chem.Eng. (JCR Sci.Ed.2019). DOI: 10.1016/j.jiec.2020.10.013

**Bibliographic review:** M. Santos; S. Serrano-Ducar; J. Gonzalez-Valdivieso; R. Vallejo; A. Girroiti; P. Cuadrado; F.J. Arias. 2018. Genetically engineered biopolymers for pharmaceutical and biomedical applications. *Current Medicinal Chemistry*. 26, pp.7117-7146. JIF: 3.894; 12/61; Q1 Chem/Med, 55/267 Pharmacology & pharmacy. (JCR Sci.Ed.2018). DOI: 10.2174/0929867325666180508094637. Cites: 7 (Scopus, 01/02/2019)

**Scientific article:** M.J. Pasual-Villalobos; M. Canto; R. Vallejo; S. Rodriguez-Rojo; P. Guirao; M.J. Cocero. 2017. Use of nanoemulsions of plant essential oils as aphid repellents Use of nanoemulsions of plant essential oils as aphid repellents. *Industrial Crops and Products*. 110, pp.45-57. JIF: 3.849; 2/14; Q1 Agricultural engineering, 6/67 Q1 (TOP 10-10%) Agronomy. (JCR Sci.Ed.2017). DOI: 10.1016/j.indcrop.2017.05.019. Cites: 23 (Scopus 01/02/2021)

## Congress contributions

**Title of the work:** Encapsulation of docetaxel with elastin like recombinamers by supercritical CO<sub>2</sub> for advanced anticancer applications.

**Authors:** Reinaldo Vallejo Vicente; Juan González-Valdivieso; Mercedes Santos García; Soraya Rodríguez Rojo; Francisco Javier Arias Vallejo.

**Type of contribution:** Oral communication

**Name of the conference:** ECCE 12 The European Congress of Chemical Engineering

**Corresponding author:** Yes

**City of event:** Florencia, Toscana, Italy

**Date of event:** 15/09/2019 **End date:** 19/09/2019

**Title of the work:** Encapsulation of docetaxel with Elastin Like Recombinamers by supercritical CO<sub>2</sub> for advanced anticancer applications in biomedicine

**Authors:** Reinaldo Vallejo Vicente; Soraya Rodríguez Rojo; Mercedes Santos García; Francisco Javier Arias Vallejo; María José Cocero Alonso.

**Type of contribution:** conference poster

**Name of the conference:** NanoBio&Med 2018

**Corresponding author:** Yes

**City of event:** Barcelona, Catalonia, Spain

**Date of event:** 20/11/2018 **End date:** 22/11/2018

**Title of the work:** Nanocoating of High Hydrophobic Drugs with Elastin-like Recombinamers by Supercritical CO<sub>2</sub>

**Authors:** Reinaldo Vallejo Vicente; Soraya Rodríguez Rojo; Mercedes Santos García; Francisco Javier Arias Vallejo; María José Cocero Alonso.

**Type of contribution:** conference poster

**Name of the conference:** Supergreen 2017

**Corresponding author:** Yes

**City of event:** Nagoya University, Japan

**Date of event:** 01/12/2017 **End date:** 03/12/2017

## **R&D Contracts with public or private entities**

- 1** Analysis and improvement of coffee impact aroma PROSOL, S.A. IP: Soraya Rodriguez Rojo. (University of Valladolid). 22/01/2020-30/09/2020.
- 2** Study for the formulation of nanoemulsions of active compounds of essential oils for fungicidal applications. Desarrollo Agrícola y Minero, S.A. IP: Soraya Rodriguez Rojo. (University of Valladolid). 22/01/2020-30/09/2020.
- 3** Design and manufacture of in vivo and ex vivo BALB/c mouse holders for nuclear magnetic resonance by 3D printing. Laboratory of Instrumental Techniques of the University of Valladolid. F.J. Arias Vallejo. (University of Valladolid) 2019.
- 4** Extraction of beta-glucans from barley, Semillas Batlle, S.A. IP: Esther Alonso Sánchez. (University of Valladolid). 12/03/2019-12/04/2019.
- 5** Extraction of tannins and polyphenols from Eucalyptus Nittens and Pinnaster Pine by industrial microwave, Química del Nalón, S.A. IP: Rafael Mato Chain. (University of Valladolid). 01/10/2018-31/12/2018.
- 6** Modification of UHMWPE and UHMWPEvitE grains via supercritical CO<sub>2</sub> for orthopaedic applications, Robert Mathys Foundation. IP: Soraya Rodriguez Rojo. (University of Valladolid). 01/12/2014-16/03/2016.

